

**SYNTHESIS AND CHARACTERIZATION OF  
ORGANO-INORGANIC CONDUCTING  
POLYMER BASED NANOCOMPOSITES FOR  
ELECTROCHEMICAL POWER SOURCES**

**BY**

**A.VADIVEL MURUGAN**

**AUGUST 2004**

**SYNTHESIS AND CHARACTERIZATION OF  
ORGANO-INORGANIC CONDUCTING POLYMER  
BASED NANOCOMPOSITES FOR  
ELECTROCHEMICAL POWER SOURCES**

**THESIS**

SUBMITTED TO THE  
**UNIVERSITY OF PUNE**  
FOR THE DEGREE OF  
**DOCTOR OF PHILOSOPHY**  
IN  
**CHEMISTRY**

BY

**A.VADIVEL MURUGAN**

UNDER THE GUIDANCE OF

**Dr.K.VIJAYAMOHANAN**

PHYSICAL AND MATERIALS CHEMISTRY DIVISION  
NATIONAL CHEMICAL LABORATORY  
PUNE- 411 008

AUGUST 2004



**Dr. K. Vijayamohan**  
**Scientist**

Physical & Materials Chemistry Division  
**National Chemical Laboratory**  
Pune -411 008, INDIA  
Tel: 91-020-25893300 Extn:2270  
Res:91-020-25893307  
Fax:91-020-25893044  
Email:viji@ems.ncl.res.in

**NCL**

---

## **CERTIFICATE**

This to certify that the work incorporated in the thesis “**Synthesis and Characterization of Organo-Inorganic Conducting Polymer based Nanocomposites for Electrochemical Power sources**” submitted by **Mr.A.Vadivel Murugan** was carried out by him under my supervision at National Chemical Laboratory, Pune. All the materials from other sources have been duly acknowledged in this thesis.

**Date:**

**(K.Vijayamohan)**  
**Research Guide**



*Dedicated to the  
Memory of My Father*



## **ACKNOWLEDGEMENTS**

This PhD thesis is simply the culmination of a few years of ardent learning and research experience. Throughout these years, I have received much support from my family, research guide and friends. Indeed, my doctoral thesis is a dream of my *late* father **Thiru.V.Arumugam** coming true. This is not just the words in these pages but each word acknowledges my deep gratitude to all those who played a pivotal role in the same and without whom this thesis would not have been possible.

I acknowledge my sincere gratitude to my research guide of this thesis **Dr. K. Vijayamohanam**, Scientist, Physical & Materials Chemistry Division, National Chemical Laboratory, Pune for his excellent guidance and constant encouragement. Thank you so much Sir for being there with all these words of inspiration, wisdom and optimism that always helped me to see the bright side of things. You kept me going when my faith was faltering.

I am very grateful to Dr. Guy Campet, Directeur de Recherche au Institut de Chimie de la Matière Condensée de Bordeaux (ICMCB), CNRS, and his group Dr. Chai-Won Kwon, Dr. M. H. Delville, and Dr. Mathieu Quintin from France for all their help in electrochemical studies and also being kind to provide the encouragement throughout. I will never forget their help and kindness and still our collaboration is continuing.

I express my sincere thanks to and Dr. Chinnakonda S. Gopinath, Scientist, Catalysis Division, NCL for his timely help and also being kind and considerate throughout my XPS studies.

I would like to express my profound gratitude to Dr. S. Sivaram, Director, and Dr. B. D. Kulkarni, Scientist, NCL, Pune for providing me this opportunity to get registered for PhD through NCL. I gratefully acknowledge Dr. B. K.Das, Executive Director, C-MET for his kind support during the course of this studies.

I would like to acknowledge my deepest gratitude to Dr. Murali Sastry, Scientist, NCL for his encouragement throughout my studies. I would also like to gratefully acknowledge Dr. Sourav Pal, Head, Physical & Materials Chemistry Division and Dr. P. A. Joy, Scientist, and his group, Physical & Materials Chemistry Division, NCL, Pune.

Most helpful during my doctoral work were Drs. Sainker, Mandale, Jog, Raja, Manikandan, Selvaraj, Adyanthya from NCL and *Late*. Dr. Subbanna, IISc, Bangalore. If there were not energetic cooperation and help of my NCL friends and Lab mates, Vijayaraj, Priya, Nirmalya, Trupti, Girish, Balachandra, Jadap, Selvakanan, Nirranjan, Deepali, Mukta and Mahima, this work would not have been done.

I am particularly thankful to Dr. B. B. Kale, Scientist C-MET to encourage me with constant support to pursue my PhD research and for arranging infrastructural facilities throughout the study. I am also thankful to Dr. D. P. Amalnerkar, Mr. P. I. Sadanandan and Mr. G. Venkatachalam from C-MET also have supported me during this work and I thank them all financial assistance from both Ministry of Non-conventional Energy Sources and Department of Information Technology, Government of India are gratefully acknowledged.

I should also truly be thankful for much help from my C-MET scientists & colleagues; Mr. S. K. Apte, R. S. Sonawane, Ganegar, R. K. Goyal, G. P. Rao, R. Marimuthu, S. Roy and S. Prasankar. Mrs. Shany, Aarti, Lalita, Sonali and Subangi, Drs. Tanay Seth, Rane and Potty. Munificent support from my friends, Mr. V. V. V. S. Subbarao played a great part for the completion of this thesis. I am profoundly grateful to M/s. Bayer AG, Germany & Mr. Joshi Bayer India Ltd. Mumbai for kindly provided EDOT monomer.

Most importantly, the deepest thanks from the bottom of my heart should be dedicated to my brothers **Mr.Sethupathy, Mr.Ramanathan, Mr.Narendren**, my sister **Mrs.Shanthi**, and especially my mother **Mrs.Yasothai** who have always supported me.

Finally I am grateful to my wife **Mrs.Amutha** without whose emotional support and dedication, this would never been possible. She is the person who was on my side with tremendous perseverance at each and every difficult stage during this work and I thank you **Amutha** for all the patience.

**(A. Vadivel Murugan)**

# INDEX

<b>Chapter</b>	<b>Title</b>	<b>Page</b>
<b>1</b>	<b>Introduction</b>	<b>1-49</b>
1.1	Introduction to Nanoscience and technology	2
1.2	Nanostructured Materials	4
1.2.1	Classes of Nanostructured Materials	5
1.3	Composite Materials	6
1.3.1	Classes of Composite Materials	7
1.4	Nanocomposite Materials – In Search of Synergic Effects	7
1.4.1	Guest-Host Materials interacting in Nanocomposites	9
1.4.2	Conducting Polymer based Nanocomposites and their Classification	11
1.4.3	Inorganic-Organic (I-O) Nanocomposites	12
1.4.3.1	Nanocomposites prepared by “Core-Shell” strategy	12
1.4.4	Organic-Inorganic (O-I) Nanocomposites	14
1.4.4.1	Nanocomposite prepared by Exfoliative and Intercalative strategies	14
1.4.5	Newly emerging Applications	17
1.5	Introduction to Electrochemical Power Sources	19
1.5.1	Fuel Cells	20
1.5.2	Supercapacitors	22
1.5.3	Batteries	24
1.5.3.1	Primary Batteries	24
1.5.3.2	Secondary Batteries	25
1.6	Introduction to Lithium Batteries	29
1.6.1	Lithium Insertion Materials for Negative Electrodes	32
1.6.2	Lithium Insertion Materials for Positive Electrodes	35
1.6.2.1	One-Dimensional Hosts as Positive Electrode Materials	36
1.6.2.2	Two-Dimensional Hosts as Positive Electrode Materials	36
1.6.2.3	Three-Dimensional Hosts as Positive Electrode Materials	38
1.6.3	Electrolytes for Lithium Batteries	40

1.7	Conclusions and Perspectives	41
1.8	Motivation, Scope and Organization of the thesis	42
1.9	Aim and Scope of the Present Study	43
1.10	References	46
<b>Chapter</b>	<b>Title</b>	<b>Page</b>
<b>2</b>	<b>Novel Organo-Inorganic Poly (3,4- Ethylene dioxythiophene) PEDOT /V<sub>2</sub>O<sub>5</sub> Nanocomposites by Redox Intercalative Polymerization</b>	<b>50-72</b>
2.1	Introduction	51
2.2	Experimental Section	52
2.2.1	Materials	52
2.2.2	Synthesis of Poly(3,4-ethylenedioxythiophene) / V <sub>2</sub> O <sub>5</sub> Nanocomposites	53
2.2.3	Characterization techniques	53
2.2.4	Electrochemical measurements	54
2.2.5	Elemental Analysis	54
2.3	Results and Discussion	55
2.3.1	FTIR Spectroscopy	55
2.3.2	Powder X-ray diffraction (XRD)	56
2.3.3	X-ray Photoelectron Spectroscopy (XPS)	58
2.3.4	Thermogravimetric Analysis (TGA/DTA)	59
2.3.5	Scanning Electron Microscopy (SEM)	60
2.3.6	Transmission Electron Microscopy (TEM)	60
2.3.7	Electronic conductivity	62
2.3.8	Electrochemical lithium insertion	63
2.3.9	Cyclic Voltammetry	64
2.3.10	Charge-Discharge Properties	65
2.3.11	Cycle life	67
2.4	Conclusions	68
2.5	References	69



<b>Chapter</b>	<b>Title</b>	<b>Page</b>
<b>3</b>	<b>New Organo-Inorganic Intercalative Nanocomposite: Entrapment of Poly (3,4-Ethylenedioxythiophene) between VS<sub>2</sub> Layers</b>	<b>73-92</b>
3.1	Introduction	74
3.2	Experimental Section	75
3.2.1	Materials	75
3.2.2	Preparation of Li <sub>x</sub> VS <sub>2</sub> (0 ≤ x ≤ 1)	75
3.2.3	Synthesis of Poly(3,4-ethylenedioxythiophene) / VS <sub>2</sub> Nanocomposite	76
3.2.4	Characterization techniques	77
3.2.5	Electrochemical measurements	77
3.3	Results and Discussion	78
3.3.1	FTIR Spectroscopy	78
3.3.2	Powder X-ray diffraction (XRD)	79
3.3.3	X-ray Photoelectron Spectroscopy (XPS)	81
3.3.4	Thermogravimetric Analysis (TGA)	82
3.3.5	Scanning Electron Microscopy (SEM)	83
3.3.6	Transmission Electron Microscopy (TEM)	83
3.3.7	Electronic conductivity	84
3.3.8	Electrochemical lithium insertion	85
3.3.9	Cyclic Voltammetry	86
3.3.10	Charge-Discharge Properties	87
3.3.11	Cycle life	89
3.4	Conclusions	89
3.5	References	91

<b>Chapter</b>	<b>Title</b>	<b>Page</b>
<b>4</b>	<b>Intercalation of Poly (3,4-Ethylenedioxy thiophene) between MoO<sub>3</sub> Layers <i>via in situ</i> Oxidative Polymerization</b>	<b>93-111</b>
4.1	Introduction	94
4.2	Experimental Section	95
4.2.1	Materials	95
4.2.2	Preparation of Li <sub>x</sub> MoO <sub>3</sub>	95
4.2.3	Exfoliation and Polymer Intercalation Strategy	96
4.2.4	Characterization techniques	97
4.2.5	Electrochemical measurements	97
4.3	Results and Discussion	97
4.3.1	FTIR Spectroscopy	97
4.3.2	Powder X-ray diffraction (XRD)	99
4.3.3	X-ray Photoelectron Spectroscopy (XPS)	101
4.3.4	Thermogravimetric Analysis (TGA/DTA)	102
4.3.5	Scanning Electron Microscopy (SEM)	103
4.3.6	Transmission Electron Microscopy (TEM)	103
4.3.7	Electronic conductivity	104
4.3.8	Electrochemical lithium insertion	105
4.3.9	Cyclic Voltammetry	106
4.3.10	Charge-Discharge Properties	107
4.3.11	Cycle life	108
4.4	Conclusions	109
4.5	References	110

<b>5</b>	<b>Poly (3,4-Ethylenedioxythiophene) Nanosheet formation in between MoS<sub>2</sub> Layers by Exfoliation and Restacking process</b>	<b>112-130</b>
5.1	Introduction	113
5.2	Experimental Section	114
5.2.1	Materials	114
5.2.2	Preparation of Li <sub>x</sub> MoS <sub>2</sub>	114
5.2.3	Preparation of Exfoliated and Reflocculated MoS <sub>2</sub>	115
5.2.4	Polymer Intercalation and Restacking of MoS <sub>2</sub>	115
5.2.5	Characterization techniques	115
5.2.6	Electrochemical measurements	115
5.3	Results and Discussion	116
5.3.1	Synthesis of MoS <sub>2</sub> Intercalation compound	116
5.3.2	Structure of 1T-MoS <sub>2</sub>	116
5.3.3	Structure of PEDOT/MoS <sub>2</sub> Intercalation Compound	117
5.3.4	FTIR Spectroscopy	117
5.3.5	Powder X-ray diffraction (XRD)	119
5.3.6	X-ray Photoelectron Spectroscopy (XPS)	121
5.3.7	Thermogravimetric Analysis (TGA)	122
5.3.8	Scanning Electron Microscopy (SEM)	122
5.3.9	Transmission Electron Microscopy (TEM)	123
5.3.10	Electronic conductivity	124
5.3.11	Electrochemical lithium insertion	125
5.3.12	Cyclic Voltammetry	125
5.3.13	Charge-Discharge Properties	126
5.3.14	Cycle life	127
5.4	Conclusions	128
5.5	References	129
<b>6.0</b>	<b>Summary and Future Prospects</b>	<b>131-136</b>

## Abbreviations

<b>Abbreviations</b>	<b>Meanings</b>	<b>Chapter</b>
AFC	Alkaline fuel cells	1
BE	Binding Energy	2,3,4,5
CNT	Carbon nanotube	1
CV	Cyclic Voltammetry	2,3,4,5
DMC	Dimethyl Carbonate	2,3,4,5
EC	Ethylene Carbonate	2,3,4,5
EDLC	Electric Double Layer Capacitor	1,4
EDOT	Ethylenedioxythiophene	2,3,4,5
EV	Electric Vehicle	1
eV	Electron Volt	2,3,4,5
FET	Field-Effect Transistors	1
F/g	Farad per gram	1,4
FTIR	Fourier Transform Infrared Spectroscopy	2,3,4,5
ICP-OES	Inductively Coupled Plasma Optical Emission Spectroscopy	2,3,4,5
I-O	Inorganic-Organic	1,2,3,4
K	Kelvin	2,3,4,5
LED	Light Emitting Diodes	1
mAh/g	Millie Ampere hour per gram	2,3,4,5
MCFC	Molten carbonate fuel cells	1
MoO <sub>3</sub>	Molybdenum trioxide	4
MoS <sub>2</sub>	Molybdenum disulfide	5
NASICON	Sodium superionic conductors	1
OCPs	Organic Conducting Polymers	1,2
OCV	Open Circuit Voltage	2,3,4,5
O-I	Oragno-Inorganic	1
PAni	Polyaniline	1,2
PEDOT	Poly(3,4-Ethylenedioxythiophene)	2,3,4,5
PEMFC	Polymer membrane or proton exchange membrane fuel cells	1
PPV	Poly(p-phenylene vinylene)	1,4
PPy	Polypyrrole	1,2
PTFE	Polytetrafluroethylene	2,3,4,5
SEM	Scanning Electron Microscope	2,3,4,5
SET	Single Electron Tunneling	1
SOFC	Solid oxide fuel cells	1
TEM	Transmission Electron Microscope	2,3,4,5
TGA/DTA	Thermogravimetric analysis/Differential Thermal Analysis	2,3,4,5
V <sub>2</sub> O <sub>5</sub>	Vanadium pentoxide	2
VS <sub>2</sub>	Vanadium disulfide	3
XPS	X-ray Photoelectron Spectroscopy	2,3,4,5
XRD	X-ray Diffraction	2,3,4,5

ABSTRACT OF THE THESIS

**SYNTHESIS AND CHARACTERIZATION OF  
ORGANO-INORGANIC CONDUCTING POLYMER  
BASED NANOCOMPOSITES FOR  
ELECTROCHEMICAL POWER SOURCES**

SUBMITTED TO THE  
**UNIVERSITY OF PUNE**

FOR THE DEGREE OF  
**DOCTOR OF PHILOSOPHY**

IN  
**CHEMISTRY**

BY  
**A.VADIVEL MURUGAN**

UNDER THE GUIDANCE OF  
**Dr.K.VIJAYAMOHANAN**

PHYSICAL AND MATERIALS CHEMISTRY DIVISION  
NATIONAL CHEMICAL LABORATORY  
PUNE-411 008

AUGUST 2004

Recently, nanoscale building blocks, such as nanoclusters, nanotubes and nanowires have attracted extensive interest because of their low dimensionality and size dependant properties which are different from those of the atomic and bulk counterparts, enabling them to tune for a wide-range of applications. Indeed, this precise tuning of the molecular level interactions of dissimilar organic and inorganic components to form unique functional materials, has generated a new theme of hybrid nanocomposite materials entailing several challenges and opportunities.

The use of conducting polymers as an organic guest for preparing such organo-inorganic hybrid materials is specially attractive for electrochemical applications mainly for electronic conducting properties. First, these conjugated molecules can be tuned to provide percolation pathways for electron transport. More importantly, the charge transfer rates can be remarkably fast in the case of these organic conjugated molecules which can be chemically bound to nanocrystalline inorganic material, which normally has a high density of electronic states. Consequently, nanocomposites of these conducting polymers inserted into layered transition metal oxides and sulfides have been extensively studied in this thesis for applications in electrochemistry particularly insertion electrodes in rechargeable lithium batteries and supercapacitors.

Poly(3,4-ethylene dioxythiophene), hitherto referred to as PEDOT, is one of the recently found excellent more “eco-friendly” polymers, which has not been investigated in this regard, despite its superior features like better thermal and electrochemical stability, improved performance in several applications including antistatic transparent films, electrochromic, supercapacitor and lithium battery electrodes. Thus, we have selected this compound to develop a new class of organo-inorganic conducting polymer based nanocomposite materials which can act as cathodes for rechargeable lithium batteries. The specific use of Poly (3,4-ethylene dioxythiophene) (PEDOT) as an organic guest into inorganic transition metal oxides / sulfides host is expected to offer several advantages in terms of intercalation cathodes due to a more flexible design for  $\text{Li}^+$  ion transport and tuning of conductivity. The design of better electrode materials for rechargeable lithium batteries has become increasingly important due to a multitude of applications in both portable consumer electronics and electric vehicles.

In the present work, we report the synthesis and characterization of such hybrid nanocomposite materials formed between Poly (3,4-ethylenedioxythiophene) (PEDOT) and two dimensional layered transition metal oxides and disulfides host materials such as  $V_2O_5$ ,  $VS_2$ ,  $MoO_3$  and  $MoS_2$  by intercalation. The usefulness of these hybrid materials as high energy density cathodes for rechargeable lithium batteries and supercapacitor have been demonstrated in comparison with their respective pristine oxides and sulfides.

The thesis comprises of 6 chapters. After a brief introduction to the Organo-inorganic nanocomposite materials in search of synergic activity, their important features are discussed in **Chapter 1**. The primary emphasis is on the intercalation of organic conducting polymer guest molecules into layered inorganic host materials. In these cases, at least in principle, the structure of inorganic guest dominates the structure of the hybrid and the polymers adapt to it. Indeed, the key to the preparation of many of these nanocomposite materials rely upon in-situ polymerization into the inorganic host. The characterization techniques have been extensively used to clearly indicate that such systems can potentially show hybrid properties synergistically derived from the guest-host system. The possible applications of these electro-active functional nanocomposite materials for rechargeable lithium batteries and supercapacitor have been discussed along with their limitations.

**Chapter.2** discusses the redox intercalative polymerization 3,4-ethylenedioxy thiophene (EDOT) into the highly oxidizing host such as Vanadium pentoxide ( $V_2O_5$ ). A systematic study of the synthesis of the nanocomposites by direct *in situ* reaction of 3,4-Ethylenedioxythiophene (EDOT) with crystalline  $V_2O_5$  powder shows that upon intercalation, the interlayer spacing of  $V_2O_5$  expands in two stages, i.e., first from 4.32 to 13.84 Å and further to 19.04 Å. The interlayer separation is consistent with the existence of two phases in the PEDOT/  $V_2O_5$  system corresponding to the intercalation of one and two mono-layers of PEDOT respectively in the  $V_2O_5$  framework. The unique properties of the organo-inorganic composites are investigated by electronic conductivity measurements, powder X-ray diffraction (XRD), FTIR-sepectroscopy, Thermal analysis (TGA/DTA), X-ray photoelectron spectroscopy (XPS), Electron

Paramagnetic Resonance (EPR), Scanning Electron Microscopy (SEM) and High Resolution Transmission Electron Microscopy (HR-TEM) indicating that the highly crystalline vanadium oxide is separated by alternating organic conducting polymer nanoribbons in this hybrid material. The application potential of these composites as cathode materials in rechargeable lithium batteries is also demonstrated by the electrochemical intercalation of lithium into the PEDOT/  $V_2O_5$  nanocomposites, where an enhancement in the discharge capacity is observed compared to that of pristine  $V_2O_5$ .

Since, we have investigated redox intercalative polymerization (RIP) process, which works only with suitably oxidizing hosts, the scope of intercalation chemistry of other layered non-oxidizing hosts has been investigated using other synthetic strategies. Indeed, Layered transition-metal disulfide is another class of versatile intercalation host which can accommodate a wide variety of guest species. **Chapter.3** discusses the encapsulation of Poly (3,4-ethylenedioxythiophene) in Vanadium disulfide ( $VS_2$ ), giving rise to novel nanoscale molecular composite with synergic properties. In this chapter, we describe the synthesis and various physico-chemical characterization of a novel Poly (3,4-ethylenedioxythiophene)PEDOT/ $VS_2$  intercalative nanocomposite with an objective of demonstrating their applications as an better electrode material for lithium batteries.

**Chapter.4** contains another type of transition metal oxide such as Molybdenum trioxide ( $MoO_3$ ), as a weakly oxidizing host structures for introducing polymer intercalation. Indeed, PEDOT /  $MoO_3$  nanocomposite has been successfully synthesized using an exfoliation and restacking strategies. Resulting nanocomposites with Poly (3,4-ethylenedioxythiophene) were characterized by, electronic conductivity, TGA/DTA, XRD, FTIR spectroscopy, XPS, SEM and TEM. This PEDOT/ $MoO_3$  nanocomposite gives an unusual electrochemical double layer capacitance and significant enhancement in the discharge capacities compared to that of their respective pristine Molybdenum trioxide. In conclusion, this nanocomposite can act as promising electrode materials for Supercapacitors and better cathode for rechargeable lithium batteries.

Another new class of nanocomposite materials that is made up of layered transition metal sulfide and chains of Poly (3,4-ethylenedioxythiophene) by exfoliative intercalation strategy has been discussed in **Chapter 5**. One of the most important



achievements described here is the encapsulation of an intractable, infusible Poly (3,4-ethylenedioxythiophene) in a non-oxidizing host such as Molybdenum disulfide ( $\text{MoS}_2$ ) using a suitable external oxidant. PEDOT nanosheet intercalated in between  $\text{MoS}_2$  layers has been investigated by electronic conductivity measurements, XRD, XPS, FTIR Spectroscopy, TGA analysis, SEM and TEM. The resulting nanocomposite material has been found to act as a better electrode material for rechargeable lithium batteries.

**Chapter.6** outline a summary of all the major conclusions of the present study suggesting the general principles of synthesis and characterization Organo-Inorganic nanocomposite, which could merge the best properties of both the organic conducting Poly(3,4-ethylenedioxythiophene) and oxidizing and non-oxidizing inorganic hosts such as  $\text{V}_2\text{O}_5$ ,  $\text{VS}_2$ ,  $\text{MoO}_3$  and  $\text{MoS}_2$ , frequently with complementary strength to form new functional materials. The intercalation of PEDOT macromolecules is consistent with both the expansion of the interlayer distance and structural stabilization of inorganic hosts. However, common to all these hybrid nanocomposite materials is the underlying search for synergy. This synergy has also been explicitly discussed and the improvement in electrochemical performance is attributed to higher electric conductivity and enhanced bi-dimensionality.

These results clearly suggest the benefits offered by these hybrid materials for fabricating composite cathodes for high energy density rechargeable lithium batteries and for supercapacitors, although, the degree to which the polymer-polymer interactions in the bulk is affected by the polymer-host is not clear. Similarly, questions related to how the polymer-host interactions sequester the polymer chains effecting either the polymer conformation, chain length, and / or bulk electron-transport properties need more investigations, especially if we want to improve the cycle life. Despite these limitations, these type of hybrid materials may find increasing importance in the area of electrochemical power sources in the coming years.

**Dr.K.Vijayamohan**  
**Scientist & PhD Research Guide**  
**Physical and Materials Chemistry Division**  
**National Chemical Laboratory, Pune- 411008.**

**A.Vadivel Murugan**  
**Research Student**

## List of Publications

### International Journals

1. Synthesis and characterization of new Organo-Inorganic Poly (3,4-Ethylenedioxy thiophene) PEDOT/V<sub>2</sub>O<sub>5</sub> nanocomposite by intercalation.  
**A.Vadivel Murugan**, B.B.Kale, C.W.Kwon, Gay Campet, K.Vijayamohan, **Journal of Materials Chemistry**, **11 (2001) 2470-2475**
2. Electrochemical Lithium Insertion into a Poly(3,4-Ethylenedioxythiophene) PEDOT /V<sub>2</sub>O<sub>5</sub> Nanocomposite.  
**A.Vadivel Murugan**, Chai-Won Kwon, G.Campet, B.B.Kale, Trupti Manddanimata, K. Vijayamohan.  
**Journal of Power Sources** **105 (2002)1-5**
3. Poly-(3,4-Ethylenedioxythiophene) PEDOT/V<sub>2</sub>O<sub>5</sub> hybrid Cathode for Lithium Batteries., Chai-Won Kwon, **A. Vadivel Murugan**, Guy Campet, Josik Portier, B.B. Kale, K. Vijayamohan, Jin-Ho Choy.  
**Electrochemistry Communications**, **4 (2002)384-387**
4. Conductive Polymer/Transition Metal Oxide Hybrid Materials for Lithium Batteries. Chai-Won Kwon, Armel Poquet, Stéphane Mornet, Guy Campet, Josik Portier, **A.Vadivel Murugan**, B. B. Kale, K. Vijayamohan and J.-H. Choy  
**Mater. Res. Soc. Symp. Proc. 726 (2002) Q11.7.1, Materials Research Society (MRS) Sanfrancisco, California, (USA)**
5. Preparation, characterization and electrochemical lithium insertion into the new organic-inorganic Poly (3,4 Ethylenedioxythiophene) /V<sub>2</sub>O<sub>5</sub> hybrid. Chai-Won Kwon, **A. Vadivel Murugan**, Guy Campet.  
**Active and Passive Electronic components**, **26 (2003) 171.**
6. A Novel Approach to Prepare Poly (3,4-Ethylenedioxythiophene) Nanoribbons between V<sub>2</sub>O<sub>5</sub> layers by Microwave Irradiation.,  
**A.Vadivel Murugan**, B.B.Kale , C.W.Kwon, G.Campet, A.B.Mandale, S.R.Sainker, Chinnakonda S.Gopinath and K.Vijayamohan  
**Journal of Physical Chemistry-B**, **108 (2004) 10736-10742,**
7. New Organo-inorganic intercalative nanocomposite: entrapment of Poly (3,4-Ethylenedioxythiophene) between VS<sub>2</sub>.  
**A.Vadivel Murugan**, G.Campet, M.Quintin, M.H.Delville, Chinnakonda S. Gopinath and K.Vijayamohan  
**Journal of Material Chemistry (Communicated)**

8. Intercalation of Poly(3,4-Ethylenedioxythiophene) between MoO<sub>3</sub> layers via in situ oxidative Polymerization.,  
**A.Vadivel Murugan**, G.Campet, M.Quintin, M.H.Delville, Chinnakonda S. Gopinath, K.Vijayamohan  
**Chemistry of Materials (Communicated)**
9. New Organo-Inorganic Nanocomposite electrode architecture and improved Supercapacitor performance from the smart use of Poly(3,4-Ethylenedioxythiophene).,  
**A.Vadivel Murugan**, Chinnakonda S.Gopinath and K.Vijayamohan  
**Advanced Materials (Communicated)**
10. Poly(3,4-Ethylenedioxythiophene) Nanosheet formation in between MoS<sub>2</sub> layers by exfoliation and restacking process.,  
**A.Vadivel Murugan**, G.Campet, M.Quintin, M.H.Delville, Chinnakonda S. Gopinath, K.Vijayamohan  
**Chemistry of Materials (Communicated)**

### **International Conferences and Symposia**

1. Electrochemical Li-Insertion into new Poly (3,4 Ethylenedioxythiophene) PEDOT/V<sub>2</sub>O<sub>5</sub> hybrids. Chai-Won Kwon, Armel Poquet, Gay Campet, Etienne Duguet, Josik Portier, **A. Vadivel Murugan**, B.B. Kale, K. Vijayamohan. Published in **International Symposium on Intercalation Compounds (ISIC) at Moscow on May 2001 and Extended abstract published in Molecular and Liquid crystals.**
2. Conductive Polymer/Transition Metal Oxide Hybrid Materials for Lithium Batteries. Chai-Won Kwon, Armel Poquet, Stéphane Mornet, Guy Campet, Josik Portier, **A.Vadivel Murugan**, B. B. Kale, K. Vijayamohan and Jin-Ho Choy. ( Q11.7) **International symposium on Hybrid Organic-Inorganic Materials April 1-5, 2002, Materials Research Society (MRS) Sanfrancisco, California,(USA)**
3. Electrochemical behavior of Inorganic Nanocrystalline and Hybrid Nanocrystalline Electrode materials for Lithium batteries Chai-Won Kwon, Christine Labrugere, Gay Campet, **A. Vadivel Murugan**, B.B. Kale, K. Vijayamohan. **Seventh International Symposium on Advances in Electrochemical Science and Technology, (ISAEST-VII)27-29 Nov, 2002 Chennai, India.(P3.37)**
4. Novel Organo-inorganic Poly (3,4 Ethylenedioxythiophene) PEDOT/V<sub>2</sub>O<sub>5</sub> nonocomposite, "Application as a high capacity cathode material for rechargeable lithium batteries". **A. Vadivel Murugan**, B.B. Kale, Chai-Won Kwon, Gay Campet, Josik Portier, , K. Vijayamohan. **Seventh International Symposium on Advances in Electrochemical Science and Technology, (ISAEST-VII)27-29 Nov, 2002 Chennai, India.(P3.44)**

5. Sonochemically Synthesized Conducting Polymer/ $V_2O_5$  nanocomposite cathode for lithium rechargeable batteries.  
**A.Vadivel Murugan**, B.B.Kale, G.Campet, Jin-Ho Choy and K.Vijayamohanana., **1<sup>st</sup> International conference on Polymer batteries and Fuel Cells, June 1-6, 2003, Jeju Island, Korea, P-TU-081, organized by Korean Electrochemical Soc., & The Electrochemical Soc., Inc.**
6. Novel Organo- inorganic Nanocomposite Materials-In Search of Synergic Activity.,  
**A.Vadivel Murugan**, K.Vijayamohanana <sup>b</sup>, **Royal Society of Chemistry West India Section Students Symposium- 19<sup>th</sup> - 20<sup>th</sup> September, 2003 at National Chemical Laboratory, Pune, India**
7. Inorganic and organic-inorganic nanomaterials as Electrodes for rechargeable lithium batteries.  
G.Campet, O.Devos, M.H.Delville, S.J.Hwang, C.W.Kwon, **A.Vadivel Murugan**, M.Quintin. **5<sup>th</sup> Korean battery meeting, 28 Nov, 2003, at ETRI, Daejeon, Korea.**
8. Novel Organo- Inorganic nanocomposite materials for use in high energy density batteries for electronic applications **A.Vadivel Murugan**, B.B.Kale, Chai-Won Kwon, Guy Campet and K.Vijayamohanana., **International Conference on Nanoscience and Technology (ICONSAT-2003) 17-20 December-2003, Kolkata, India.**
9. Novel Organic-Inorganic Hybrid Functional Nanostructured Material for the Future Energy Storage Application  
**A.Vadivel Murugan**, B.B.Kale, Chai-Won Kwon, Guy Campet, K.Vijaymohanana and B.K.Das.  
**Materials for the Future MF- 2004, March 22-23, 2004, Materials Research Centre, Indian Institute of Science, IISc, Bangalore, India.**

## **Patent**

1. A Novel Process for the Preparation of Nanostructured Organo-Inorganic Hybrid Materials as High Energy Density Cathode for Rechargeable Lithium Batteries.  
**A. Vadivel Murugan**, B.B. Kale, B.K.Das, K. Vijayamohanana.  
**(US Patent filed-Application No. by DOE 915/DEL/2002)**

This chapter presents an overview of science and technology of nanostructured materials as a recently emerged, unique and powerful interdisciplinary research activity. This is followed by a discussion of the “*Bottom-up*” approach for materials synthesis based on molecular design, where organic-inorganic hybrid materials reveal remarkable synergistic effects highlighting a wide range of unique properties (e.g., optoelectronic, energy storage, electrocatalysis and magnetic applications) associated with different types of nanostructures. Various methods and types of organization of nanocomposite materials for electrochemical power sources are mentioned with special emphasis on rechargeable lithium batteries. This chapter also gives the major objectives and the overall organization of the thesis.

## Nanostructured Materials

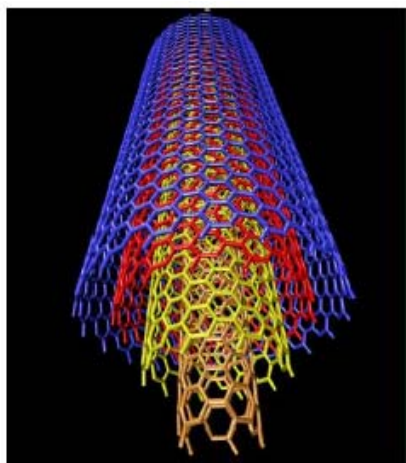


Figure 1a. Representation of a Multiwalled Carbon Nanotube<sup>1b</sup>

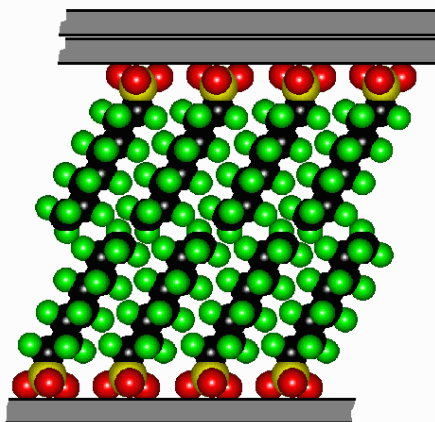


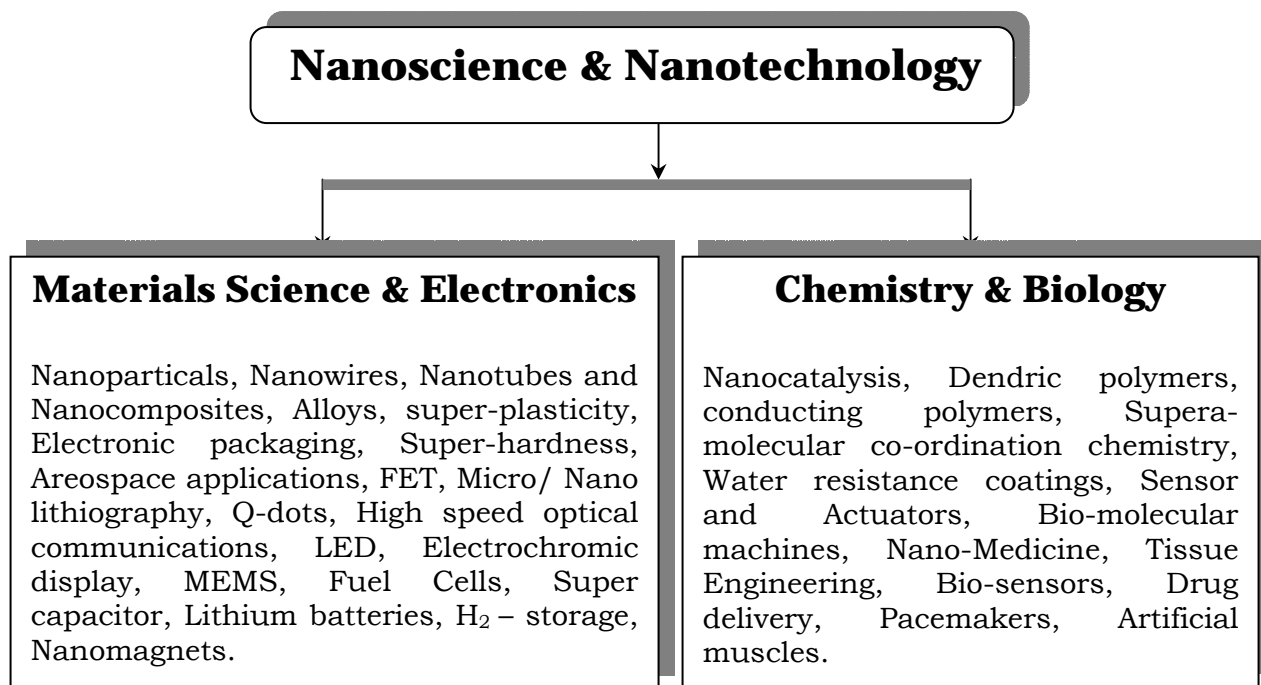
Figure 1b. Simulated structure of Organo-Inorganic Interactive Nano-composite<sup>1c</sup>

## 1.1 Introduction to Nanoscience and Technology

The recently emerged nanoscience and nanotechnology as a unique and powerful interdisciplinary research activity, has generated several futuristic ideas that are now slowly becoming vibrant areas of research and development. For example, the realization of Feynman's prophecy "**there is plenty of room at bottom**" in 1959)<sup>1a</sup> though originated from the ability of researchers to manipulate matter at the nanometer scale, has resulted in materials with novel and significantly improved physical, chemical, and biological properties.<sup>2</sup> Since, nanotechnology implies the control of matter at the atomic and molecular level which requires working across boundaries of classical disciplines, it is essential to work within a very basic scheme of the interdisciplinary character of nanotechnology realizing the overlap between nanotechnology and its related fields. This is especially significant since a strong hope (also much hype!) is now put on nanomaterials and nanotechnology resembling a sort of dream in which nanotechnology will solve all the current problems in any scientific field ranging from electronics, optoelectronic and photonics to energy storage, medicine and biology. For example, miniaturization in electronics through improvements in the so-called "**top-down**" fabrication techniques is approaching the point where fundamental issues are expected to limit the dramatic increase in computing speed. Obviously, there is also the pressing issue of fabrication cost as the feature size reaches the sub-100 nm region. As a result, nanostructured materials like carbon nanotube (CNTs) have recently been explored as building blocks to fabricate nanoscale electronic devices through self-assembly-a typical "**bottom-up**" approach. The prototype devices that have been demonstrated include field-effect transistors (FETs), p-n junctions, bipolar junction transistors and resonant tunneling diodes.<sup>3</sup> It is believed that the "**bottom-up**" approach to nanoelectronics has the potential to go beyond the limits of the traditional "**top-down**" manufacturing techniques, ultimately enabling nanodevices to emerge from the balance between these two complementary nanofabrication approaches.

Many of the architects of the nanoscience and nanotechnology (e.g., condensed-matter physicists, molecular biologists, chemists, chemical engineers, electrical engineers and others) further recognize that most of the action often is at physical interfaces-and interfaces, of course, are the domain of electrochemists. It will be exciting to see over the next few years, just how far, and in what ways, electrochemists take molecular materials in the development of functional

nanoarchitectures. What follows is a discussion based on two representative (*Scheme 1.1*) reports that emphasize the construction and function of nanostructured materials, from a molecular perspective. First, **Feldheim** describes molecule-organized nanoscale metallic structures that



**Scheme 1.1. Representation of the interdisciplinary area of the science and technology of nanostructured materials and their applications**

display, among other things, quantized charging behavior and single electron conductivity.<sup>4</sup> This exotic behavior, which is absent for microscale structures, illustrates several emerging concepts in the field of molecular electronics. More significantly, **Crooks** describes the use of 2-D assemblies of nanoscale 3-D polymers (monodispersed hyper-branched or dendritic polymers commonly known as “dendrimers”) as nanoscale catalytic reactors, as gates for molecular transport, and as selective receptors for chemical sensing.<sup>5</sup> Lastly, **Hupp** and **Nguyen** describe the advantage of soft materials that are constructed using the design strategies of supramolecular coordination chemistry. Most of these materials also possess extraordinary nanoscale porosity- a property that makes them suitable for sieving, selective chemical sensing, and enzyme-like chemical catalysis.<sup>6</sup>

Many researchers in this exciting field do recognize that these reports indeed are only representative, not comprehensive. Several missing elements could be identified such as the descriptions of molecule-labeled quantum dot technology, biomolecule-derived technology (e.g. ATP-driven flagellar motors for propelling tiny man-made and naturally occurring objects; nanoscale materials for clinical diagnostics, gene therapy, templated cell growth and “human repair;” membranes containing nanometer-wide protein pores for stochastic sensing and identification of single molecules; etc.), nanoscale light emitting diode assemblies, self-replicating and self-repairing assemblies, ultra small electronic and ionic conductors based on carbon nanotube (CNT) and fullerene technology, nanostructured materials for light-to-electrical energy conversion ( “artificial leaf ” technology), and a host of other demonstrated or emerging nanoscale molecular materials applications. Also missing are descriptions of equally exciting non-molecular, nanostructured materials, including a tremendous variety of templated materials comprising nanoscale tubes, wires and cylinders for catalysis, transport, chemical sensing, and electrochemical energy storage periodic structures for an extraordinary number of emerging photonics applications; and so on. It will be exciting to see which of these futuristic ideas ultimately succeed in enhancing the quality of human life and which of the successful technologies involving electrochemical processes will compete in the market.<sup>7</sup>

## 1.2 Nanostructured Materials

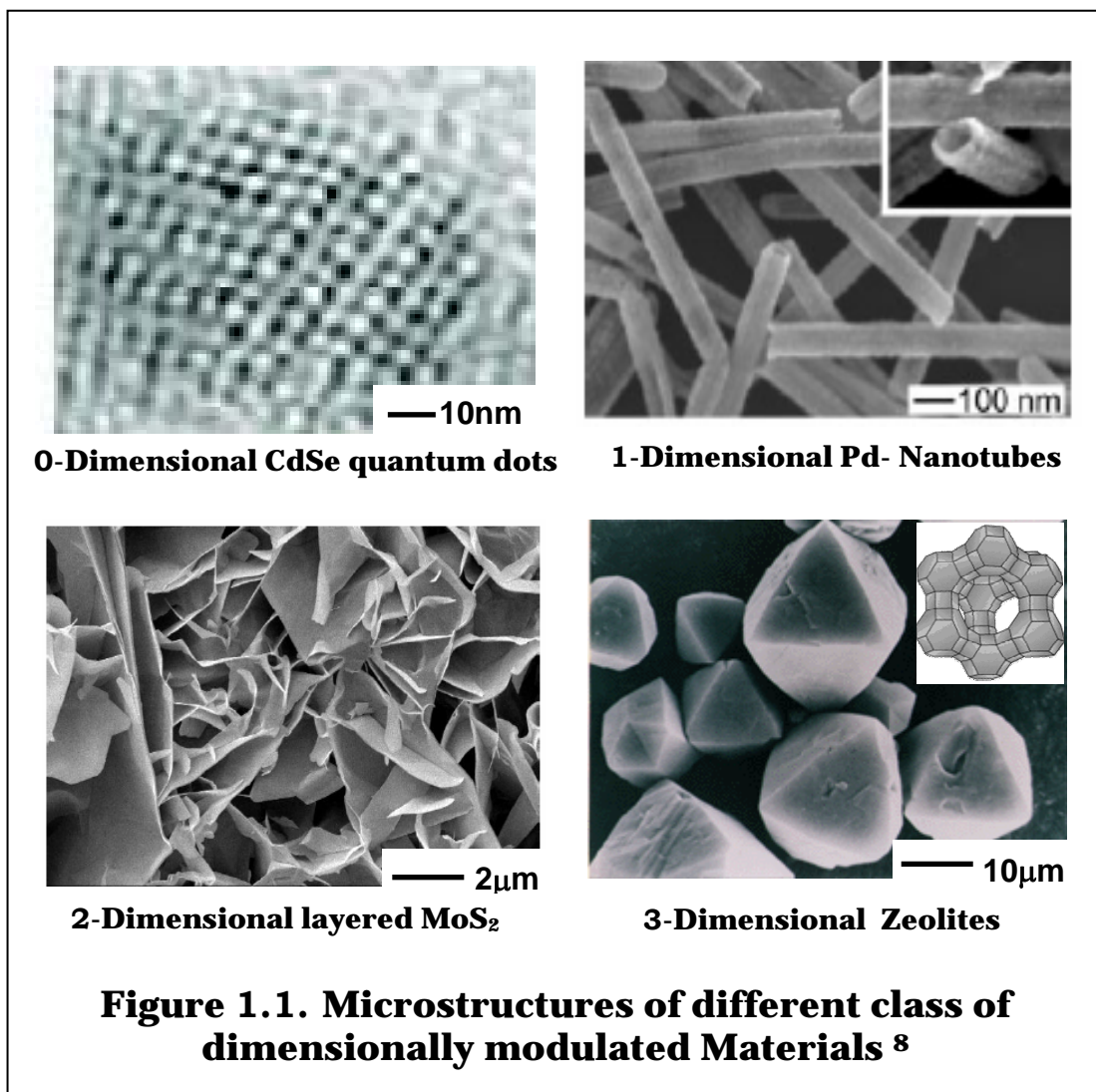
**“Nanostructures”**- structures that are defined as having at least one dimension in the range of 1-100 nm have attracted steadily growing interest as a result of their peculiar and fascinating properties, as well as their unique applications that are superior to their bulk counterparts<sup>8</sup>. The ability to generate such small structures is essential to the advancements of many areas in modern science and technology. In recent years physicists and chemists have devoted increasing attentions to these materials, and this interest is expected to multiply further in the near future. For example in electronics, the ever-increasing complexity in microprocessor and memory chips means that for every two years there is a doubling of the chip density. This brings the individual electronic components, having dimension in 100 nm or smaller, to the low dimensional regime, facilitating them to exhibit novel electronic and optical properties. This was demonstrated in the 1970s with the fabrication of quantum well and superlattice devices. Consequently, the physics



and chemistry of the one- and two-dimensional systems have been extensively investigated to demonstrate a large number of opportunities and some are yet to be realized by making new type of nanostructures from currently existing hybrid molecular materials.

### 1.2.1 Classes of Nanostructured Materials

There are different types of nanostructured materials. These range from zero dimensional atomic clusters (quantum dots) to three dimensional structures, where *at least one dimension is in the nanometer range*, as shown in *Figure 1.1*. In comparison, atoms, clusters, quantum dots and filaments are defined as “*Zero modulation dimensionality*” (0-D) systems which can have any aspect ratio ranging from 1 to  $\infty$ . Any wires, rods, belts and tubes in the nanometer range is classified as *One-dimensionally modulated* (1D) and this way of classification provides a good system to investigate the dependence of electrical, thermal and optical or mechanical properties on the dimensionality and size reduction (quantum confinement). Some of the established examples include size-dependent excitation or emission, quantized or ballistic conductance, coulomb blockade or single electron tunneling (SET) and metal-insulator transition<sup>9</sup>. Many of these properties play an important role when interconnects and active components are fabricated in nanoscale electronic, optoelectronic, electrochemical, and electromechanical devices. The most important two-dimensional Layers (2-D) in the nanometer thickness range consisting of ultrafine grains (nanometer range diameter) are “*Two-dimensionally modulated*”. This class includes insertion materials such as graphite and layered-type dichalcogenides and oxides of the transition metals Ti, Nb, Ta, Mo, W and V, which are of interest as positive and negative insertion electrode materials for electrochemical power sources<sup>10</sup>. Some of these materials also function as solid lubricants because of their layered character. The last class is that consisting of “*Three dimensionally modulated*” microstructures or nanophase framework where cross linked channels allow ion insertion if the size of the channels is sufficiently large to accommodate the ions<sup>11</sup>. For example, 3D-zeolitic solids containing aluminum, silicon, and oxygen with regularly spaced pores within the molecular framework can have nanopores enabling them to be useful for adsorbing small molecules, ions, or gases -just like how a sponge sucks up water. The pores are normally filled with positively charged ions, such as calcium or sodium which can be easily exchanged. These



materials also have potential applications as nuclear waste scavengers and are also useful as quantum confinement hosts for semiconductor q-dots or for the intercalation of ions. However, due to size-tunability, these materials provide are commonly considered as better model systems for investigating the dependence of electronic/ionic transport, optical and mechanical properties on size confinement and dimensionality.

### 1.3 Composite Materials

Society has always wanted and continued to seek materials that are strong, tough, and light. In this quest, it was discovered that the macroscopic combinations of two or more different

materials resulting in a new material with improved properties could be described as “**composite**”<sup>12</sup>. Naturally occurring composites are bone, bamboo, feathers, natural fibers, and wood. Bone is an organic-inorganic composite of protein (collagen) and minerals (calcium apatite) and bamboo is cellulose reinforced by silica. These combinations make a hard material with high impact strength. The cellulose cell structure of wood and fiber is bound together with lignin, a natural polymeric substance.

### **1.3.1 Classes of Composite Materials**

There are three major classes of composite materials: (1) Fibrous, (2) Laminar, and (3) Particulate.

Fibrous composites are composed of reinforced fibers in a matrix. During 1970s, many in the reinforced plastics industry began to talk about “high-strength composites” and “Advanced composites”. These terms have been generally associated with reinforcements that offered stiffer, stronger composites than the traditional composite of glass fibers in a polyester matrix.

Laminar composites are composed of two or more layers of materials held together by the matrix binder. Examples are automobile parts, like windshields and laminated glass, where, isotropic layers of materials are bonded together to form nonhomogeneous composite laminates.

Particulate composites consist of particles dispersed in a matrix. These particulates may be powdered, crystalline or amorphous. They may be metallic or ceramic containing natural or artificially prepared materials. The matrix must be capable of being forced around the reinforcement during some stage in the manufacture of composite. There are a number of matrix materials, including carbon, ceramic, glass and polymers. Concrete and solid rocket propellants are familiar examples of particulate composites<sup>12</sup>.

## **1.4 Nanocomposite Materials- In Search of Synergistic Effects**

Conventional, macroscopic composite materials such as adobe is a mixture of clay and straw that serves as an effective structural composite material which has been used to make bricks and wall in arid regions and these along with reinforced concrete has shaped our world during the past. Yet when it comes to the microscopic world, reduced particle size boosts the importance of the interphase in composite mixtures and this is especially important for a new class of recently developed materials named, the nano-composites.

The definition of **“nano-composite material”** has broadened significantly to encompass a large variety of systems such as one-dimensional, two-dimensional, three-dimensional materials, amorphous or crystalline, made of distinctly dissimilar components which are mixed at the nanometer scale. Nanocomposite is a distinct form of composite materials, which involves embedding nano or molecular domain sized particles into an organic polymer, metal or ceramic matrix material. In all cases, it is perceived that the intimate inclusion of these nanoparticles in these matrices can completely change the properties of these materials. The nanoparticles can serve as matrix reinforcement in order to change the physical properties of these base materials. With such small inclusions, a large amount of interfacial phase material is now included in the bulk of these nanocomposites, enabling a complete transformation of the material’s chemical, mechanical and morphological domain structure. Much of today’s research activity in the field of polymer based organic-inorganic hybrid nanocomposites exhibits mechanical, electrical properties superior to those of their separate components.

Nanocomposite plastics have their origin in the 1970's with the use of sol-gel technology to form homogeneous dispersions of small sized inorganic particles throughout a polymer matrix. In such systems, the inorganic phase may or may not be chemically attached to the organic phase. These *first generation nanocomposites* have been found to be useful in coating applications. Subsequently during 1980's, *second generation nanocomposites* emerged as a result of the resurgence in the use of fine particles, minerals and clay fillers for plastics. Limited compatibility between the filler and polymers as well as complex polymer processing requirements was needed to form these nanocomposites. In the 1990’s and beyond, a new form of nanocomposite has emerged *third generation nanocomposites* where polymeric materials are reinforced with nanofibers such as carbon nanotubes, SiC whiskers, colloidal silica, nano-clay particles etc. This unique ability to obtain control of the nanoscale structures via innovative *“bottom-up”* synthetic approaches has consequently entailed several challenges and opportunities. Undertaking this challenge provides an opportunity for developing new materials with synergic behavior leading to improved performance<sup>13</sup>.

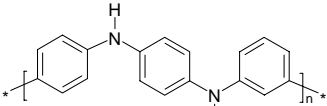
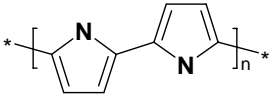
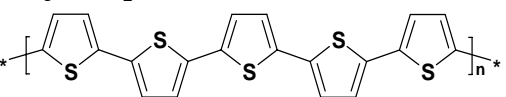
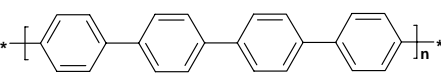
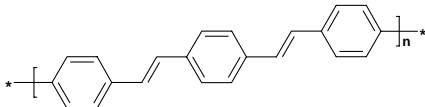
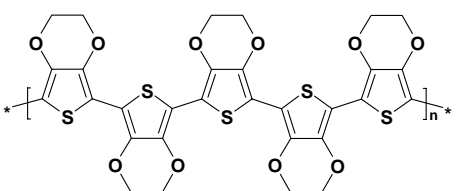
### 1.4.1 Guest-Host Materials interacting in Nanocomposites

A great variety of nanocomposite materials can be formed by guest-host interactions between organic and inorganic species. When we consider the myriad of extended and molecular inorganic species, small organic molecules and polymers available for the design of these hybrid materials, it becomes clear that the variety of combinations is huge. *Table 1.1* shows the host and guest types of inorganic materials derived from different structural dimensions with various classes of organic materials as both guests and hosts and vice versa.

During last two decades, the field of organic conducting polymers (**OCPs**) which is also referred as synthetic metals has enjoyed a dramatic transition from chemical curiosities to revolutionary new plastic materials that continues to receive great attention in such a way that recent reviews tend to center on particular polymers or applications. The vast majority of reports dealing with OCPs involve the study of p-doped polymers, for example polyaniline (PAni), polypyrrole (PPy), poly(p-phenylene vinylene) (PPV), polythiophene (PTh) and their derivatives. Among their properties and applications the most frequently studied systems (*Table 1.1*) relate to their semiconducting nature and electroactivity, and range from their use as plastic conductor or light emitting diodes (LED), electrochromic display and smart windows, corrosion inhibitor, field effect transistors (FET), Electromagnetic interference (EMI) shielding, and more significantly energy storage applications such as batteries, supercapacitors and fuel cells<sup>14-17</sup>.

The assortment would include innovative combinations of OCPs with a wide variety of available inorganic components like three-dimensional framework systems of zeolites, two-dimensional layered materials such as clays, metal oxides, metal phosphates, chalcogenides, and even one-dimensional nanowires, nanotubes,  $(\text{Mo}_3\text{Se}_3)_n$  chains and zero-dimensional materials such as CdS, CdSe nanoclusters. Experimental work has generally shown that virtually all types and classes of nanocomposite materials lead to new and improved properties when compared to their macrocomposite counterparts. Therefore, nanocomposites promise new applications in many fields such as mechanically reinforced lightweight components, non-linear optics, battery cathodes, sensors and optoelectronics. The general class of organic-inorganic nanocomposites may also be of relevance to issues of bio-ceramics and biomineralization in which *in-situ* growth and polymerization of biopolymer and inorganic matrix also occurs<sup>13-17</sup>.

**Table 1.1. Organic and Inorganic Guest-Host Materials**

<b>Inorganic Materials</b>	<b>Organic Materials</b>	<b>References</b>
<p><b>Zero Dimensional, 0-D</b> Nano clusters- Au, Ag, Pd, Pt and CdS, CdSe, colloidal metallic/ semiconducting nanoparticles.</p> <p><b>One Dimensional, 1-D Materials.</b> Metal/Metal Oxide Nano wires and Nanotubes, Nano rods: Au, Pt, SiO<sub>2</sub>, TiO<sub>2</sub>, MnO<sub>2</sub>, ZrO<sub>2</sub>, CuO, MnO<sub>2</sub>, Ta<sub>2</sub>O<sub>5</sub>, CeO<sub>2</sub>, RuO<sub>2</sub>, <math>\gamma</math>-F<sub>2</sub>O<sub>3</sub>, WO<sub>3</sub>, ZnO, (Mo<sub>3</sub>Se<sub>3</sub>)<sub>n</sub> chains, Carbon nanotubes (SWCNT, MW CNT)</p> <p><b>Two Dimensional, 2-D Layered materials</b> Transition Metal Oxides- V<sub>2</sub>O<sub>5</sub>, Li<sub>x</sub>MoO<sub>3</sub>, Li<sub>x</sub>WO<sub>3</sub>, Cs<sub>x</sub>TiO<sub>2</sub>, Li<sub>x</sub>MnO<sub>2</sub>. Dichalcogenides- VS<sub>2</sub>, VSe<sub>2</sub>, MoS<sub>2</sub>, MoSe<sub>2</sub>, TaS<sub>2</sub>, TiS<sub>2</sub>, NbS<sub>2</sub>, NbSe<sub>2</sub>, WS<sub>2</sub> Oxychlorides- FeOCl. Phosphates: <math>\alpha</math>-VOPO<sub>4</sub>, UO<sub>2</sub>PO<sub>4</sub> Inorganic layered Clays</p> <p><b>Three Dimensional, 3-D Materials</b> Zeolitic solids, LiM<sub>2</sub>O<sub>4</sub>, H<sub>3</sub>PMo<sub>12</sub>O<sub>40</sub>, Fe<sub>2</sub>O<sub>3</sub>, <math>\gamma</math>-MnO<sub>2</sub>, <math>\lambda</math>-MnO<sub>2</sub>, Mn<sub>3</sub>O<sub>4</sub>, FePO<sub>4</sub>, LiMnVO<sub>4</sub>, Li[Li<sub>1/3</sub>Ti<sub>5/3</sub>]O<sub>4</sub></p>	<p><b>Organic Conducting Polymers</b></p> <p>Polyaniline: PAni </p> <p>Polypyrrole: PPy </p> <p>Polythiophene: PTh </p> <p>Poly(p-phenylene), PPP </p> <p>Poly (p-phenylenevinylene):PPV </p> <p>Poly(3,4-ethylenedioxythiophene): PEDOT </p> <p>Nonconducting organic molecules and Polymers. Naphthalene, Poly(ethylene oxide), PEO, Poly(ethyleneglycol), PEG</p> <p>Biomolecules- Enzymes, proteins, DNA, collagen, Cellulose.</p>	<p>18</p> <p>19</p> <p>20</p> <p>21</p> <p>22</p> <p>23</p> <p>24</p> <p>25</p> <p>26</p> <p>27</p> <p>28</p> <p>29</p>

### 1.4.2 Conducting Polymer based Nanocomposites and their Classification

According to the nature of the organic-inorganic interface (focusing more on the inorganic materials) these nanocomposites could be classified into two types: nanoparticles and nano-structured layered materials. Depending upon the nature of association between the inorganic and organic components, these nanocomposites can also be classified into two categories as illustrated in *Table 1.2*; one in which the inorganic nanoparticles are embedded in organic matrix is called “*Inorganic-Organic nanocomposite*” (*IO-materials*) to denote hybrids where the organic phase is host to an inorganic guest. The other type is “*Organic-inorganic nanocomposite*” (*OI-materials*) where the guest organic polymer is confined into inorganic host layers. In each case however, the composite formation demands some entrapment or encapsulation rather than simple blending or mixing.

**Table 1.2. Conducting Polymer Nanocomposites Classifications**

Inorganic-in-organic	Organic-in-Inorganic	References
1.Nanocomposite with surface functional group ( -NH <sub>2</sub> , -COOH on colloidal particles (SiO <sub>2</sub> , SnO <sub>2</sub> , BaSO <sub>4</sub> etc as core materials)	1.Nanocomposite with functionalized structural materials with superior mechanical properties, (Clay-polymer intercalative nanocomposite with polymer like nylon-6, PMMA, styrene, polypropylene intercalation into the layered silicates- sodium montmorillonite, hectorite etc)	21-26 22-23
2,Nanocomposite with improved physical and mechanical properties (Fe <sub>2</sub> O <sub>3</sub> , ZrO <sub>2</sub> ,TiO <sub>2</sub> etc as incorporated materials).	2.Nanocomposite with novel electronic anisotropic material and thermoelectric power, catalysis ( V <sub>2</sub> O <sub>5</sub> , MoO <sub>3</sub> , FeOCl, MoS <sub>2</sub> , TiS <sub>2</sub> , RuCl <sub>3</sub> , α-VOPO <sub>4</sub> , UO <sub>2</sub> PO <sub>4</sub> , CdPS <sub>3</sub> , NiPS <sub>3</sub> )	24-25 27-29
3.Nanocomposites with magnetic susceptibility (using Fe <sub>3</sub> O <sub>4</sub> , γ-Fe <sub>2</sub> O <sub>3</sub> etc magnetic particles.)	3.Nanocomposite for energy storage, enhanced electrochemical properties for lithium batteries, fuel cells, and supercapacitors (using V <sub>2</sub> O <sub>5</sub> , MoO <sub>3</sub> , FeOCl, MoS <sub>2</sub> , TiS <sub>2</sub> , MnO <sub>2</sub> )	18-19 30 and their in
4.Nanocomposites with dielectric, piezoresistive, catalytic activities (with BaTiO <sub>3</sub> , PMo <sub>12</sub> , TiO <sub>2</sub> , Pt, Pd, etc incorporation)		
5.Naocomposites with energy storage, optical and electrochromic activities (incorporation of MnO <sub>2</sub> , SnO <sub>2</sub> , WO <sub>3</sub> , SiO <sub>2</sub> , TaO <sub>2</sub> . LiMn <sub>2</sub> O <sub>4</sub> Prussian blue, CdS, CdSe.		

### 1.4.3 Inorganic-Organic (I-O) Nanocomposites

In this section of *inorganic-in-organic* system, such nanocomposite not only bridge the world of microparticles with that of the macromolecules, but often makes successful strides towards overcoming the processing problems of OCPs, thus also enhancing their importance to a large extent. Inorganic nanoparticles can be introduced into the matrix of a host-conducting polymer either by some suitable chemical route or by an electrochemical incorporation technique. However, each synthesis opens a way to a group of materials with complementary behavior between two components. Chemical origin as well as the special properties viz. its colloidal stability, optical, catalytic, electrochemical, magnetic susceptibility, etc., always add new dimensions to the characteristic of the resulting composite.

#### 1.4.3.1 Nanocomposites prepared by “Core-Shell” strategy

Encapsulation of inorganic nano-particles inside the core of conducting polymers has become more popular leading to some interesting aspects of nanocomposite synthesis. Several numbers of different metal and metal oxide particles have so far been encapsulated into the core of conducting polymers giving rise to a host of nanocomposites. These materials differ from pure polymers in some of the physical and chemical properties and at the same time differ from each other also. It is important to keep the polymer in a stable colloidal form and this stream of investigation was pioneered by Armes et al. when they succeeded in incorporating silica nanoparticles with polypyrrole (PPy) and polyaniline (PAni)<sup>21</sup>. Aniline was polymerized by  $(\text{NH}_4)_2\text{S}_2\text{O}_8$  (APS) in HCl while  $\text{FeCl}_3 \cdot 6\text{H}_2\text{O}$  and salicylic acid were used for pyrrole. Polymerization of the respective monomers in the presence of the preformed colloids at low concentration of monomer and oxidant was the key to synthesize two stable colloids. This technique allowed the slowing down of the rate as well as the degree of polymerization thus promoting the polymerization on the surface rather than in bulk. A high resolution TEM picture obtained by Gill et al. revealed an unusual “raspberry” morphology where the inorganic particles were “glued” with the chains of Polyaniline<sup>21</sup>. Composite particles were polydispersed in nature with an average particle diameter of 1.5-3.0 $\mu\text{m}$ . Small-angle X-ray scattering (SAXS) studies revealed<sup>21</sup> that silica particles were 0.4 $\mu\text{m}$  apart from one another suggesting that the polyaniline was adsorbed onto the surface of silica particles as a thin layer of individual polymer chains. These polymer-inorganic oxide nanocomposites are represented in *Figure 1.2*.<sup>21</sup> The same technique was repeated by Maeda et al.<sup>21</sup> for synthesizing stable PPy-SiO<sub>2</sub> colloids using 20 nm



SiO<sub>2</sub> particles as dispersant. The critical SiO<sub>2</sub> concentration was kept at ~1.0% and fraction of PPy % in the composites varied from ~37% to ~70% depending upon the reaction parameters. A good solid-state conductivity (4 Scm<sup>-1</sup>) was obtained characteristic of the “raspberry” morphology

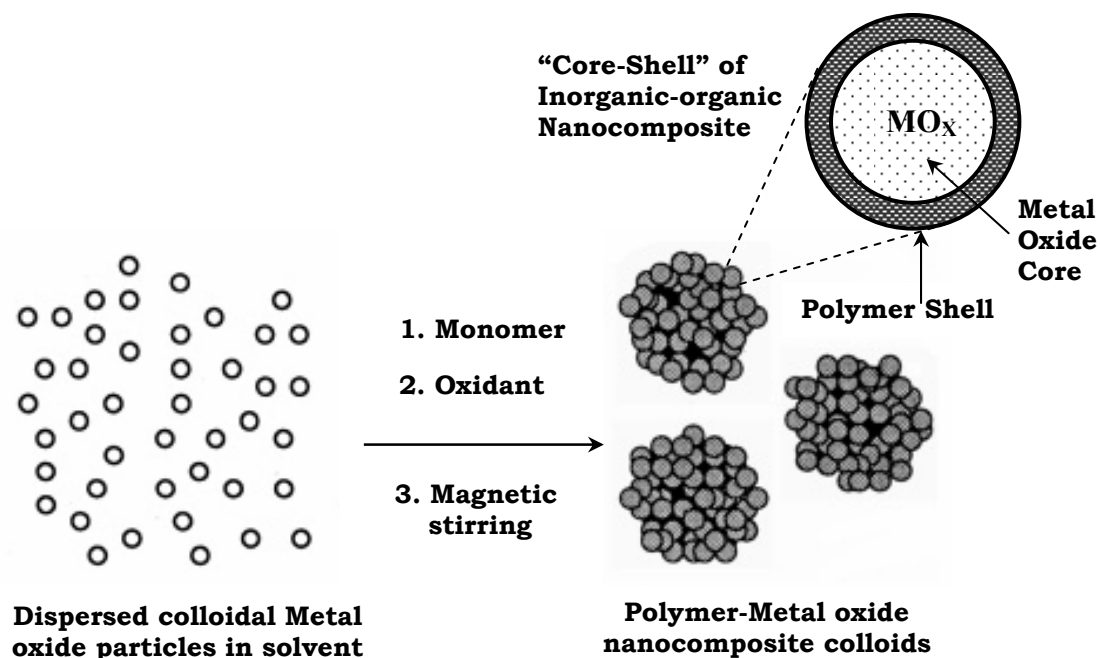


**Figure 1.2. Schematic representation of Inorganic-Organic (I-O) Nanocomposite formation<sup>21</sup>**

observed from TEM (*Figure 1.2.*)<sup>21</sup>. This was subsequently extended to a broad spectrum of metal oxide colloids viz. SiO<sub>2</sub>, SnO<sub>2</sub> (pristine and antimony doped), TiO<sub>2</sub>, Sb<sub>2</sub>O<sub>3</sub>, ZrO<sub>2</sub> and Y<sub>2</sub>O<sub>3</sub> for synthesizing PPy-based colloidal nanocomposites. However, except the SiO<sub>2</sub> and SnO<sub>2</sub>, all others failed to form core-shell structure perhaps due to the macroscopic precipitation of the resulting nanocomposites.

Another excellent technique for preparing PPy-(colloidal) gold nanocomposite was recently introduced by Marinakos et al.<sup>31</sup>. Although the work started with template-guided polymerization, it ultimately provided a template-free nanocomposite (particles, tubes, or wires). Au nanoparticles were arranged within the pores of an Al<sub>2</sub>O<sub>3</sub> membrane using a vacuum filtration technique. PPy was grown within the pores of the respective film supporting the Au particles and the Au-PPy composite was grown inside. After that the template membrane was dissolved using

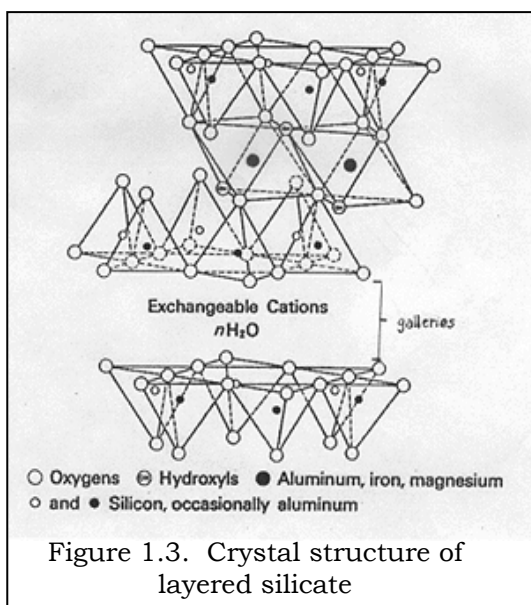
0.5 M KOH to set the composite particles free in solution. The TEM picture showed the organized clusters of the interconnected arrays of PPy-Au nanocomposite.

#### 1.4.4 Organic-Inorganic (O-I) Nanocomposites

A second group of nanocomposite materials is constituted by those in which the organic polymer is confined into the inorganic layers for a broad range of applications. Since the inorganic layered materials exist in great variety possessing a well defined, ordered intralamellar space potentially accessible by foreign species they can act as matrices or hosts for polymers, yielding interesting lamellar “*organic-in-inorganic nanocomposite*” materials. Lamellar nano-composites can be divided into two distinct classes, intercalated and exfoliated. In the former, the polymer chains alternate with the inorganic layers in a fixed compositional ratio and have a well defined number of polymer layers in the intralamellar space. In exfoliated nanocomposites the number of polymer chains between the layers is almost continuously variable and the layers stand  $>100 \text{ \AA}$  apart. The intercalated nanocomposites are also more compound-like because of the fixed polymer/layer ratio, and they are interesting for their electronic and charge transport properties. On the other hand, exfoliated nano-composites are more interesting for their superior mechanical properties.

##### 1.4.4.1 Nanocomposites prepared by Exfoliative and Intercalative strategies

It is well known that layered silicates have crystal structure is shown in *Figure 3*. with two dimensional spacings in the nanometer range. Exchangeable cations and water usually



occupies the spacings to balance the negative charges in the ionic lattice. Clay-Polymer nanocomposites have recently attracted a great deal of attention as they offer enhanced mechanical and thermal properties as compared to conventional materials. For example, recently Okada et al prepared new molecular scale nanocomposites from saturated polymers (Nylon-6 and other plastic) intercalated in clay layers<sup>32</sup>. These products show extraordinary mechanical strength compared to that expected by

simple mixing of the individual components. Because of these enhanced properties, they find extensive applications in automobile, and furnishing industries. However, the enhancement of material properties has been linked to the interfacial interaction between the polymer matrix and the organically modified layered silicate filler structure. The filler particles provide a very high surface area and the polymer can be incorporated either as oligomeric species itself or via the monomer, using in situ polymerization to form polymer-clay nanocomposites. The latter is a more successful approach although it probably limits the ultimate utility of these systems. The synthetic route of choice for making a nanocomposite depends on exfoliated hybrid (*Figure 1.4*). In the case of an intercalate, the organic component is inserted between the layers of clay such that the inter-layer spacing is expanded, but the layers still bear a well-defined spatial relationship to each other. In an exfoliated structure, the layers of the clay have been completely separated and the individual layers are distributed throughout the organic matrix. Another alternative is to disperse clay particles (tactoids) completely within the polymer matrix, although this simply represents the use of the clay as conventional filler. In recent years, there has been extensive study of the factors which control whether a particular organo-clay hybrid can be synthesized as an intercalated or exfoliated structure. Since clay nanocomposites can produce dramatic improvements in a variety of properties, it is important to understand the factors which affect the delamination of the clay. These factors include the exchange capacity of the clay, the polarity of the reaction medium and the chemical nature of the interlayer cations (e.g. onium ions). The correct selection of modified clay is essential to ensure effective penetration of the polymer or its monomer into the interlayer spacing of the clay which results in the desired exfoliated or intercalated product. Indeed, further development of the compatibiliser chemistry is undoubtedly a key to the expansion of this nanocomposite technology beyond the systems where success has been achieved to date<sup>32</sup>.

Despite their relatively large molecular weights, electronically conducting polymers can play the role of intercalated guest molecules inserted within the van der Waals gaps of layered inorganic phases resulting in a special class of intercalative nanocomposites is shown in *Figure 1.4* termed as “*organic-in-inorganic nanocomposites*”. At least in principle, in these cases the structure of the inorganic host dominates the structure of the hybrid and the polymers adapt to it. The insertion of conducting polymers in layered inorganic host materials and other structurally organized environments is a topic of considerable interest because the resulting organic-inorganic

nanostructures can possess novel multifunctional properties useful for opto-electronic and electrochemical devices. Such systems can potentially show hybrid properties synergistically derived from both the host and the guest. These polymer-inorganic nanocomposites have been synthesized by various intercalative methods as proposed by Kanatzidis et al <sup>25c</sup>. Among these, the *in situ* redox intercalative polymerization with suitable oxidizing hosts is the most direct method, since its topotactic character leastly disturbs the crystalline structure of the host <sup>25</sup>. This type of reaction requires a strongly oxidizing host to provide the driving force to pull the

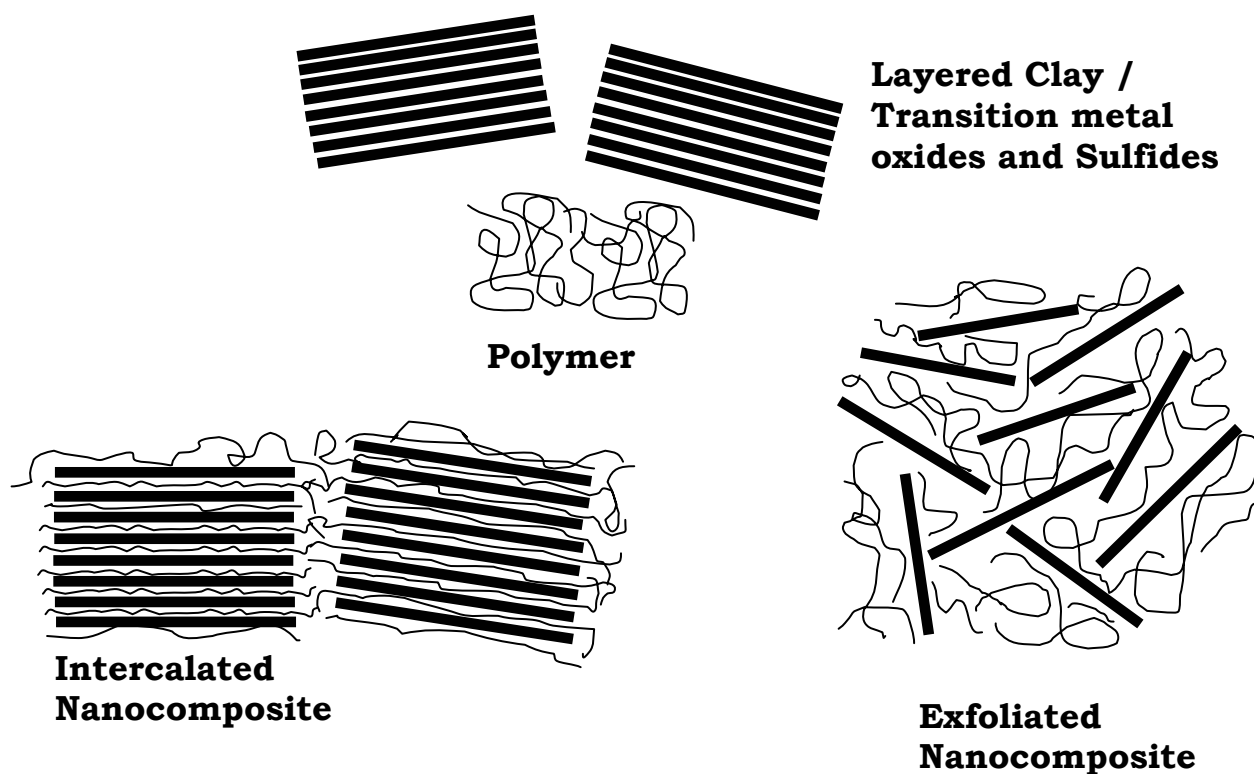


**Figure 1.4. Schematic representations of different types of Nanocomposite formation**

monomers into the galleries before oxidizing them into polymers. Because of the scarcity of such highly oxidizing hosts, the number of illustration has been limited. The groups of Kanatzidis, Nazar, Buttry, and Gomez-Romero et al have successfully intercalated several conducting and non-conducting organic polymers into the highly oxidizing hosts via “intecalative strategies”<sup>22-25</sup>. The detailed synthesis, characterization and applications of various organic-inorganic nanocomposites will be discussed in subsequent chapters.

## 1.4.5 Newly emerging Applications

### (i) Electronic and Optoelectronic Devices

Nanometer-size particles possessing hybrid molecular and bulk behavior define a new class of materials with several interesting optical and electronic applications. For example, light emitting diodes have been developed recently that are based on new materials such as porous silicon<sup>33a</sup>. By taking advantage of the developments in the preparation and characterization of direct-gap semiconductor nanocrystals<sup>33b</sup> and of electroluminescent polymers<sup>33c</sup>, Colvin et al has constructed a hybrid inorganic-organic electroluminescent device<sup>33d</sup>. Light emission arises from the recombination of holes injected into a layer of p-type semiconducting poly p-phenylene vinylene (PPV)<sup>33e</sup> with electrons injected from n-type cadmium selenide nanocrystals. Because of the quantum size effect<sup>33f</sup> the color of the emission can be tuned from red to yellow by changing the nanocrystals size.

### (ii) Electrochemical Energy storage

Recently, Yoneyama et al<sup>34a</sup> has successfully attached oxide particles having very low isoelectric points, such as  $\text{WO}_3$ ,  $\text{SiO}_2$  and  $\text{Ta}_2\text{O}_5$  into polypyrrole film by electrochemical oxidation of pyrrole in the presence of oxide suspensions especially if the pH of the deposition is higher than the isoelectric point of the oxide. These composites have been found to be useful as electrode materials for batteries and electrochromic applications. Oxide particles which do not belong to this class, such as  $\text{TiO}_2$ , can also be incorporated into polypyrrole if small amount of electrolyte anions having specific adsorption to the oxide e.g.,  $\text{SO}_4^{2-}$ , are added to the deposition baths containing oxide suspensions<sup>34b</sup>. As polypyrrole is one of the most popular conducting polymers, its technological applications as cathode material for rechargeable lithium batteries has been widely studied<sup>34c</sup>. Even with the use of highly porous polypyrrole, however, the volumetric energy density is not very high, because the amount of electrolyte anions involved in the redox reaction is limited. This limitation can be improved by incorporating electrochemically active anion-adsorbed  $\text{MnO}_2$  as a dopant<sup>34d</sup>. Although Manganese dioxide is one of the promising materials as a cathode material for Li-batteries<sup>35e</sup>, it possesses an extremely low conductivity, and it is essential to have a conducting net work for complete utilization of the active material had also for accomplishing high power density. Usually some conducting form of carbon like acetylene black or graphite powder is mixed with  $\text{MnO}_2$  particles. If PPy films containing  $\text{MnO}_2$  particles could be used as cathode materials, it can form PPy/ $\text{MnO}_2$  nano composite which would

not only act as conducting network for MnO<sub>2</sub> but also as efficient active materials. For example,

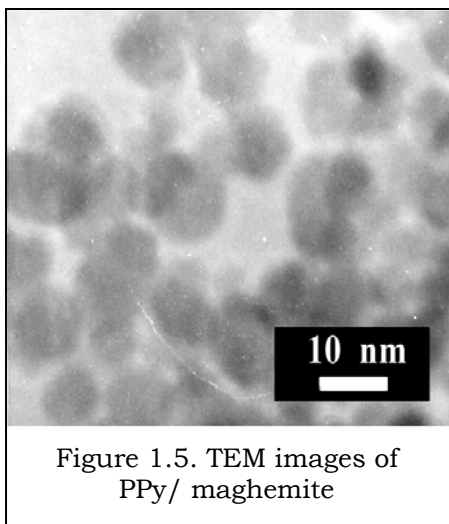


Figure 1.5. TEM images of PPy/ maghemite

Yoneyama et al has recently, reported that MnO<sub>2</sub> particles incorporated into conducting polymer film works well as an active material, causing enhanced charge-discharge capacity<sup>34f</sup>. Similarly, a new “core-shell” polypyrrole (PPy) / maghemite ( $\gamma$ -Fe<sub>2</sub>O<sub>3</sub>) nanocomposite prepared by Kwon et al<sup>34g</sup> via surface modification has improved the electrochemical discharge capacity compared to that of the pristine oxide of TEM is shown in *Figure 1.5*. More recently, Mastragostino and co-workers have reported the improvement in electronic conductivity, discharge capacity

and open circuit voltage up to 4V for LiMn<sub>2</sub>O<sub>4</sub> particles, after mixing with Poly (3,4-ethylenedioxythiophene) PEDOT<sup>27c</sup>.

Growing demand for miniaturized power sources of high-power density has also stimulated great interest in electrochemical capacitors in recent years. For example, carbon powder and conducting polymers do possess large double layer capacitance (and also have high surface area) while oxides of multivalent metals such as ruthenium and iridium exhibit large faradaic pseudocapacitance and hence these two classes of materials find extensive applications in supercapacitor<sup>34h</sup>. Jong-in Hong et al has recently reported<sup>34i</sup> the use of conducting polymers with metal oxides for electrochemical capacitors. More specifically, RuO<sub>2</sub> when deposited on Poly (3,4-ethylenedioxythiophene), is found to exhibit large specific capacitance 420 F/g.

### **(iii) Application in Electro-Catalysis**

Another important application of these hybrid nanostructured composite material is in electro-catalysis. For example many fuel cell reactions like the electro-oxidation of methanol in principal, requires an efficient reversible redox process where catalyst need sustained stability. Since, some of the important fuel cells operate in acid medium which requires both the catalyst and support to be highly stable the building of efficient nanocomposite electrode is very important. This principle has been followed by several researchers, describing the preparation of nanocomposites in which nanoparticles of Pt, Pd, Cu, etc. are combined with PPy, PANi, PTh etc to form efficient electrocatalytic electrodes. The dispersion of Pt particles in PANi matrix and their ability for enhancing methanol oxidation has been extensively discussed by Hable et al<sup>35a</sup>.

Similarly, the formation of a series of such mono and bimetallic electrodes using Pd, Cu, Pd/Cu and Cu/Pd catalyst in conjunction with PANi has been reported to show efficient oxidation of formic acid and methanol<sup>35b</sup>.

#### **(iv) Magnetic Applications**

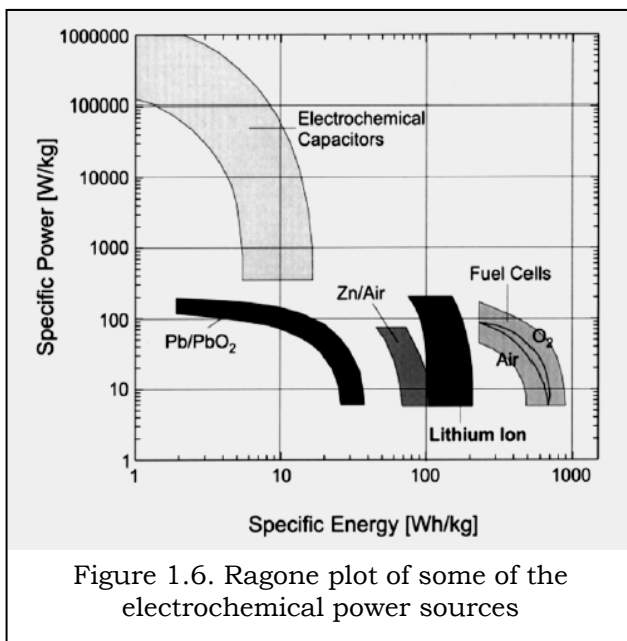
Several nanostructured materials show interesting size dependence magnetic properties like superparamagnetism and quantum tunneling of magnetization and hence some of this unique nanostructured magnetic materials have been used to form composites with promising applications for diverse area<sup>36a,b</sup>. A versatile process for the preparation of maghemite/polyaniline ( $\gamma\text{-Fe}_2\text{O}_3/\text{PANi}$ ) nanocomposite was first reported by Ben Zhong Tang et al<sup>36c</sup>. In this case  $\gamma\text{-Fe}_2\text{O}_3$  nanoparticles were coated with PANi chains doped by anionic surfactants. Both the coated  $\gamma\text{-Fe}_2\text{O}_3$  and the doped PANi were soluble in common organic solvents, and casting of the homogeneous solutions gives free-standing nanocomposite films with good electrical conductivity ( $\sigma = 82 - 237\text{Scm}^{-1}$ ) much higher than that of the iron oxide/conducting polymer system prepared by mixing. The nanocomposite films were superparamagnetic, showing no hysteresis loop at 300K. Since these nanocomposites, formed by nanometer-size particles of metals or metallic compounds dispersed in OCPs constitute a good example of hybrid nanomaterials their detailed preparation and properties have been reviewed recently<sup>30</sup>.

### **1.5 Introduction to Electrochemical Power Sources**

Electrochemistry plays a crucial role in both the generation and storage of energy. Electrochemical method of energy storage possesses several advantages over other mode of energy storage. Further, electrochemical energy generation and storage has become extremely important with increasing environmental pollution as it can decrease our dependence on limited fossil fuels<sup>37a, b</sup>. Moreover, the rapid development of modern electronic and information technologies create a strong demand for miniaturization of electronics coupled with consumer demand for light weight portable electrochemical power sources, for a range of applications including communication devices, electric vehicles, spaceships and pacemaker etc<sup>37c, d</sup>.

Electrochemical power sources, allow the direct conversion of the free energy of a chemical reaction to electrical energy without any loss of efficiency associated with the second law of thermodynamics (Carnot limitations). Such a conversion of chemical energy stored in the active materials into electrical energy takes place by electrochemical oxidation-reduction

reactions, involving the flow of electrons through an external circuit. The electrochemical cell



essentially consists of an anode, which sustains an oxidation reaction and a cathode, which sustains a reduction reaction contained in an electrolyte which provides ionic path for electrical conduction. Commercial systems also contain a separator between the anode and the cathode to prevent accidental electronic shorts between these electrodes. A comparison of different type of commonly used electrochemical power sources is shown in *Figure 1.6. (Ragone plot)*, with respect to their ability to deliver energy and power<sup>10a</sup>. These

electrochemical power sources, can be broadly classified in to three types; Fuel Cells, Supercapacitors, and Batteries.

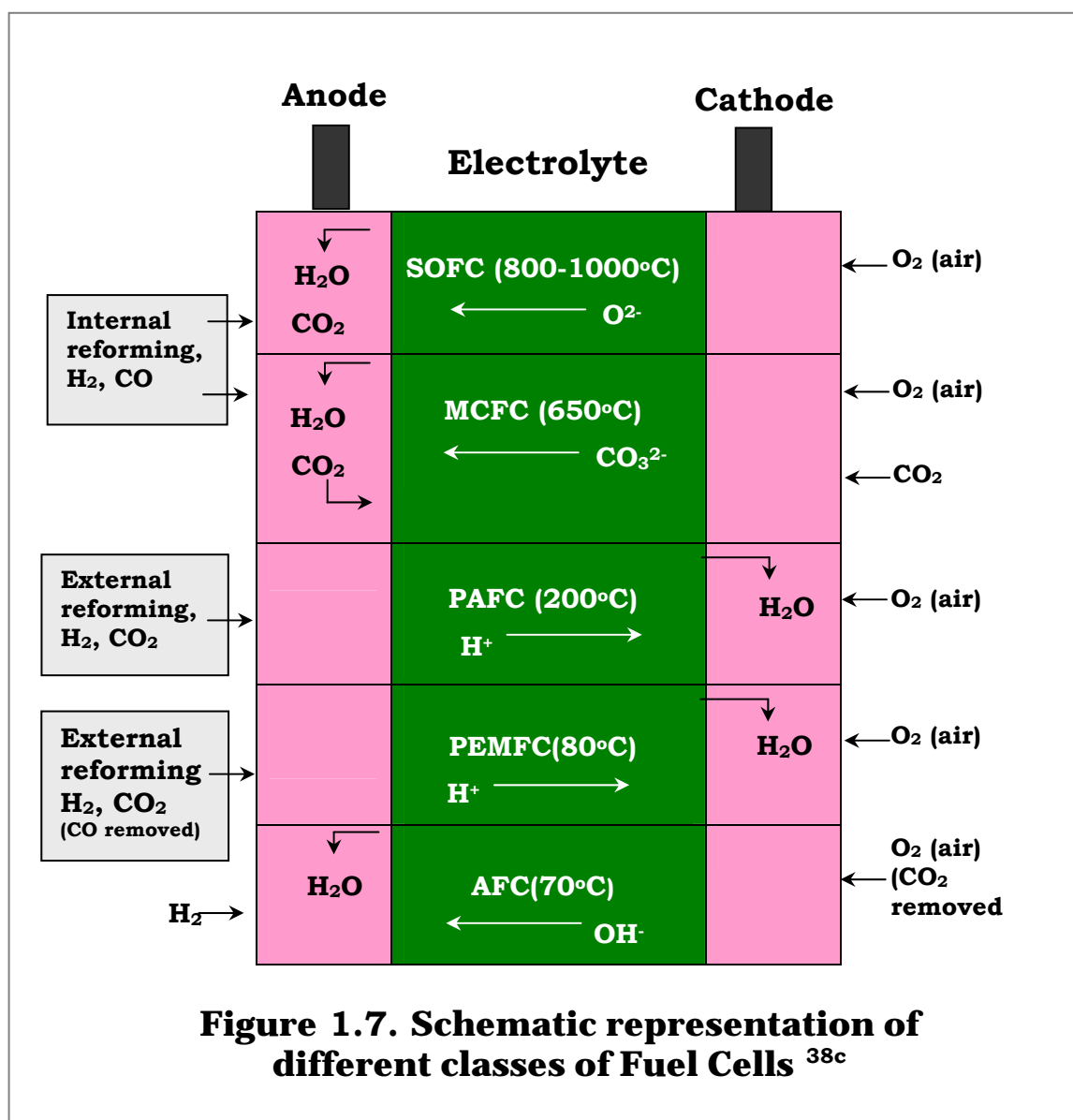
### 1.5.1 Fuel Cells

Fuel cells are electrochemical devices which convert the free energy change of a chemical reaction directly into electrical energy in an essentially invariant electrode-electrolyte system<sup>38a, b</sup>. They operate continuously in the discharge mode and the reactants have to be supplied from outside. The hydrogen-Oxygen fuel cell utilizing potassium hydroxide, sulfuric acid or phosphoric acid electrolytes is one of the most common examples. Depending on the type of electrolyte employed, fuel cells can be conveniently classified into Alkaline fuel cells (AFC), Phosphoric acid fuel cells (PAFC), Molten carbonate fuel cells (MCFC), Solid oxide fuel cells (SOFC) and Polymer membrane or proton exchange membrane fuel cells (PEMFC). Some of these systems such as PAFC and PEMFC have reached commercial maturity in recent times while continued attempts are being made to improve other types. Different types of fuel cells under active development are summarized in *Figure 1.7*.

During the operation, oxidation reaction takes place at the anode thus liberating electrons (for example,  $H_2 = 2H^+ + 2e^-$ ) which travel round the external circuit producing electrical energy of the external load, to participate in the reduction reaction (for example,  $1/2O_2 + 2e^- = O^{2-}$ ). This way of generation of electrical energy also produces heat and combined heat power generation



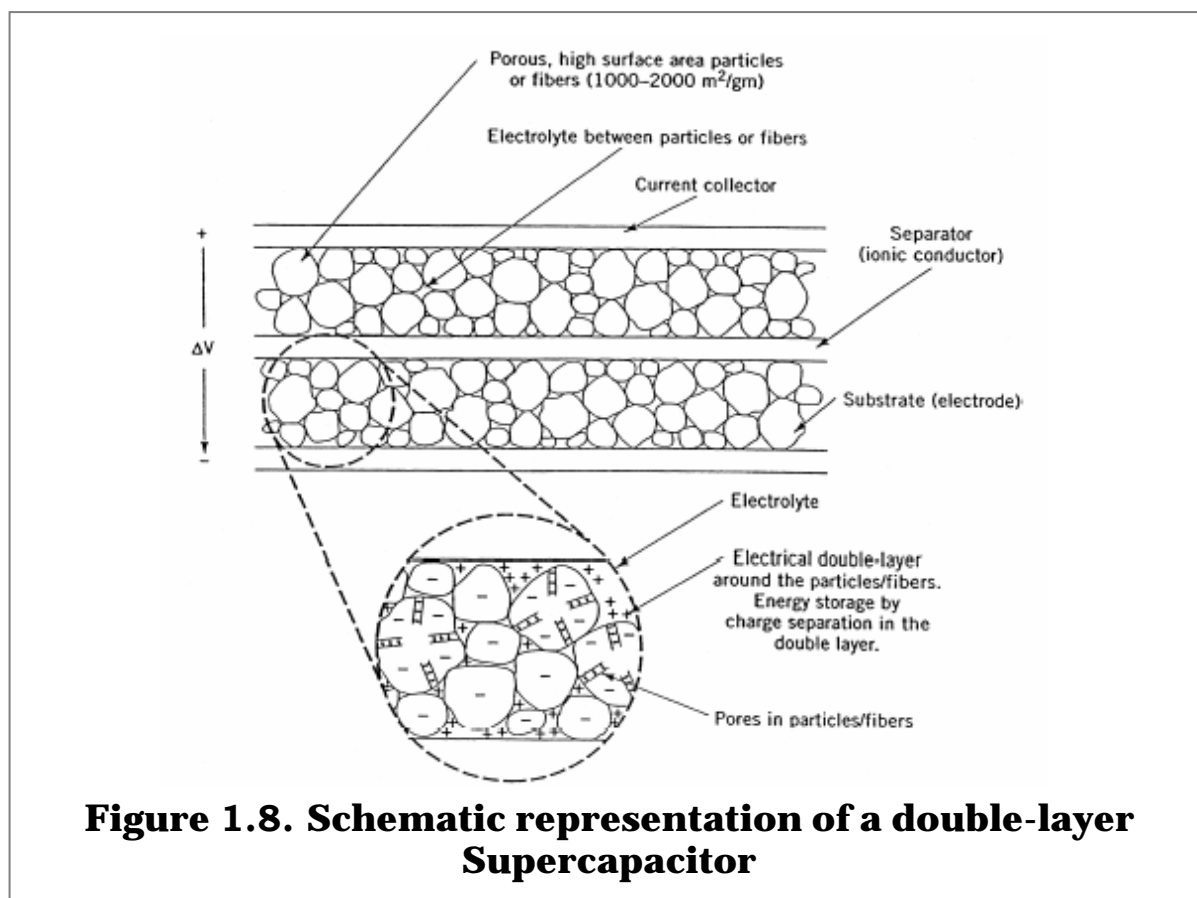
(co-generation) is specially an attractive characteristic for SOFC. The reaction products are formed at the anode for SOFC, MCFC and AFC types, while the cathode accumulates them for PAFC and PEMFC types<sup>38c</sup>. This difference has significant implications for the design of the entire fuel cell system; including pumps and heat exchangers. The major advantages of these systems are their high efficiency, environment-friendly operation, low solution resistance, easy transportation and low day-to-day maintenance. However, their difficulties like use of expensive materials, electrode degradation, and uncertainty in lifetime, high concentration polarization and ohmic losses hamper their wider commercial applications, although several electrocatalysts have been recently developed to alleviate some of the problems<sup>38d</sup>.



## 1.5.2 Supercapacitors

Capacitors store electrical energy by charge separation in a thin layer of dielectric material that is supported by metal plates that can also act as the terminals for the device. The energy stored in a capacitor is given by  $\frac{1}{2} CV^2$ , where  $C$  is its capacitance (Farads) and  $V$  is the voltage between the terminal plates. The maximum voltage of the capacitor is dependent on the breakdown characteristics of the dielectric material. The charge  $Q$  (coulombs) stored in the capacitor is given by  $CV$  and the capacitance depends critically on the dielectric constant ( $\epsilon$ ), thickness ( $t$ ) of the dielectric and its geometric area ( $A$ ) as expressed by,  $C = \epsilon A/t$ <sup>39a</sup>.

In comparison to both ceramic multilayer capacitors and electrolytic capacitors commonly used in electronic circuits, a new type of capacitor called Electrochemical capacitor (ECC), (also known as supercapacitors or an ultracapacitors), have attracted attention during the



last three decades due to their unique capability of higher charge storage several hundred times more than that of conventional capacitor, using an electrode-electrolyte interface. These are different from both batteries and fuel cells since they can generate repeated bursts of power for

certain types of applications. The state-of-charge is a simple function of voltage and this coupled with high power density and good cycle-life enable them to be useful in several applications ranging from light-weight electronic fuses, memory back-up power sources, and surge protection devices to pulse power sources for smart weapons. Such devices are also likely to help the global transition to a more energy-efficient society, since they can be coupled with both batteries and fuel cells to form hybrid power sources, especially suitable for Electric Vehicle (EV) applications<sup>39a-c</sup>. ECCs can also be sometimes classified as electric double layer capacitor (EDLC) or a pseudocapacitor (or a redox capacitor) depending on the nature of interfacial processes. The former has a capacitance associated with the non-faradaic charging and discharging of the electrical double layer at the electrode-electrolyte interface and is hence called electrical double layer capacitors (EDLCs) while the latter has faradaic surface redox reactions or adsorption induced pseudocapacitance as the cause or origin<sup>39c</sup>. A schematic representation of an electrical double layer capacitor is shown in *Figure 1.8*.<sup>39d</sup> While EDLCs with capacities of many tens of farads per gram of the electrode material have been achieved employing high surface-area carbon powders, fibers, or felts, much higher capacitance values (even hundreds of F/g) are accomplished with pseudo capacitors employing certain high surface-area oxides or conducting polymers.(*Table 1.3*) The large capacitance exhibited by some of these systems has been demonstrated to originate from a combination of the double-layer capacitance and pseudocapacitance associated with the participation of adsorbed intermediates in the surface redox-type reactions.

**Table 1.3. The specific capacitance of selected electrode materials for Supercapacitor<sup>39c</sup>**

Materials for Capacitor	Density (g/cm <sup>3</sup> )	Electrolyte	F/g	F/cm <sup>3</sup>
<b>Double layer capacitance</b>				
Carbon cloth	0.35	KOH, Organic	200,100	70, 35
Carbon black	1.0	KOH	95	95
Aerogel carbon	0.6	KOH	140	84
<b>Pseudo-capacitance</b>				
Anhydrous RuO <sub>2</sub>	2.7	H <sub>2</sub> SO <sub>4</sub>	150	405
Hydrous RuO <sub>2</sub>	2.0	H <sub>2</sub> SO <sub>4</sub>	650	1300
Conducting polymers	0.7	Organic	450	315

### 1.5.3 Batteries

As worldwide concern grows over fossil fuel usage, in terms of global warming, resource depletion, and other related issues there will be a progressive swing to the effective use of renewable energy sources. This will necessitate the development of improved methods of generating and storing electricity, from abundant resources without causing any environmental contamination. Electrochemical methods of energy storage has several superior features as explained above for fuel cells and ultracapacitors and another important method to convert electrical energy to chemical energy is by using rechargeable batteries. *A battery can be defined as an electrochemical storage device which converts electrical energy to chemical energy and vice versa during its charge-discharge operations involving various components such as anode (negative plate), and a cathode (positive plate) immersed in a suitable electrolyte.* Batteries are electrochemical cells comprising of an electrolyte existing in between anode, which sustains an oxidation reaction, and a cathode which sustains a reduction reaction and the cell emf allows one to estimate the amount of energy available. In practical batteries, some times a separator is also used in between the anode and cathode to avoid direct shorting and to improve the performance.

Based on reversibility of the electrochemical reactions batteries can be broadly divided into primary and secondary types.

#### 1.5.3.1 Primary Batteries

Primary cells have only limited amount of reactants and after their complete utilization these

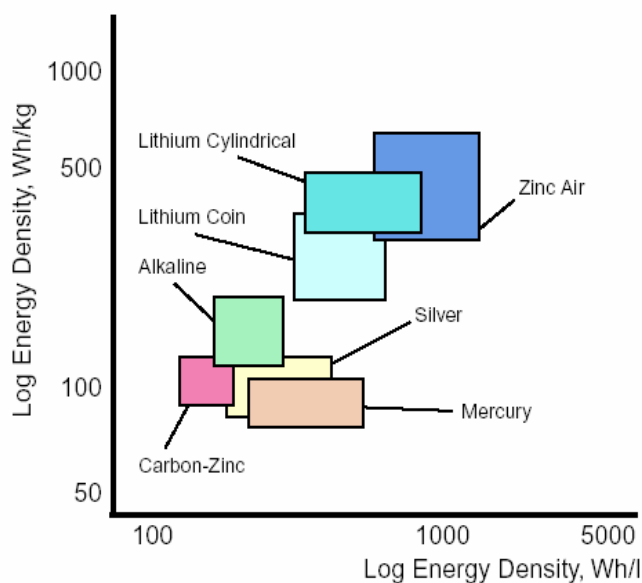


Figure 1.9. A Comparison of the energy storage capability of various primary battery systems<sup>40a</sup>

batteries have to be discarded. Most commonly available primary cells include Zinc-carbon cells (Leclanché cells) or alkaline Zn-MnO<sub>2</sub>, dry cells where both give 1.5V open circuit, despite their difference in a number of important respects. For example, Zinc-carbon cells have a central carbon collector immersed in the cathode active material mix (a mixture of impure MnO<sub>2</sub> and carbon), a container of metallic zinc as the anode, and

an electrolyte of aqueous  $\text{NH}_4\text{Cl}$  and/or  $\text{ZnCl}_2$  and these cells are traditional and inexpensive. Alkaline  $\text{MnO}_2$  cells, on the other hand, are more expensive and superior, as they use finely divide Zinc powder as the anode, which fills the centre of the cell, with a brass pin to make contact with the base. The electrolyte is concentrated  $\text{KOH}$  solution and the cathode material-a mix of chemically or electrochemically prepared  $\gamma\text{-MnO}_2$  and carbon-forms a concentric annulus around the zinc powder and the separator. These cells have a longer shelf life and are particularly useful for high drain (power) applications, where their useful life is several times than that of zinc-carbon type cells. *Figure 1.9.* illustrates the energy storage capability of the commonly employed primary batteries <sup>40a</sup>.

Several primary battery manufacturers also offer 3V lithium- $\text{MnO}_2$  cells by employing a lithium foil negative and an organic electrolyte coupled to  $\text{MnO}_2$  or other transition metal oxide/sulfide cathode. They are available as cylindrical cells, using spiral-wound electrodes ('jelly roll' configuration) is shown in *Figure.1.10*, or as button cells. Their advantages include high gravimetric and volumetric energy densities, high pulse rate capability, long shelf life and the ability to operate over a wide temperature range ( $-40^\circ\text{C}$  to  $+60^\circ\text{C}$ ). Button and coin cells are used widely in watches and pocket calculators. They may be either alkaline manganese cells (1.5V), zinc-silver oxide cells (1.5V), or 3V lithium cells with several possible cathodes (usually  $\text{MnO}_2$  or  $\text{CF}_x$ ). There are also several metal (Zn, Al etc.)-air button cells, employing a fuel cell type air cathode, which find

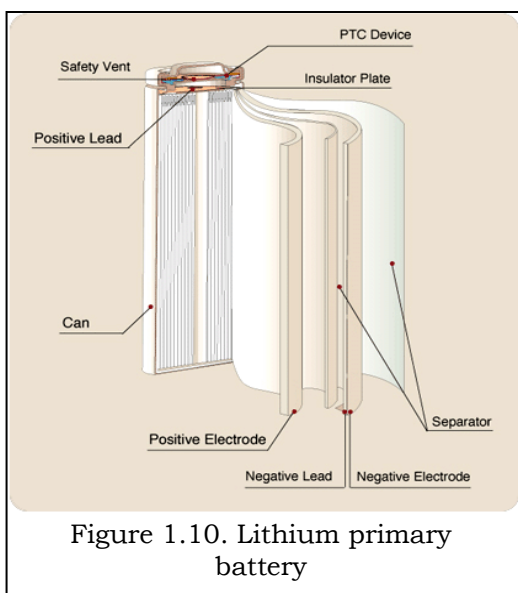


Figure 1.10. Lithium primary battery

interesting applications like hearing aid. Altogether there are over 40 different sizes and chemistries of button and coin cells <sup>40b</sup> and some of them are miniaturized to the extent of stamp or pin type of cells with good shelf life of 8-10 years.

### 1.5.3.2 Secondary Batteries

Secondary or rechargeable batteries store a fixed amount of chemical energy and may be recharged several times when the electrochemical active materials in them have been exhausted. Some of the common rechargeable batteries include

1. Lead-Acid batteries,

2. Nickel-Cadmium batteries,
3. Nickel-Metal Hydride batteries, and
4. Lithium batteries.

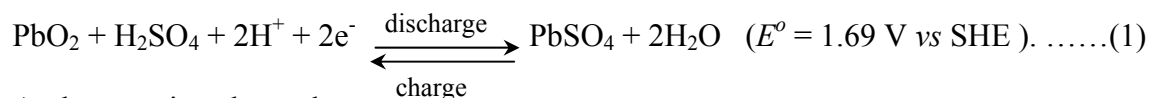
Due to the possibility of rechargeability arising from the reversibility of the cell reaction, the electrode design plays a very important role in controlling the cycle life of these batteries. A porous electrode is normally used along with a metallic current collector where the active materials like Zinc, Cd, Pb, Fe or Li acts as the negative electrode whereas  $\text{MnO}_2$ ,  $\text{PbO}_2$ ,  $\text{NiOOH}$ , etc., act as the positive electrode when kept in a matrix to give sufficient cycle life. The electrodes are separated by an electrolyte (and polymeric separator) that conducts ions which also must be an electronic insulator to avoid internal short-circuits. In most conventional batteries, the electrolyte is an aqueous solution, such as  $\text{ZnCl}_2$ ,  $\text{KOH}$  or  $\text{H}_2\text{SO}_4$ , although some advanced batteries use non-aqueous solution, ion conducting ceramics, polymers or molten salts as electrolytes<sup>41</sup>.

### (i) Lead-Acid Batteries

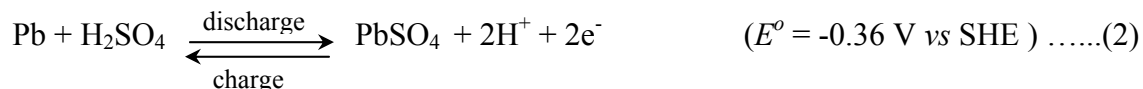
The lead-acid battery is one of the most successful electrochemical systems ever developed. Although it was first demonstrated as early as in 1859 by Gaston Planté and many other rechargeable batteries have been developed since then, the lead-acid battery still continues to be one of the most widely used rechargeable batteries. The electrochemistry of the lead-acid battery is shown in *Box 1*. There are three types of lead-acid batteries in common use: (a) batteries with excess or flooded electrolyte, (b) low-maintenance batteries with either starved electrode or immobilized electrolyte with or without a pressure-sensitive valve usually referred to

#### Box 1. Electrochemistry of the Lead-Acid Battery

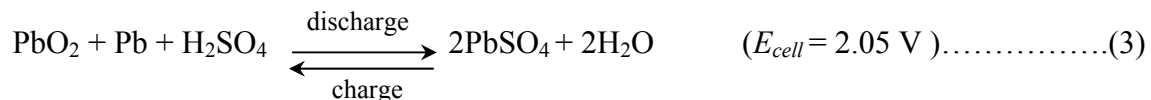
At the positive electrode:



At the negative electrode:



The net reaction is accordingly given by.



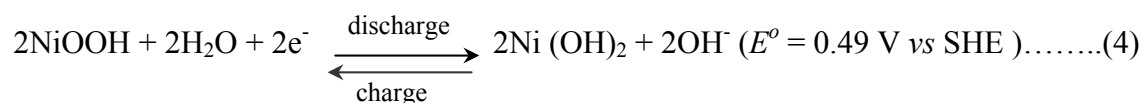
as valve-regulated lead-acid (VRLA) and (c) sealed fully maintenance free lead-acid batteries (SLA). The key issues, which in the past have made the Lead-acid batteries to seek improvements for certain type of applications, are short-life, high-maintenance, and inadequate energy density. Additional issues such as safety, environmental impact and material recyclability are becoming more critical than in the past. Although manufacturers of rechargeable batteries are exploring other advanced technologies<sup>41</sup> by keeping these factors in mind, lead-acid batteries still continues to be most popular type of cheapest rechargeable power sources.

## (ii) Nickel-Cadmium Batteries

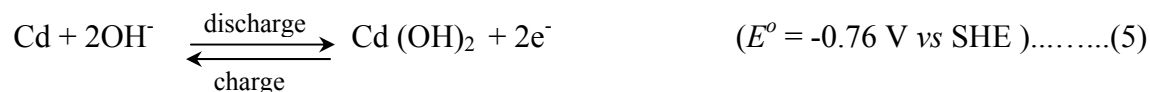
Compared to lead-acid batteries, alkaline rechargeable batteries such as nickel-cadmium (Ni-Cd), nickel-iron (Ni-Fe) and nickel-zinc (Ni-Zn) batteries represent a better balance between specific energy, specific power, cycle life and reliability. The Ni-Cd battery has a positive plate

### Box 2. Electrochemistry of the Nickel-Cadmium Battery

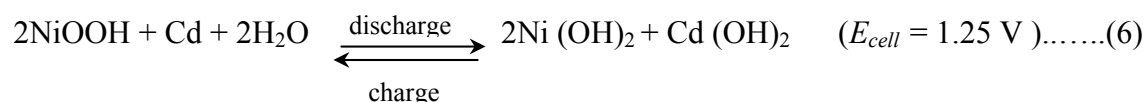
At the positive electrode:



At the negative electrode.



Accordingly, the overall charge and discharge reactions for the cell are:



of nickel oxyhydroxide (NiOOH), a negative plate of cadmium (Cd), and an aqueous solution of potassium hydroxide (KOH), for the electrolyte. The battery can endure a lot of abuse both physically and electrically, especially if designed using sintered electrodes and completely sealed (hydrogen-oxygen recombinant type) forms are also available. Also, the alkaline electrolyte does not enter into the discharge reaction as the acid does in the lead-acid battery and hence does not get depleted as the battery discharges. During discharge, NiOOH in the positive plate is converted to Ni(OH)<sub>2</sub>. This reaction results in a change in the Ni-oxidation state from +3 to +2. During the cell recharge, NiOOH is retrieved. The cadmium of the negative plate is converted to Cd(OH)<sub>2</sub> during the cell discharge and retrieved during the cell charge. The mechanism of the

electrode reaction (Box 2.) involves diffusion of protons through the solid-state lattice of Ni(OH)<sub>2</sub> and NiOOH so that there is a continuous change in the composition of the active material between Ni(OH)<sub>2</sub> and NiOOH. As the transformation of Ni(OH)<sub>2</sub> to NiOOH and vice-versa is a bulk feature, and so the process is considered to be homogeneous in nature. By contrast, reaction eqn. 5. (Box 2.) involves both solid and liquid phases, and hence is heterogeneous in nature. *Due to their higher cranking-power, lower weight and corrosion free atmosphere, nickel-cadmium batteries have found ample applications in defence and space.* Nickel-cadmium batteries suffer from the memory effect, which burdens the user with having to at least occasionally flow a time-consuming rechargeable regime in order to maintain their rated capacity. The effect appears to be due to the growth of abnormally large crystals on cadmium electrode. These crystals reduce the surface area of the cadmium electrode thereby increasing the battery's effective internal resistance. Besides, nickel-cadmium batteries store only slightly more energy per unit weight than lead-acid units and have a fairly high-rate of self-discharge at high temperatures. Lastly, cadmium is scanty and also toxic<sup>41</sup>. Iron and zinc negative electrodes also works in similar fashion forming Fe(OH)<sub>2</sub> and Zn(OH)<sub>2</sub> respectively instead of cadmium hydroxide upon discharge.

### (iii) Nickel-Metal Hydride Batteries

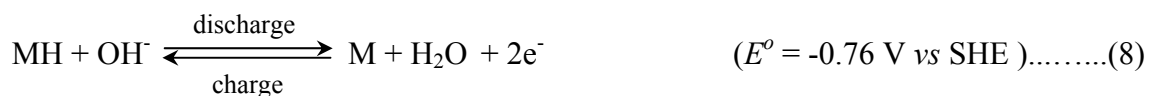
*The limitation of cadmium has encouraged the development of nickel-metal hydride (Ni-MH) battery as an attractive alternative, which is not only cadmium-free but can also store more energy than comparatively sized Ni-Cd, Ni-Fe or Ni-Zn alkaline cells.* Similar to all these cells, the Ni-MH units also employ nickel-positive plates with NiOOH/ Ni(OH)<sub>2</sub> as the active material

#### Box 3. Electrochemistry of the Nickel-Metal Hydride Battery

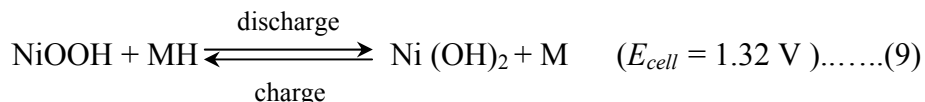
At the positive electrode:



At the negative electrode: charge



Accordingly, the net cell reactions during its charge and discharge are given as:





in an aqueous KOH electrolyte. The difference is that the active material in the negative plate is hydrogen adsorbed in a metal alloy. The metal alloys in which hydrogen is stored fall into two categories: (a) the  $AB_5$  –alloys based on mixtures of nickel and rare earth, and (b) the  $AB_2$  –alloys based on nickel commonly blended with titanium, vanadium and zirconium. Although, in the beginning,  $AB_5$ -type alloys were employed as battery electrodes, at present,  $AB_2$ -type alloys are preferred as they yield superior energy densities, compared to  $AB_5$ -type, which can still hold hydrogen more strongly thus lowering the self-discharge rate. The electrochemistry of Ni-MH battery is shown in *Box 3*. Several companies like Ovonic make attractive modules of Ni-MH batteries and some of these are used to replace Ni-Cd for space applications due to good reliability. Nevertheless, Ni-MH batteries deliver less power, have a faster self-discharge and are less tolerant to overcharge like the nickel-cadmium batteries<sup>41</sup>.

## 1.6 Introduction to Lithium Batteries

The miniaturization in electronics and the rapid advances in portable electronic devices as camcorders, digital watches, laptop computers, cellular phones, portable computers, have created an increasing demand for lightweight, high-energy density batteries<sup>10a, 40a</sup>. Also, there is an

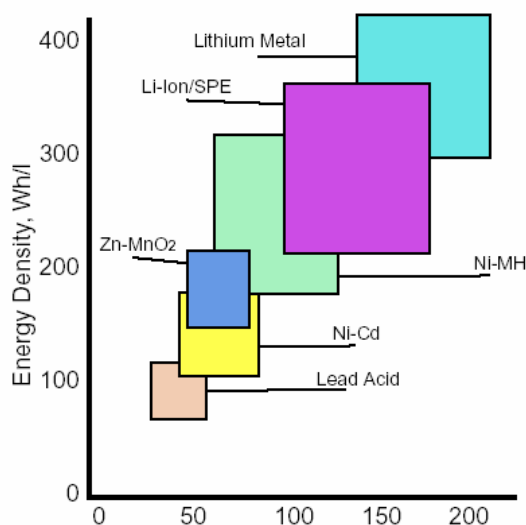


Figure 1.11. A Comparison of the energy storage capability of common rechargeable battery systems<sup>40a</sup>

enormous interest to develop advanced high-energy density batteries for electric vehicle, space and defence propulsions<sup>40b</sup>. Moreover, NASA's planetary exploration missions require advanced rechargeable batteries that can operate at extreme temperatures, and with high specific energy and power densities. Since conventional aerospace rechargeable battery systems are inadequate due to mass and volume constraints and also to poor performance at sub-zero temperatures, lithium rechargeable batteries are being selected as baseline for these missions. More specifically, the 2003 Mars Exploration Rover mission, which

deploys twin rovers onto Mars with longer mission duration than the previous Sojourner rover, has lithium rechargeable batteries for the first time in a major NASA mission<sup>40a,b</sup>.

Lithium batteries have become attractive for these applications because lithium, with an atomic mass of 6.94, is the lightest of all the metals and has a high specific capacity ( $3.86\text{Ahg}^{-1}$ ) along with a much higher electrochemical potential ( $-3.045\text{V}$ ). Consequently, Li anode has become an obvious choice to provide higher energy density and higher voltage compared to other anodes for rechargeable systems. From a comparison of the volumetric and gravimetric energy densities of the various rechargeable systems, lithium batteries stand separately since they are much lighter and smaller than other systems. A comparison of energy storage capability of common rechargeable cells for various applications clearly illustrates this as shown in *Figure 1.11. & Table 1.4.*<sup>40a, 41</sup>. This interest in lithium batteries was initially explored using a lithium foil negative electrode coupled with several transition metal oxide/ sulfide cathode materials and many systems are commercially available from several suppliers. Nevertheless, lithium metal is highly reactive and for safety reasons, especially during recharging, lithium metal negative does not seem to work well although much research is still in progress especially after alloying with various elements like Si and Al.

**Table 1.4. A comparison of the important features of rechargeable batteries<sup>41</sup>**

Cell type	Nominal voltage (V)	Specific energy (Wh/kg)	Energy density (Wh/l)	Specific power (W/kg)	Power density (W/L)	Self discharge (% month)	Cycle life
Lead-acid	2.0	35	70	~200	~400	4-8	250-500
Nickel-Cadmium	1.2	40-60	60-100	140-220	220-350	10-20	300-700
Nickel-Metal Hydride	1.2	60	220	130	475	30	300-500
Lithium-ion	3.6	115	260	20-250	400-500	5-10	500-1000
Lithium -Polymer	3.0	100-200	150-350	>200	>350	~1	200-1000

The lithium-ion battery, the rising star of the 1990's, circumvents most of these problems by using lithiated carbonaceous solids as safer anode materials. One property that makes graphite the most commonly used lithium metal substitute is its ability to reversibly intercalate (insert) lithium atoms between its carbon sheets without significantly altering its structure. The lithium-ion battery is normally made of electrode materials capable of cyclic transfer of lithium ions between the two electrodes, lithium intercalated graphite as anode and transition metal oxide/ sulfide as cathode placed in an organic electrolytes comprising dissolved lithium salts. One of the essential features of the lithium-ion battery is that they at no stage in the charge-discharge cycle have any lithium metal present. Rather, lithium ions are intercalated into the positive electrode in

the discharged state and into the negative electrode in the charged state and because of this movement of  $\text{Li}^+$  ions across the electrolyte, these cells are sometimes called to work by "a rocking chair" principle. This principle of operation is fundamentally different and safer than that of a rechargeable lithium metal battery and a schematic representation of the transfer of lithium

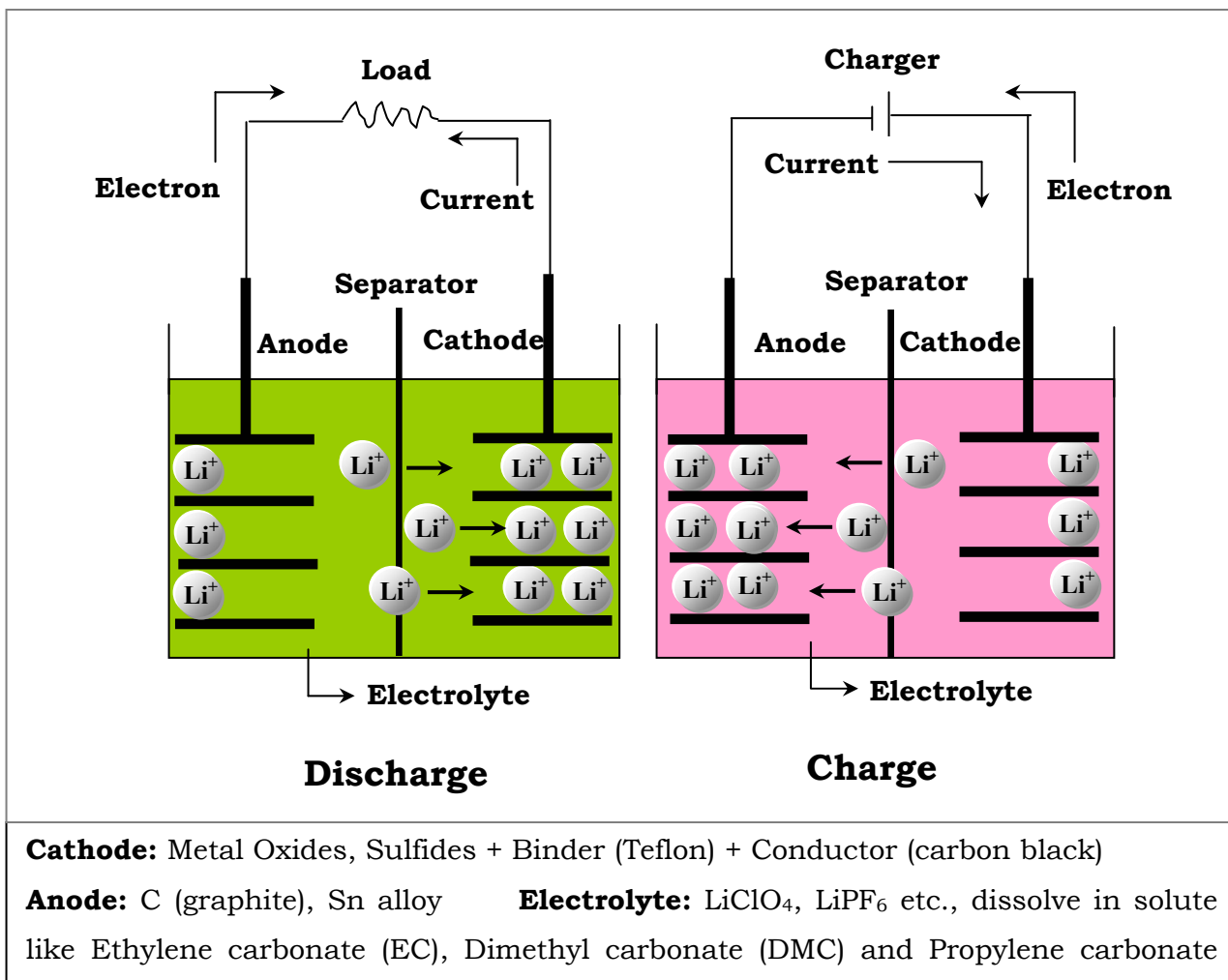


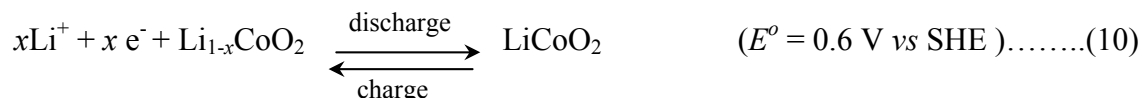
**Figure 1.12. Schematic representation of Lithium-ion battery: Lithium ion intercalation into cathode and anode during Charge and Discharge process**

ions during charge/ discharge processes is shown in *Figure 1.12*. The electrochemistry of the lithium-ion battery is shown in *Box 4*. The origin of the cell voltage can then be understood as the difference in free energy between  $\text{Li}^+$  ions in the crystal structures of the two electrode materials. The selection of electrode material has special importance, because the capacity is

mostly limited by the choice of the electrode material and in order to reach the goal of a high specific energy/power density, two fundamental requirements must be met by the electrode materials: i) a high specific charge (in Ah/kg) and charge density (in Ah/L), i.e., a large number of available charge carriers per mass and volume unit of the material; and ii) a high (positive

#### Box 4. Electrochemistry of the Lithium-Ion Battery

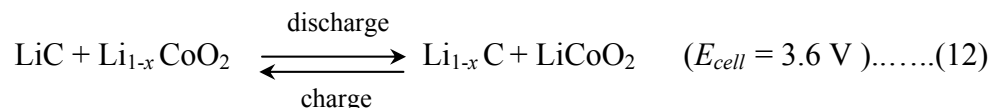
At the positive electrode:



At the negative electrode:



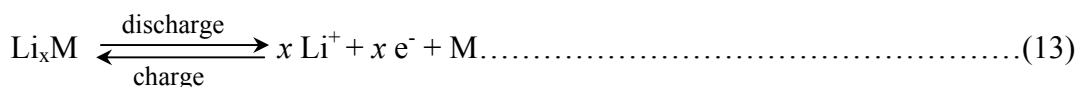
Accordingly, the net cell reactions during the charge and discharge process of the cell are written as bellow:



electrode) and low (negative electrode) standard redox potential of the respective electrode reactions, leading to a high cell voltage. Moreover, the cell reactions at both negative and positive electrodes are to be highly reversible so that charge-discharge operations could be carried out for several thousands of cycles. Limited cycle life due to capacity fading is a major limitation and *present research and development activities are mainly focused on preparing such highly reversible insertion electrode materials*<sup>41</sup>.

### 1.6.1 Lithium Insertion Materials for Negative Electrodes

Various insertion materials have been proposed for negative electrodes of high energy density rechargeable lithium batteries, which work as follows:



For example, several  $\text{Li}^+$  ion intercalating transition metal oxides/ chalcogenides, carbon have been used as anode materials as illustrated in *Table 1.5*. Both the specific charges and the power densities of lithium insertion materials are theoretically lower than that of metallic lithium<sup>10a</sup>.

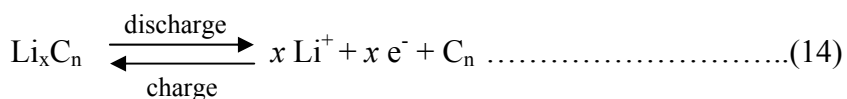
However, considering that the cycling efficiency of metallic lithium is  $\leq 99\%$ , one has to employ a large excess of lithium<sup>10a</sup> to reach sufficient cycle life. The practical charge density of a secondary lithium electrode is therefore much lower than the theoretical one, so that it is comparable with the charge densities of alternative lithium-containing compounds shown in Table 1.5.

**Table 1.5. A comparison of the main characteristics of representative negative electrode materials for lithium batteries<sup>10a</sup>**

Negative electrode Materials	Molecular weight	Density [kg/L]	Theoretical specific charge* [Ah/kg]
Li (primary)	6.94	0.53	3862
Li <sub>4</sub> (secondary)	27.76	0.53	965
LiC <sub>6</sub> (graphite)	79.00 (72.06)	2.24 (2.25)	339 (372)
LiAl	33.92 (26.98)	1.75 (2.70)	790 (993)
Li <sub>21</sub> Sn <sub>5</sub>	739.31 (593.55)	2.55 (7.28)	761 (948)
LiWO <sub>2</sub>	222.79 (215.85)	11.30 (12.11)	120 (124)
LiMnO <sub>2</sub>	134.88 (127.94)	6.06 (6.47)	199 (209)
LiTiS <sub>2</sub>	118.94 (112.01)	3.06 (3.22)	225 (239)

\* In some cases a considerably lower amount of the specific charge can be cycled reversibly in practice<sup>10a</sup>

At present mostly carbon is used as the negative electrode in commercial rechargeable Li-ion batteries since they exhibit both higher specific charges and more negative redox potentials than the most metal oxides/ sulfides and more significantly, due to their dimensional stability, facilitating better cycling performance than that of Li-alloys. The incorporation of lithium ions into carbon habitually named “insertion”, proceeds according to the following equation:



Due to electrochemical reduction (charge) of the carbon host, lithium ions from the electrolyte penetrate into the carbon to form a lithium/carbon intercalation compound, Li<sub>x</sub>C<sub>n</sub>. The reaction is reversible and the carbon that enables reversible lithium intercalation can roughly be classified as graphitic and non-graphitic. Lithium intercalation into graphitic carbon material, Li<sub>x</sub>C<sub>n</sub> has

been known since the mid 1950s<sup>10a</sup>. At ambient pressure, a maximum lithium content of one Li-guest atom per six carbon host atoms can be reached for highly crystalline graphitic carbon ( $n \geq 6$  in  $\text{LiC}_n$  or  $x \leq 1$  in  $\text{Li}_x \text{C}_6$ ). The intercalation reaction normally occurs only at prismatic surfaces although it is also possible for basal planes through defect sites<sup>10a</sup>. During the intercalation of  $\text{Li}^+$  into graphite, the stacking order of the carbon layers (named graphene layers) shifts to AA. Thus, two neighboring graphene layers in  $\text{LiC}_6$  directly face each other (Figure 1.13 a b).

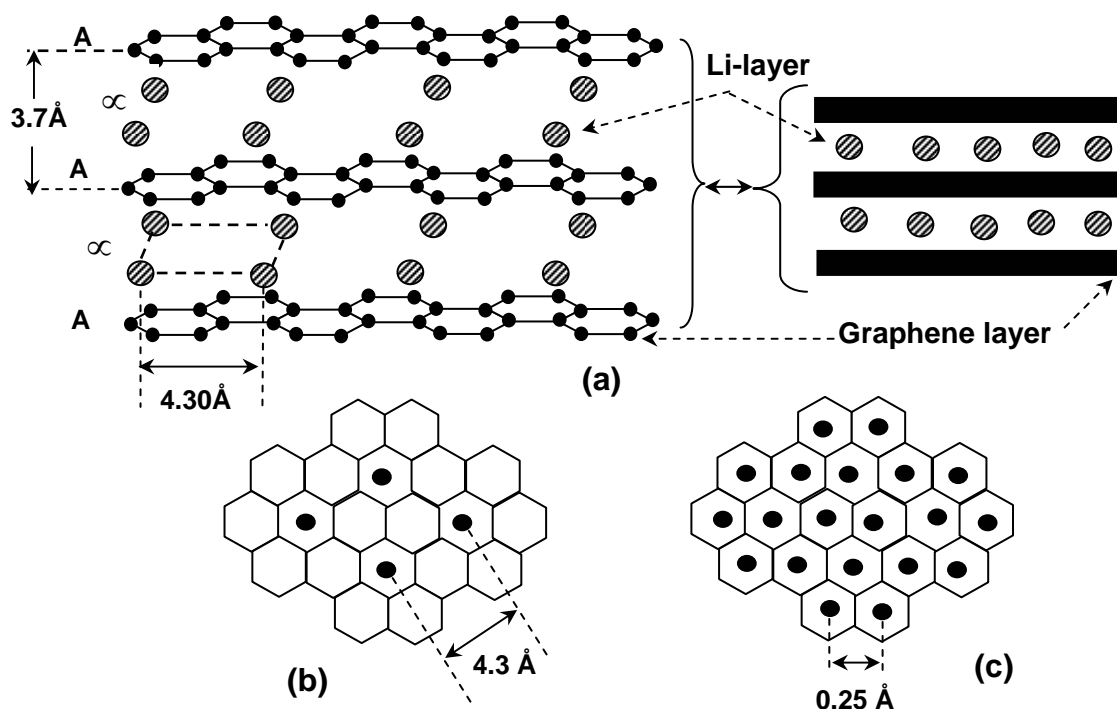
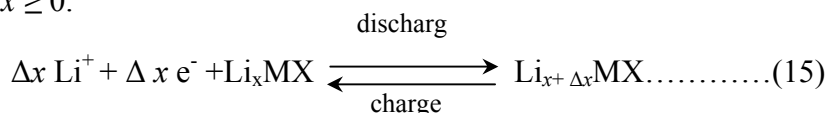


**Figure 1.13. Structure of  $\text{LiC}_6$  (a) schematic drawing showing the AA layer stacking sequence and the  $\infty\infty$  interlayer ordering of the intercalated lithium (b, c) view perpendicular to the basal plane of  $\text{LiC}_6$**

Owing to lithium intercalation the interlayer distance between the graphene layers increases moderately (10.3%) and this has been calculated for  $\text{LiC}_6$ <sup>10a</sup>. The stacking order of the lithium interlayer is  $\infty\infty$  (a  $\text{Li-C}_6\text{-Li-C}_6\text{-Li}$  chain exists along the  $c$ -axis)<sup>10a</sup>. If the negative electrode consists of lithiated graphite then the choice of the electrolyte is restricted to non-aqueous electrolytes only.

### 1.6.2 Lithium Insertion Materials for Positive Electrodes

Numerous intercalation compounds have been proposed as positive electrodes for rechargeable lithium batteries. These materials can be divided into three main groups: i) inorganic transition-metal oxides and chalcogenides, ii) organic molecules and iii) polymers. At present mostly inorganic transition-metal oxides and sulfides are used as positive electrodes in commercial rechargeable lithium batteries and *Table 1.6.* shows an overview of some of these materials. Their specific charges are based on a reversible range  $\Delta x$  of the lithium content during the charge/ discharge process as shown in *equation-15*, where X = oxide or chalcogenide;  $x \geq 0$ .



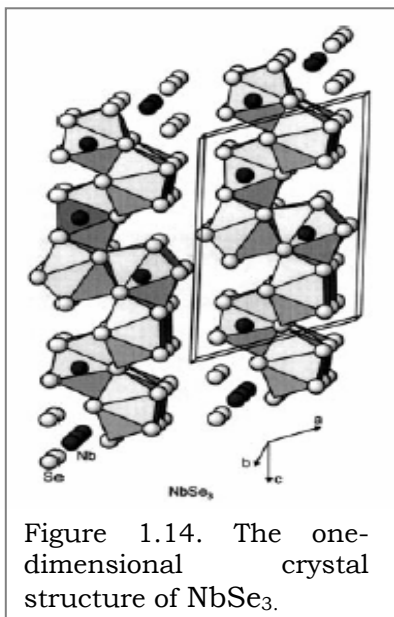
These positive electrode materials can be structurally classified into one-, two-, or three-dimensional inorganic structured based on the type of void spaces available for lithium insertion, as illustrated below.

**Table 1.6. Characteristics of representative positive electrode materials for lithium batteries <sup>10a</sup>. The values are either for fully lithiated (#discharged) host materials or lithium-free (\*charged) host materials, and the specific charges are based on a reversible range  $\Delta x$  of the lithium content during the charging/discharging process.**

Positive electrode materials	Molecular weight	Density [kg/L]	Reversible range $\Delta x$	Theoretical specific charge[Ah/kg]
*TiS <sub>2</sub>	112.01	3.27	1.0	239
*MoS <sub>2</sub>	160.06	5.06	0.8	134
*V <sub>2</sub> O <sub>5</sub>	181.88	3.36	1.0	147
*V <sub>6</sub> O <sub>13</sub>	513.64	3.91	3.6	188
*MnO <sub>2</sub>	86.94	5.03	0.5	154
*NbSe <sub>2</sub>	329.81	8.70	3.0	244
#LiCoO <sub>2</sub>	97.87	5.16	0.5	137
#LiNiO <sub>2</sub>	97.63	4.78	0.7	192
#LiMn <sub>2</sub> O <sub>4</sub>	180.82	4.28	1.0	148

### 1.6.2.1 One-Dimensional Hosts as Positive Electrode Materials

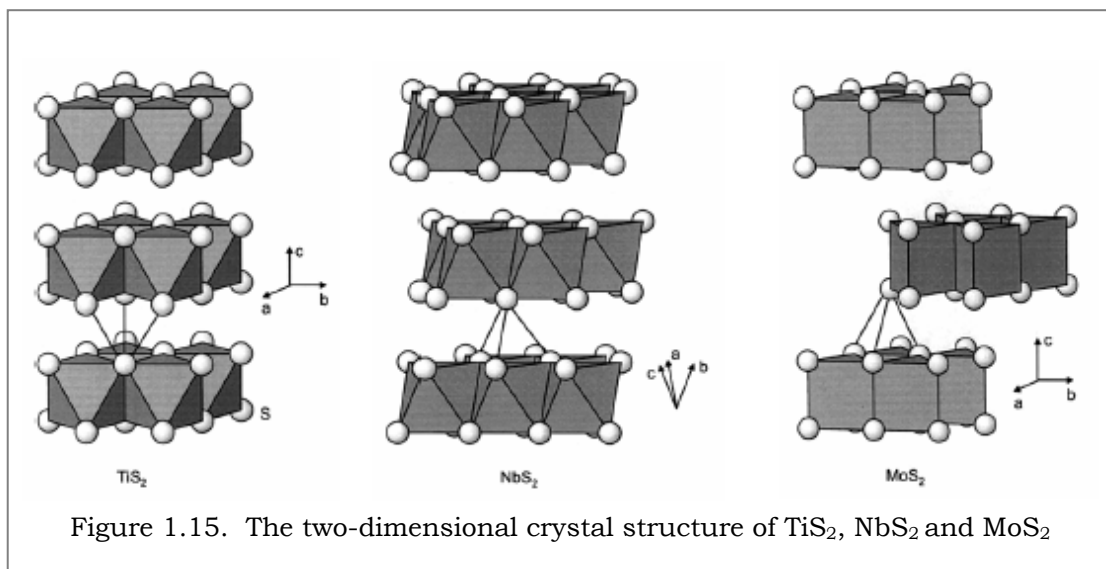
The electrochemically interesting representatives of this class of insertion hosts are crystalline  $\text{TiS}_3$  and  $\text{NbSe}_3$ <sup>10a</sup>. The crystal structures of  $\text{TiS}_3$  and  $\text{NbSe}_3$  are quite similar,



consisting of chains of face-sharing trigonal prismatic  $[MX_6]$  units. The chains are staggered in such a way that the metal ‘ $M$ ’ can coordinate with two additional chalcogenides, ‘ $X$ ’ from different adjacent chains to form a bicapped trigonal prism<sup>10a</sup>. The resulting ribbons are linked together by weak van der Waals forces in the crystallographic  $b$ -direction, which leads to the fibrous morphology of the materials (Figure.1.14).  $\text{TiS}_3$  can be viewed as  $\text{Ti}^{4+} \text{S}_2^{2-} \text{S}^{2-}$  with a disulfide ion  $\text{S}_2^{2-}$  and an isolated sulfide  $\text{S}^{2-}$ <sup>10a</sup>. In  $\text{NbSe}_3$  the negative charge is delocalized over the selenium atoms, since there is no Se-Se bond.

### 1.6.2.2 Two-Dimensional Hosts as Positive Electrode Materials

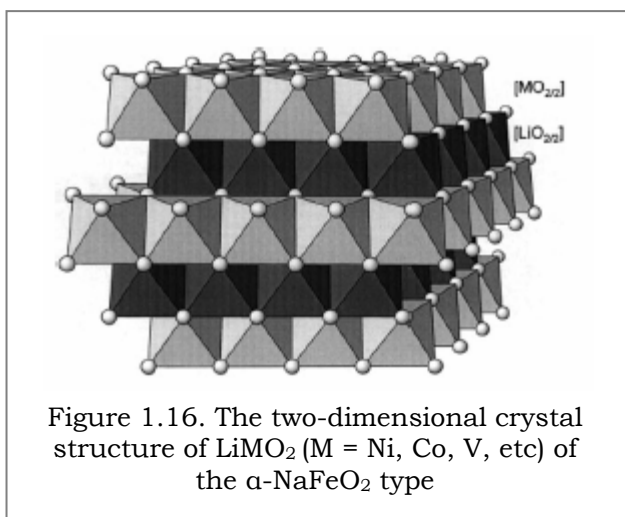
The most important two-dimensional insertion compounds, layered-type dichalcogenides of the transition metals Ti, Nb, Ta, Mo and W, as well as dioxides of the transition metals V, Cr, Fe, Co and Ni are of interest as positive insertion electrode materials<sup>10a</sup>.





The structural features of the transition-metal dichalcogenides  $MX_2$  with  $CdI_2$  -type structures are blocks of two hexagonally close-packed chalcogen layers between which the transition metals reside in either prismatic or octahedral coordination of six chalcogens. This coordination symmetry together with different stacking arrangement of the  $X-M-X$  layers gives rise to the different polymorphs as shown in *Figure.1.15*.<sup>10a</sup>. One of the key features of all these polymorphs is the van der Waals gap between the  $X-M-X$  sheets, which provides the space for guest reactant in intercalation reactions. During the intercalation of lithium, complete charge transfer occurs involving the reduction of  $M^{4+}$  to  $M^{3+}$  concomitant with the diffusion of  $Li^+$  into the van der Waals gaps,<sup>10a</sup> resulting in the expansion of the host structure along the crystallographic  $c$ -direction. The van der Waals force between the layers is thereby replaced by coulombic interactions. In all these polymorphs, octahedral and tetrahedral interstitial sites are available for the intercalation of lithium ions.

The structure of a typical two dimensional lithium transition-metal oxide is shown in *Figure 1.16*. The oxide with general formula  $LiMO_2$  with  $M= V, Cr, Fe, Co$  and  $Ni$ <sup>10a</sup> adopt the  $\alpha$ - $NaFeO_2$  -type structure, which can be regarded as a distorted rock salt superstructure. In a cubic close-packed oxygen array the lithium and transition-metal atoms are distributed in the octahedral interstitial sites in such a way that  $MO_2$  layers are formed consisting of edge-sharing  $[MO_2]$  octahedral. In between these layers lithium resides in octahedral  $[LiO_6]$  coordination,



leading to alternating (111) planes of the cubic rock-salt structure (*Figure 1.16*). This ordering induces a slight distortion of the lattice to hexagonal symmetry. Complete deinsertion of the lithium ions results in the layered  $CdCl_2$  structure type. These oxides are thermodynamically stable only in the intercalated state  $LiMO_2$  since the high electronegativity of oxygen leads to a higher ionic character of the metal-oxygen bonds in

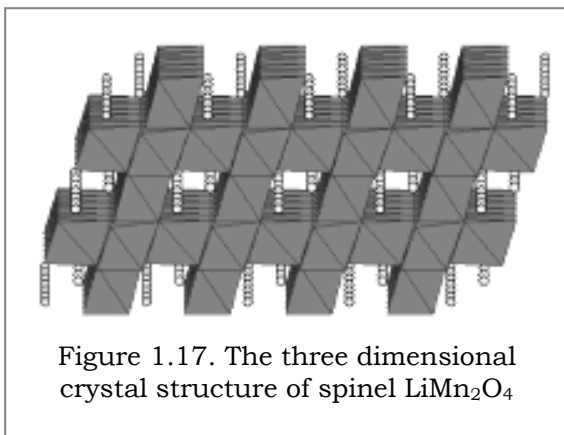
comparison to the covalent nature of metal-chalcogen bonds. The resulting negative charge of the transition metal-oxygen layers causes repulsive interactions between adjacent layers which need compensation for the positively charged ions between the adjacent oxygen layers<sup>10a</sup>.

Among the above-mentioned isostuctural dioxides, particularly  $\text{LiCoO}_2$ ,  $\text{LiNiO}_2$ ,  $\text{LiMnO}_2$  and the recent mixed oxides  $\text{Li}_x\text{Ni}_y\text{Co}_{1-y}\text{O}_2$  and  $\text{Li}_x\text{Mn}_y\text{Co}_{1-y}\text{O}_2$  have gained promising attention as positive electrode materials for rechargeable lithium batteries.

### 1.6.2.3 Three-Dimensional Hosts as Positive Electrode Materials

Three-dimensional framework structures have cross-linked channels allowing efficient ion insertion especially if the size of the channel is sufficiently large to accommodate the ions. The advantage of three-dimensional frameworks over two-dimensional layered structures are i) the possibility of avoiding, for steric reasons, the co-insertion of bulky species such as solvent molecules; and ii) the smaller degree of expansion/ contraction of the framework structure upon lithium insertion / deinsertion.

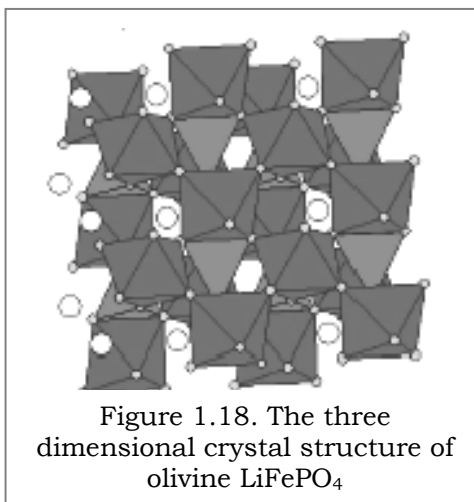
Besides  $\text{LiNiO}_2$  and  $\text{LiCoO}_2$ , lithiated spinel  $\text{LiMn}_2\text{O}_4$  is at present a very popular lithium-containing positive electrode material<sup>10a</sup>. It has cubic spinel structure as shown in *Figure 1.17.*, and can be described as a cubic close packed oxygen array with the oxygen anions on the crystallographic 32e sites of  $Fd3m$  space group. The manganese cations occupy half of the octahedral interstitial sites, 16d, and the lithium cations, one eighth of the tetrahedral sites, 8a.



The interstitial space group in the  $[\text{Mn}_2]\text{O}_4$  framework represents a diamond type network of tetrahedral 8a sites and the surrounding octahedral 16c sites. These empty tetrahedra and octahedra are interconnected with one another by common faces and edges to form 3D pathways for  $\text{Li}^+$  ion diffusion<sup>10a</sup>. The electrochemical  $\text{Li}^+$  ion deinsertion from the tetrahedral sites of  $\text{LiMn}_2\text{O}_4$  is reversible and proceeds at about +4 V *Vs*  $\text{Li}/\text{Li}^+$ . During charge-discharge operation in the “4 V” potential range, the cubic symmetry of the structure is maintained<sup>10a</sup>. Good rechargeability and stable cycling behavior of  $\text{LiMn}_2\text{O}_4$  is attributed to the fact that  $\text{Li}^+$  is deinserted from the cubic structure with a minimal contraction of the unit cell over a wide composition range. However, at practical potentials ( $\ll 5$  V *Vs*  $\text{Li}/\text{Li}^+$ ) it is not possible to extract all the lithium electrochemically to form  $\lambda\text{-MnO}_2$ . It is also possible to insert additional  $\text{Li}^+$  in empty octahedral 16c sites of  $\text{LiMn}_2\text{O}_4$ . The electrochemical insertion/deinsertion occurs

at about +3 V *Vs* Li/ Li<sup>+</sup>, despite rather poor cycling performance. The poor cycling behavior of Li/ LiMn<sub>2</sub>O<sub>4</sub> cells in the “3 V” range is attributed to an asymmetric lattice expansion /contraction of the Li<sub>1+z</sub>Mn<sub>2</sub>O<sub>4</sub> electrode during the discharge /charge reactions. This lattice distortion is largely a result of the Jahn-Teller effect of the Mn<sup>3+</sup> ion. This effect transforms the cubic crystal symmetry of the spinel electrode into tetragonal symmetry. Thus, the electrochemical performance in the “3 V” potential window can be significantly improved by decreasing the amount of Mn<sup>3+</sup> in the spinel compound. However, on long term cycling, even optimized cells show a slight capacity fading<sup>10a</sup>. This fading is attributed to the instability of the organic-based electrolyte at the very high voltage reached when charging the cells, resulting in the slow dissolution of the Li<sub>x</sub>Mn<sub>2</sub>O<sub>4</sub> electrode in the electrolyte (Mn<sup>2+</sup> is a soluble species that is produced from Mn<sup>3+</sup> by the disproportionation reaction to Mn<sup>2+</sup> and Mn<sup>4+</sup>), as well as to an onset of the Jahn-Teller effect in deeply discharged Li<sub>x</sub>Mn<sub>2</sub>O<sub>4</sub> electrodes (i.e., at x = 1)<sup>10a</sup>. Replacing some manganese in LiMn<sub>2</sub>O<sub>4</sub> with mono- or multivalent cations (e.g., Li<sup>+</sup>, Mg<sup>2+</sup> or Zn<sup>2+</sup>) or, alternatively doping the oxide with additional oxygen increases the average manganese oxidation state slightly above 3.5, suppressing the Jahn-Teller effect on the deep discharge, thus leading to an improved rechargeability. Other approaches like the substitution of the Jahn-Teller ion Mn<sup>3+</sup> by the other trivalent cations (Al<sup>3+</sup>, Fe<sup>3+</sup>, Ni<sup>3+</sup>, Co<sup>3+</sup> or Cr<sup>3+</sup>) have also been tried<sup>10a</sup> and the application of many of these mixed oxides has promising future.

Recently, lithium iron phosphates and sulfates were shown to be good candidates for



positive electrode materials. Li<sub>x</sub>Fe<sub>2</sub>(SO<sub>4</sub>)<sub>3</sub>, Li<sub>3</sub>Fe<sub>2</sub>(PO<sub>4</sub>)<sub>3</sub>, Li<sub>3</sub>V<sub>2</sub>(PO<sub>4</sub>)<sub>3</sub> belong to the family of compounds with an open NASICON framework structure while LiFePO<sub>4</sub> and FePO<sub>4</sub> are phosphor-olivines as shown in *Figure.1.18*. Additionally, they all are inexpensive, non-toxic, and environmentally benign. Although the specific charges are relatively low (ca.100 Ah/kg), these compounds might point to a new direction in solid-state electrochemistry for the design of advanced battery materials<sup>10a</sup>.

### 1.6.3 Electrolytes for Lithium Batteries

Lithium electrodes in contact with aqueous electrolytes like that used in conventional acidic and alkaline rechargeable batteries cause a variety of problems, which in the worst case can lead to fires and explosions. Therefore, one of the most promising approaches is that of the “rocking-chair” Li-ion cells employing non-aqueous electrolytes comprising lithium salts dissolved in an organic solvent. The main issues in selecting an electrolyte are its compatibility with Li, good solubility for Li salts, low vapor pressure and thermal stability and a comparison of commonly employed organic solvents especially for low temperature applications is shown in Table 1.7.

**Table 1.7.A comparison of commonly employed organic solvents especially for low temperature applications.<sup>42 b</sup>**

Solvent	Dielectric Constant	Conductivity, mS/cm		Viscosity, kg.m <sup>-1</sup> s <sup>-1</sup>		T FREEZE Deg C
		25°C	-20°C	25°C	-20°C	
Ethylene Carbonate, EC	89.6	5.2	-	1.9	-	39.4°C
Propylene Carbonate, PC	64.4	6.9	1.1	2.33	7.41	-49 °C
Diethyl Carbonate, DEC	2.82	2.9	1.4	0.75	-	-43 °C
Dimethyl Carbonate, DMC	3.1	6.5	1.4	0.59	-	3 °C
Ethylmethyl Carbonate, EMC	2.4	4.3	2.2	0.7	1.29	-55 °C
Ethyl Acetate, EA	6	11	6.6	0.51	0.85	-83 °C

If the negative electrode consists of lithiated graphite then the choice of the electrolyte is restricted to systems based on ethylene carbonate (EC) since those based on other solvents tend to cause exfoliation of the graphite. On the other hand, the use of lithiated coke for the negative electrode provides a much wider choice with diethyl carbonate (DEC), propylene carbonate (PC), dimethyl carbonate (DMC), and many other solvents that may be used alone or in combination. The favorite solute is lithium hexafluorophosphate (LiPF<sub>6</sub>) although other lithium

salts such as Lithium perchlorate, ( $\text{LiClO}_4$ ), Lithium hexafluoroarsenate, ( $\text{LiAsF}_6$ ), Lithium hexafluoroantimonate, ( $\text{LiSbF}_6$ ) may as well be used. The ionic conductivity of these mixtures is about two orders of magnitude lower than that of aqueous electrolytes; nevertheless, this is high enough to make practical batteries for use at or above room temperatures. Indeed, even at  $0^\circ\text{C}$ , an ionic conductivity of about  $10^{-3} \text{ Scm}^{-1}$  for these electrolytes is sufficient for the practical use. The conductivity, however, varies quite appreciably with temperature, ranging from  $0.2 \times 10^{-3}$  at  $-40^\circ\text{C}$  to  $1.5 \times 10^{-2} \text{ Scm}^{-1}$  at  $40^\circ\text{C}$  for  $\text{LiPF}_6$  dissolved in 1:1 volume mixture of ethylene and propylene carbonate (EC: PC). During the cell operation, lithium ions move back and forth between the two electrodes across the electrolyte as the cell is alternatively charged and discharged.

However, because of the high oxidation potential of the transition-metal oxide cathodes, these batteries may suffer from decomposition reactions of the organic electrolyte. Therefore, the replacement of the liquid electrolyte with thin 'solid polymer electrolyte' membrane (SPE) comprising lithium salts dissolved in a suitable polymer matrix would be highly desirable. For example, Polyethylene oxide (PEO), Polypropylene oxide (PPO), Polyphosphazene (MEEP) and Poly (*p*-Phenylene) (PPP) can be used as polymer matrix for preparing these solid polymer electrolytes (SPE) containing lithium salts. The electrolyte serves as a medium to transport  $\text{Li}^+$  ions during the charging/discharging cycle of the cell. In addition, the function of ceramic or polymer separators often placed between the electrodes, can also be carried out by this polymeric electrolyte, thus realizing both functions (-ion conduction and avoiding electronic shorts) in a single thin membrane when polymer electrolytes are used. Recently, the choice of polymer electrolyte for lithium-ion batteries has been reviewed by W.H.Meyer<sup>42a</sup>.

## 1.7 Conclusions and Perspectives

Lithium-ion cells are emerging as one of the prime electrochemical power sources for several important applications compared to other rechargeable systems<sup>10a, 41</sup>. In fact the term rechargeable lithium batteries now essentially means those based on insertion electrodes and the one using layered  $\text{LiCoO}_2$  as the cathode (positive electrode) offers excellent capacity in the 4 V range. There is an enormous interest in increasing the energy density further by designing new materials which can provide higher cell voltage and/or capacity. Since, cobaltate is both expensive and toxic as a cathode material, there is extensive worldwide research interest to

develop alternate cathode materials. Although layered  $\text{LiMnO}_2/\text{LiNiO}_2$  has recently drawn much attention, both  $\text{LiNiO}_2$  and spinel  $\text{LiMn}_2\text{O}_4$  exhibit capacity fading due to the lattice deformations arising from Jahn-Teller distortion associated with the low spin ( $\text{Ni}^{3+}: 3d^7$ ) and high spin ( $\text{Mn}^{3+}: 3d^4$ ) ions respectively<sup>10a</sup>. Consequently, the last decade has witnessed, much efforts to improve the performance of these electrode materials and several groups have focused on the synthesis of new nanostructured cathode materials, in order to ameliorate this limitations. Design of new hybrid nanocomposites can be an attractive solution since many of this organo-inorganic materials based on new concepts can increase the capacity with low cost.

## 1.8 Motivation, Scope and Organization of the thesis

Inorganic layered materials exist in a great variety and possess well defined, ordered intralamellar space. It has also been demonstrated that most of the 2D-transition metal oxides, sulfides, oxy chlorides and phosphates that are layered such as  $\text{V}_2\text{O}_5$ ,  $\text{MoO}_3$ ,  $\text{FeOCl}$ ,  $\text{VOPO}_4$ ,  $\text{TaS}_2$ ,  $\text{TiS}_2$ ,  $\text{VS}_2$  and  $\text{MoS}_2$  act as beneficial lithium battery cathodes despite their shortcomings like low electronic conductivity, structural instability during lithium insertion/ extraction and poor capacity retention upon cycling (capacity fading). This ability enables them to act as matrices or hosts for polymers, yielding interesting hybrid nanocomposite materials. Nevertheless, despite the irreversible character of the process, the inclusion of conducting polymers within the structure of extended solid phase leads in many cases to remarkable hybrid materials with synergistic properties. Although, conductive polymers have high electronic conductivity, their processability, stability and capacity are not sufficient to match with that of lithium for fabricating an efficient rechargeable lithium battery. Consequently, several groups have focused efforts on the synthesis of new cathode materials with special emphasis on organo-inorganic conducting polymer based intercalative nanocomposites.

In this context, Poly (3,4-ethylenedioxythiophene) (PEDOT), is one of the recently found excellent “eco-friendly” conducting polymers. It is also a low band gap material which has attracted wide interest due to its high electronic conductivity, good stability in the p-doped state and reversible electrochemistry. From an electrochemical point of view it is interesting to note that PEDOT even when de-doped, has an electronic conductivity high enough to operate as its own electrode material. Upon re-doping this could be used also for designing such a hybrid

cathode material. Indeed, it appears to be one of the most stable conducting polymers currently available and has been attracting growing interest for applications in microwave “smart” windows, antistatic transparent films, electroplating, supercapacitors etc.,<sup>28-34</sup>.

## 1.9 Aim and Scope of the Present Study

From the above critical review, it is clear that several aspects pertaining to the effect of conducting polymer intercalation into transition metal oxides/sulfides on the electrochemical behavior of composite electrodes are not completely elucidated, despite the extensive use of conducting polymers during the last decades. More specifically Poly (3,4-ethylenedioxy thiophene) (PEDOT) has not been used for intercalation into transition metal oxides/sulfides although, the benefits due to intercalation of this conducting polymer has been mention in improving the capacity and cycle life. Accordingly, the main objectives of the present thesis are as follows.

- (i) to prepare and characterize new Organic-inorganic nanocomposites by two efficient soft chemistry (“*Chimie douce*”) intercalative methodologies such as redox intercalative polymerization and *in situ* oxidative polymerization coupled with encapsulative precipitation from solution of exfoliative lamellar solids for introducing Poly (3,4-ethylenedioxythiophene) (PEDOT) into different inorganic hosts
- (ii) to establish these methods for the preparation of organic-inorganic nanocomposites by various oxidizing and non-oxidizing inorganic hosts via intercalative process
- (iii) to estimate if such nanocomposites can potentially show hybrid properties synergistically derived from both host and the guest
- (iv) to understand how intercalation of Poly (3,4-ethylenedioxythiophene) (PEDOT) conducting polymer affects the structural and physicochemical properties of pristine inorganic hosts
- (v) to demonstrate their applications as effective cathode materials for rechargeable lithium batteries.
- (vi) to analyze the electrochemical charge-discharge properties and cycle-life of inorganic host material with and without polymer intercalation

(vii) to evaluate the electrochemical performance of the nano composites prepared from different inorganic host material as a cathode material for rechargeable lithium battery application.

This thesis comprises of six chapters. After a brief introduction to the general features of nanostructured materials for various applications in electronics, **Chapter-1** deals with the novel nanocomposites resulting from the tuning of molecular level interactions of dissimilar inorganic host components with organic guest species to form structural and functional nanocomposites having unique properties and wide application potential in the field of optoelectronics, magnetic devices, electro-catalysis and particularly electrode materials for rechargeable lithium batteries.

**Chapter-2** discusses the redox intercalative polymerization of new 3, 4-ethylenedioxy thiophene (EDOT) into the highly oxidizing host such as Vanadium pentoxide ( $V_2O_5$ ). A systematic study of the synthesis of the nanocomposites by direct *in situ* reaction of 3, 4-ethylenedioxythiophene (EDOT) with crystalline  $V_2O_5$  powder shows that upon intercalation, the interlayer spacing of  $V_2O_5$  expands with the existence of two phases in the PEDOT/  $V_2O_5$  system corresponding to the intercalation of one and two mono-layers of PEDOT in the  $V_2O_5$  framework. The unique properties of the organo-inorganic composites are investigated by various physicochemical characterization techniques. The application potential of these composites as cathode materials in rechargeable lithium batteries is also demonstrated by the electrochemical intercalation of lithium into the PEDOT/  $V_2O_5$  nanocomposites, where an enhancement in the discharge capacity is observed compared to that of pristine  $V_2O_5$ .

**Chapter-3** is concerned with the encapsulation of Poly (3, 4-ethylenedioxy thiophene) (PEDOT) in homologous layered-type dichalcogenides of Vanadium such as Vanadium disulfide ( $VS_2$ ). The structural features of the Vanadium-metal dichalcogenides  $VX_2$  with  $CdI_2$  -type structures are explained using blocks of two hexagonally close-packed chalcogen layers between which the Vanadium metals reside in either prismatic or octahedral coordination of six chalcogens. The synthesis and various physico-chemical characterization of a novel Poly (3,4-ethylenedioxythiophene) (PEDOT) /  $VS_2$  intercalative nanocomposite are discussed with an objective of demonstrating their applications as an efficient cathode material for lithium batteries.



**Chapter-4** contains results and discussion related to another type of transition metal oxide i.e., Molybdenum trioxide ( $\text{MoO}_3$ ), as a weakly oxidizing host structures for introducing polymer intercalation. Indeed, PEDOT /  $\text{MoO}_3$  nanocomposite has been successfully synthesized using an exfoliation and restacking strategies and the resulting nanocomposites with Poly (3, 4-ethylenedioxythiophene) have been characterized by different physicochemical techniques. This PEDOT/ $\text{MoO}_3$  nanocomposite gives significant enhancement in the discharge capacities compared to that of their respective pristine Molybdenum trioxide and the enhanced activity has been explained using a model.

**Chapter-5** describes one of the important achievements of encapsulation of an intractable, infusible Poly (3,4-ethylenedioxythiophene) in a non-oxidizing homologous layered-type dichalcogenides of Molybdenum ( $\text{MoS}_2$ ) using a suitable external oxidant. PEDOT/  $\text{MoS}_2$  nanocomposites have been investigated by electronic conductivity measurements, X- ray diffraction, FTIR Spectroscopy, Thermo-gravimetric analysis, SEM and TEM. The resulting nanocomposite material has been found to act as a better cathode material for rechargeable lithium batteries.

**Chapter-6** outline a summary of all the major conclusions of the present study suggesting the general principles of synthesis and characterization of Organo-Inorganic nanocomposites, which could merge the best properties of both the organic conducting Poly (3,4-ethylenedioxythiophene) and oxidizing and non-oxidizing inorganic hosts such as  $\text{V}_2\text{O}_5$  ,  $\text{VS}_2$  ,  $\text{MoO}_3$  and  $\text{MoS}_2$ , have been demonstrated to possess complementary strength as new hybrid functional materials. The intercalation of PEDOT macromolecules is consistent with both the expansion of the interlayer distance and structural stabilization of inorganic hosts. However, common to all these hybrid nanocomposite materials is the underlying search for synergy. This synergy has also been explicitly discussed and the improvement in electrochemical performance is attributed to higher electronic conductivity and enhanced bi-dimensionality.

These results clearly suggest the benefits offered by these hybrid materials for fabricating composite cathodes for high energy density rechargeable lithium batteries, although, the degree to which the polymer-polymer interactions in the bulk is affected by the polymer-host is not clear. Similarly, questions related to how the polymer-host interactions sequester the polymer chains effecting either the polymer conformation, chain length, and / or bulk electron-transport

properties need more investigations, especially if we want to improve the cycle life. Despite of these limitations, these type of hybrid materials may find increasing importance in the area of electrochemical power sources in the coming years.

## 1.10 References

1. (a) Richard Feynman's classic talk on Dec.1959, annual meeting of American Physical Soc., at the California Institute of Technology, published in Caltech's Engineering and Science, Feb.1960. ([www.zyvex.com/nanotech/feynman.html](http://www.zyvex.com/nanotech/feynman.html)). (b) Richard E. Smalley Image Gallery (c) Nanotech web.org.
2. (a) Synthesis, Functionalization, and Surface Treatment of Nanoparticles, M.-I. Baraton Editor, American Scientific Publishers, Stevenson Ranch (CA, USA), 2002.; (b) K.E.Gonsalves, M.-I. Baraton, R.Singh, H.Hofmann, J.X.Chen, and J.A.Akkara (eds.), in Surface Controlled Nanoscale Materials for High-Added-Value Applications, *Proceedings of the Materials Research Society*, Vol.501, Warrendale, PA, USA (1998). (c) N.Lane, *J.Nanopart.Research*, 3(2001) 95.
3. P.G.Collins, M.S.Arnold and P.Avouris, *Science*, **292** (2001) 706.
4. R.S.Lee, H.J.Kim, J.E.Fischer, A.Thess, R.E.Smally, *Nature*, **388** (1997)255.
5. "Functional Nanostructured Molecular Materials," J. T. Hupp and S. T. Nguyen, *Interface*, **10** (2001) 28. Cover feature.
6. Merlau, M. L., Mejia, M. D. P., Nguyen, S. T. and Hupp, J. T. *Angew. Chem. Int. Ed. Engl.* **40** (2001) 4239.
7. "Electrochemistry in Nanostructured Inorganic Molecular Materials," M. E. Williams and J. T. Hupp, *Proceedings of the Materials Research Society*, **676** (2001) Y1.5.1.
8. (a)Y.Xia, P.Yang, Y.Sun, Y.Wu, B.Mayers, B.Gates, Y.Yin, F.Kim and H.Yan *Adv.Mater* **15** (2003) 352 (Review Article) (b) C.Ros., *Annu.Rev.Mater.Sci.* **31**(2001)203.
9. (a)K.K.Likharev, T.Claeson, *Sci.Am* 1992, June, p-80 (b) K.K.Likharev, *IBM, J.Res.Dev*, **32** (1998)144 (c) G.Markovich, C.P.Collier, S.E.Henrichs, F.Remacle, R.D.Levine, J.R.Heath. *Acc.Chem.Res* , **32** (1999) 415.
10. (a) M.Winter, J.O.Besenhard, M.E.Spahr and Petr Novak, *Adv.Mater* **10** (1998) 725 (b) J.A.Wilson, A.D.Yoffe, *Adv.Phys*, **18** (1969)193.

11. R.W. Siegel, *Nanophase Materials, Encyclopedia of Applied Physics*, **11**, VCH Publishers 1994, 173.
12. Composites: A design guide, Terry Richardson, Industrial Press Inc. 200 Madison Avenue, New York, 1987, P-1-12.
13. Gomez-Romero, P. *Adv Mater*, **13** (2001)163. (Review Article) their in
14. H.Shirawa, E.J.Louis, A.G.MacDiarmid, C.K.Chiang and A.Heeger, *J.Chem Soc Chem. Communication* (1977)578.
15. K.Gurunathan, A.Vadivel Murugan, R.Marimuthu, U.P.Mulik, D.P. Amalnerkar, *Mater Chem & Phys*. **61** (1999) 173 (Review Article)
16. (a)G.Gustaffson, Y.Gao, G.M.Treacy, F.Klavetter, N.Colaneri, A.J.Heeger, *Nature*, 357 (1992) 477(b) Y.Yang, A.J. Heeger, *Nature*, **372** (1995) 344
17. (a)Petr Novak, K.Muller, K.S.V.Santhanam, O.Hass, *Chem Rev.* **97** (1997)207; (b)J.C.Carlberg,O.Inganas, *J.Electrochem.Soc.*, **144** (1997) L61.
18. (a) Z.Qi, P.G.Pickup, *Chem.Commun.*1998,15 (b) Z.Qi, P.G.Pickup, *Chem. Commun.* (1998) 2299.
19. (a) K.G.Neoh, K.K.Tan, P.L.Goh, S.W.Huang, E.T.Kang, K.L.Tan, *Polymer*,**40** (1999) 887 (b)S.W.Huang, K.G.Neoh, E.T.Kang, H.S.Han, K.L.Tan, *J. Mater. Chem*, **8** (1998) 1743. (c) S.Pethkar, R.C.Patil, J.A.Kher, K.Vijayamohanan, *Thin Solid Films*, **394** (1999)105.
20. (a) C.Downns, J.Nugent, P.M.Ajayan, D.J.Duquette, K.S.V.Santhanam, *Adv. Mater*, **11** (1999)12 (b) K.Jurewicz, S.Delpeux, V.Bertagna, F.Beguine, E. Frackowiak, *Chem.Phys.Lett* , **347** (2001) 36.
21. (a) S.Maeda, S.P.Armes, *Chem.Mater*,7(1995)171(b) S.Maeda, S.P.Armes, *Synth.Met*, **69** (1995) 171.(c) S.Maeda, S.P.Armes, *J.Mater.Chem*, **4** (1994)935. (d) S.Maeda, S.P. Armes, *J. Colloid Interface Sci.***159** (1993) 257.(e) S.P.Arms, et al *ibid* **174** (1995)510.
22. Wu,C-G.;DeGroot, D.C.;Marcy, H.O.; Schindler, J.L.; Kannewurf, C.R.; Liu. Y.-J.; Hirpo,W.; Kanatzidis, M.G. *Chem.Mater.* **8** (1996) 1992.
23. (a)Lira-Cantu, M.; Gomez-Romero, P. *J. Electrochem. Soc*, **146** (1999) 2029.(b) Shouji, E.; Buttry, D. A.; *Langmuir*. **15** (1999) 669.

24. (a) T.A.Kerr, H.Wu, L.F.Nazar, *Chem.Mater*, 1996, 8, 2005 (b) T.A.Kerr, F.Leroux, L.F.Nazar, *Chem.Mater*, **10** (1998) 2588 (c) L.Wang, J.Schindler, C.R.Kannewurf, M.G.Kanatzidis, *J.Mater.Chem*, **7**(1997)1277.
25. (a) H.Nakajima, G.Matsubayashi, *Chem.Mater* **5** (1993) 423.(b) Y.-J.Liu, M.G. Kanatzidis, *Chem. Mater.* **7** (1995) 1525 (c) M.G.Kanatzidis, R.Bissessur, D.C.DeGroot, J.Schindler, C.R.Kannewurf, *Chem.Mater* **5** (1993) 595.
26. (a) T.Kyotani, T.Mori, A.Tomita *Chem.Mater.* **6** (1994) 2138 (b) H.Shi, T.Lan, T.J.Pinnavaia, *Chem.Mater.* **8** (1996)1584.
27. (a) A.H.Gemeay, H.Nishiyama, S.Kuwabata, H.Yoneyama, *J. Electrochem. Soc.* **142** (1995) 4190. (b) M.Nishizawa, K.Mukai, S.Kuwabata, C.R.Martin, H.Yoneyama, *J. Electrochem. Soc.* **144** (1997) 1923. (c) C.Arbizzani, M. Mastragostino, M.Rossi, *Electro Chem. Comm* **4** (2002) 545.
28. P.G.Romero, M.L.Cantu, *Chem.Mater* **9** (1997)144 (b) M.L.Cantu, P.G.Romero, *Chem.Mater* **10** (1998)698 (c) A.Vadivel Murugan, Chai-Won Kwon, Guy Campet, B.B.Kale, *Active and Passive Electronic components*, **26** (2003) 81-86.
29. (a) C.G.Wu, T.Bein, *Science* **264** (1994)1757, C.G.Wu, T.Bein, *Chem.Mater*, **6** (1994)1109 (b) A.G.Pattantyus-Abraham, M.O.Wolf, *Mater.Res.Soc.Symp.Proc*, **560** (1999) 291.
30. R.Gangopadhyay, A.De, *Chem.Mater*, **12** (2000) 608 (Review Article) their in.
31. S.M.Marinakos, L.C.Brousseau, A.Jones, D.L.Feldheim, *Chem.Mater*, **10** (1998) 1214.
32. (a) A.Okada, Y.Kojima, A.Usuki, M.Kawasumi, Y.Fukushima, T.Kurauchi, O.Kamigaito, *J.Mater.Res.*, **8** (1993)1185. (b) A.Usuki, Y.Kojima, M.Kawasumi, A.Okada, Y.Fukushima, T.Kurauchi, O.Kamigaito, *J.Mater.Res.*, **8** (1993)1179.
33. (a) A. Bsiesy, *Phys. Rev. Lett* **71**, (1993) 637; (b) C.B.Murray, D.B.Norris, M.G.Bawendi, *J.Am.Chem.Soc*, **115** (1993) 8706; (c) D.D.C.Bradley, *Synthetic Metals* **54** (1993) 401. (d) V.L.Colvin, M.C.Schlamp, A.P.Alivisatos, *Nature*, **370** (1994)354; (e) C.Zhang, D.Braun, A.J.Heeger, *J.Appl.Phys*, **73** (1993) 5177.(f) A.Hasselbarth, A.Eychmuller, H.Weller, *Chem.Phys.Lett*, **203** (1993) 271.
34. (a) H.Yoneyama, Y.Shoji, K.Kawai, *Chem.Lett*, (1989) 1067.; (b) O.Ikeda, H.Yoneyama, *J. Electroanal. Chem*, **265** (1989) 323. (c) K.Ogura, N.Endo, M. Nakayama, *J.Electrochem. Soc.* **145** (1998) 3801; (d) K.Kawai, N.Mihara, S.Kuwabata, S.P.Arnes,

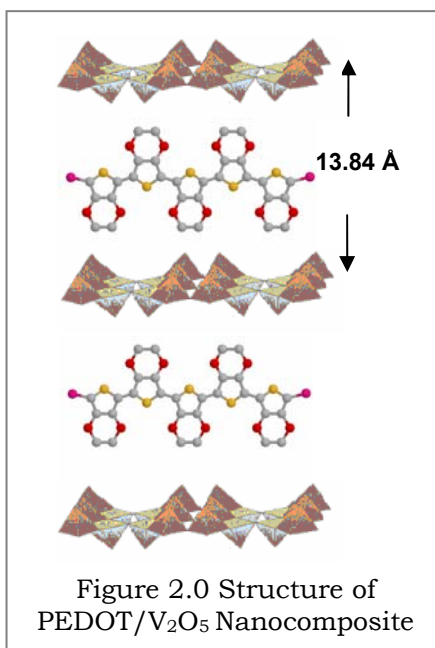
- J. Electrochem. Soc.* **137** (1990) 1793; (e) G.Wang, H.Chen, H.Zhang, Y.Shen, C.Yuan, C.Lu, W.Yang, *Phys.Lett.A*, **237**(1998) 165. (f) H.Yoneyama, Y.Shoji, *J. Electrochem. Soc.* **137** (1990) 3826; (g) Chai-Won Kwon, A.Poquet, S.Mornet, Guy Cmpet, J.Portier, Jin-Ho Choy, *Electro Chem. Comm* **4** (2002)197. (h) J.PZheng, T.R.Jow. *J. Electrochem.Soc*, **142** (1995) L6. (i) Jong-in Hong, In- Hyeong Yeo, Woon-kie Paik, *J. Electrochem.Soc*, **148** (2001) A -156.
35. C.T.Hable, M.S.Wrighton, *Langmuir*, **7** (1991) 1305; (b) A.A.Athawale, B.Deore, *Proceedings of Polymers '99: Int. Symp. On Polymers Beyond AD2000*, New Delhi, India, 1999, p-792.
36. (a) Nano-magnetism; Hernando, A., Ed.; Kulwer Academic Publishers: Dordrecht, The Netherlands, 1993 (b) R.Weissler, M. Papicov, *Rev.Magn, Reson. Med* **4** (1992)1. (c) B.Z.Tang, Y.Geng, J.W.Y.Lam and B.Li., *Chem Mater.* **11** (1999)1581.
37. (a)M.M.Thackeray, W.I.F.David, P.G.Bruce, J.B.Goodenough, *Mater. Res.Bull.* **18** (1983) 461. (b) Scrosati, *Nature* **373** (1995) 557; (c) J.Kim and A.Manthiram, *Nature* **390** (1997)265. (d) A.Manthiram, J.Kim, *Transaction of the SAEST*, **34** (1999) 1.
38. (a)K.V.Kordesch, G.R.Simader, *Chem. Rev* **95** (1995) 191, (b) D.Linden "Handbook of Batteries and Fuel Cells" McGraw-Hill Book Co., New York, (1984).(c) Brian C.H.Steele, Angelika Heinzl, *Nature*, **414** (2001)345; (d) K.V.Kordesch, *J. Electrochem.Soc*, **125** (1978) 77.
39. (a)B.E.Conway, *Electrochemical supercapacitors: Scientific fundamentals and technological applications*, Kluwer Academic/Plenum Publishers, NY,1999. (b) S.Sarangapani, B.V.Tilak and C.P.Chen, *J. Electrochem.Soc*, **143** (1996) 3791. (c)A.K.Shukla, S.Sampath, K.Vijayamohanan, *Current Science*, **79** (2000)12. (d) Andrew Burke, *J.Power Sources*, **91** (2000) 37.
40. (a)The electrochemical Soc., *Interface.fall* 1999, p-21(b) Chemistry in Britain March 2000 p-34-39
41. Electrochemical Power sources, 1.Rechargeable Batteries, A.K.Shukla , S.K.Martha, Resonance, *J. Science Education* , **6** (2001) 52.
42. (a) W.H.Meyer, *Adv. Mater*, **10** (1998) 439. (Review article) and their in.(b) Low temperature batteries, K.Nechev & R.Staniewicz, SAFT, America, 2003.

# NOVEL ORGANO-INORGANIC POLY (3,4-ETHYLENEDIOXYTHIOPHENE) PEDOT/V<sub>2</sub>O<sub>5</sub> NANOCOMPOSITES BY REDOX INTERCALATIVE POLYMERIZATION

## Chapter

# 2

This chapter primarily deals with the preparation of a novel nanocomposite material, PEDOT/V<sub>2</sub>O<sub>5</sub> by inserting Poly (3,4-ethylenedioxythiophene) PEDOT in crystalline V<sub>2</sub>O<sub>5</sub> layers using redox-intercalative polymerization. A systematic study of the synthesis of the nanocomposites by direct *in situ* reaction of 3,4-ethylenedioxythiophene (EDOT) with V<sub>2</sub>O<sub>5</sub>



fine powder shows that upon intercalation, the interlayer spacing of V<sub>2</sub>O<sub>5</sub> expands in two stages, i.e., first from 4.32 to 13.84 Å and further to 19.04 Å. The interlayer separation is consistent with the existence of two phases in the PEDOT/V<sub>2</sub>O<sub>5</sub> system corresponding to the intercalation of one and two mono-layers of PEDOT respectively, in the V<sub>2</sub>O<sub>5</sub> framework. The unique properties of the organo-inorganic composites are investigated by various characterization techniques. The application potential of these nanocomposites as cathode materials in rechargeable lithium batteries is demonstrated by the electrochemical insertion of lithium into the PEDOT/V<sub>2</sub>O<sub>5</sub> nanocomposite by coupling with a Li-foil

anode in 1M LiClO<sub>4</sub> dissolved in a mixture of ethylene carbonate and dimethyl carbonate (50/50 by volume), where an enhancement in the discharge capacity significantly larger than that of pristine V<sub>2</sub>O<sub>5</sub> is clearly observed.

\* Various parts of the work discussed in this chapter have been published in: Journal of Materials Chemistry, 11 (2001) 2470-2475; Journal Power Sources 105 (2002) 1-5; Electrochemistry Communications, 4 (2002) 384-387; Materials Research Society Symposium. Proceedings, 726 (2002) Q11.7.1, Materials Research Society (MRS) Sanfrancisco, California, (USA); Journal of Physical Chemistry B 108 (2004) 10736-10742; Seventh International Symposium on Advances in Electrochemical Science and Technology, (ISAEST-VII) 27-29 Nov, 2002 Chennai, India. (P3.44); International Conference on Nanoscience and Technology (ICONSAT-2003) 17-20 December-2003, Kolkata, India.

## 2.1 Introduction

Recently, soft chemistry ( "*Chimie douce*" ) has been shown to offer many effective methods for the preparation of conducting polymer based nanocomposites for several applications such as light emitting diodes, supercapacitors, chemical sensors, and nonlinear optics.<sup>1-4</sup> In particular, the low temperature processing of such nanocomposites is especially relevant in the area of rechargeable lithium-ion batteries where the composition and structure can be modulated to obtain many advantages such as the formation of amorphous matrices to facilitate lithium ion transport, flexibility with respect to fabrication, high energy density and good cycle life.<sup>5-8</sup> Although early studies on two-dimensional or layered oxides/sulfides of transition metals primarily involved the intercalation of simple, small molecules or ions into the van der Waals gap, later several new classes of these materials were developed based on the extension of these concepts, including the incorporation of macromolecular species.<sup>9,10</sup> In particular, the insertion of conjugated polymers has been extensively examined over the past few years.<sup>11-23</sup> One approach is based on the oxidation of the polymer backbone (p-doping), where the method provides materials that are highly conductive and possess fascinating questions as to the change in their properties upon intercalation. For example, the degree to which the polymer-polymer interactions in the bulk are affected by the polymer host is not clear and questions related to how the polymer-host interactions sequester the polymer chains affecting either the polymer conformation, chain length, and / or bulk electron-transport properties are not fully elucidated. In addition, there is also the possibility of electron or hole transfer between the polymer and the inorganic component especially if the latter is a transition metal oxide with conductive properties.<sup>24</sup> More significantly, the application of either conjugated polymers<sup>25</sup> or transition metal oxide<sup>26</sup> individually as positive electrodes in rechargeable lithium batteries also suggests that when these polymer/ oxide materials are blended together at a "nanoscale" level new properties are possible due to synergistic effects.

During the past several years many conducting polymers have been inserted into layered transition metal oxides to form nanocomposites. For example, several groups have inserted polyaniline, one of the few conducting polymers that is completely air stable in the p-doped form into  $V_2O_5$  to form a nanocomposite.<sup>27-30</sup> Unfortunately, owing to the possible presence of benzidine moieties in the polymer backbone, the application of these systems is limited since

they might yield toxic (carcinogenic) products upon degradation.<sup>31</sup> Consequently, numerous industrial and academic groups have considered many alternatives to polyaniline including the (hetero) aromatic polypyrrole and polythiophene, two more “eco-friendly” systems, as already discussed in *Chapter-1*.<sup>32</sup> In this context it may be better to use poly(3,4 ethylenedioxy thiophene) (PEDOT), one of the recently found excellent conducting polymers, as it has been reported to exhibit enhanced stability compared to polypyrrole and polyaniline.<sup>33,34</sup> Indeed, it appears to be one of the most stable conducting polymers currently available<sup>35</sup> and has been attracting growing interest for applications in supercapacitors<sup>36,37</sup> and lithium ion batteries.<sup>38-40</sup>

In this chapter we report the successful preparation of PEDOT/ V<sub>2</sub>O<sub>5</sub> nanocomposites by a soft method of intercalation, where the resulting nanocomposite shows improved room temperature conductivity and enhanced lithium ion mobility compared to the pristine vanadium pentoxide. The primary objective is to characterize the redox intercalation reactions of EDOT with V<sub>2</sub>O<sub>5</sub> powder and the subsequent polymerization chemistry associated with this system to demonstrate the existence of two phases in the PEDOT/ V<sub>2</sub>O<sub>5</sub> system corresponding to the intercalation of one and two monolayers of PEDOT respectively into V<sub>2</sub>O<sub>5</sub>. These observations are adequately, supported by several physicochemical data and the microstructure of PEDOT/ V<sub>2</sub>O<sub>5</sub> nanocomposites, attributed in part, to the polymer propping open the inorganic layers, thus effectively reducing the electrostatic and steric effects which hinder lithium diffusion through the material. Preliminary measurements of the energy storage ability of PEDOT/ V<sub>2</sub>O<sub>5</sub> nanocomposite during few initial charge-discharge cycles show an excellent capacity of 330 mAhg<sup>-1</sup> compared to that of pristine V<sub>2</sub>O<sub>5</sub>, after coupling these nanocomposites as cathodes with lithium foil anode using 1M LiClO<sub>4</sub> in a mixed electrolyte of ethylene and dimethyl carbonate. To our knowledge, this is the first study of electrochemical Li-insertion into a PEDOT/ vanadium oxide nanocomposite, which shows that the improvement in electrochemical capacity is related to the presence of the conducting polymer in the interlamellar region.

## 2.2 Experimental Section

### 2.2.1 Materials

Vanadium pentoxide(V<sub>2</sub>O<sub>5</sub>, 99%), Lithium foil (99.9%), Lithium perchlorate (LiClO<sub>4</sub>, 99.99%) and dimethyl carbonate (DMC, 99%), from Aldrich were used without any further



purification. Ethylenedioxythiophene (Bayer AG Germany) was distilled under vacuum prior to use; Ethylene carbonate (EC, Prolabo 99%), Chevron Carbon black and PTFE (Teflon) binder were used as received. All the experiments were conducted with double distilled water.

### **2.2.2 Synthesis of Poly (3, 4- ethylenedioxythiophene) / V<sub>2</sub>O<sub>5</sub> Nanocomposites**

Insertion of PEDOT into V<sub>2</sub>O<sub>5</sub> in aqueous medium was carried out by dissolving a given amount of EDOT in double distilled water and refluxing this with crystalline vanadium pentoxide for 12 h. The molar ratio of EDOT/ V<sub>2</sub>O<sub>5</sub> was systematically varied from 0.02 to 0.6 in five different compositions. After completion of the reaction, the solid was filtered off and washed repeatedly with water and acetone until the initial light yellow color in the filtrate was totally absent, and the resultant bluish black powder was dried in air.

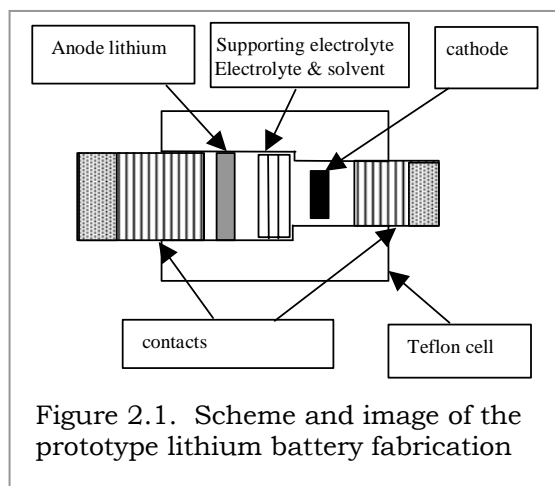
### **2.2.3 Characterization techniques**

Fourier transform infrared (FTIR) spectra were recorded from pressed KBr pellets using a Perkin-Elmer spectrum-2000 FTIR spectrometer. The X-ray powder diffraction studies were carried out with a Bruker AXS D5005 instrument in the range 3- 80° using Cu-K $\alpha$  radiation. X-ray photoemission spectra (XPS) were recorded on VG Microtech Multilab ESCA 3000 spectrometer using non-monochromatized AlK $\alpha$  X-ray source ( $h\nu = 1486.6$  eV). Base pressure in the analysis chamber was maintained at 10<sup>-10</sup> Torr range. The energy resolution of the spectrometer was set at 1.0 eV with AlK $\alpha$  radiation at a pass energy of 50 eV. Binding energy (BE) calibration was performed with Au 4f<sub>7/2</sub> core level at 83.9 eV and BE of adventitious carbon at 284.9 eV was utilized for charging correction with all the samples. The error in all the BE values reported here is within  $\pm 0.1$  eV. Thermogravimetric analysis (TGA/DTA) was performed with a Shimadzu TGA-50 thermal analyzer using dry oxygen as a carrier gas. The TGA experiments were conducted from room temperature to 800° C at a linear heating rate of 10°C min<sup>-1</sup>. Electronic conductivity measurements were carried out on compacted pellets by using a four probe conductivity method, while scanning electron microscopy (SEM) images were taken on a Philips XL-30 microscope after mounting samples on Al stubs with gold coatings. For TEM imaging (TEM model JEM-2010, JEOL) the powder was first dispersed in ethanol by ultrasonication, and then the suspension was deposited drop wise onto a carbon coated copper grid. The electrochemical measurements were performed using a computer controlled Tacussel,

PGS 201T model Potentiostat/galvanostat. Elemental analysis was carried out using inductively coupled plasma optical emission spectroscopy (ICP-OES, Perkin-Elmer 1000) and a CE-Instrument-EA 1110 CHNS-O Analyzer.

## 2.2.4 Electrochemical measurements

Electrochemical measurements were carried out using composite cathodes, prepared by mixing the PEDOT/  $V_2O_5$  nanocomposite powder with carbon black and PTFE binder (70:25:5



by weight), followed by compaction and drying under a primary vacuum for 3 h at 80°C. This composite cathode was subsequently coupled with a lithium foil anode in 1M  $LiClO_4$  dissolved in a mixture of ethylene carbonate and dimethyl carbonate (50/50 by volume) to form an electrochemical cell. All manipulations of air sensitive materials as well as the cell assemblies were carried out in an argon filled glove box and

schematic representation of the prototype lithium battery fabrication is shown in *Figure 2.1*. Using this experimental setup, charge-discharge measurements were performed in galvanostatic mode using a computer controlled potentiostat/ galvanostat.

## 2.2.5 Elemental Analysis

The Vanadium content was determined by ICP-OES analysis of the sample solution that was prepared by placing the composite powder in concentrated sulfuric acid to dissolve  $V_2O_5$  in the composite, followed by dilution with water and filtration to remove the dispersed polymer solid samples. Other elements presents in the polymer were analyzed by CHNS-O analysis. This combined elemental analysis of the nanocomposites give the following information: [a]  $(C_6H_4O_2S)_{0.02} V_2O_5$ : C, 0.84; H, 1.15; S, 0.17; V, 44.53. [b]  $(C_6H_4O_2S)_{0.04} V_2O_5$ : C, 1.35; H, 1.48; S, 0.28; V, 43.67. [c]  $(C_6H_4O_2S)_{0.08} V_2O_5$  : C, 2.12; H, 1.61; S, 1.09; V, 39.15. [d]  $(C_6H_4O_2S)_{0.40} V_2O_5$  :C, 6.92; H, 1.54; S, 3.77; V, 34.36. [e]  $(C_6H_4O_2S)_{0.60} V_2O_5$  :C, 9.01; H, 1.07; S, 4.86 and V, 33.66.

## 2.3 Results and Discussion

The intercalation of EDOT in  $V_2O_5$  is a redox reaction in which EDOT is oxidatively polymerized, concomitantly reducing the vanadium (V) ions to form a relatively semi-crystalline layered material, which is also associated with a dramatic color change to dark blue. Generally if the solvent containing EDOT is able to swell the  $V_2O_5$  powder, the intercalation reaction is observed to be fast whilst no swelling (or intercalation) occurs if  $V_2O_5$  is refluxed with neat EDOT. This could be understood since water is reported to be a good solvent for the completion of polymeric intercalation in oxide layers, in comparison with organic solvents<sup>29</sup> as water

molecules can be expelled from the slightly hydrophobic intragallery space during intercalation, thus allowing the insertion of more polymer. The resultant composite obtained from the reaction between EDOT and  $V_2O_5$  in aqueous medium shows good lamellar order, as judged by the results of the following characterization techniques.

### 2.3.1 FTIR Spectroscopy

Figure 2.2 shows a comparison of the FTIR spectra of different samples of pristine (a)  $V_2O_5$  and (b)-(f) PEDOT/ $V_2O_5$  nanocomposites synthesized with various amount of EDOT as described above. The spectrum for (d) (EDOT/ $V_2O_5$  = 0.08), is discussed as a representative example, since it presents the distinct characteristic bands corresponding to PEDOT (bands in the range 1049 -1600  $cm^{-1}$ ) as well as bands at lower frequencies assigned to  $V_2O_5$  (523 and 759  $cm^{-1}$  for V-O-V stretching modes and 1003  $cm^{-1}$  for V=O stretching). The changes in the position and shape of the vibrational peaks of the vanadium oxide framework are also significant. The V=O peak shifts from 990 to 1003  $cm^{-1}$  while the V-O-V vibrational peaks shift from 852 and 530  $cm^{-1}$  to 758 and

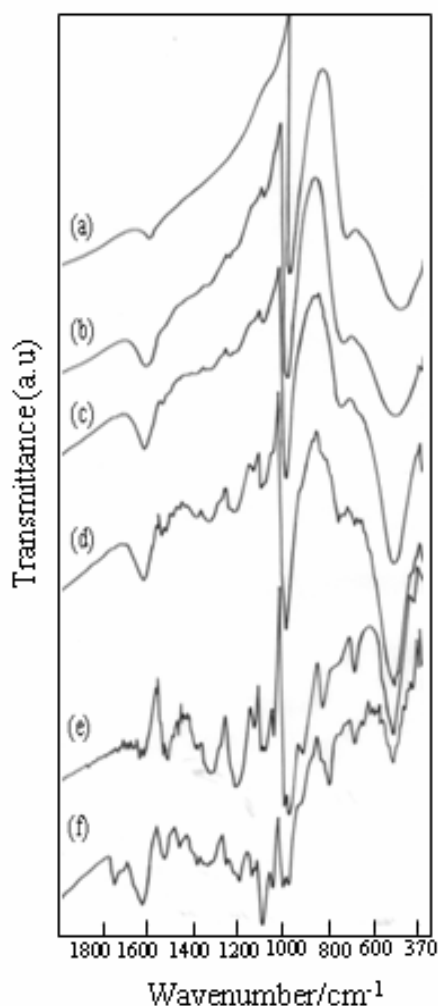


Figure 2.2. FTIR spectra of (a) pristine  $V_2O_5$  and PEDOT/ $V_2O_5$  nanocomposites obtained with different EDOT/ $V_2O_5$  ratios; (b) 0.02, (c) 0.04, (d) 0.08, (e) 0.40, and (f) 0.60.

523  $\text{cm}^{-1}$ , respectively. These changes are attributed to the larger number of  $\text{V}^{4+}$  centers in the nanocomposite. The mechanism of this remarkable all-solid-state intra-lamellar polymerization is presumed to be coupled to the ability of vanadium centers<sup>41</sup> to activate oxygen. Therefore, vanadium oxide plays a direct role in this redox event, which is consistent with its ability to catalyze several oxidation reactions of organic molecules.<sup>42</sup> The qualitative difference between spectra of (e) and (f) relative to those of nanocomposites (b)-(d) demonstrate bands at 1218 and 1105  $\text{cm}^{-1}$  owing to the presence of excess PEDOT in these two samples.

### 2.3.2 Powder X- ray diffraction (XRD)

*Figure 2.3.* shows a comparison of the powder XRD patterns for the PEDOT / $\text{V}_2\text{O}_5$  composite of sample (a)- (e) and pure  $\text{V}_2\text{O}_5$  respectively to demonstrate subtle structural changes upon intercalation. The strongest peak observed at the low angle, corresponding to the (001) plane of the layered  $\text{V}_2\text{O}_5$  structure is directly related to the interlayer spacing. The main features of the  $\text{V}_2\text{O}_5$  diffraction pattern in the composites are clearly modified by the appearance of a sharp diffuse scattering feature and an increase in the intensity of the (001) peak. Within the series of nanocomposites, a clear change in the position of the peak takes place, indicating the difference between samples. In particular, samples (a)-(c) with EDOT/ $\text{V}_2\text{O}_5$  ratios of 0.02 - 0.08 show the (001) peak at  $2\theta$  value from 6.6 - 6.4°, which corresponds to an interlayer spacing of 13.84-14.02 Å., respectively, in comparison with the 4.32Å interlayer spacing of  $\text{V}_2\text{O}_5$ . More interestingly, this peak in the patterns for (d) and (e) is shifted to lower angle, (5.0 to 4.5°), corresponding to an interlayer spacing from 17.8 to 19.04 Å, respectively, which is substantially larger than that found for samples (a)-(c). This behavior is summarized in *Figure 2.3* and also in the inset, where the evolution of  $c$  parameter is shown in relation to the nominal EDOT / $\text{V}_2\text{O}_5$  ratio used in the preparation of each sample. There are two regions with qualitatively different features, which confirm the existence of phases with distinct structures. This suggests that PEDOT intercalation occurs in two steps, leading to the formation of two correspondingly different phases. The first one represents an expansion from 4.32 to 13.84 Å, and can be explained by the monolayer formation of PEDOT. On the other hand, the formation of the second phase, associated with an additional expansion of the  $c$  parameter to 19.04 Å indicates double amount of PEDOT between layers per  $\text{V}_2\text{O}_5$  unit as reported recently for the PANI/ $\text{V}_2\text{O}_5$  system.<sup>30</sup> Thus it is likely that these materials constitute a new PEDOT / $\text{V}_2\text{O}_5$  nanocomposite

phase consisting of a double layer of PEDOT chains intercalated within the  $V_2O_5$  interlayer spacing. (see Scheme 2.1)

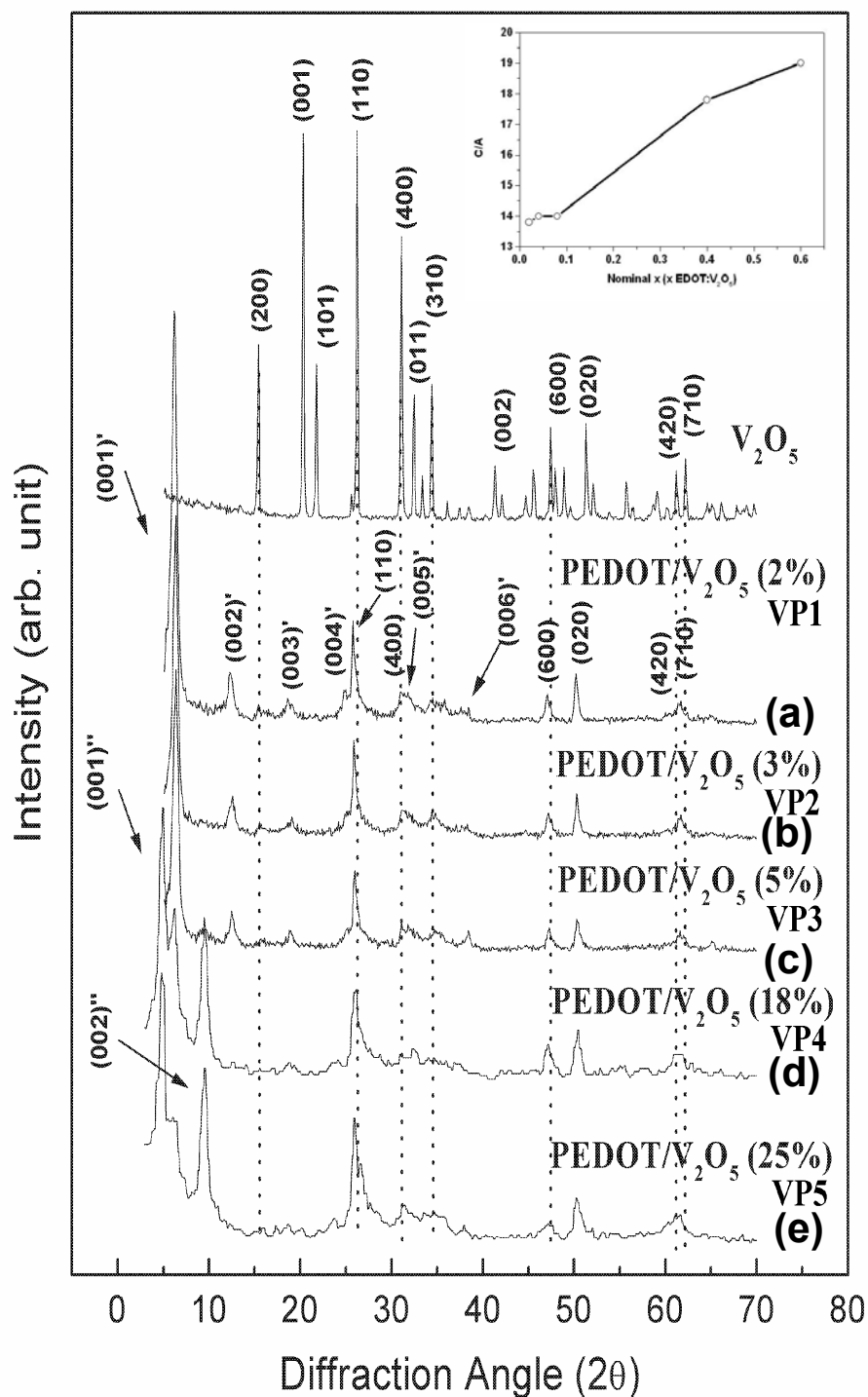
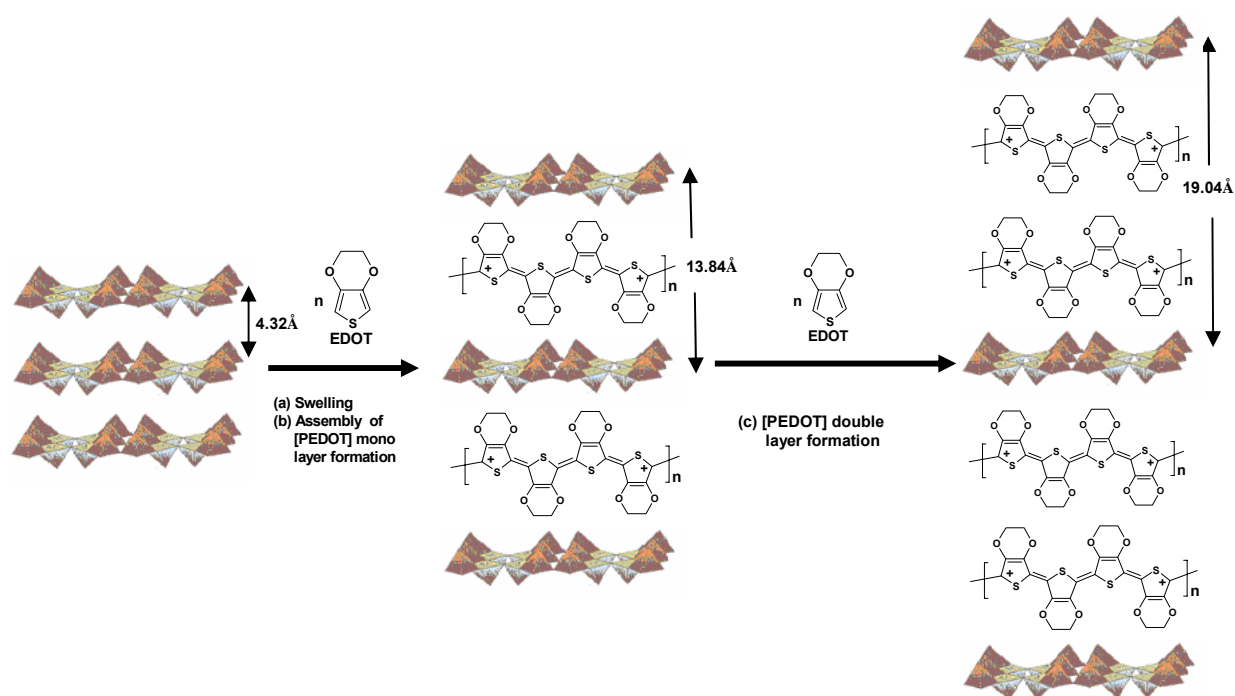


Figure 2.3. Comparative powder X - ray diffraction patterns of  $V_2O_5$  powder and PEDOT/  $V_2O_5$  nanocomposites synthesized with different ratios of EDOT/ $V_2O_5$ . The inset figure shows the interlayer spacing in  $V_2O_5$  ('c' parameter in Å, calculated from the position of 001 peaks) vs. the EDOT/  $V_2O_5$  ratio



**Scheme 2.1. Schematic diagram of the swelling and assembly of monolayer and double layer formation of PEDOT into  $V_2O_5$  layers during the preparation of the nano composite.**

### 2.3.3 X-ray Photoelectron Spectroscopy (XPS)

X-ray photoelectron spectroscopy (XPS) is a surface specific technique to study the polymer-

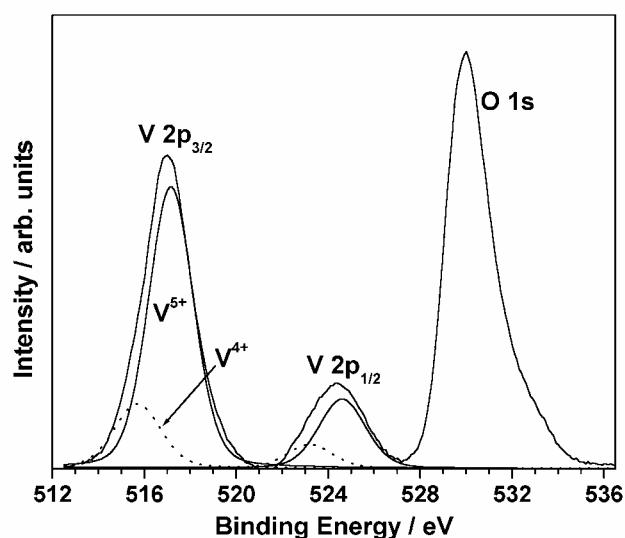


Figure 2.4. X-ray photo electron spectra of PEDOT/ $V_2O_5$  nanocomposite prepared using a EDOT/ $V_2O_5$  ratio of 0.02

$V_2O_5$  interaction and the change in the vanadium ( $V^{5+}/V^{4+}$ ) oxidation state of the sample before and after the redox polymer intercalation. XPS results from both V 2p and O 1s core level of polymer intercalated nanocomposite are shown in *Figure 2.4* after the removal of O 1s X-ray satellite around 518-520 eV and also after Shirley background subtraction. A low binding energy (BE) feature is apparent for  $V^{5+}$  species at 517.2 eV,

although deconvolution of the V 2p core levels clearly shows one additional low BE feature at 515.7 eV, which could be attributed to  $V^{4+}$ . The above BE values are in good agreement with the corresponding BE values of the standard compounds<sup>35</sup>. Using the deconvoluted peak area and the photoionization cross section of the V 2p<sup>3/2</sup> level, the amount of  $V^{4+}$  calculated is, 19 % of the total vanadium, which clearly indicates charge transfer from polymer to  $V_2O_5$  revealing the effectiveness of the interaction between the polymer and  $V_2O_5$ . It is speculated that the above interaction might be through S atom of the polymer, as it is electron-rich; nevertheless, the above suggestion could not be confirmed since the S 2p signal is hardly seen in XPS, perhaps due to low photoionisation cross section.<sup>36</sup>

### 2.3.4 Thermogravimetric Analysis (TGA/DTA)

The thermal stability of these materials in air was examined by TGA experiments. Two distinct stages of decomposition are observed in the thermogravimetry and differential thermal analysis (TGA-DTA) curves as shown in *Figure 2.5*. The first step, up to 120°C, corresponds to

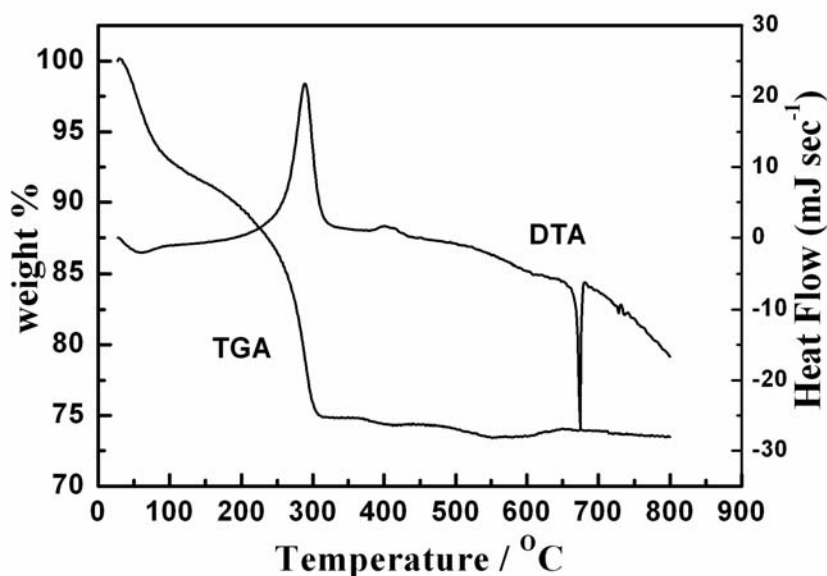


Figure 2.5. TGA-DTA curves of the composite of PEDOT /  $V_2O_5$  synthesized from EDOT/  $V_2O_5$  ratio of 0.08

the removal of the reversibly bound water, whereas the second step at  $\sim 215^\circ\text{C}$  corresponds to the loss of more strongly bound water perhaps bound between the layers. This is followed by a continuous weight loss up to  $\sim 310^\circ\text{C}$  which could be attributed to the combustion of the organic polymer component, which is in good agreement with the exothermic peak in the DTA curve. A subsequent mass gain up to  $650^\circ\text{C}$  can be attributed to the phase transformation (melting) of  $V_2O_5$ .<sup>72</sup> Indeed, further evidence from the DTA curve shows a relatively sharp endotherm at  $650^\circ\text{C}$ , suggesting that the insertion and polymerization of the 3, 4-ethylenedioxythiophene (EDOT) monomer is accompanied by 'sacrificial' reduction of the  $V_2O_5$  layers.

### 2.3.5 Scanning Electron Microscopy (SEM)

The scanning electron microscopic (SEM) images of both  $V_2O_5$  and PEDOT / $V_2O_5$  composites are illustrated in *Figure 2.6* a and b respectively, where the later forms a continuous and relatively homogeneous matrix with a distinct lamellar morphology. Although, the

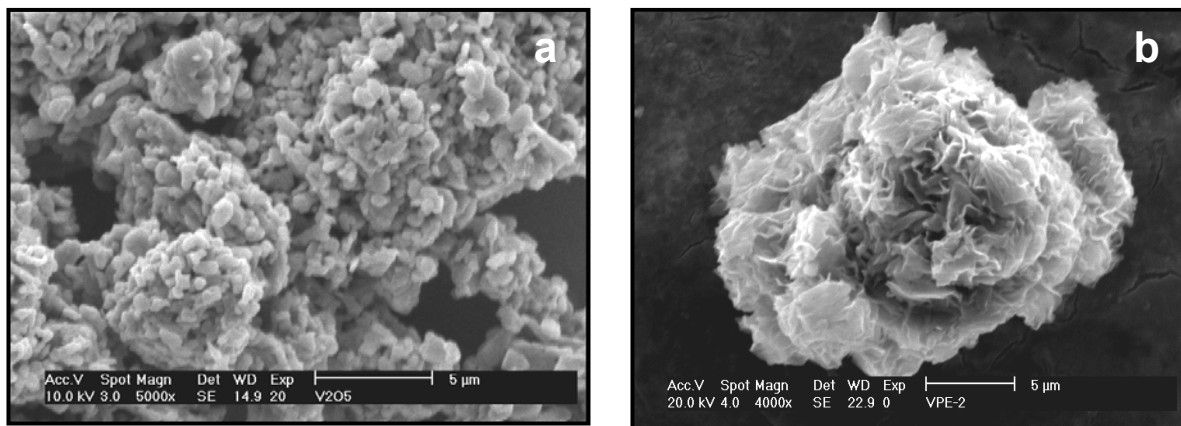


Figure 2.6. SEM micrographs of (a)  $V_2O_5$  and (b) PEDOT/  $V_2O_5$  nano composite synthesized with ratio of EDOT /  $V_2O_5$  is 0.08

incorporation of PEDOT into the  $V_2O_5$  leads to morphological changes in agreement with the results of XRD patterns, these can be seen only at high resolution. More significantly, the SEM images also suggest that there is no bulk deposition of polymer on the surface of the micro-crystallites.

### 2.3.6 Transmission Electron Microscopy (TEM)

A more accurate observation of particle morphology and structure can be realized using transmission electron microscopy (TEM) as illustrated in *Figure 2.7*. In particular particles of nanocomposite consist of well-developed (*a-b*) planes stacked along with *c*-axis (*Figure 2.7a, b*). Interestingly, the stacking length in *c*-direction is much shorter compared with that in both *a* and *b* directions for the hybrids, which would be considered as the enhancement of ‘bidimensionality’. The interlayer spacing of sample (a) has been estimated by measuring the length from one dark line to the nearest one, which gives  $\sim 14 \text{ \AA}$ , a value in good agreement with the XRD results.

More significantly, High resolution-transmission electron microscopy (HR-TEM) image shows nanoribbon morphology of the PEDOT- $V_2O_5$  composite of sample (a), as illustrated in *Figure 2.7c*, thus suggesting that the *in situ* redox intercalative polymerization by soft chemistry



route is topotactic and that it does not disrupt the structure of the host. As can be seen from HRTEM images, the  $V_2O_5$  host consists of several conducting polymer nanoribbons and the low scattering power causes bright contrast for white lines, each about  $\sim 1.4$  nm between two dark fringes of vanadate layers.

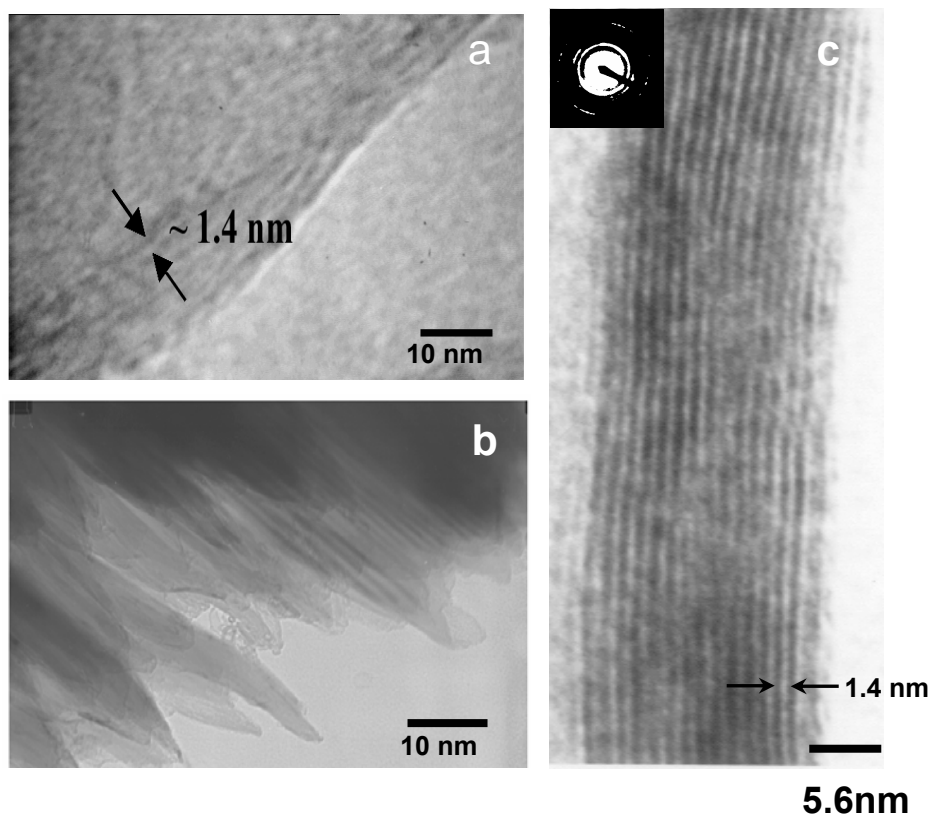


Figure 2.7. TEM images (a), (b) and HRTEM image (c) of PEDOT nanoribbons intercalated into  $V_2O_5$  layers during nanocomposite formation with the ratio of EDOT/  $V_2O_5$  is 0.02

The same ribbon thickness of about 1.384 nm can be evaluated from the most pronounced intensity maximum found in the broad X-ray diffraction pattern  $d(001)$  (Figure. 2.3). Thus, from the HRTEM image of the nanocomposite material, we conclude that highly crystalline vanadium oxide is separated by alternating organic conducting polymer nanoribbons in this hybrid material. This type of a structure of  $V_2O_5$  / PEDOT nanocomposite can be described (Scheme 2.1) by the assembly of well-defined bilayers of single  $V_2O_5$  layers of square pyramidal  $VO_5$  units with PEDOT nanoribbons residing between them. The distance of closest approach between the bilayers is approximately 1.4 nm. This is in good agreement with the recent proposition of

Petkov et al,<sup>54</sup> where a chain based slab structure is found to be responsible for the formation of long nanoribbons in both crystalline  $V_2O_5$  and  $V_2O_5 \cdot nH_2O$  xerogel.

### 2.3.7 Electronic conductivity

The electrical transport of nanocomposite can be understood by considering the insertion of poly(3,4-ethylenedioxythiophene) in  $V_2O_5$  as a composite system in which, two different types of low-dimensional electronic conductors coexist at the molecular level in a dimensionally

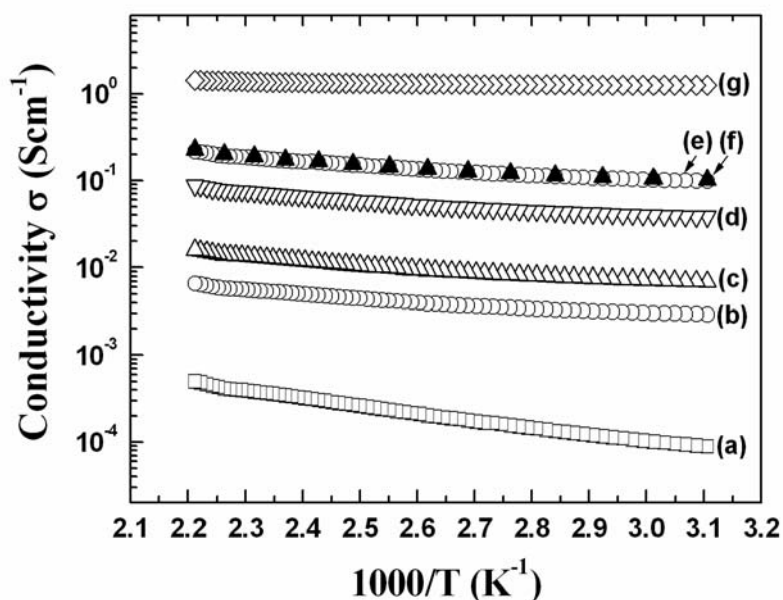


Figure 2.8. Four-probe, variable-temperature electrical conductivity of (a) crystalline- $V_2O_5$  and all PEDOT/  $V_2O_5$  nano composites synthesized with different EDOT/ $V_2O_5$  ratios; (b) 0.02, (c) 0.04, (d) 0.08, (e) 0.40, (f) 0.60 and (g) PEDOT

constrained environment. Two types of charge carriers can be present in these materials, small polarons (electrons) associated with the  $d^1$  ( $V^{4+}$ ) centers on the vanadium oxide lattice, and large polarons on the Poly (3,4-ethylene dioxythiophene) backbone.<sup>29</sup> The actual nature of charge transport would depend on the relative mobility of these two different types of carriers as demonstrated by the fact that the electronic conductivity of PEDOT/ $V_2O_5$  is about  $10^4$  times higher than that of pristine  $V_2O_5$ . In all samples, the conductivity is almost exclusively electronic under our experimental conditions, and increases with temperature as has been observed in most intercalated compounds and conjugated polymers.<sup>12-42</sup> For similar PEDOT/ $V_2O_5$  samples synthesized with different nominal EDOT/  $V_2O_5$  ratios, the room temperature conductivity varies from  $10^{-1}$  to  $10^{-5}$  S  $cm^{-1}$ . The increase in conductivity is probably due to a continued process of growth of the organic polymer network and the conductivity increases as the length of polymer chain increases from (a)-(e) although the exact mechanism may be complex (*see Table 2.1 & Figure 2.8*) involving percolation phenomena.

constrained environment. Two types of charge carriers can be present in these materials, small polarons (electrons) associated with the  $d^1$  ( $V^{4+}$ ) centers on the vanadium oxide lattice, and large polarons on the Poly (3,4-ethylene dioxythiophene) backbone.<sup>29</sup> The actual nature of charge transport would depend on the relative mobility of these two different types of carriers as demonstrated by the fact that the electronic conductivity of PEDOT/ $V_2O_5$  is about  $10^4$  times higher than

**Table 2.1 Comparison of room temperature conductivity, inter layer spacing and open circuit voltage of nanocomposits with the corresponding EDOT/V<sub>2</sub>O<sub>5</sub> ratio**

Name of the materials	Nominal 'x' ('x' EDOT: V <sub>2</sub> O <sub>5</sub> )	Interlayer Spacing (Å)	Electronic Conductivity (σ) S cm <sup>-1</sup>	Discharge capacities* (mAh/g)	Open circuit voltage* (V)
V <sub>2</sub> O <sub>5</sub>	-	4.32	8.78×10 <sup>-5</sup>	241	3.43
Nanocomposite- <b>a</b>	0.02	13.84	2.92×10 <sup>-3</sup>	330	3.74
Nanocomposite- <b>b</b>	0.04	14.00	6.97×10 <sup>-3</sup>	280	3.76
Nanocomposite- <b>c</b>	0.08	14.02	3.84×10 <sup>-2</sup>	304	3.77
Nanocomposite- <b>d</b>	0.40	17.80	9.82×10 <sup>-2</sup>	283	3.62
Nanocomposite- <b>e</b>	0.60	19.04	1.01×10 <sup>-1</sup>	250	3.61

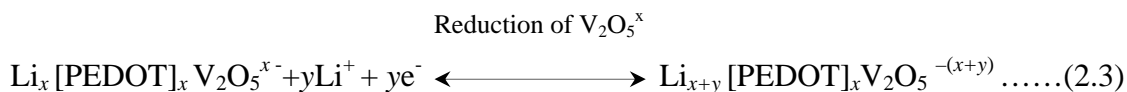
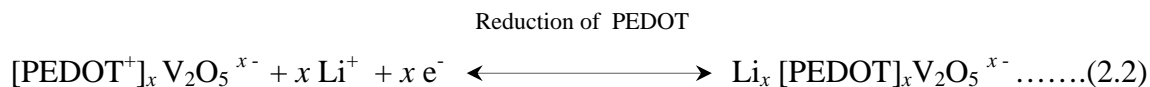
\*The discharge capacity and open circuit voltage (OCV) were obtained from the charge-discharge measurements of V<sub>2</sub>O<sub>5</sub> and PEDOT/ V<sub>2</sub>O<sub>5</sub> nanocomposites synthesized from EDOT/ V<sub>2</sub>O<sub>5</sub> ratio from 0.02 to 0.6, as a cathode material by coupling with lithium metal anode using 1M LiClO<sub>4</sub> in a mixed electrolyte of ethylene and dimethyl carbonate

### 2.3.8 Electrochemical lithium insertion

Vanadium oxide host lattice has been proposed as a good cathode material in secondary Li-batteries, mainly due to its layered structure which is highly suitable for Li-insertion.<sup>43-44</sup> For battery applications, the rate limiting step is reported to be the reduction of V<sub>2</sub>O<sub>5</sub> during discharge accompanied by Li<sup>+</sup> insertion.<sup>45</sup> One common strategy to achieve higher efficiency and lithium uptake is to use high surface area materials, so that the distance over which Li<sup>+</sup> must diffuse through the host material is minimized.<sup>46-50</sup> For example, V<sub>2</sub>O<sub>5</sub> nanotubes have been recently reported to give rise to a discharge capacity of 186 mAhg<sup>-1</sup> compared to 140 mAhg<sup>-1</sup> observed for bulk oxide.<sup>51</sup> Another approach that has not been completely explored yet is the manipulation of the interlayer spacing in these layered materials using various intercalants so as to enhance the rate of Li<sup>+</sup> migration since it is well-known that intercalation leads to changes in the interlayer spacing for layered materials.<sup>52,53</sup> Examples of such intercalants includes pyrrole and aniline, which are known to oxidatively polymerize when intercalated into highly oxidizing materials such as V<sub>2</sub>O<sub>5</sub><sup>15-23</sup>. The electrochemical insertion of Li in V<sub>2</sub>O<sub>5</sub> can be described by the redox eqn.(2.1).



For PEDOT/ V<sub>2</sub>O<sub>5</sub> nanocomposites, we can write analogous electrochemical reactions [eqns. (2.2) and (2.3)] corresponding to the incorporation of lithium ions between the layers.



### 2.3.9 Cyclic Voltammetry

Figure 2.9 shows comparative cyclic voltammograms of (a) crystalline  $\text{V}_2\text{O}_5$ , and two [(b) and (c)] PEDOT/ $\text{V}_2\text{O}_5$  nanocomposites respectively illustrating a drastic change in electrochemical properties induced by the polymer insertion. For example, during the first cathodic scan, from the open-circuit voltage to 2.2 V vs  $\text{Li}/\text{Li}^+$ , the crystalline  $\text{V}_2\text{O}_5$  undergoes a

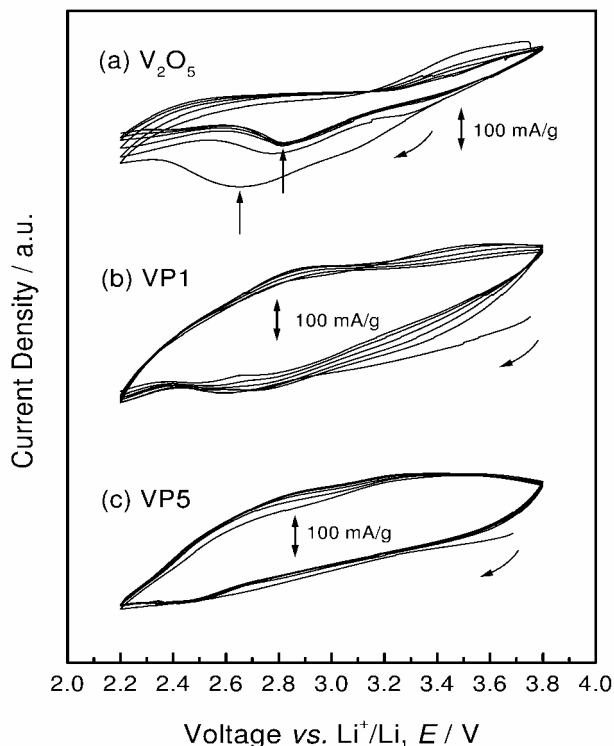


Figure 2.9. Cyclic voltammograms of (a) pristine  $\text{V}_2\text{O}_5$ , and PEDOT/ $\text{V}_2\text{O}_5$  nanocomposites with ratios of EDOT /  $\text{V}_2\text{O}_5$  (a) 0.02 and (c) 0.60 at 0.6 mV/s between 2.2 and 3.8 V vs.  $\text{Li}^+/\text{Li}$ .

well-known phase transformation and the stabilization occurs after the third cycle (Figure 2.9a). The irreversible shift in the cathodic peak from 2.65 V (first cathodic scan) to 2.82 V (third and following cathodic scans) suggests that the structural change is permanent as reported elsewhere.<sup>55-58</sup> This type of voltammogram of crystalline  $\text{V}_2\text{O}_5$  is different from that of vanadium pentoxide xerogels  $\text{V}_2\text{O}_5 \cdot n\text{H}_2\text{O}$  as reported by Anaissi *et al*<sup>58</sup> since, amorphous xerogels are known to exhibit enhanced electrochemical behavior in terms of faradaic yields and reversibility. Further, the weak interactions between the interlamellar layer, allow fast insertion of  $\text{Li}^+$  ions between the ribbons rather than that in the channels of crystalline vanadium pentoxide<sup>58</sup>.

In contrast, for the PEDOT/ $\text{V}_2\text{O}_5$  hybrids, there is no sign of any irreversible structural change (Figure 2.9b,c), although the broad cathodic peak resembles that of 2D- $\text{V}_2\text{O}_5$  compounds.<sup>55-58</sup> The broad and diffuse peak shape can,

therefore, be correlated with the layer stacking derived by the polymer incorporation, as previously deduced from X-ray diffraction data.

### 2.3.10 Charge-Discharge Properties

Figure 2.10. demonstrates plot of potential vs. Li composition for the first two cycles carried out at 15 mA/g in the voltage range of 2.0 ~ 4.2 V (vs.  $\text{Li}^+/\text{Li}$ ) for  $\text{V}_2\text{O}_5$  and 2.0 ~ 4.4 V for the hybrids, corresponding to the uptake of ~ 2 lithium per  $\text{V}_2\text{O}_5$  unit. The pristine  $\text{V}_2\text{O}_5$  shows distinctive plateau due to structural changes from  $\alpha\text{-V}_2\text{O}_5$  to  $\varepsilon\text{-Li}_x\text{V}_2\text{O}_5$ , then further to  $\delta\text{-Li}_x\text{V}_2\text{O}_5$ ,<sup>55</sup> whereas the potential decreases more smoothly down to ~ 2.7 V for the hybrid samples. Similar continuous decrease in potential has also been observed for  $\text{V}_2\text{O}_5$  xerogel<sup>59-62</sup>, 2D- $\text{V}_2\text{O}_5$ <sup>63-67</sup> and polymer/ $\text{V}_2\text{O}_5$  xerogel hybrids<sup>6</sup>, of which the common structural feature is the separation of vanadium oxide layers owing to the presence of interlayer molecules. A plausible

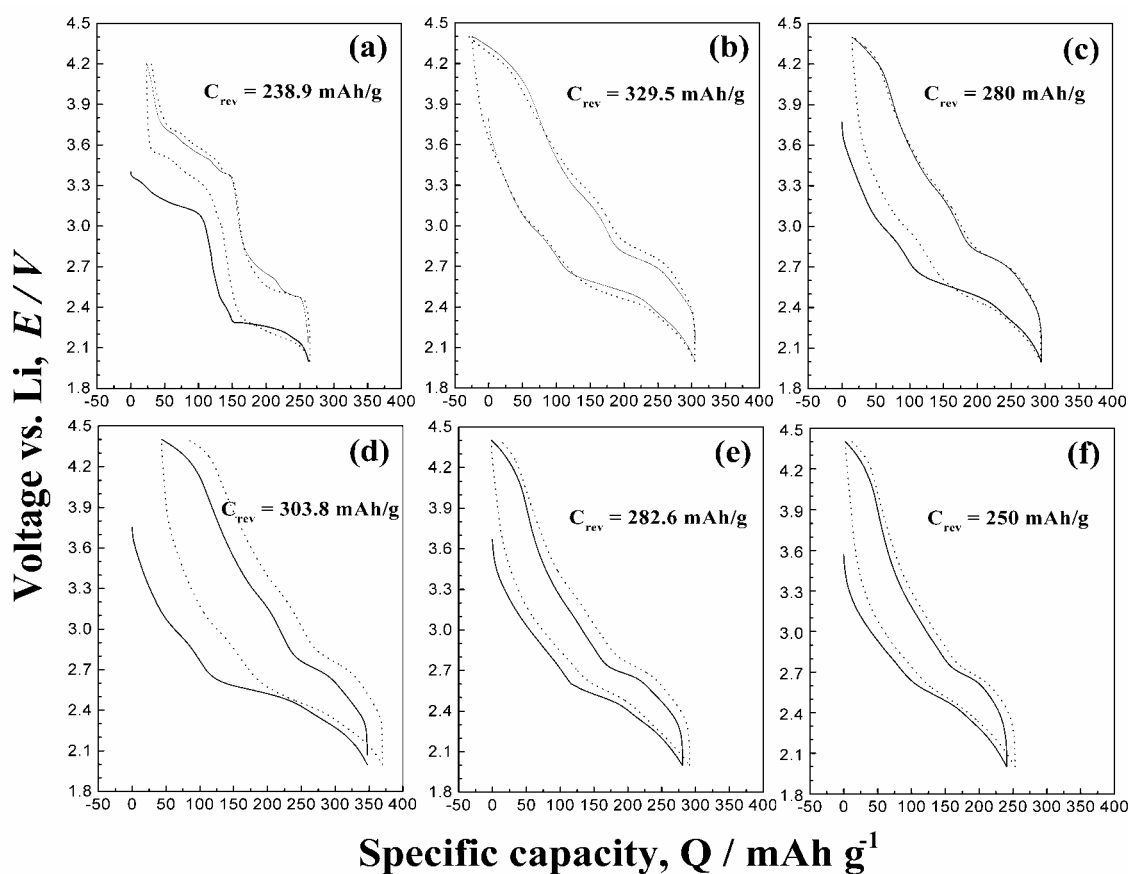


Figure 2.10. Potential vs. specific capacity plots for the first two cycles of (a) pristine  $\text{V}_2\text{O}_5$ , and PEDOT/ $\text{V}_2\text{O}_5$  nanocomposites with different EDOT/ $\text{V}_2\text{O}_5$  ratios (b) VP1, (0.02) (c) VP2, (0.04) (d) VP3, (0.08) (e) VP4 (0.4) and (f) VP5 (0.6). The potential range was set from 2.0 to 4.4 V vs. Li for  $\text{V}_2\text{O}_5$  and all the hybrids. The current density was fixed to 15 mA/g. by coupling with a lithium metal anode in 1M  $\text{LiClO}_4$  in ethylene and dimethylcarbonate using the electrode surface area ~1cm<sup>2</sup>.

explanation is that the disturbed layer stacking derived by the separation of layers which would make structural disorders, (e.g. reduced covalency of bondings between some vanadium and oxygen atoms) thereby creating empty sub-bandgap  $V^{5+}:3d^0$  energy states rather uniformly distributed between  $\sim 3.7$  and  $\sim 2.7$  V.<sup>68, 69</sup>

The next lithium insertion into the pristine  $V_2O_5$  occurs at  $\sim 2.3$  V and is accompanied by the irreversible structural changes to  $\gamma\text{-Li}_xV_2O_5$  phase,<sup>55-58</sup> leading to a transformation of curve

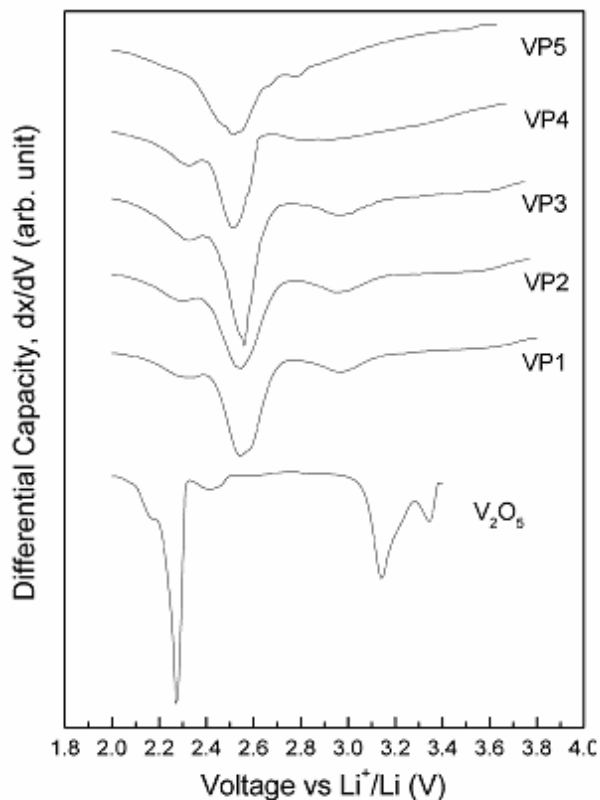


Figure 2.11. The first differential capacity profiles of the first discharges of the pristine  $V_2O_5$  and nanocomposites.

shape in second cycle, while the hybrids display a plateau at  $\sim 2.5$  V like  $V_2O_5$  xerogel or 2D- $V_2O_5$ . The fact that about 2.1 moles of lithium could be inserted per  $V_2O_5$  unit, similar to the case of 2D- $V_2O_5$  compounds, also advocates the above-mentioned assertion. Although, sample (a) and (e) deliver 328 and 251 mAh/g, respectively, the pristine  $V_2O_5$  produces 241 mAh/g on the second discharge. It is worth while to mention that (a) reveals a larger capacity in the first discharge. It would be accounted for the presence of  $V^{4+}$ , which can be easily oxidized by an electrochemical method, as already observed in the case of PPy/ $V_2O_5$  and PTh/ $V_2O_5$  hybrids.<sup>70</sup> Sample (a) shows the largest reversible capacity ( $\sim 330$  mAh/g) among the hybrids, while sample (e) delivers the smallest value ( $\sim 250$  mAh/g). It is

probably due to the fact that the formula weight of sample (a) ( $\sim 185$  g/mol) is smallest and that of sample (e) ( $\sim 217$  g/mol) is largest.

A more accurate inspection of insertion voltage is accomplished by the analysis of differential coulombic capacity profiles of the first discharge (Figure 2.11). The sharp peaks of pristine  $V_2O_5$  are typical traits of the phase transformations, while on the contrary, the hybrids exhibit broad peaks, which would sustain our above argument on the sub-bandgap states  $V^{5+}:3d^0$

energy states rather uniformly distributed between  $\sim 3.7$  and  $\sim 2.7$  V.<sup>68, 69</sup> Sample (a) shows three peaks at 2.9, 2.5 and 2.3 V analogous to PPy/V<sub>2</sub>O<sub>5</sub> and PAni/V<sub>2</sub>O<sub>5</sub> hybrids<sup>70</sup>. In the case of PAni/V<sub>2</sub>O<sub>5</sub> hybrids, the 2.3 V peak could be increased after appropriate oxygen treatment, which could be attributed to the polymer.<sup>71, 72</sup> But in our case, the hybrids also display 2.3 V peak although PEDOT has no redox capacity around 2.3 V. We, therefore, suggest a possibility that the 2.3 V capacity might be from the synergetic interaction between V<sub>2</sub>O<sub>5</sub> layers and polymer chains, and not from the polymers alone. For sample (e), the 2.9 V peak shifts down to 2.7 V, and 2.3 V peak is less obvious, which also supports this thought.

### 2.3.11 Cycle life

In order to clarify the role of the polymer incorporation on the electrochemical performance for extended cycling, the variation of discharge capacity was measured for sample (a) (VP-1) and (e) (VP-5) as representative for monolayer and double-layer incorporated system, respectively (Figure 2.12). Sample (a) maintains capacities over 300 mAh/g for ten cycles. All the hybrids provide larger capacity and better cyclability than the pristine V<sub>2</sub>O<sub>5</sub>. The improved

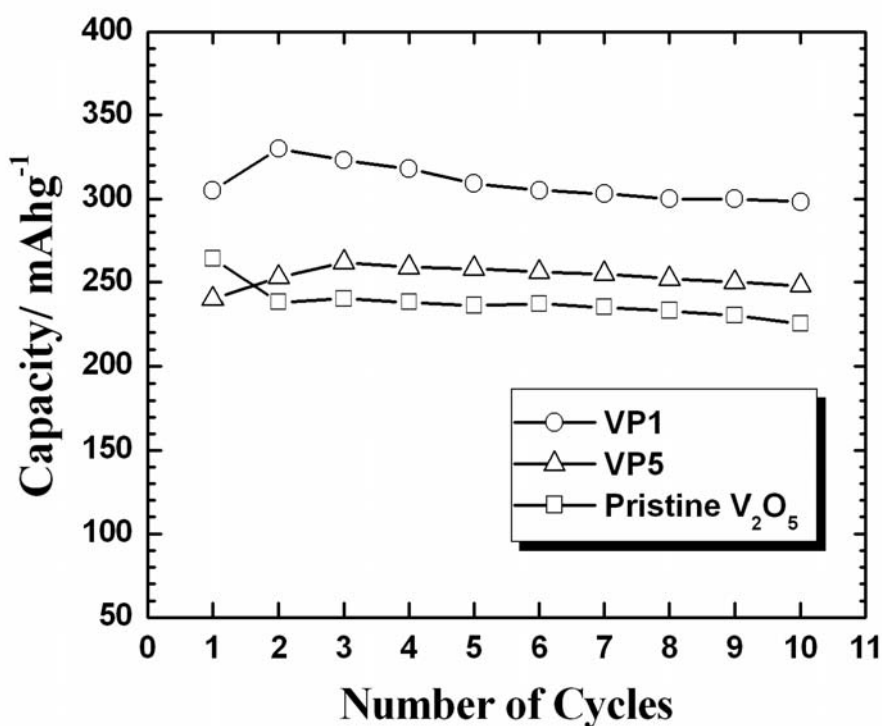


Figure 2.12. Evolution of the discharge capacity with the number of cycles for pristine V<sub>2</sub>O<sub>5</sub> and nanocomposites (VP1, VP5). The data were obtained at a current density of 15 mA/g. The potential range was set to 2.0-4.4 V vs Li

performance is presumably due to a higher electrical conductivity and to the separation between vanadium oxide layers, leading to an enhanced bidimensionality. More rigorous evaluation of charge-discharge behavior for several hundreds of cycles is desired before realizing the industrial applications.

## 2.4 Conclusions

We have found a novel method of interleaving poly (3,4-ethylenedioxythiophene) between the layers of  $V_2O_5$  using a soft process of intercalation. The reaction takes place with the *in situ* polymerization of EDOT within the framework of  $V_2O_5$  with different nominal EDOT/ $V_2O_5$  ratios to give two distinct phases. These two phases can be distinguished by the different interlayer spacing as detected from powder X-ray diffraction patterns. The fact that two distinct phases rather than a continuum of compositions is obtained in this system suggests the existence of a significant interaction between the host and guest beyond simple insertion into the van der Waals gaps and is closer to the formation of true compounds. Analysis of the experimental data presented here suggests that the polymerization proceeds concomitantly with the intercalation. The polymer chains appear fixed in the interlamellar space, and the ring flips observed in the bulk form of PEDOT are frozen in these materials. Therefore, there is considerable bonding interaction between the organic and inorganic components, probably due to hydrogen bonding. In addition, X-ray photoelectron spectrum shows the presence of both  $V^{4+}/V^{5+}$  species in the nanocomposite suggesting the increased number of  $V^{4+}$  centers in the  $V_2O_5$  framework. These results also do confirm the redox intercalation process and charge transfer from the polymer to the  $V_2O_5$  framework while the HRTEM suggests that the interlayer distance of crystalline  $V_2O_5$  expands upon the incorporation of the polymer nanoribbons. According to electrochemical measurements, the hybrids show reversible specific capacities up to  $\sim 330$  mAh/g at 15 mA/g rate between 2 ~ 4.4 V vs.  $Li^+/Li$ . This improvement of electrochemical performance compared with pristine  $V_2O_5$  is attributed to higher electric conductivity and enhanced bidimensionality. The influence of intercalants on  $Li^+$  diffusion rates and charge capacity in the PEDOT/ $V_2O_5$  nanocomposite is increased relative to that for  $V_2O_5$ . The results also suggest that, the polymer nanocomposite acts as a better cathode material than the pristine  $V_2O_5$  material by enhancing lithium diffusion.



## 2.5 References

1. V.L. Colvin, M.C. Schlamp, and A.P. Alivisatos, *Nature* **370** (1994) 354.
2. C. Arbizzani, M. Mastragostino, L. Meneghello, R. Paraventi, *Adv. Mater.* **8** (1996) 331.
3. M-I. Baraton, L. Merhara, J. Wang and K. E. Gonsalves, *Nanotechnology*, **9** (1998) 356.
4. B. R. Mattes, E. T. Knobbe, P. D. Fuqua, F. Nishid, E. W. Chang, B. M. Pierce, B. Dunn and R. B. Karner, *Synth. Metal* **43** (1991) 3183
5. S. Kakuda, T. Momma, T.Osaka, B. G. Appetecchi and B. Scrosati, *J. Electrohem. Soc.* **142** (1995) L1.
6. F. Leroux, B. E. Koene and L. F. Nazar, *J. Electrochem. Soc.* **143** (1996) L181.
7. E. Shouji, and A. D. Buttry, *Langmuir* **15** (1999) 669.
8. A.J. Jacobson, M.S. Whittingham, Intercalation chemistry, Academic Press: New York, 1982
9. J.P. Pereira-Ramos, *J. Power Sources*, **54** (1995)120.
10. J.P. Pereira-Ramos, N.Baffier, G. Pistoia, in lithium batteries, New Materials, Developments and Perspectives. Pistoia, G.; Editor, P.281, Elsevier, Amsterdam (1994)
11. E. Ruiz-Hitzky, *Adv. Mater.* **5** (1993) 334.
12. H. H. Javadi, K. R. Cromack, A. G. Mac Diarmid and A. Epstein, *J. Phys. Rev. B.* **39** (1989) 3579.
13. H. H. S. Javadi, R. Laversanne, A. J. Epstein, R. K. Kohli, E. M. Sherr and A. G. Mac Diarmid, *Synth. Met*, **29** (1989) E439.
14. F. Zuo, M. Angelopoulos, A. G. Mac Diarmid and A. Epstein, *J. Phys. Rev.B*, **39**(1989) 3570.
15. M. G. Kanatzidis, C.-G. Wu, H. O. Marcy and C. R. Kannewurf, *J. Am. Chem. Soc.* **111** (1989) 4139.
16. C.-G. Wu, M. G. Kanatzidis, H. O. Marcy, D. C. Degroot and C. R. Kannewurf, *Polym. Mater. Sci. Eng.* **61** (1989) 969.
17. C.-G. Wu, M. G. Kanatzidis, H. O. Marcy, D. C. Degroot and C. R. Kannewurf, NATO Advanced Study Institute, *Lower Dimensional Systems and Molecular Devices* Metzger R. M.; Ed.; Plenum Press : New York, 1991; P427.
18. M. G. Kanatzidis, H. O. Marcy, D. C. Degroot, C. R. Kannewurf, *Chem. Mater.* **2** (1990) 221.

19. C.-G. Wu, M. G. Kanatzidis, *Symposium on Solid State Ionics* G. Nazri, R. A. Huggins, D. F. Shriver, M. Balkanski, Eds.; *MRS Symp. Proc.* **210** (1991)429.
20. D. C. Degroot, J. L. Schindler, C. R. Kannewurf, Y. -J. Liu, -C. G. Wu and M. G. Kanatzidis, *Symposium on Submicron Multiphase Materials*. R Baney, L. Gilliom, H. Schmidt, and S. -I. Hirano, Eds. *Mater. Res. Soc. Symp. Proc.* 1992, 133.
21. C.-G. Wu, D. C. Degroot, H. O. Marcy, J. L. Schindler, C. R. Kannewurf, T. Bakas, V. Papaefthymiou, W. Hirpo, J. Yes-nowski, Y. -J. Liu and M. G. Kanatzidis, *J. Am. Chem. Soc.* **117** (1995) 9229.
22. M. G. Kanatzidis, C.-G. Wu, H. O. Marcy, D. C. Degroot, J. L. Schindler, C. R. Kannewurf, M. Benz and E. Le Goff, *Supramolecular Chemistry in two and Three Dimensional*; T. Bein, Ed.; *ACS Symp. Ser.* **499** (1992) 194.
23. M. G. Kanatzidis, C.-G. Wu, D. C. Degroot, J. L. Schindler, M. Benz, E. Le Goff and C. R. Kannewurf, *NATO Advanced Study Institute in Chemical Physics of Intercalation*; P. Bernier, J. E. Fischer, S. Roth, S. Solin, Eds.; Plenum Press; New York, 1993; P63.
24. P. Day, *Philos. Trans. R. Soc. London A*, **A314** (1985) 145.
25. F. Bonino and B. Scrosati, *In Materials for Solid State Batteries*: B. V. R. Chowdari, S. Radhakrishna, Eds.; *World Scientific: Singapore*, 1986, P53.
26. J. Desilvestro and O. Haas, *J. Electrochem. Soc.* **137** (1990) 5C
27. Y.J. Liu, D.C. DeGroot, J.L. Schindler, C.R. Kannewurf and M.G. Kanatzidis, *J. Chem. Soc., Chem. Commun.* 1993, 593.
28. M.G. Kanatzidis and C. Wu, *J. Am. Chem. Soc.* **111** (1989) 4139.
29. -G.Wu, D.C. DeGroot, H.O. Marcy, J.L. Schindler, C.R. Kannewurf, Y.-J. Liu, W. Hirpo and M.G. Kanatzidis, *Chem. Mater.* **8** (1996)1992.
30. P.Gomez-Romero and M. Lira-Cantu. *J.Solid.State.Chem.* **147** (1999) 601.
31. F. Lux, *Farbe & Lack*, **104** (1998) 32.
32. L.B. Groenendaal, F. Jonas, D. Freitag, H. Pielartzik and R. J. Reynolds, *Adv. Mater.* **12** (2000)481.
33. G. Heywang and F. Jonas, *Adv. Mater.* **4**, (1992)116.
34. H. Yamato, M. Ohwa and W. Wernet, *J. Electroanal. Chem.* **397** (1995)163.
35. I. Winter, C. Reese, J. Hormes, G. Heywang and F. Jonas, *Chem. Phys.* **194** (1995) 207.
36. S. Ghosh, and O. Ingnas, *Adv. Mater.* **11** (1999)1214.

37. P. Novak, O. Inganas, and R. Bjorklund, *J. Electrochem. Soc.* **134** (1987) 1341.
38. P. Novak, K. Muller, K. S. V. Santhanam, O. Haas, *Chem. Rev.* **97** (1997) 207.
39. M. Dietrich, J. Heinze, G. Heywang and F. Jonas, *J. Electroanal. Chem.* **369** (1994) 87.
40. Tomoyuki Nakamura and Michio Inagaki.; *The 39<sup>th</sup> Battery Symposium in Japan Nov. 25-27, 1998, Sendai, P 283-284.*
41. G. Geneti, D. Pinelli, and F. Trifiro, *J. Mol. Catal.* **59** (1990) 221.
42. R. A. Ross, and C. Fairbridge, *Can. J. Chem.* **62** (1984) 1483.
43. D.B. Le, S. Passerini, A.L. Tipton, B. B. Owens and W. H. Smyrl, *J. Electrochem. Soc.* **142** (1995) L102.
44. D.B. Le, S. Passerini, J. Guo, J. Ressler, B. B. Owens and W.H. Smyrl, *J. Electrochem. Soc.* **143** (1996) 2099.
45. S. Megahed, B. M. Barnett, L. Xie, Eds. *Rechargeable Lithium and Lithium ion Batteries; Electrochemical Society; New Jersey, 1995; Electrochemical Society Proceedings Series PV 94-28.*
46. D.B. Le, S. Passerini, J. Guo, J. Ressler, B. B. Owens and W. H. Smyrl, *J. Electrochem. Soc.* **143** (1996) 2099.
47. M. S.Wittingham, A. J. Jacobson, *Intercalation Chemistry, Academic Press; New York, 1982.*
48. F. R. Gamble, F. J. Disalvo, R. A. Klemm and T. H. Geballe, *Science*, **168** (1970) 568.
49. D. W. Murphy and G. W. Hull, *J. Chem. Phys.* **62** (1975) 973.
50. A. Lerf and R. Schollhorn, *Inorg. Chem.* **11** (1977) 2950
51. M. E. Spahr, P. Stoschitzki-bitterli, R. Nesper, O. Haas and P. Novak, *J. Electrochem. Soc.* **146** (1999) 2780.
52. J. P. Lemmon and M. M. Lerner, *Chem. Mater.* **6** (1994) 207.
53. C. O.Oriakhi and M. M. Lerner, *Chem. Mater.* **8** (1996) 2016.
54. Petkov, V.; Trikalitis, P.N.; Bozin, E.S.; Billinge, S.J.L.;Vogt, T.; Kanatzidis, M.J. *J.Am.Chem.Soc.* **124** (2002)10157.
55. J. M. Cocciantelli, M. Broussely, J. P. Doumerc, J. Labat and M. Pouchard, *J. Power Sources*, **34** (1991) 103.
56. A. Tranchant, J. M. Blengino, J. Farcy and R. Messina, *J. Electrochem. Soc.*, **139** (1992) 1243.

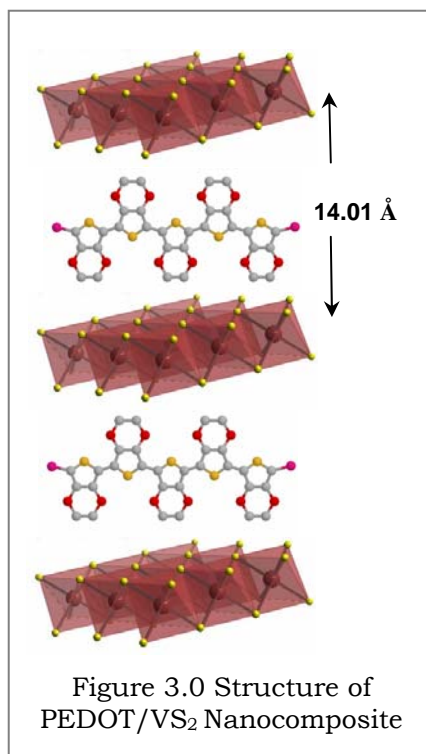
57. K. West, B. Zachau-Christiansen, T. Jacobsen and S. Skaarup, *Solid State Ionics*, **76** (1995) 15.
58. F.J Anaissi, G. J. F Demets, H. E. Toma, *Electrochem. Commun.*, **1** (1999) 332.; J. M. Cocciantelli, M. Ménétrier, C. Delmas, J. P. Doumerc, M. Pouchard, M. Broussely and J. Labat, *Solid State Ionics*, **78** (1995), 143. & J .Livage,. *Chem Mater.*,**3** (1991) 578.
59. H. K. Park and W. H. Smyrl, *J. Electrochem. Soc.*, **141** (1994) L25.
60. K. Salloux, F. Chaput, H. P. Wong, B. Dunn and M. W. Breiter, *J. Electrochem. Soc.*, **142** (1995) L191.
61. F. Coustier, S. Passerini and W. H. Smyrl, *J. Electrochem. Soc.*, **145** (1998) L73.
62. J. H. Harreld, W. Dong and B. Dunn, *Mater. Res. Bull.*, **33** (1998) 561.
63. W. Dong, D. R. Rolison and B. Dunn, *Electrochem. Solid-State. Lett.*, **3** (2000) 457.
64. Y. Sato, T. Nomura, H. Tanaka and K. Kobayakawa, *J. Electrochem. Soc.*, **138** (1991) L37.
65. Y. Sato, T. Asada, H. Tokugawa and K. Kobayakawa, *J. Power Sources*, **68** (1997) 674.
66. Y. Sato, T. Matsueda, H. Tokugawa and K. Kobayawa, *Chem. Lett.*, (1993) 901.
67. M. Ugaji, M. Hibino and T. Kudo, *J. Electrochem. Soc.*, **142** (1995) 3664.
68. Amorphous Semiconductors, 2nd ed., M. H. Brodsky (Ed.), *Topics in Applied Physics* Vol. 36, *Springer-Verlag, Berlin* (1985).
69. G. Campet, S. J. Wen, S. D. Han, M. C. R. Shastry, J. Portier, C. Guizard, L. Cot, Y. Xu and J. Salardennet, *Mater. Sci. Eng. B*, **18** (1993) 201.
70. G. R. Goward, F. Leroux and L. F. Nazar, *Electrochim. Acta.*, **43** (1998), 1307.
71. M. Lira-Cantu and P.Gomez-Romero, *Int. J. Inorg. Mater.*, **1** (1999), 111.
72. M. Lira-Cantu and P.Gomez-Romero, *J. Electrochem. Soc.*, **146** (1999), 2029.

# NEW ORGANO-INORGANIC INTERCALATIVE NANOCOMPOSITE: ENTRAPMENT OF POLY (3,4-ETHYLENEDIOXYTHIOPHENE) BETWEEN VS<sub>2</sub> LAYERS

Chapter

3

This chapter deals with the study of a new class of nanocomposite including their synthesis by direct *in situ* oxidative polymerization of 3, 4-ethylenedioxythiophene (EDOT) with VS<sub>2</sub> as a host material in the presence of an external oxidizing agent. Upon intercalation, the



interlayer spacing of VS<sub>2</sub> expands from 5.79Å to 14.01Å, followed by exfoliation and restacking process facilitating an expansion of the lattice in a direction perpendicular to the dichalcogenide layers. This change in interlayer separation is consistent with the existence of two phases of organic and inorganic species in the nanocomposites corresponding to the intercalation of PEDOT in the VS<sub>2</sub> framework. The resulting nanocomposite is characterized by thermal analysis (TGA), X-ray diffraction, FTIR, SEM, TEM, XPS and four-probe electrical conductivity measurements. The application potential of the nanocomposite as cathode materials for rechargeable lithium batteries is also demonstrated by the electrochemical intercalation of lithium into the PEDOT/VS<sub>2</sub> nanocomposite, where a significant enhancement in the

first discharge capacity is observed (~130 mAh/g) compared to that (80 mAh/g) for pristine VS<sub>2</sub>.

### 3.1 Introduction

The insertion of conjugated polymers in layered host materials and other structurally organized environments is a topic of considerable interest because the resulting organic-inorganic nanostructures can possess novel electrical, structural, and mechanical properties.<sup>1, 2</sup> Such systems can potentially show hybrid properties synergistically derived from both the host and guest.<sup>3</sup> We have already discussed in the second chapter that the redox intercalative polymerization (RIP) of 3, 4-ethylenedioxythiophene in  $V_2O_5$  produces well-ordered compounds with enhanced electrical and  $Li^+$  ion diffusion properties.<sup>4,5</sup> Since, this process works only with suitable oxidizing host, this experimental strategy could be applied to other hosts to extend that they can also accept electrons at low enough potential. However, non-oxidizing hosts such as layered transition-metal sulfides are not suitable for RIP, and hence we must use other synthetic methodologies for introducing polymers into non-oxidizing hosts.<sup>6</sup>

Layered transition-metal sulfides are versatile intercalation hosts which can accommodate the steric demands of a wide variety of guest species.<sup>7</sup> Their ability to form intercalation compounds is known to be strongly dependent on the electronic structure of dichalcogenides.<sup>8</sup> This may be traced to the requirement for the host structure to possess low-lying empty electronic states, as a result of redox process which accompanies the intercalation reaction. Hence, transition metals dichalcogenides of groups 4B and 5B such as  $TiS_2$ ,  $TaS_2$ ,  $NbSe_2$  readily form intercalation compounds with a wide variety of guest species.<sup>9</sup> This may be achieved electrochemically or chemically, either by direct reaction with electron donors such as organic Lewis bases or with chemically reducing agents. In contrast, the group 5B dichalcogenide materials like  $VS_2$  result in a very limited intercalation chemistry, mainly restricted to alkali metals as guest species.<sup>10</sup> It is surprising that  $VS_2$  alone of these group 5B dichalcogenide compounds has not been prepared by direct combination of elements especially since  $VSe_2$  is readily prepared. This is specially significant, since there are only a few reports on the synthesis and characterization of  $VS_2$  despite the considerable current interest in the van der Waals bonding of this metal chalcogenide and also due to the immense utility of this compounds with lithium as potential cathode electrodes in nonaqueous lithium batteries.<sup>11,12</sup> Thus, to broaden the scope of these new hybrid materials to other layered systems, in this chapter we focused on the intercalation of poly (3,4-ethylenedioxythiophene) into  $VS_2$ . The primary objective is to

investigate the successful entrapment of poly (3,4-ethylenedioxythiophene) chains between VS<sub>2</sub> layers, giving rise to a novel nanoscale molecular composite by soft chemistry method of intercalation. More significantly, we attempt to characterize the entrapment of PEDOT with VS<sub>2</sub> powder by *in situ* oxidative polymerization associated with this system to demonstrate the existence of two organic and inorganic phases in the PEDOT/ VS<sub>2</sub> system corresponding to the intercalation of monolayers of PEDOT into VS<sub>2</sub>.

These observations are supported by several physicochemical data and microstructure of PEDOT/ VS<sub>2</sub> nanocomposite, where the resulting nanocomposite shows improved room temperature conductivity with unusual charge-transport and electrochemical properties compared to the polymer free vanadium disulfide. The preliminary electrochemical measurement of PEDOT / VS<sub>2</sub> nanocomposite during the initial charge-discharge cycles shows an enhanced capacity of 130 mAhg<sup>-1</sup> compared to that of pristine VS<sub>2</sub> (i.e., 80 mAhg<sup>-1</sup>) after coupling these nanocomposite as cathode with lithium metal anode using 1M LiClO<sub>4</sub> in propylene carbonate. To our knowledge, this is the first study of the electrochemical Li-insertion into a PEDOT/ vanadium disulfide nanocomposite, which clearly suggests that the improved capacity could be related to the presence of the conducting polymer in the interlamellar region.

## 3.2 Experimental Section

### 3.2.1 Materials

Vanadium disulfide (99%) was synthesized in our laboratory by reacting Li<sub>2</sub>CO<sub>3</sub> and V<sub>2</sub>O<sub>5</sub> under a H<sub>2</sub>S atmosphere. Lithium metal foil (99.9%), LiClO<sub>4</sub> (99.99%) and Dimethyl carbonate (DMC, 99%), purchased from Aldrich were used without any further purification. Ethylenedioxythiophene (Bayer AG Germany) was distilled under vacuum prior to use; Propylene carbonate (PC, Aldrich 99.7%), Carbon black and PTFE (Teflon) binder were used as received. All the experiments were conducted with double distilled water.

### 3.2.2 Preparation of Li<sub>x</sub>VS<sub>2</sub> (0 ≤ x ≤ 1)

The LiVS<sub>2</sub> was prepared according to previously described procedure<sup>13</sup> except that V<sub>2</sub>O<sub>5</sub> was used instead of V<sub>2</sub>O<sub>3</sub>. In brief, stoichiometric amount of Li<sub>2</sub>CO<sub>3</sub> and V<sub>2</sub>O<sub>5</sub> were mixed thoroughly and heated in a graphite crucible under a H<sub>2</sub>S atmosphere at 500°C for 10 h and the resultant product was powdered and further heated in H<sub>2</sub>S atmosphere at 700°C for 24 h and subsequently cooled down slowly.



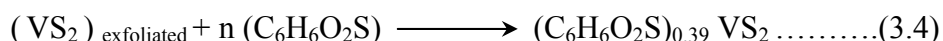
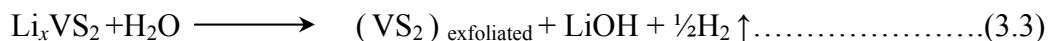
Iodine solutions of ~0.2N prepared from freshly sublimed I<sub>2</sub> and acetonitrile, freshly distilled from P<sub>2</sub>O<sub>5</sub> were standardized with standard sodium thiosulfate. Li<sub>x</sub>VS<sub>2</sub> (0 ≤ x ≤ 1) bronze was prepared by the oxidation of LiVS<sub>2</sub> with iodine in acetonitrile according the equation



In a typical procedure, Li<sub>x</sub>VS<sub>2</sub> (1.32 g) was treated with 50 ml of Iodine solution in acetonitrile (~ 0.24 N) and stirred. Within five minutes the solution was colorless and the stirring was continued for 28 h. VS<sub>2</sub> was prepared with slight excess of Iodine solution, which was titrated after filtration. Inductive Coupled Plasma Optical Emission Spectrometer (ICP-OES, Perkin-Elmer 1000) confirmed the absence of Li in VS<sub>2</sub> and X-ray fluorescence indicated the absence of iodine. EDAX analysis and CHNS-O elemental analyzer confirmed the stoichiometry as [V 25.5; S 45.1] VS<sub>1.768</sub>. Furthermore, X-ray diffraction pattern confirmed the compound as hexagonal P3m1 (CdI<sub>2</sub> type) with *a* = 3.218Å, *b*=3.218 and *c* =5.698Å; α= 90° β= 90° γ=120° which is in good agreement with the reported structural parameters.<sup>11,13</sup>

### 3.2.3 Synthesis of Poly (3,4-ethylenedioxythiophene) / VS<sub>2</sub> Nano-composite

0.202 g of Li<sub>x</sub>VS<sub>2</sub> was exfoliated in 20 ml of water by sonication for 0.5 h to form a suspension with a concentration of 0.08 g ml<sup>-1</sup> followed by refluxing for 16 h. To this suspension, 3,4-ethylenedioxythiophene (EDOT) monomer (4.6 mmol) was added drop wise and was refluxed further for 0.5 h to ensure complete mixing. Then 8.5 g of iron (III) chloride (FeCl<sub>3</sub>) in 10 ml water was added drop wise in to this suspension under refluxing condition for another 2 h. The blue-black powder was washed with excess of ethanol to remove unreacted monomer present in the composite and the excess of FeCl<sub>3</sub> after the reaction was removed by repeated washing with water unless the filtrate became colorless.



The Vanadium content was determined by Inductive Coupled Plasma Optical Emission Spectrometer (ICP-OES) analysis after dissolving in concentrated sulfuric acid followed by



dilution with water and filtration to remove the dispersed polymer. The other elements (C,H,S,O) were analyzed by CHNS-O analyzer and a combined analysis confirmed the stoichiometry of pure VS<sub>2</sub> [V=25.5 %; S=45.1%] as VS<sub>1.768</sub> and nanocomposite as (C<sub>6</sub>H<sub>4</sub>O<sub>2</sub>S)<sub>0.39</sub> VS<sub>2</sub>: C, 6.92; H, 1.54; S, 48.97; V, 24.63.

### 3.2.4 Characterization techniques

Fourier transform infrared (FTIR) spectra were recorded from pressed KBr pellets using a Perkin-Elmer spectrum-2000 FTIR spectrometer. The X-ray powder diffraction was carried out with a Bruker AXS D5005 instrument from 3- 80° using CuK $\alpha$  radiation. Thermogravimetric analysis (TGA) was performed with a Shimadzu TGA-50 thermal analysis system using dry oxygen as a carrier gas. The TGA experiments were conducted from room temperature to 800° C at a linear heating rate of 10° C per minute. Electronic conductivity was measured on compacted pellets using a four probe conductivity method.

X-ray photoemission spectra (XPS) were recorded on VG Microtech Multilab ESCA 3000 spectrometer using non-monochromatized AlK $\alpha$  X-ray source (hv = 1486.6 eV). Base pressure in the analysis chamber was maintained at 10<sup>-10</sup> Torr range. The energy resolution of the spectrometer was set at 1.0 eV with AlK $\alpha$  radiation at a pass energy of 50 eV. Binding energy (BE) calibration was performed with Au 4f<sub>7/2</sub> core level at 83.9 eV and BE of adventitious carbon (284.9 eV) was utilized for charging correction with all the samples. The error in all the BE values reported here is within  $\pm 0.1$  eV. Scanning Electron Microscopy (SEM) was carried out with Philips XL-30 microscope at an accelerating voltage of 20 kV after mounting samples on Al stubs with gold coatings. The Elemental analysis was carried out by Inductive Coupled Plasma Optical Emission Spectrometer (ICP-OES, Perkin-Elmer 1000) and CE-Instruments-EA 1110 CHNS-O Analyzer.

### 3.2.5 Electrochemical measurements

The electrochemical measurements were performed using a button-type cell configuration with the help of a computer-controlled PGS201T (Tacussel) potentiostat/galvanostat system. The working electrode was prepared by mixing the PEDOT/ VS<sub>2</sub> nanocomposite powder or pristine VS<sub>2</sub> with carbon black and PTFE binder (70:25:5) by weight, followed by compaction and drying under a primary vacuum for 3 hrs at 80°C. The electrolyte was 1M LiClO<sub>4</sub> in PC and a

lithium foil was used as the anode. A constant current of 0.5-0.75 mA was applied between 1.0 and 3.0 V (vs.  $\text{Li}^+/\text{Li}$ ) for charge/discharge experiments. Cyclic Voltammetry was conducted on similar working electrodes by scanning the potential between -1.0 and 1.0 V vs.  $\text{Ag}/\text{Ag}^+$ , at 0.6 mV/s rate in 1M  $\text{LiClO}_4$  in 1:1 mixture (by volume) of EC/DMC and a Pt foil was used as the anode.

### 3.3 Results and Discussion

#### 3.3.1 FTIR Spectroscopy

Figure 3.1 shows a comparison of the FTIR spectra of PEDOT/  $\text{VS}_2$  nanocomposite with that of both individual components of  $\text{VS}_2$  and poly (3,4-ethylenedioxythiophene). The 500-1500  $\text{cm}^{-1}$  region of the infrared spectrum is particularly sensitive to C-H vibrations and hence any shift

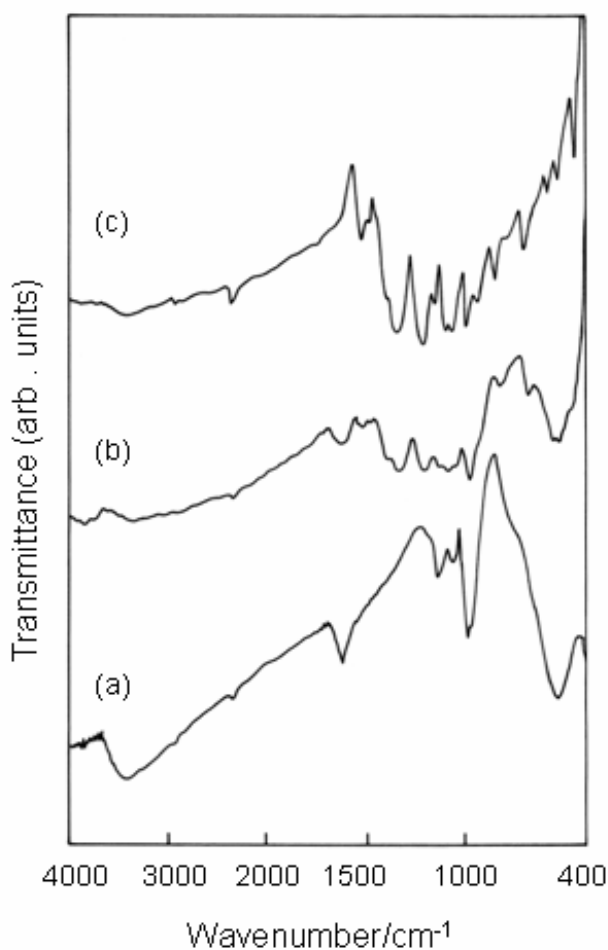


Figure 3.1. FTIR spectra of the (a)  $\text{VS}_2$  (b) PEDOT/ $\text{VS}_2$  nanocomposite (c) PEDOT

in the region can be used to identify changes in the polymer structure during the nanocomposite formation. The positions of the vibrational peaks arising from the encapsulated PEDOT are close to those of pure PEDOT polymer peak vibrations at 1520 and 1388  $\text{cm}^{-1}$  attributed to the stretching of C=C and C-C in the thiophene ring.<sup>14-15</sup> Further vibration from C-S bond in the thiophene ring can be seen at 835 and 680  $\text{cm}^{-1}$  respectively<sup>16-17</sup> and other vibrations at 1142-1128, 1093-1076 and 1052-1047  $\text{cm}^{-1}$  could be assigned to stretching in the alkylenedioxy group.<sup>14-17</sup> Doping induced bands originating from changes in the conjugated backbone due to electron withdrawing (oxidation) from the polymer chain and counter balance also seen during polymerization do appear at

1332, 1202, 1142, 1048 and 918  $\text{cm}^{-1}$  which are interpreted to be from the stretching in the ethylenedioxy ring and from the C-S bond after doping with  $\text{Cl}^-$ .<sup>14,15</sup> A Comparison of the PEDOT/  $\text{VS}_2$  spectrum with that of pure  $\text{VS}_2$  confirms the presence of  $\text{V}^{4+}$  oxidation state in the composite. There is no significant change in the features of both V=S and V- S -V peaks, which could be attributed to the greater number of  $\text{V}^{4+}$  centers present in the nanocomposite. While the positions of the peaks 529, 562 and 978  $\text{cm}^{-1}$  are due to the  $\nu$  (V-S-V) doubly bounded  $\text{S}^{2-}$ , doubly bridged  $\text{S}^{2-}$  and  $\nu$  (V=S) terminal S stretches respectively for  $\text{VS}_2$  are slightly shifted to higher wave numbers, suggesting that the  $\text{VS}_2$  layers in the nanocomposite are oxidized.

### 3.3.2 Powder X- ray diffraction (XRD)

Figure 3.2 shows a comparative XRD patterns of both pristine  $\text{VS}_2$  and poly (3,4-ethylenedioxy thiophene) PEDOT/  $\text{VS}_2$  nano composite. The  $\text{VS}_2$  prepared by this method is stable in air and the compound is hexagonal ( $\text{CdI}_2$  type) with  $a = 3.217\text{\AA}$  and  $c = 5.712\text{\AA}$  as

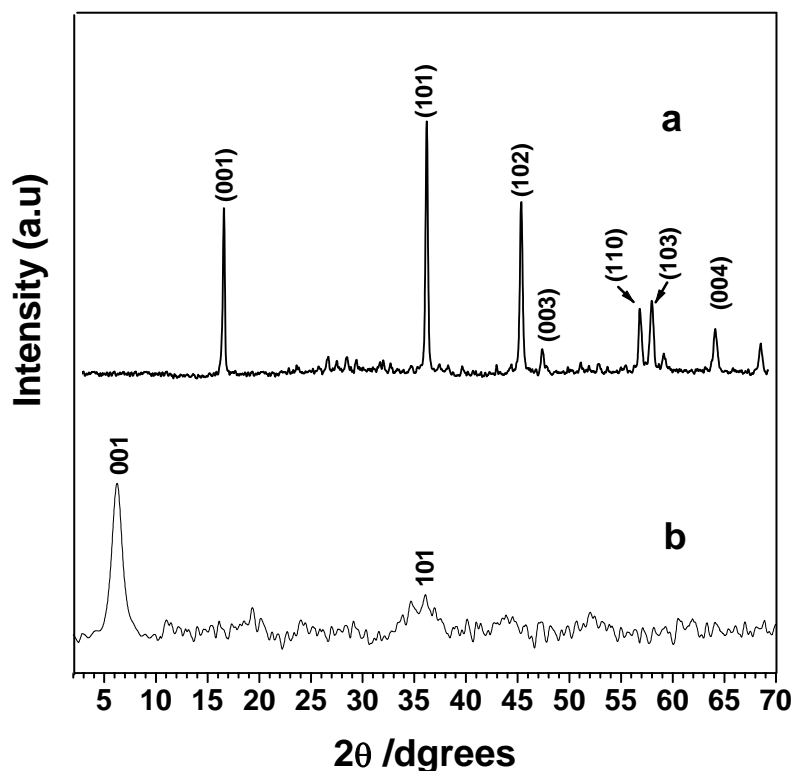
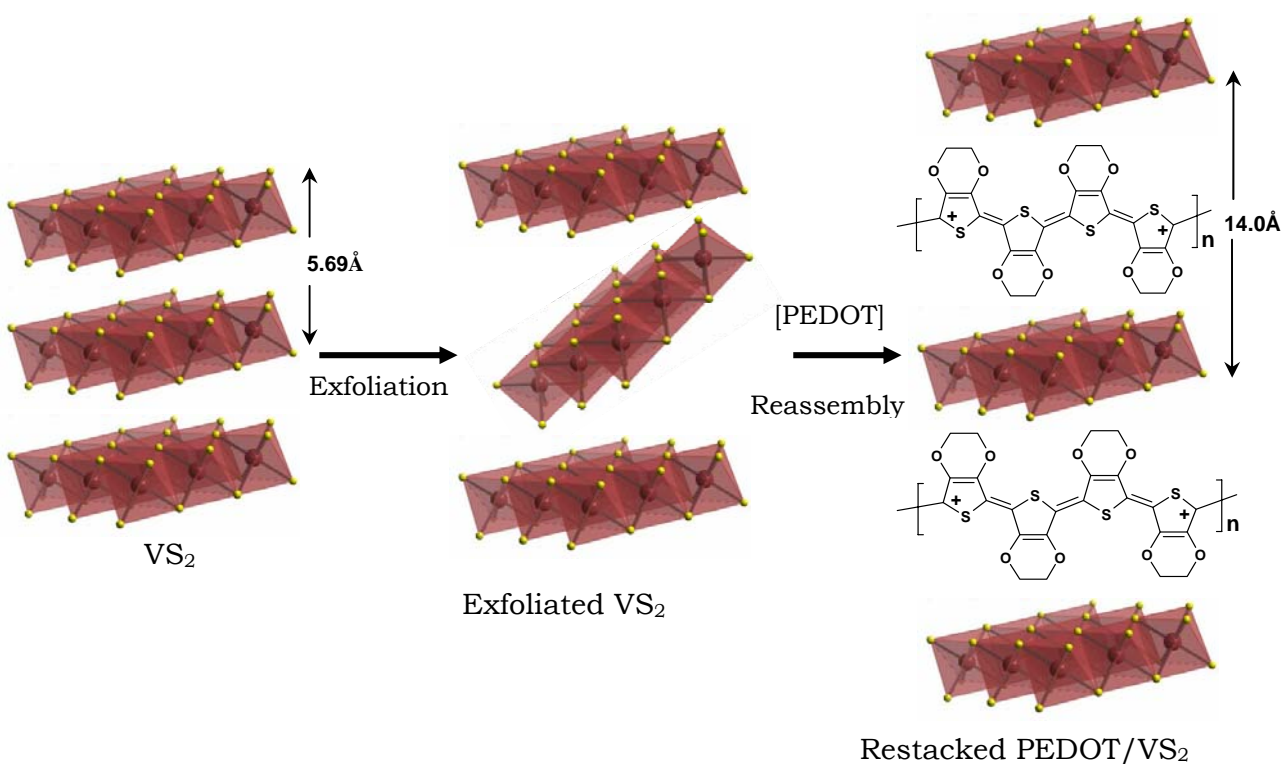


Figure 3.2. X-ray diffraction patterns of (a)  $\text{VS}_2$  (b) PEDOT/ $\text{VS}_2$  nanocomposite

demonstrated by the powder diffraction, (Figure 3.2a).<sup>11</sup> In comparison, the X-ray diffraction pattern of composite (Figure 3.2 b) reveals an increase in the interlayer distance of the pristine disulfide,  $\text{VS}_2$ , from 5.712 to 13.90 $\text{\AA}$ , indicating substantial incorporation of organic conducting polymeric material between the layers. However, the sharp and intense peak observed at the low angle corresponding to the (001) plane of the layered well

stacked  $\text{VS}_2$  structure could be directly related to the interlayer spacing. Thus the main features of the  $\text{VS}_2$  diffraction patterns in the composites are clearly modified by the appearance of a sharp

diffused scattering feature and an increase in the intensity of (001) peak. In addition, the XRD characterization of nanocomposite has shown that the change in interlayer distance is consistent with the interstitial PEDOT chains being oriented with the planes of the thiophene rings perpendicular to the layers. The introduction of polar substituents to thiophene favors a perpendicular orientation of the guest in the interlayer space, permitting a higher degree of their incorporation. Accordingly, a high degree of ordering along the axis perpendicular to the layers is evident in our (PEDOT)<sub>0.39</sub>/VS<sub>2</sub> nanocomposite from the intense sharp peaks that are obtained. These results suggest that the polymer chains lie parallel to each other in the “valleys” of the disulfide sheets and this high degree of ordering has already been supported by several reports.<sup>18</sup> Thus it is likely that these materials constitute a new PEDOT / VS<sub>2</sub> composite phase consisting of a monolayer of PEDOT chains intercalated within the VS<sub>2</sub> interlayer spacing. (see Scheme 3.1)



**Scheme 3.1. Schematic diagram of the exfoliation and reassembly of monolayer formation of PEDOT into the VS<sub>2</sub> layers during the preparation of the nanocomposites**

### 3.3.3 X-ray Photoelectron Spectroscopy (XPS)

PEDOT and PEDOT/ $\text{VS}_2$  composite materials were subjected to XPS analysis and the results from vanadium 2p, oxygen 1s, sulfur 2p and carbon 1s core levels of the above samples are shown in *Figure 3.3 a, b and c*, respectively. Composite materials were made into pellets and the surface was scraped *in situ* in the XPS spectrometer to remove any atmospheric degradation on the composite surface. The PEDOT/ $\text{VS}_2$  surface analyzed prior to scraping (not included) shows large amount of oxidized V and S species- $\text{VOS}$ ,  $\text{VO}_x$  and  $\text{SO}_x$ , respectively. Although the contamination level has decreased after a thorough scraping, the presence of a large amount of oxidized species clearly indicates that the  $\text{VS}_2$  could have undergone oxidation during the oxidative polymerization of EDOT using  $\text{FeCl}_3$ . Another possibility is the slow atmospheric

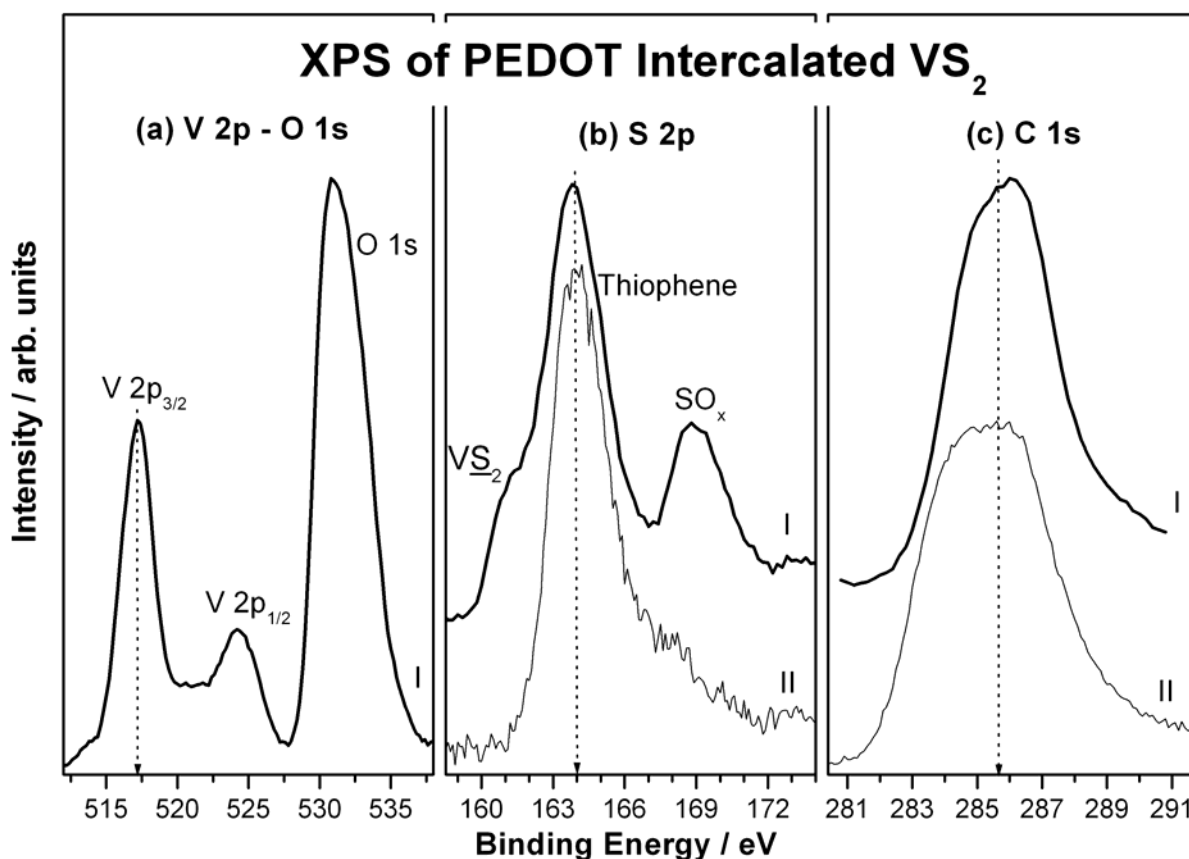


Figure 3.3 XPS of (a) V 2p and O 1s core levels, (b) S 2p core level and (c) C 1s core level from PEDOT intercalated  $\text{VS}_2$  (I) and PEDOT (II). PEDOT/ $\text{VS}_2$  results were recorded after scraping the surface.

oxidation causing the transformation of  $\text{V}^{4+}$  to  $\text{V}^{5+}$  state. The BE value observed for vanadium  $2p_{3/2}$  core level corresponds to  $\text{V}_2\text{O}_5$  type species and the presence of a large amount of oxygen at

531 eV (after keeping longer period in air) indicates that  $\text{VS}_2$  is not stable. Further S 2p core level from PEDOT/ $\text{VS}_2$  shows sulfur from  $\text{VS}_2$ , thiophene units and sulfur oxidized species all at increasing BE values in *Figure 3.3b*. In comparison, Carbon 1s core level from PEDOT and PEDOT/ $\text{VS}_2$  shows essentially the same features, except for a shift in BE which is likely due to the overall oxidation.

### 3.3.4 Thermogravimetric Analysis (TGA)

The thermal analysis of  $\text{VS}_2$  and PEDOT/ $\text{VS}_2$  nanocomposite of these materials in air was carried out to understand their relative stability. A comparative differential thermal analysis (TGA) curve of pure crystalline  $\text{VS}_2$  and  $\text{VS}_2$ / PEDOT nanocomposite is shown in *Figure 3.4*.

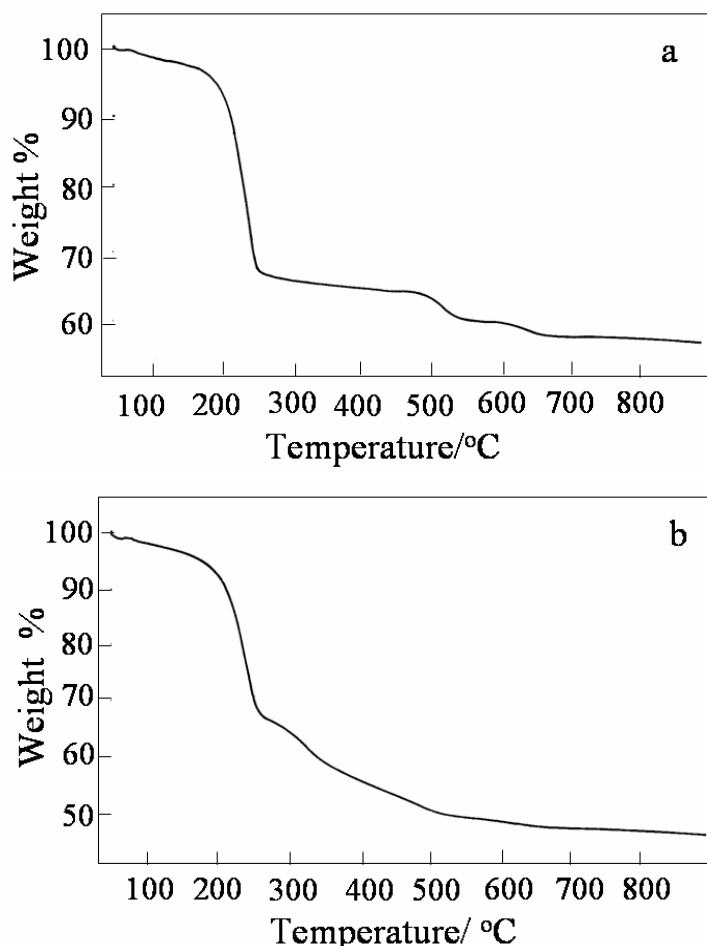


Figure 3.4. Thermal analysis (TGA) of (a) pristine  $\text{VS}_2$  (b) PEDOT/ $\text{VS}_2$

The TG curve shows a two step decomposition of the intercalated PEDOT/ $\text{VS}_2$  nanocomposite (*Figure 3.4b*). The mass loss which occurs at the first step, up to 245°C, can be understood in terms of the loss of sulfur molecule by the decomposition of  $\text{VS}_2$  present in the nanocomposite. This is evidenced by the differential thermal analysis (TGA) curves of pristine  $\text{VS}_2$  shown in *Figure 3.4a*. This mass loss is followed by a continuous weight loss up to  $\sim 500^\circ\text{C}$ , which can be attributed to the complete decomposition of polymer intercalated into  $\text{VS}_2$  layers. However, the mass continues to decrease slowly and the curve does not show a precise ending and this

could be attributed to the subsequent oxidation of vanadium  $\text{V}^{4+}$  into higher oxidation state of  $\text{V}^{5+}$  followed by a phase transformation.

### 3.3.5 Scanning Electron Microscopy (SEM)

Scanning electron micrographs (SEM) of both  $\text{VS}_2$  and PEDOT /  $\text{VS}_2$  composite are illustrated in *Figure 3.5a,b* respectively. It is apparent that pristine  $\text{VS}_2$  sample comprises of flat particles, about  $1\mu\text{m}$  thick and  $3\text{-}10\mu\text{m}$  in diameter. These, however, form large agglomerates, ranging from  $5\text{-}50\mu\text{m}$ , after the polymer intercalation between  $\text{VS}_2$  layers, indicating a relatively homogeneous matrix with layer morphology. It is evident that the incorporation of PEDOT into the  $\text{VS}_2$  accompanies morphological changes in agreement with the results of XRD patterns, which can be seen only under high resolution.

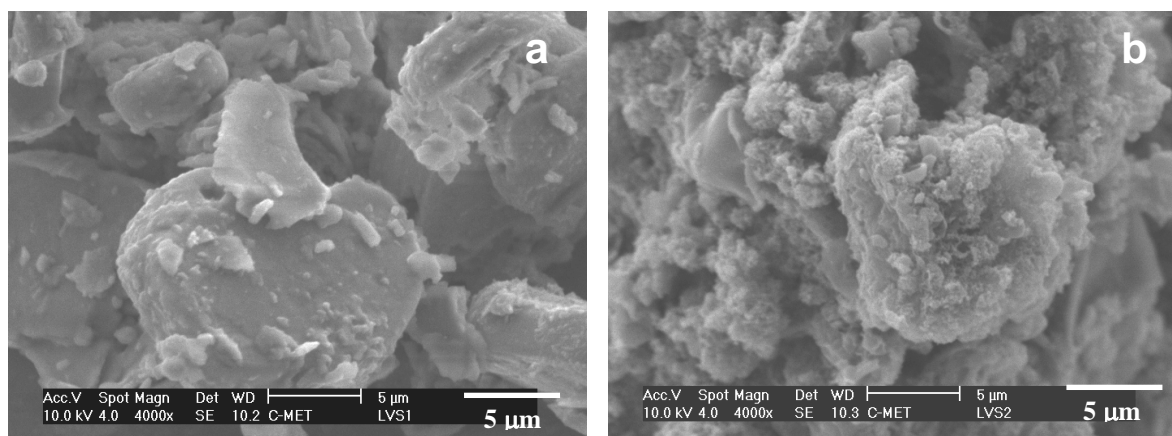


Figure 3.5. SEM micrographs of (a)  $\text{VS}_2$  and (b) PEDOT/  $\text{V}_2\text{S}$  nanocomposite

### 3.3.6 Transmission Electron Microscopy (TEM)

The transmission electron microscopy (TEM) images shows thick particles of  $\text{VS}_2$  with micrometer order (*Figure 3.6a*), whereas the nanoribbon morphology of the PEDOT/  $\text{VS}_2$

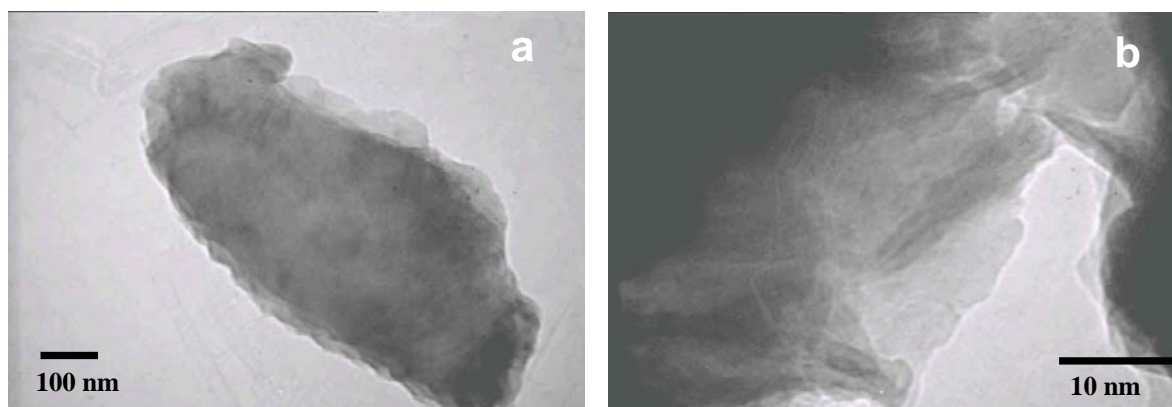


Figure 3.6. TEM images of (a)  $\text{VS}_2$  (b) PEDOT/ $\text{VS}_2$  nanoribbons intercalated into  $\text{VS}_2$  layers to form as a nanocomposite

nanocomposite, is illustrated in *Figure 3.6b*, thus suggesting that the *in situ* oxidative polymerization is topotactic. As can be seen from TEM images, the  $\text{VS}_2$  host consists of conducting polymer nanoribbons whose order could be evaluated from the most pronounced intensity maximum in the broad X-ray diffraction pattern  $d(001)$  (*Figure. 3.1b*). Thus, from the TEM image of the nanocomposite material, we conclude that the highly crystalline vanadium disulfide is separated by organic conducting polymer nanoribbon in this hybrid material.

### 3.3.7 Electronic conductivity

The electrical transport behavior of nanocomposite can be understood by considering the insertion of Poly (3,4-ethylenedioxythiophene) in  $\text{VS}_2$  powder as a composite system in which, two different type of low-dimensional electronic conductors coexist at the molecular level in a

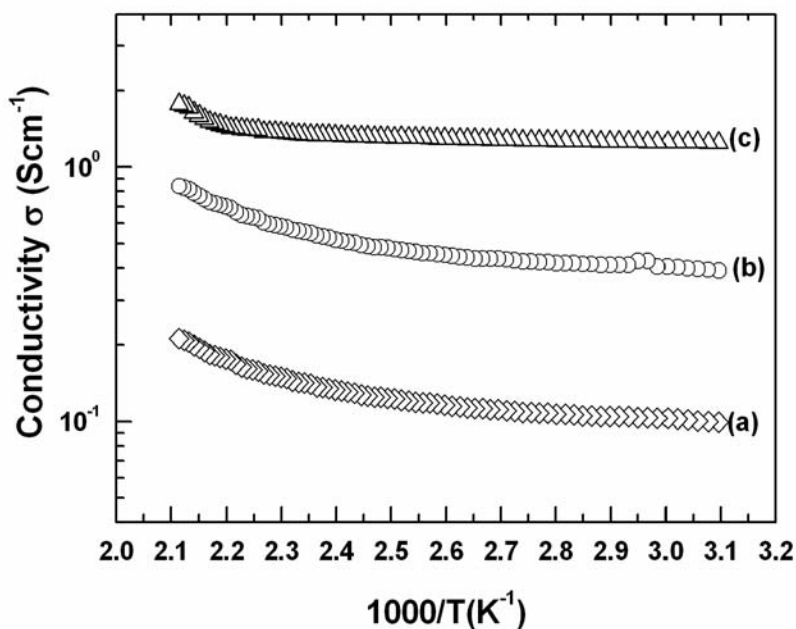


Figure 3.7. Four-probe variable-temperature electrical conductivity of (a) crystalline- $\text{VS}_2$  (b) PEDOT/  $\text{VS}_2$  nano composite and (c) PEDOT

dimensionally constrained environment. Two type of charge carriers are generally assumed to be present in these materials: small polarons (electrons) associated with the  $d^1$  ( $\text{V}^{4+}$ ) centers on the vanadium sulfide lattice, and large polarons on the poly (3,4-ethylenedioxy thiophene) backbone.<sup>4</sup> The actual nature of charge transport would depend on the relative mobility of these two different-kinds of carriers as demonstrated by the fact that

the electronic conductivity of PEDOT/  $\text{VS}_2$  is ten times higher than that of pristine  $\text{VS}_2$ . The room temperature conductivity for the PEDOT/  $\text{VS}_2$  composite is  $3.9 \times 10^{-1} \text{ Scm}^{-1}$ , while pristine vanadium disulfide is a semiconductor with a room temperature conductivity of  $9.9 \times 10^{-2} \text{ Scm}^{-1}$ . The conductivity of PEDOT/  $\text{VS}_2$  is therefore substantially increased over that of pristine  $\text{VS}_2$ . It is, nevertheless surprisingly lower than that of bulk PEDOT ( $\sim 1.25 \text{ Scm}^{-1}$ ) and it is instructive to



compare this data with that of PEDOT/V<sub>2</sub>O<sub>5</sub>, prepared by the reaction of EDOT with crystalline V<sub>2</sub>O<sub>5</sub>, (Chapter-2) where the conductivity is a linear function of PEDOT content ensuing a three order of magnitude increase compared to that of pristine oxide.<sup>4</sup> In this sample, the conductivity is almost exclusively electronic under our experimental conditions, increasing with the rise of temperature as has been observed in most intercalated compounds and conjugated polymers (Figure .3.7). The comparative electronic conductivity data, open circuit voltage and discharge capacity of nanocomposite and their composition are listed in Table 3.1.

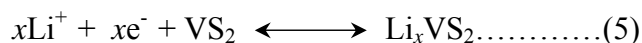
**Table 3.1. A Comparison of the physicochemical properties of the PEDOT/VS<sub>2</sub> nanocomposite**

Sample	Interlayer Spacing/ Å	Electronic conductivity, $\sigma/\text{Scm}^{-1}$ (R.T)	Discharge capacity/mAhg <sup>-1</sup>	Open circuit voltage* / V
VS <sub>2</sub>	5.69	$9.907 \times 10^{-2}$	86	2.43
PEDOT/VS <sub>2</sub>	14.01	$3.906 \times 10^{-1}$	127	2.68
PEDOT	-	$1.248 \times 10^0$		

\*The open circuit voltage is obtained from the discharge measurements of VS<sub>2</sub> and PEDOT/ VS<sub>2</sub> nanocomposite, as a cathode material by coupling with lithium metal anode using 1M LiClO<sub>4</sub> in a electrolyte of propylene carbonate.

### 3.3.8 Electrochemical lithium insertion

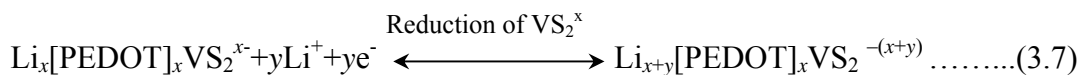
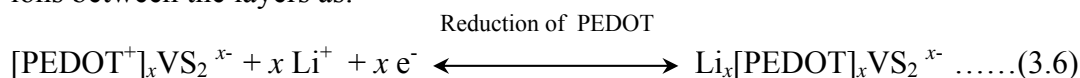
Transition metal dichalcogenides, MX<sub>2</sub> (M= V, Ti, Ta and X= S, Se) which form layered compounds (especially groups 4B and 5B) that can act as host lattice with lithium ions are of significant interest as the basis for developing high energy density cathodes for rechargeable lithium batteries. In particular, Li<sub>x</sub>VS<sub>2</sub> has been proposed as one of the attractive cathode materials in nonaqueous lithium batteries as the electrochemical insertion of Li in VS<sub>2</sub> material can be described by the following redox couple.



The most striking aspects of the Li<sub>x</sub>VS<sub>2</sub> system is the occurrence of two slightly distorted phases  $\alpha$  and  $\beta$ .<sup>11</sup> This phase transition in the Li<sub>x</sub>VS<sub>2</sub> appears to be related to electronic instabilities in the VS<sub>2</sub> layers. Such instabilities could take the form of a charge density wave (CDW),<sup>19</sup> as observed in many MX<sub>2</sub> layered compounds including VSe<sub>2</sub> although some may be more similar to Mott-like transitions observed in vanadium oxides such as VO<sub>2</sub>,<sup>20</sup> V<sub>2</sub>O<sub>3</sub><sup>21</sup> etc., as these compounds span the range from d<sup>1</sup> to d<sup>2</sup>, as does Li<sub>x</sub>VS<sub>2</sub> as x increases from 0 to 1. When both d<sup>1</sup>

and  $d^2$  Vanadium are present in the oxides (mixed valent), two transitions are frequently observed.<sup>11</sup>

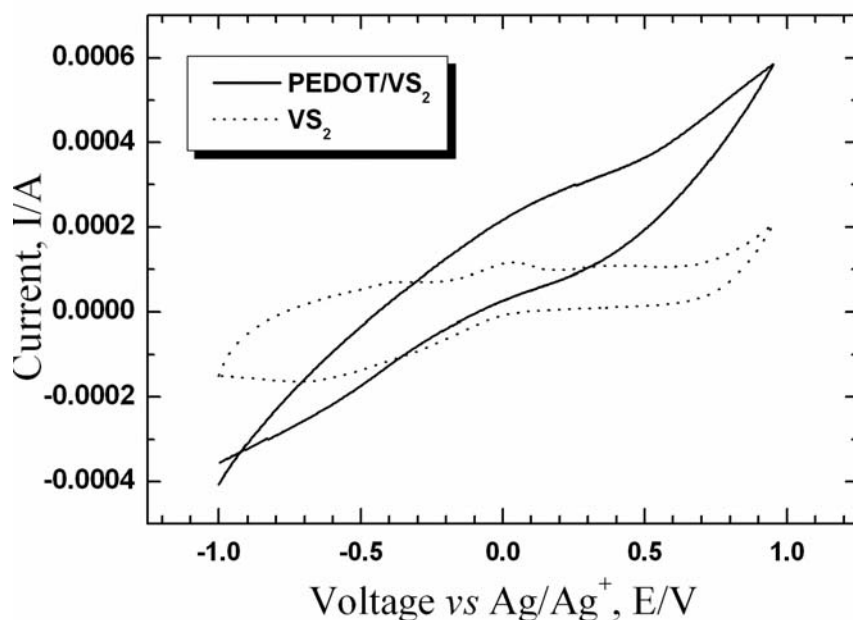
The occurrence of phase transitions in  $\text{Li}_x\text{VS}_2$  from hexagonal to distorted phases suggest the possibility of suppressing these transitions by substituting other metals for V, or using macromolecules intercalated in between  $\text{VS}_2$  layers, thereby introducing disorder and modifying the electronic structure of the Vanadium d-band. For example, Di Salvo has reported<sup>22, 23</sup> that CDW and polytype transformation in layered compounds may be reduced by alloy formation. In particular, conducting polymers seems to be an attractive substitute because of their improved room temperature conductivity and lithium ion mobility compared to that of polymer free inorganic hosts.  $\text{VS}_2$  and  $\text{Li}_x\text{VS}_2$  are regular 1T hexagonal structures, although their composition intermediate in lithium are distorted over most of the range. Furthermore, the nature of polymer intercalated  $\text{Li}_x\text{VS}_2$  distortions may be somewhat different than that of  $\text{Li}_x\text{VS}_2$  and this may give rise to interesting variants in the electrical behavior. For the case of PEDOT/  $\text{VS}_2$  nanocomposites, we can write analogous electrochemical reactions after incorporating lithium ions between the layers as:



### 3.3.9 Cyclic Voltammetry

Electrochemical measurements were performed based on the cell configuration of the Pt|1M  $\text{LiClO}_4$  in EC/DMC (1:1 v/v)| PEDOT/ $\text{VS}_2$  nanocomposite electrode. *Figure 3.8* shows comparative cyclic voltammograms of pristine  $\text{VS}_2$  and PEDOT/ $\text{VS}_2$  nano composite, illustrating a drastic change in electrochemical properties induced by the polymer insertion. During the first cathodic scan, from -1.0 V to 1.0 vs  $\text{Ag}/\text{Ag}^+$ , the crystalline  $\text{VS}_2$  undergo a well-known phase transformation and the stabilization occurs after the fifth cycle (*Figure 3.8*). The irreversible shift in the cathodic peak from -0.32 V (first cathodic scan) to -0.20 V (third and following cathodic scans) suggests that the structural change is permanent as reported elsewhere.<sup>20</sup> Further, the weak interactions between the interlamellar layer, allow fast insertion of  $\text{Li}^+$  ions between the ribbons

rather than that in the crystalline vanadium disulfide<sup>9</sup>. In contrast, for the PEDOT/VS<sub>2</sub> hybrids, there is no sign of any irreversible structural change (Figure 3.8), although the broad cathodic



peak, resembles that of 2D inorganic layered compounds.<sup>36-39</sup> The broad and diffuse peak shape can, therefore, be correlated with the layer stacking derived by the polymer incorporation, as previously deduced from X-ray diffraction data.

Figure 3.8. Cyclic voltammetry of pristine VS<sub>2</sub> and PEDOT/VS<sub>2</sub> nanocomposite at 100 mV/s between -1.0 and 1.0 V vs. Ag/Ag<sup>+</sup>

### 3.3.10 Charge-Discharge Properties

Figure 3.9 demonstrates potential vs. capacity curves for the first discharge carried out for VS<sub>2</sub> and the hybrids at a constant current of 0.5-0.75 mA/cm<sup>2</sup> in the voltage range of 1.0 ~ 3 V (vs. Li<sup>+</sup>/Li), corresponding to the uptake of ~ 1.5 lithium per VS<sub>2</sub> unit. The discharge curve for pristine Li<sup>+</sup>/Li<sub>x</sub>VS<sub>2</sub> (Figure.3.9) shows distinctive plateaus due to structural changes near the beginning of discharge, possibly associated with transition from  $\alpha$ -VS<sub>2</sub> to  $\beta$ -Li<sub>x</sub>VS<sub>2</sub> phase. Preliminary results indicate that the reduced capacity of Li<sup>+</sup>/Li<sub>x</sub>VS<sub>2</sub> cells is intimately related to the distorted intermediate phases either by reduced Li<sup>+</sup> ion mobility or by a sluggish nucleation.

Clearly, the Li / PEDOT/ VS<sub>2</sub> cells give improved capacity and cycling behavior over Li<sup>+</sup>/Li<sub>x</sub>VS<sub>2</sub> cells. The first cycle of a PEDOT/VS<sub>2</sub> discharge plateau shows (Figure 3.9) the continued presence of distorted intermediate phases as evidenced by a mild break near the middle of these curves, although their properties are apparently modified from those of Li<sub>x</sub>VS<sub>2</sub> allowing easy reversibility. Rechargeable cells prepared with these compositions give good capacity and reversible behavior as shown in Figure 3.9. The lithium insertion into the pristine VS<sub>2</sub> occurs at ~

2.43 V and is accompanied by irreversible structural changes to  $\beta\text{-Li}_x\text{VS}_2$  phase<sup>20</sup>, leading to a transformation of curve shape in first cycle. The open circuit voltage of this cell increases after polymer intercalation into  $\text{VS}_2$  such that the OCV for PEDOT/ $\text{VS}_2$  is 2.68 V and it delivers a coulombic capacity of  $\sim 130$  mAh/g during its first discharge in comparison to 80 mAh/g for

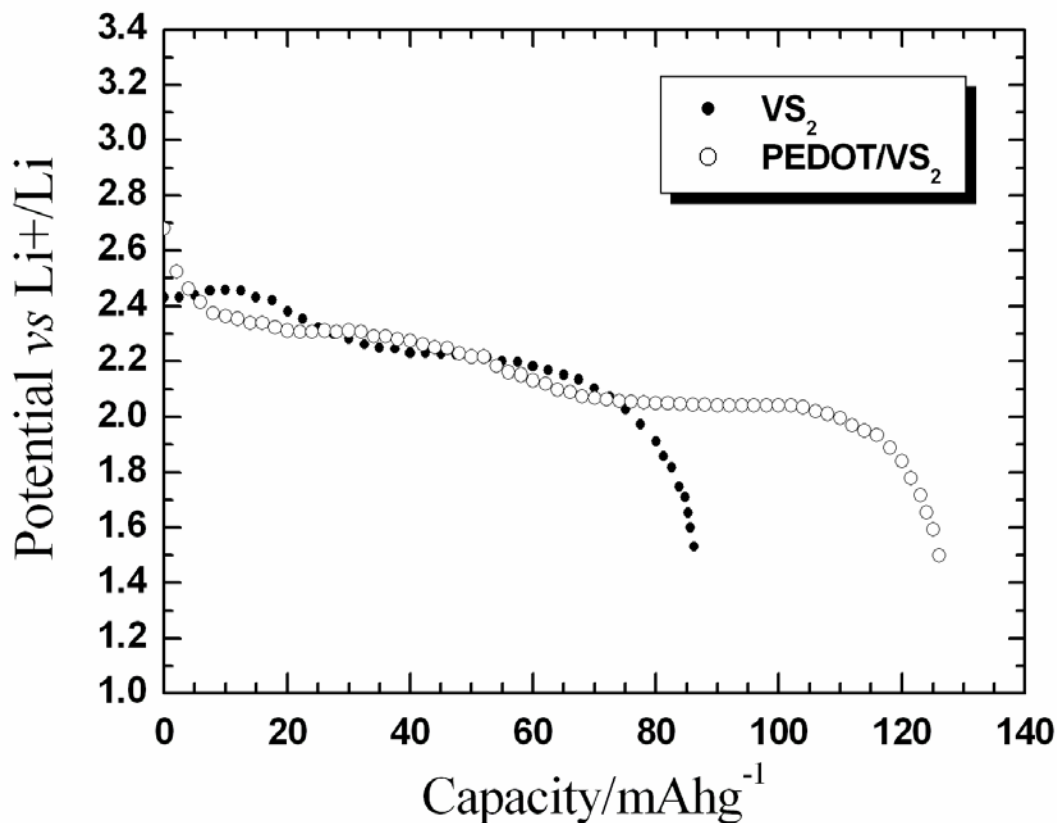


Figure 3.9. Potential *vs.* specific capacity curves for the second cycle of pristine  $\text{VS}_2$ , and PEDOT/ $\text{VS}_2$  nanocomposite after coupling with lithium metal anode using 1M  $\text{LiClO}_4$  in propylene carbonate using a constant current of 0.5-0.75 mA/cm<sup>2</sup>. The potential range is from 1.0 ~ 3.0 V *vs.* Li and the electrode surface area is  $\sim 1\text{cm}^2$ .

pristine  $\text{VS}_2$  despite the common structural feature of the separation of vanadium disulfide layers owing to the presence of  $\text{Li}^+$  ions. It would be, hence, a plausible explanation that the disturbed layer stacking derived by the separation of layers would make structural disorders. The improved performance of the hybrid material is presumably due to the larger separation between vanadium oxide layers, leading to an enhanced “bidimensionality”.

### 3.3.11 Cycle life

In order to clarify the role of the polymer incorporation on the electrochemical performance for extended cycling, the variation of discharge capacities with cycle number for  $\text{VS}_2$  and

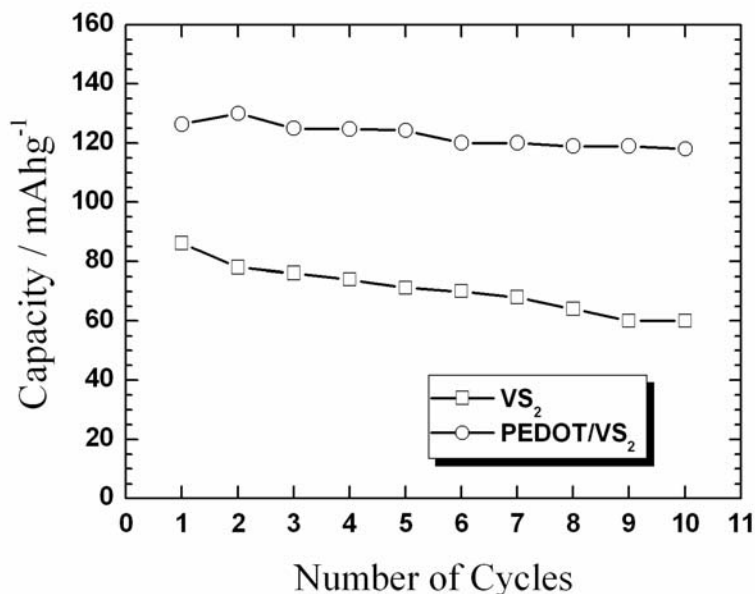


Figure 3.10. Evolution of discharge capacity with the number of cycles for pristine  $\text{VS}_2$  and  $\text{PEDOT}/\text{VS}_2$ . The data were obtained at a current of 0.5-0.75  $\text{mA}/\text{cm}^2$ . The potential range was set to 1.0 ~ 3.0 V vs. Li .

$\text{PEDOT}/\text{VS}_2$  cathodes are shown in *Figure 3.10*. Apparently,  $\text{PEDOT}/\text{VS}_2$  nanocomposite maintains higher capacities of *ca.* 120  $\text{mAh}/\text{g}$  for several cycles suggesting better cyclability than cathodes made up of the pristine  $\text{VS}_2$ . The improved performance is presumably due to a higher electrical conductivity and to the altered separation between vanadium sulfide layers, leading to enhanced lithium ion mobility.

## 3.4. Conclusions

We have found a novel method of interleaving poly (3,4-Ethylene dioxythiophene) between the layers of  $\text{VS}_2$  using a soft process of intercalation. The reaction takes place with the *in situ* polymerization of EDOT within the framework of  $\text{VS}_2$ . These two phases can be distinguished by the different interlayer spacing as detected from powder X-ray diffraction patterns. The fact that two distinct phases rather than a continuum of compositions are obtained in this system suggests the existence of a significant interaction between the host and guest rather than a simple insertion into the van der Waals gap. The experimental data presented here suggest that the polymerization proceeds concomitantly with intercalation. The polymer chains appear fixed in the interlamellar space, and the ring flips observed in the bulk form of PEDOT are frozen in these materials. Therefore, there is considerable bonding interaction between the organic and

inorganic components, probably due to hydrogen bonding. X-ray photoelectron spectrum shows the presence of oxidized species indicating that the  $\text{VS}_2$  could have undergone oxidation either during oxidative polymerization of EDOT or upon atmospheric exposure to transfer  $\text{V}^{4+}$  to  $\text{V}^{5+}$  state. These results are also confirmed by XRD, where the intercalation process and charge transfer from the polymer to the  $\text{VS}_2$  framework reveal clear signatures. The SEM and TEM results suggest that the interlayer distance of crystalline  $\text{VS}_2$  expands upon the incorporation of the polymer nanoribbons. According to electrochemical measurements, the hybrids shows reversible specific capacities up to  $\sim 130\text{mAh/g}$  and the improvement of electrochemical performance compared with that of pristine  $\text{VS}_2$  is attributed to higher electric conductivity and enhanced bidimensionality. The influence of intercalants on  $\text{Li}^+$  diffusion rates and charge capacity in the PEDOT/ $\text{VS}_2$  nanocomposite is increased relative to that for  $\text{VS}_2$ .

### 3.5 References

- 1.S.D.Cox, G.D.Stucky, J.Phys.Chem. **95** (1991) 710.
- 2.T.Bein, P.Enzel, Angew. Chem., Int.Ed.Engl. **28** (1989)1692.
- 3.L.F.Nazar, Z.Zhang, D.Zinkweg, J.Am.Chem.Soc.**114** (1992) 6239.
4. A.Vadivel Murugan, B.B. Kale, C-W.Kwon, G.Campet, K.Vijayamohanan, *J.Mater.Chem* **11** (2001) 2470
- 5.A.Vadivel Murugan, C-W.Kwon, G.Campet, B.B. Kale, T.Maddanimath and K.Vijayamohanan *J.Power Sources*, **105** (2002) 1.
6. M. G . Kanatzidis, R.Bissessur,, D. C. Degroot, J. L. Schindler, and C. R. Kannewurf. *Chem Mater.*, **5** (1993) 595.
- 7.A.V.Powell.*Annu.Rep.Prog.Chem.Sect C*.**90** (1993)177.
- 8.R.H.Friend and A.D.Yoffe. *Adv. Phys.* **36** (1987)1.
- 9.L.Kosidowski and A.V.Powell, *Chem.Comm*, (1998) 2201.
- 10.Jrouxel. *Intercalated Layered Materials*. ed.F.Lév. Dordrecht, (1979) 201
- 11.D.W.Murphy, C.Cros, F.J.Di salvo and J.V.Waszczak, *Inorganic Chem* **16** (1977)3027.
- 12.M.S.Whittingham, *J.Electrochem.Soc.*, **123** (1976)315.
- 13.B.van Laar and D.J.W.Ijdo, *J.Solid State Chem* **3** (1971) 590.
- 14.V.Hernandez, F.J.Ramirez, T.F.Otero, J.T.Lopez Navarrete, *J.Chem.Phys.* **100** (1994) 114.
- 15.G.Louarn, J.Kruszka, S.Lefrant, M.Zagorska, I.Kulshewicz-Bayer, A.Prón, *Synth.Met.*, **61** (1993) 233.
- 16.N.B.Colthup, L.H.Daly, S.E.Wiberley, *Introduction to Infrared and Raman Spectroscopy*, Academic Press, New York, (1964) 276.
- 17.R.S.Tipson, H.S.Isbell, J.E.Stewart, *J.Res.Natl.Bur.Standards.* **62** (1959) 257.
- 18.A.V.Powell, L.Kosidowski and A.McDowall, *J.Mater.Chem*, **11**(2001) 1086.
- 19.J.A.Wilson, F.J.Di Salvo, and S.Mahajan, *Adv.Phy*, **24** (1975)117.

- 20.J.P.Pouget, P.Lederer, D.S.Schreber, H.Launois, D.Wohlleben, A.Casalot and G.Villeneuve, *J.Phy.Chem.Soilds*, **33** (1972) 1961.
- 21.A.C.Gossard, A.Menth, W.W.Warren and J.P.Remeika, *Phys.Rev.B*, **12** (1975) 1187.
- 22.F.J.Di Savo, J.A.Wilson, B.G.Bagley and J.V.Waszcak, *Phys.Rev.B*, **12** (1975) 2220.
- 23.F.J.Di Savo, and J.V.Waszcak, *J.de Physique*, C **4** (1976) 157.

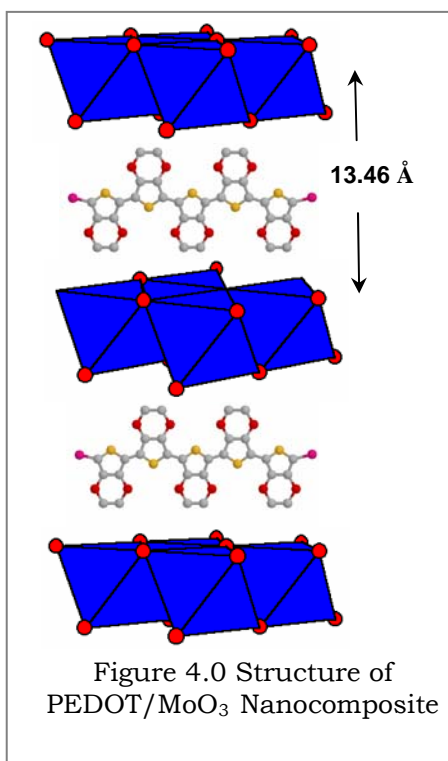


# INTERCALATION OF POLY (3,4-ETHYLENEDIOXYTHIOPHENE) BETWEEN MoO<sub>3</sub> LAYERS *via in situ* OXIDATIVE POLYMERIZATION

Chapter

4

In this chapter, we report the synthesis of a novel nanocomposite PEDOT/ MoO<sub>3</sub> material by direct *in situ* oxidative polymerization of 3, 4-ethylenedioxythiophene (EDOT) between MoO<sub>3</sub> layers in the presence of an external oxidizing agent. The interlayer spacing, upon



intercalation expands from 6.93Å to 13.46Å followed by exfoliation and restacking process. The resultant interlayer separation is consistent with the existence of two phases of organic and inorganic species in the nanocomposite corresponding to the intercalation of PEDOT in the MoO<sub>3</sub> framework. The resulting nanocomposite is characterized by thermal analysis (TGA/DTA), powder X-ray diffraction, XPS, FTIR spectroscopy, SEM, TEM, and four-probe electrical conductivity measurements. The application potential of these nanocomposite as promising electrode material for supercapacitor is investigated and it is interesting to note that the electrochemical double layer capacitance of pristine MoO<sub>3</sub> increases from ~40 mF/g to ~300 F/g after polymer intercalated into MoO<sub>3</sub>. In addition

with cathode materials for rechargeable lithium batteries is also demonstrated by the electrochemical intercalation of lithium into the PEDOT/MoO<sub>3</sub> nanocomposite cathode, where a the second discharge capacity is found to be significantly enhanced from 130 mAh/g for pristine MoO<sub>3</sub> compared to 160 mAh/g for PEDOT/ MoO<sub>3</sub> nanocomposites under similar experimental conditions. The nanocomposite displays intriguing effects with respect to electrochemical Li<sup>+</sup> insertion.

## 4.1 Introduction

There has been a great deal of interest in recent years on the ability to control nanoscale structures *via* the effective approach of innovative soft-chemistry routes for the preparation of conducting polymer based nanocomposite for several applications including light emitting diodes, chemical sensors, supercapacitors, fuel cells and lithium batteries.<sup>1-6</sup> In particular, a comparison of the application of either conjugated polymers or transition metal oxides individually with the nanocomposite as positive electrodes in rechargeable lithium batteries suggests that when these polymer/oxide materials are combined at “nanoscale” level, new properties like enhanced electrochemical Li storage ability due to synergistic effects do appears.<sup>7-14</sup>

Poly(3,4-ethylenedioxythiophene) PEDOT, one of the recently found excellent conducting polymers, has been reported to exhibit greatly enhanced stability and eco-friendly behavior compared to polypyrrole and polyaniline.<sup>15,16</sup> Indeed, it appears to be one of the most stable conducting polymers currently available and has been attracting growing interest for several applications.<sup>17,18</sup> In previous *Chapters (2 and 3)* we have demonstrated the successful intercalation of poly (3,4-ethylenedioxy thiophene) PEDOT into layered oxidizing host such as V<sub>2</sub>O<sub>5</sub>, where the influence of intercalants on lithium (Li<sup>+</sup>) diffusion rates and charge capacity in the PEDOT/V<sub>2</sub>O<sub>5</sub> nanocomposite have been found to be increased relative to that for V<sub>2</sub>O<sub>5</sub>.<sup>12-14</sup> This reaction is actually limited to hosts that fall into a redox potential range sufficient to oxidize the monomer and also to hosts possessing a structure that permits the polymer to be readily inserted between the layers ( i.e., kinetic limitations).

To broaden the scope of these new hybrid materials to other layered systems, molybdenum oxide is considered to be an attractive and it also technologically important as cathode material for non-aqueous lithium batteries<sup>19</sup>. These materials offer high energy density and wide composition intervals for lithium intercalations. MoO<sub>3</sub> is particularly interesting because: (i) the orthorhombic phase ( $\alpha$ -MoO<sub>3</sub>) has two dimensional layered structure favorable for Li<sup>+</sup> intercalation<sup>20</sup>; (ii) it exhibits higher electro chemical activity than chalcogenides; (iii) it is exceptionally stable<sup>21</sup>, and it has widespread utility as a cathode material for secondary Li-ion batteries, and electrochromic devices,<sup>19-22</sup> despite its disadvantage including relatively slow kinetics for Li-ion transport, electronically insulating state upon full oxidation and poor cycling

behavior.<sup>21, 22</sup> Thus one approach to modify the properties of a host material is through the intercalation of electronically conducting large guest species into the interlayer van der Waals gap, albeit with some difficulty. Unlike more oxidizing transition metal oxides such as  $V_2O_5$ , however, the electrochemical redox potential of  $MoO_3$  (3.2V) is not sufficiently high to oxidatively polymerize monomers during the insertion reaction. Hence we sought to follow another new technique that could be used to insert conductive polymers between the layers which utilize an external oxidizing agent, thus benefiting from the propensity of layered oxides like  $Li_xMoO_3^{x-}$  to swell in water and to undergo ion-exchange reactions followed by exfoliation.<sup>8, 22</sup>

We report in this chapter a new modification in the *in situ* intercalative polymerization reaction which, for the first time, allows the intercalation of poly (3,4-ethylenedioxythiophene) PEDOT into the van der Waals gap of  $MoO_3$  to produce a new composite. This nanocomposite is characterized by thermal analysis (TGA/DTA), powder X-ray diffraction, FTIR, X-ray photo electron spectroscopy (XPS), and electronic conductivity measurements. Furthermore the application potential of this nanocomposite, displaying some interesting effects with respect to enhancement of electrochemical properties of  $MoO_3$  by intercalation of PEDOT, has been demonstrated using this as a cathode material for rechargeable lithium batteries.

## 4.2 Experimental Section

### 4.2.1 Materials

$MoO_3$  (99.9 %), LiBr (99.9%), lithium metal foil (99.9%),  $LiClO_4$  (99.99%), polytetrafluoroethylene (PTFE; 99.99%), propylene carbonate (PC; 99.9%) and dimethylcarbonate (DMC; 99%) from Aldrich and n-hexanol (98%) from Fluka were used without any further purification. 3,4-ethylenedioxythiophene (EDOT, Bayer AG Germany) was distilled under vacuum prior to use while ethylene carbonate (EC; Prolabo 99%) and ketjenblack were used as received. All experiments were conducted with deionized water.

### 4.2.2 Preparation of $Li_xMoO_3$

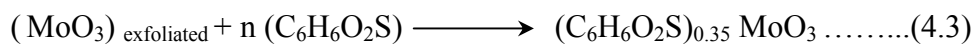
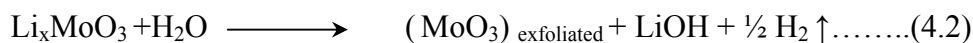
Commercially available  $MoO_3$  was used as the starting material, which was fired in an alumina crucible in presence of air at 600°C overnight to increase the particle size. This  $MoO_3$  was refluxed with LiBr in n-hexanol for 12 h to form dark purplish-blue metallic lusted  $Li_xMoO_3$  bronze, which was collected by centrifugation followed by extensive washing with

ethanol to remove excess bromine, until the filtrate became colorless. Then it was stored in N<sub>2</sub> atmosphere. This direct and single step LiBr reflux route to Li<sub>x</sub>MoO<sub>3</sub> is one of the best methods to conveniently provide the material in good yield. An additional advantage of this method is that since it is conducted in n-hexanol, this provides the anhydrous form of molybdenum bronze. The Li<sub>x</sub>MoO<sub>3</sub> prepared in this fashion, though still crystalline, shows broader diffraction maxima than that corresponding to MoO<sub>3</sub>. Further, the Li<sup>+</sup> insertion into MoO<sub>3</sub> is topotactic as evidenced by the complete indexing of the X-ray powder diffraction pattern of the product. The amount of Li in MoO<sub>3</sub> was determined by elemental analysis using ICP-OES and X-ray fluorescence respectively, suggesting 2.46 % Li and 56.39 % Mo respectively. This gives a ratio of Li to Mo as 0.6:1 corresponding to the molar ratio of LiBr used in the lithiation reaction. It is, of course, possible that *x* value might slightly differ from sample to sample in the range 0.6 < *x* < 0.7.



### 4.2.3 Exfoliation and Polymer Intercalation Strategy

The lithium molybdenum bronze exfoliates readily in water to form a stable colloidal solution, and this indeed, makes it as an appealing candidate for the polymer intercalation. Thus 50 mg of lithium molybdenum bronze was exfoliated in 20 ml of double distilled water, and after 1 h sonication to form a suspension with a concentration of 5 gl<sup>-1</sup> followed by refluxing for 8 h. To this suspension 3,4-ethylenedioxythiophene (EDOT) monomer (4.6 mM) was added drop wise and was refluxed for further 2 h to ensure complete mixing. Subsequently, 8.5 g of iron (III) chloride (FeCl<sub>3</sub>) in 10 ml of water was added drop wise to the suspension as the oxidizing agent under refluxing conditions for 10 h.



The Molybdenum content was determined by Inductive Coupled Plasma Optical Emission Spectrometer(ICP-OES) analysis after dissolving in concentrated sulfuric acid followed by dilution with water and filtration to remove the dispersed polymer. Elemental analysis of nanocomposites gave (C<sub>6</sub>H<sub>4</sub>O<sub>2</sub>S)<sub>0.35</sub> MoO<sub>3</sub> :C, 6.92; H, 1.54; S, 3.77 and Mo, 34.36.

#### 4.2.4 Characterization techniques

Powder X-ray diffraction was carried out using Rigaku X-ray Diffractometer (Rigaku miniflex) equipped with a Ni filtered Cu-K $\alpha$  (1.542Å) radiation and a graphite crystal monochromator. Fourier transform infrared (FTIR) spectra were recorded from pressed KBr pellets using a Perkin-Elmer spectrum-2000 FTIR spectrometer. Thermogravimetric analysis (TGA/DTA) was performed with a Shimadzu TGA-50 thermal analysis system using dry oxygen as a carrier gas. TGA experiments were conducted from room temperature to 800° C at a linear heating rate of 10° C per minute. Electronic conductivities were measured on compacted pellets using a four probe conductivity method.

X-ray photoemission spectra (XPS) were recorded on VG Microtech Multilab ESCA 3000 spectrometer using non-monochromatized AlK $\alpha$  x-ray source ( $h\nu = 1486.6$  eV). The base pressure in the chamber was maintained at  $10^{-10}$  Torr range. The energy resolution of the spectrometer was set at 1.0 eV with AlK $\alpha$  radiation at a pass energy of 50 eV. Binding energy (BE) calibration was performed with Au 4f $_{7/2}$  core level at 83.9 eV and BE of adventitious carbon (284.9 eV) was utilized for charging correction with all the samples. The error in all the BE values reported here is within  $\pm 0.1$  eV. Scanning Electron Microscopy (SEM) was carried out with Philips XL-30 microscope at an accelerating voltage of 20 kV after mounting samples on Al stubs with gold coatings. The Elemental analysis was carried out by Inductive Coupled Plasma Optical Emission Spectrometer (ICP-OES, Perkin-elmer 1000) and CE-Instruments-EA 1110 CHNS-O Analyser.

#### 4.2.5 Electrochemical measurements

The electrochemical measurements were performed same as already discussed in *Chapter-2*. Only, for charge/discharge experiments, a constant current of 15 mA/cm $^2$  were applied between 1.0 and 3.8 V (vs. Li $^+$ /Li) reference electrode.

### 4.3 Results and Discussion

#### 4.3.1 FTIR Spectroscopy

*Figure 4.1* shows a comparison of the FT-IR spectra of a nanocomposite PEDOT/ MoO $_3$  and its components. This IR spectrum of composite displays several characteristic bands attributed to both PEDOT and MoO $_3$  (*Table 4. 1*). In particular the vibrational spectrum of

$\text{Li}_x(\text{H}_2\text{O})_y(\text{PEDOT})_z\text{MoO}_3$  is a combination of the vibrational features of PEDOT and  $\text{MoO}_3$ . For example,  $500\text{-}1500\text{ cm}^{-1}$  region of the infrared spectrum is sensitive to C-H vibrations and the

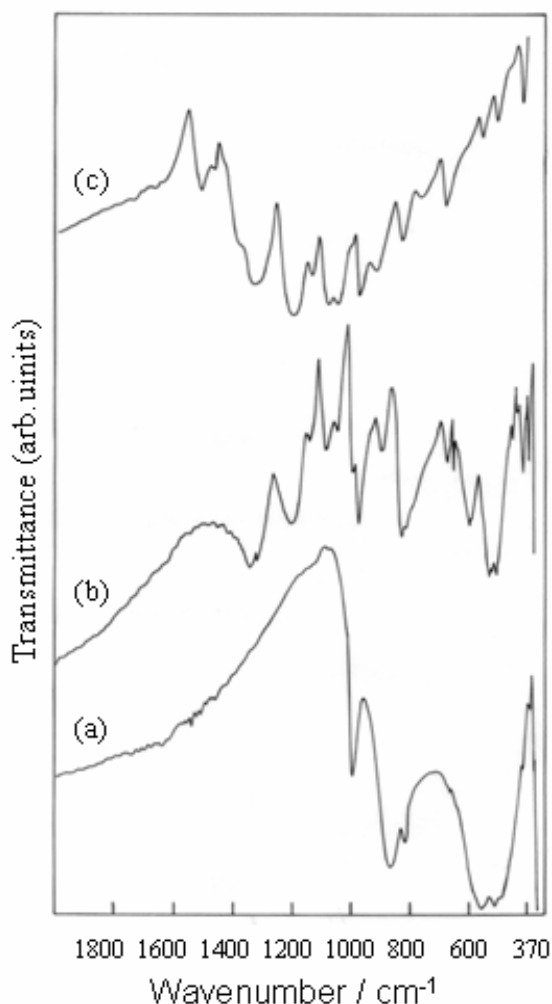


Figure 4.1. FTIR spectra of (a)  $\text{MoO}_3$  (b) PEDOT/  $\text{MoO}_3$  nanocomposite and (c) PEDOT.

stretching of C=C and C-C in the thiophene ring<sup>23,24</sup> Further vibration from C-S bond in the thiophene ring can be seen at  $930, 832$  and  $694\text{ cm}^{-1}$ <sup>23,24</sup> and other vibrations at  $1142\text{-}1128, 1093\text{-}1076$  and  $1052\text{-}1047\text{ cm}^{-1}$  are assigned to the stretching of the alkylendioxy group.<sup>25,26</sup>

Doping induced bands originated from the changes in the conjugated backbone due to electron withdrawing (oxidation) from the polymer chain and concomitant counter ion balance also appear at  $1332, 1202, 1142, 1048$  and at  $918\text{ cm}^{-1}$  which are to be interpreted to be from stretching in the ethylenedioxy ring and from the C-S bond after doping with  $\text{Cl}^-$ . The positions of the peaks at  $571, 821$  and  $995\text{ cm}^{-1}$  are due to the  $\nu(\text{O-Mo})$  triply bounded  $\text{O}^{2-}$ , doubly

shift in the region can be hence used to identify the prominent changes in the polymer structure. The positions of the vibrational peaks arising

**Table 4.1 FTIR spectra used for analysis (data from ref 8,22-26)**

Frequency $\text{cm}^{-1}$	Assignments
575	$\nu(\text{O-Mo})$ , triply bounded
697	$\delta(\text{C-S-C})$ ring
727	$\delta(\text{C-S})$
760-787	$\gamma(\text{CH})$
830	$\nu(\text{C-S})$ ring
978-1026	doping induced band
1052-1047	$\nu(-\text{COROC}-)$
1093-1076	$\nu(-\text{COROC}-)$
1144-1128	$\nu(-\text{COROC}-)$
1247-1199	doping induced band
1323-1290	doping induced band
1370	$\nu(\text{C-C})$ ring

from the encapsulated PEDOT are close to those of pure PEDOT polymer peak vibrations at  $1512, 1470$  and  $1388\text{ cm}^{-1}$  originated from the

bridged  $O^{2-}$  and  $\nu$  (Mo=O) terminal O stretches respectively for  $MoO_3$  are shifted to higher wavenumbers, suggesting that the  $MoO_3$  layers in the nanocomposite are slightly more oxidized. These results also are supported by similar data of Kerr *et al* using polyaniline with molybdenum trioxide hosts.<sup>8, 22</sup>

### 4.3.2 Powder X- ray diffraction (XRD)

Figure 4.2 shows a comparative X-ray diffraction patterns of pristine  $MoO_3$  and polymer intercalated PEDOT/ $MoO_3$  nanocomposite. Figure 4.2 (a) illustrates that  $MoO_3$ , has an Orthorhombic bipyramid structure of Pbnm type (2/m 2/m 2/m) (62) with  $a = 3.962$ ,  $b = 13.850$ ,  $c = 3.690$  (Å);  $\alpha = 90^\circ$   $\beta = 90^\circ$   $\gamma = 90^\circ$ ; however, when  $Li^+$  is intercalated into  $MoO_3$ , it become

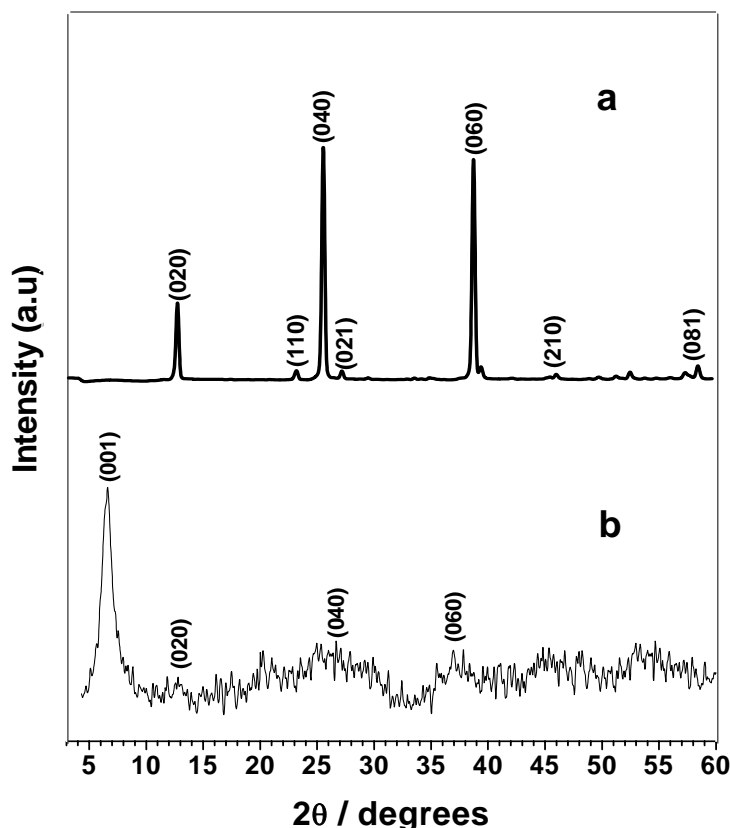
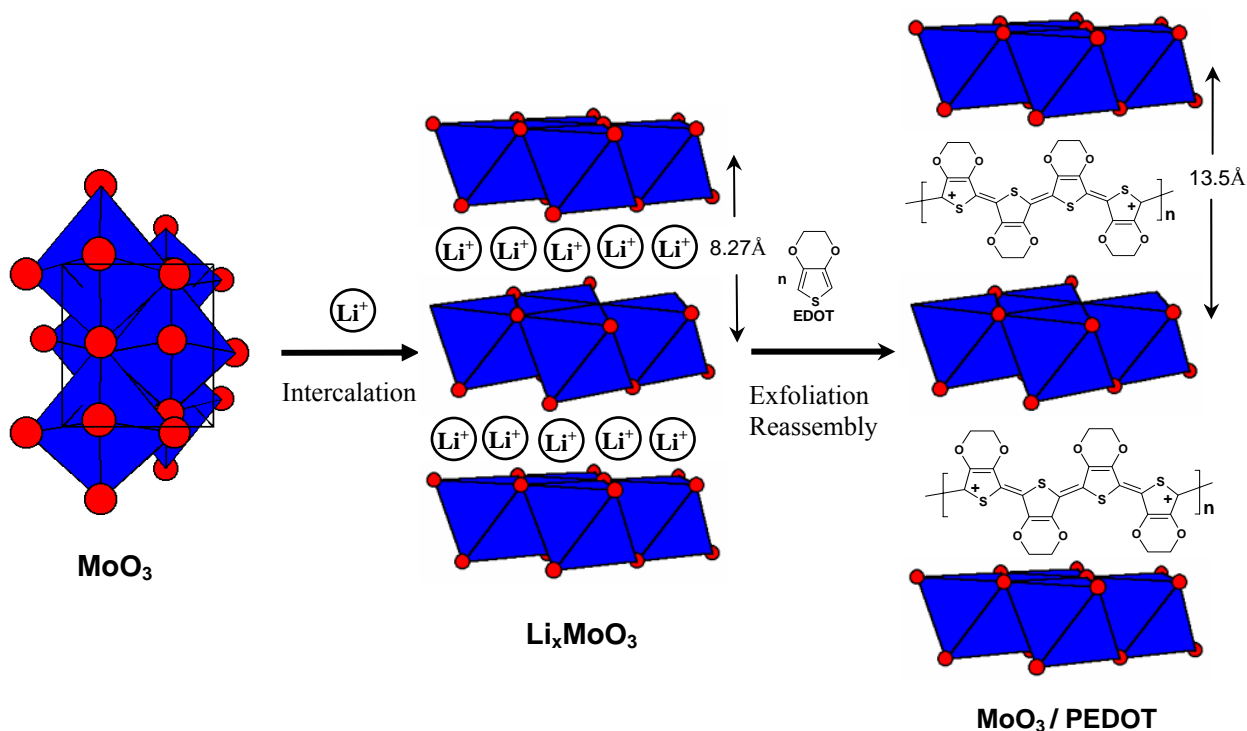


Figure 4.2. A comparative powder X - ray diffraction patterns of (a)  $MoO_3$  powder and (b) PEDOT/ $MoO_3$  nanocomposite

orthorhombic layered phase ( $\alpha$ - $MoO_3$ ) which is one exception as the structure consists of vertex-sharing chains of distorted  $MoO_6$  octahedra which share edges with two similar chains to form layers. The distortion gives to very short “Mo=O” bonds at the apical octahedral positions, that terminate at the top and bottom of the double-octahedral oxide sheets. The resultant two-dimensionally bonded layers are stacked in a staggered arrangement which is held together by weak van der Waals forces. The encapsulation of polymers inside the interlayer galleries of  $MoO_3$  is demonstrated by X-ray powder

diffraction, which shows an expansion of the gallery space. For instance, Figure 4.2 b shows the poly (3,4-ethylenedioxythiophene) PEDOT/  $MoO_3$  nanocomposite, where sharp and intense (001) reflections indicate the distinct stacking of  $MoO_3$  layers. An increase in the interlayer

distance of the pristine oxide,  $\text{MoO}_3$ , from 6.93 to 13.46 Å, indicates substantial incorporation of conducting polymeric material between the layers. In addition, the change in the interlayer distance is consistent with the interstitial PEDOT chains being oriented with the planes of the thiophene rings perpendicular to the layers as evident from the intense sharp peaks. For the  $\text{PEDOT}_{0.35}\text{MoO}_3$  nanocomposite, the polymer chains appear to be fixed in the interlamellar space, and the high degree of ordering is evident from the oriented powder XRD patterns suggesting that the PEDOT chains are aligned (at least to some degree) in the *ac* (basal) plane. Therefore, considerable bonding interaction between the organic and inorganic components is expected probably due to the hydrogen bonding. These results also suggest that the polymer chains lie parallel to each other in the “valleys” of the oxide sheets. Thus it is likely that these materials constitute a new PEDOT /  $\text{MoO}_3$  composite phase consisting of a monolayer of PEDOT chains intercalated within the  $\text{MoO}_3$  interlayer spacing and the concept is summarized in *Scheme 4.1*. This high degree of ordering is also supported by several groups working on such organic-inorganic hybrid materials of conducting polymers with transition metal oxide hosts<sup>8, 22</sup>.



**Scheme 4.1. Schematic representation Organo-Inorganic Poly(3,4-ethylenedioxythiophene) /  $\text{MoO}_3$  Nanocomposite by Intercalation**



### 4.3.3 X-ray Photoelectron Spectroscopy (XPS)

Since XPS is known to be very sensitive to the changes in electron density, it could be exploited well to study such changes in related systems<sup>27</sup>. XPS results for PEDOT and PEDOT/MoO<sub>3</sub> composites in terms of S 2p, C 1s and Mo 3d core levels are shown in *Figure 4.3a, b and c*, respectively. More significantly, S 2p core level from PEDOT displays a peak at 164 eV, typical for thiophene sulfur<sup>28</sup>. However the S 2p core level binding energy (BE) from PEDOT/MoO<sub>3</sub> shows a peak around 165 eV suggesting that on PEDOT intercalation, there is

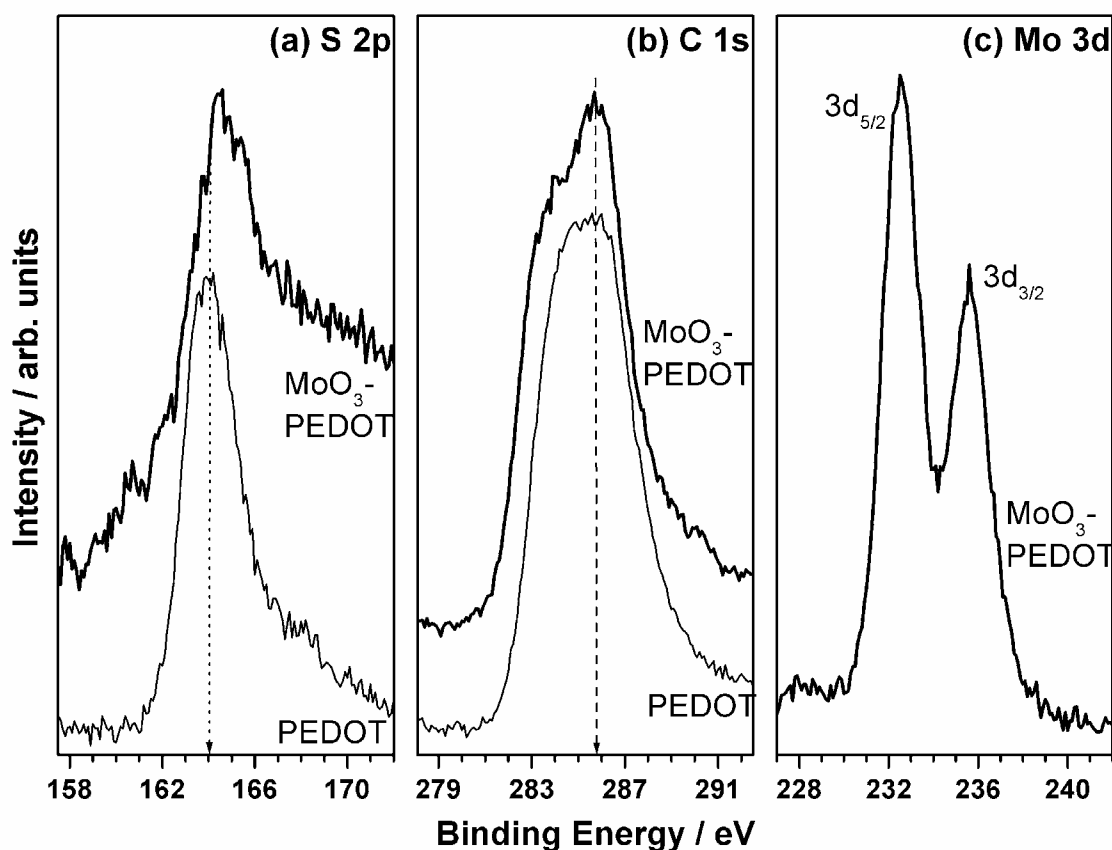


Figure 4.3. X-ray photoelectron spectra from (a) S 2p, (b) C 1s and (c) Mo 3d core levels of PEDOT and PEDOT /MoO<sub>3</sub> nanocomposite

some charge transfer from sulfur atoms. Carbon 1s core level also shows similar changes before and after intercalation in MoO<sub>3</sub>. In sharp contrast PEDOT shows a single but broad C 1s peak at 285.3 eV. It is likely that the BE of carbon atoms from thiophene and ethylenedioxy groups are somewhat similar and hence appear at close enough BE values difficult to resolve. However on intercalation, a broadening on the lower BE side and an appearance of the second peak are

visible. The C 1s peak around 286 eV is attributed to ethylenedioxy group carbon and the lower BE peak at 284 eV is attributed to the thiophene carbon atoms. The above shift in C 1s BE of thiophene group on intercalation suggests an increase in charge and broadening due to some delocalization. In comparison, the ethylenedioxy groups remain at the same BE indicating that there might be no electronic involvement from this group. Mo 3d<sub>5/2</sub> core level at 232.5 eV from PEDOT-MoO<sub>3</sub> composite is typical for MoO<sub>3</sub><sup>28</sup> and the XPS studies hint an oxidation of PEDOT after intercalation into MoO<sub>3</sub> along with some charge transfer from sulfur to MoO<sub>3</sub>. Thus the XPS results are in good agreement with results from other studies, such as XRD and SEM.

#### 4.3.4 Thermogravimetric Analysis (TGA/DTA)

Figure 4.4. shows the thermogravimetric and differential thermal analysis curves of the PEDOT intercalated molybdenum trioxide composite. The first step of decomposition up to 120<sup>o</sup> C, corresponds to the removal of the reversibly bound water. This is followed by a continuous weight loss (TGA) up to ~ 310<sup>o</sup>C which could be attributed to the combustion of the organic

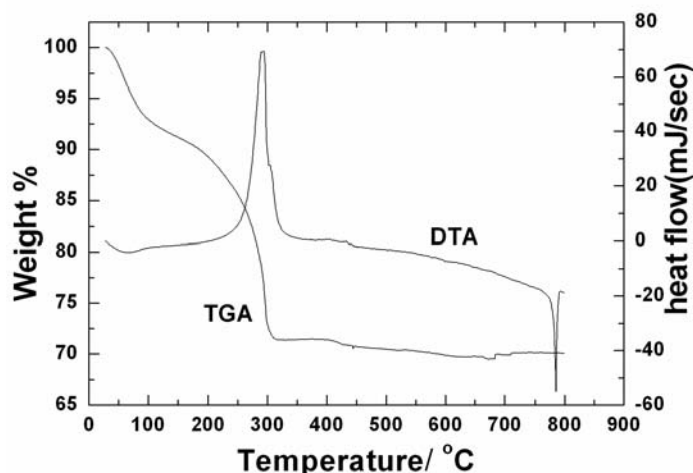


Figure 4.4 TGA/DTA curves of the PEDOT/ MoO<sub>3</sub> nanocomposite

polymer component, which is in agreement with the DTA curve where a large, relatively sharp exothermic peak at 280-310<sup>o</sup>C is distinct due to the degradation/ oxidation of the poly (3,4-ethylene dioxythiophene) between the layers. Furthermore, the weight loss from TGA curve at 740<sup>o</sup>C is in agreement with the DTA curve of a relatively sharp endotherm at 780<sup>o</sup>C, due to the melting of MoO<sub>3</sub> present in

the nanocomposite. Thus the change in these profiles could be attributed to the insertion and external oxidative polymerization of the 3,4-ethylenedioxythiophene (EDOT) between the MoO<sub>3</sub> layers.

### 4.3.5 Scanning Electron Microscopy (SEM)

A comparison of the SEM images of the  $\text{MoO}_3$  and synthesized PEDOT /  $\text{MoO}_3$  nanocomposite is presented in *Figure 4.5 a & b* respectively. It is apparent that  $\text{PEDOT}_{0.35}\text{MoO}_3$  composite forms a continuous and relatively homogeneous matrix with a clearly lamellar morphology and that the incorporation of PEDOT into the  $\text{MoO}_3$  accompanies morphological changes in agreement with the results of XRD patterns, although it can be seen only at a higher resolution. SEM micrographs also suggest that there is no bulk deposition of polymer on the surface of the micro-crystallites.

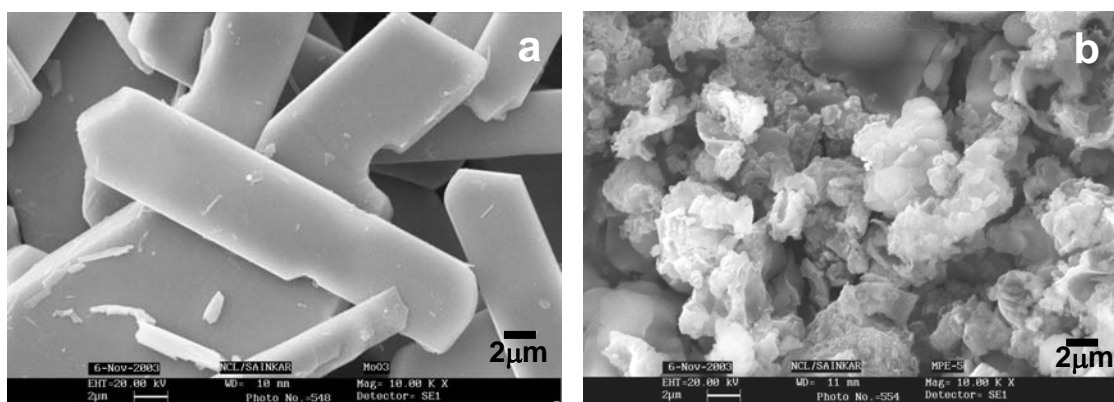


Figure 4.5. SEM micrographs of (a)  $\text{MoO}_3$  , (b) PEDOT/  $\text{MoO}_3$  nano composite

### 4.3.6 Transmission Electron Microscopy (TEM)

The transmission electron microscopy (TEM) images shows thick particles of  $\text{MoO}_3$  with micrometer order (*Figure 4.6 a*), whereas the nanoribbon morphology of the PEDOT-  $\text{MoO}_3$

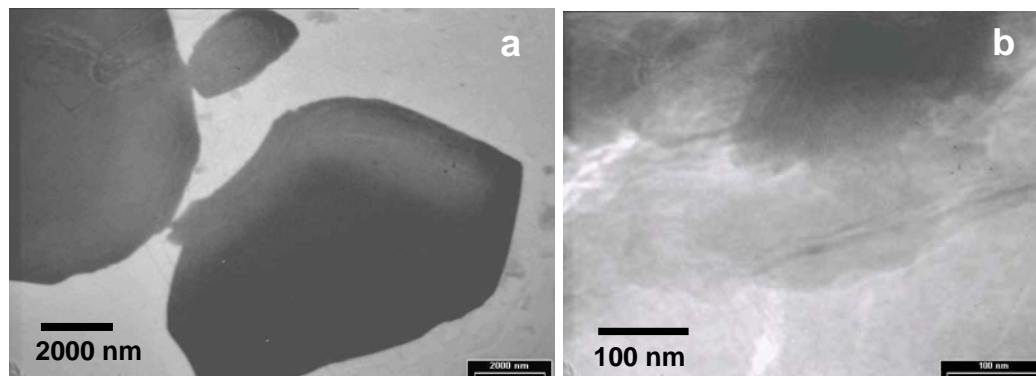


Figure 4.6. TEM images of (a)  $\text{MoO}_3$  , (b) PEDOT nanoribbons intercalated into  $\text{MoO}_3$  layers to form as a nanocomposite

nanocomposite, is also illustrated in *Figure 4.6b*, suggesting that the *in situ* oxidative polymerization by “*Chimie douce*” is topotactic. As can be seen from the TEM images, low scattering power causes bright contrast for white lines of conducting polymer nanoribbons between dark fringes of molybdenum oxide host layers. It can be evaluated from the most pronounced intensity maximum found in the broad X-ray diffraction pattern  $d(001)$  (*Figure 4.2b*). Thus, from the TEM image of the nanocomposite material, we conclude that highly crystalline molybdenum trioxide is separated by alternating organic conducting polymer nanoribbon in this hybrid

### 4.3.7 Electronic conductivity

Four probe dc electronic conductivity of PEDOT/ MoO<sub>3</sub> nanocomposite measured at variable temperature shows a linear increase in conductivity indicative of thermally activated electron transport with an activation energy of 0.2 eV (*Figure 4.7*). Similar behavior is also shown by PPV/MoO<sub>3</sub> & PANI/MoO<sub>3</sub> nano composites.<sup>8</sup> The room temperature conductivity for

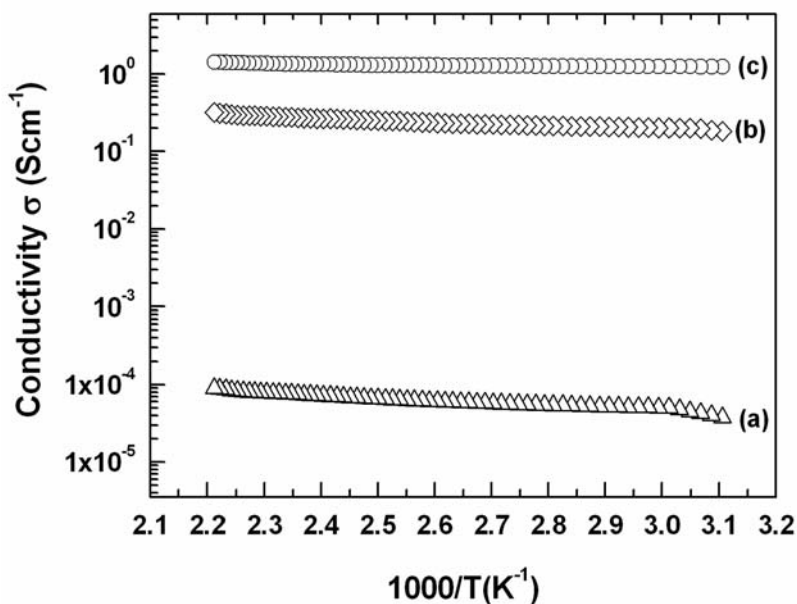


Figure 4.7. Four-probe variable- temperature electrical conductivity of (a) crystalline-MoO<sub>3</sub> (b) PEDOT/ MoO<sub>3</sub> nano composite and (c) PEDOT.

the PEDOT/ MoO<sub>3</sub> composite is  $1.82 \times 10^{-1} \text{ Scm}^{-1}$ , although pristine molybdenum trioxide is an insulator with a room temperature conductivity of  $3.78 \times 10^{-5} \text{ Scm}^{-1}$ .<sup>23</sup> The conductivity of PEDOT/ MoO<sub>3</sub> is therefore substantially increased over that of pristine MoO<sub>3</sub> and is interestingly higher than that of crystalline Li<sub>x</sub>MoO<sub>3</sub>. Surprisingly, it is not lower than that of bulk PEDOT ( $\sim 1.248 \text{ Scm}^{-1}$ ). These results also supported in the case of PEDOT/V<sub>2</sub>O<sub>5</sub>, the conductivity is a linear function of PEDOT content and interestingly there is a three order of magnitude increase in conductivity compared to that of the pristine oxide.<sup>12</sup> The polymer composition of the nanocomposite as determined by

ICP-OES, TGA data and the comparative electronic conductivity data of nanocomposite and their counterpart are listed in Table 4. 2.

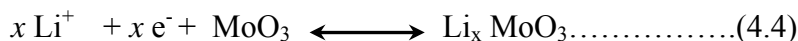
**Table 4.2. Comparison of interlayer spacing, composition analysis, electronic conductivity, discharge capacity and open circuit voltage of PEDOT/MoO<sub>3</sub> nanocomposite and its counterparts**

Sample	Interlayer Spacing/ Å	composition as per elemental analysis	Electronic conductivity, $\sigma/\text{Scm}^{-1}$ (R.T)	Discharge capacity/mAhg <sup>-1</sup>	Open circuit voltage* / V
MoO <sub>3</sub>	6.93	MoO <sub>2.8</sub>	$3.78 \times 10^{-5}$	129	3.25
Li <sub>x</sub> MoO <sub>3</sub>	8.27	Li <sub>0.6</sub> MoO <sub>3</sub>	$1.3 \times 10^{-2}$	-	-
PEDOT/ Li <sub>x</sub> MoO <sub>3</sub>	13.46	Li <sub>0.3</sub> (H <sub>2</sub> O) <sub>0.48</sub> (PEDOT) <sub>0.35</sub> MoO <sub>3</sub>	$1.82 \times 10^{-1}$	158	3.67

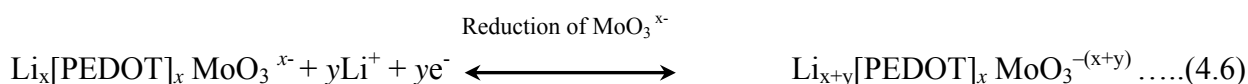
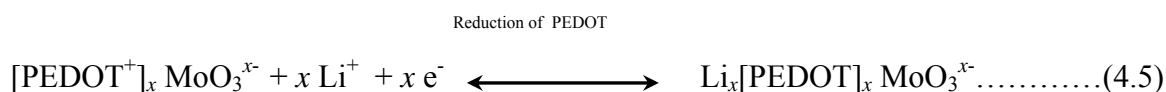
\*The open circuit voltage is obtained from the discharge measurements of MoO<sub>3</sub> and PEDOT/MoO<sub>3</sub> nanocomposite, as a cathode material by coupling with lithium metal anode using 1M LiClO<sub>4</sub> in a electrolyte of 1:1 mixture (by volume) EC/DMC, ethylene and dimethyl carbonate

#### 4.3.8 Electrochemical lithium insertion

The oxide group of the MoO<sub>3</sub> surface bears a partial negative charge and hence strongly attracts Li<sup>+</sup>. This means that a large potential barrier must be surmounted for migration of Li<sup>+</sup> from site to site in the lattice, thus hindering the ion mobility. Steric constraints in the 2D gap can also hinder mobility. As a result, diffusion constants for Li<sup>+</sup> are quite low in MoO<sub>3</sub>,<sup>22</sup> (of the order of  $10^{-11}$  to  $10^{-12}$  cm<sup>2</sup> s<sup>-1</sup>) The electrochemical insertion of Li in MoO<sub>3</sub> material can be described by the following redox couple.



For the case of PEDOT/ MoO<sub>3</sub> nanocomposites, we can write analogous electrochemical reactions after incorporating lithium ions between the layers as;



### 4.3.9 Cyclic Voltammetry

Comparative cyclic voltammograms of (a) crystalline  $\text{MoO}_3$  and (b) layered PEDOT/ $\text{MoO}_3$  nanocomposite, at several scan rates 1M  $\text{LiClO}_4$  in EC/DMC (1:1 v/v) are shown in *Figure 4.8.*, illustrating a drastic change in electrochemical properties induced by the polymer insertion. The observed linearly current increase with scan rate is expected for a strongly adsorbed electrochemical species. It is interesting to note that the double layer capacitance of pristine  $\text{MoO}_3$  increases from  $\sim 40$  mF/g to  $\sim 300$  F/g after polymer intercalated into  $\text{MoO}_3$ . During the first cathodic scan, voltage from  $-1.5$  V to  $0.25$  vs  $\text{Ag}/\text{Ag}^+$ , the crystalline  $\text{MoO}_3$  undergoes a well-known phase transformation and the stabilization occurs after the fourth cycle (*Figure 4.8a*),

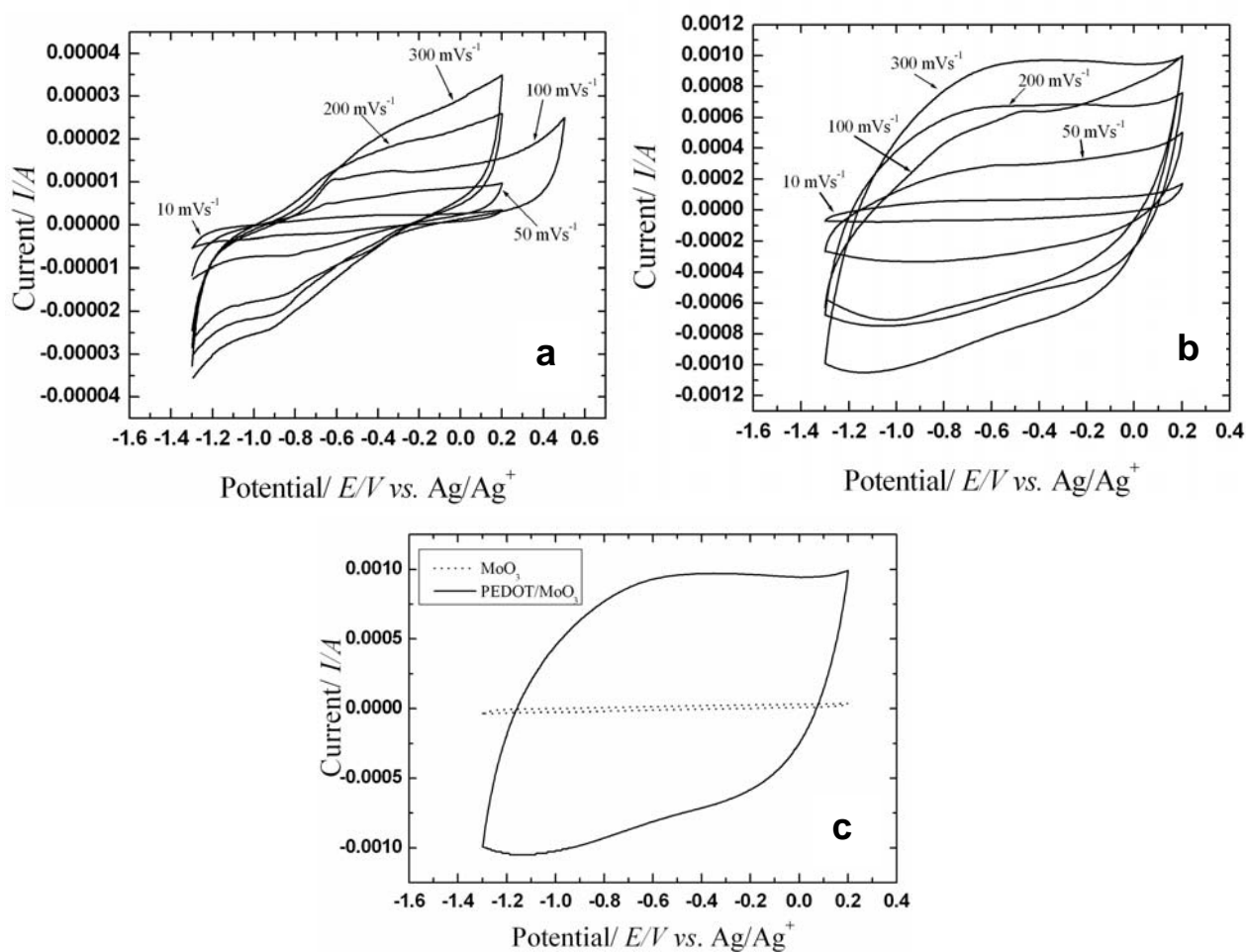


Figure 4.8. cyclic voltammograms of (a) crystalline  $\text{MoO}_3$  and (b) layered PEDOT/  $\text{MoO}_3$  nanocomposite, at several scan rates; (c) super imposed votammograme of  $\text{MoO}_3$  and the composite at  $300 \text{ mVs}^{-1}$  illustrate the supercapacitor behavior using 1M  $\text{LiClO}_4$  in EC/DMC (1:1 v/v)

suggesting that the structural change is permanent. Further, the weak interactions between the interlamellar layers, allow fast insertion of  $\text{Li}^+$  ions between the ribbons rather than that in the crystalline molybdenum trioxide<sup>22</sup>. In contrast, for the PEDOT/  $\text{MoO}_3$  hybrids, there is no sign of any irreversible structural change (Figure 4.8b); however, the broad cathodic peak, resembles that of 2D inorganic layered compounds.<sup>14</sup> The broad and diffuse peak shape can, therefore, be correlated with the layer stacking derived by the polymer incorporation, as previously deduced from the X-ray diffraction data.

#### 4.3.10 Charge-Discharge Properties

Figure 4.9 demonstrates potential vs. capacity curves for the second discharge carried out for  $\text{MoO}_3$  and the PEDOT/  $\text{MoO}_3$  hybrids at a constant current density of  $15 \text{ mA/cm}^2$  in the voltage range of  $1.0 \sim 4 \text{ V}$  (vs.  $\text{Li}^+/\text{Li}$ ), corresponding to the uptake of  $\sim 1.5$  lithium per  $\text{MoO}_3$

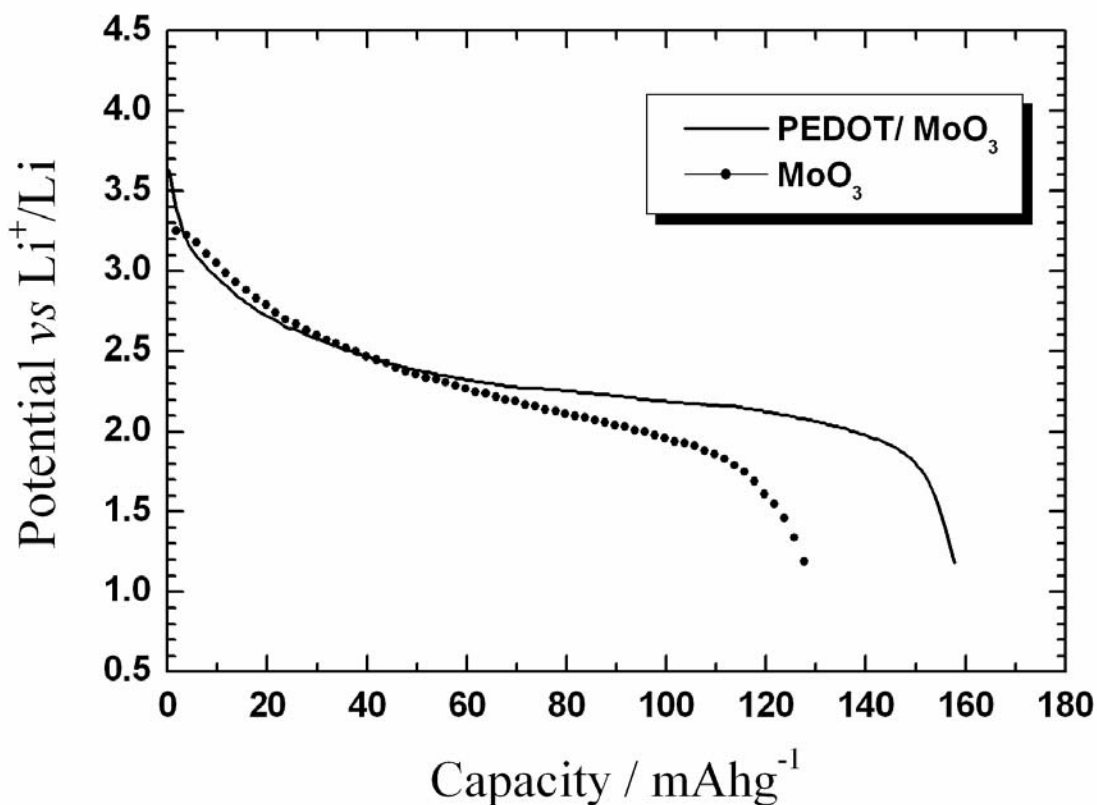


Figure 4.9. Potential vs. specific capacity curves for the second cycle of pristine  $\text{MoO}_3$ , and PEDOT/  $\text{MoO}_3$  nanocomposite. The potential range was set to  $1.0 \sim 4.0 \text{ V}$  vs.  $\text{Li}$  after coupling with lithium metal anode using  $1\text{M LiClO}_4$  in a mixed electrolyte of ethylene and dimethyl carbonate using constant current density of  $15 \text{ mA/cm}^2$ .

unit. The open-circuit voltage (OCV) of the composites when coupled with lithium metal anode is found to be a function of the PEDOT/ MoO<sub>3</sub> ratio and clearly all nanocomposites give higher OCV value (3.67V) than that observed (3.25V) for pure MoO<sub>3</sub> (Table 4.2). The discharge process of the Li / MoO<sub>3</sub> cell seems to be thermodynamically more favorable as the deviation from open circuit voltage is less for the same current density. However, the second discharge capacity is found to be significantly enhanced from 130 mAh/g for pure MoO<sub>3</sub> compared to 160 mAh/g for PEDOT/ MoO<sub>3</sub> nanocomposites under similar experimental conditions. The nanocomposite displays intriguing effects with respect to electrochemical Li<sup>+</sup> insertion. Despite relative increase in conductivity afforded by the incorporation of the polymer, the effect of the polymer is to enhance the battery performance of the PEDOT eliminating water from the interlamellar region which can augment the discharge capacity due to the additional redox capabilities of the polymer. These results also suggest that the polymer nanocomposite is a better cathode material than the pristine alkali bronze oxide due to the effect of PEDOT intercalated into the MoO<sub>3</sub> framework in enhancing the discharge capacity of MoO<sub>3</sub> material and could be attributed to the changes in the interlayer spacing due to more facile lithium ion diffusion.

#### 4.3.11 Cycle life

In order to clarify the role of the polymer incorporation on the electrochemical performance for

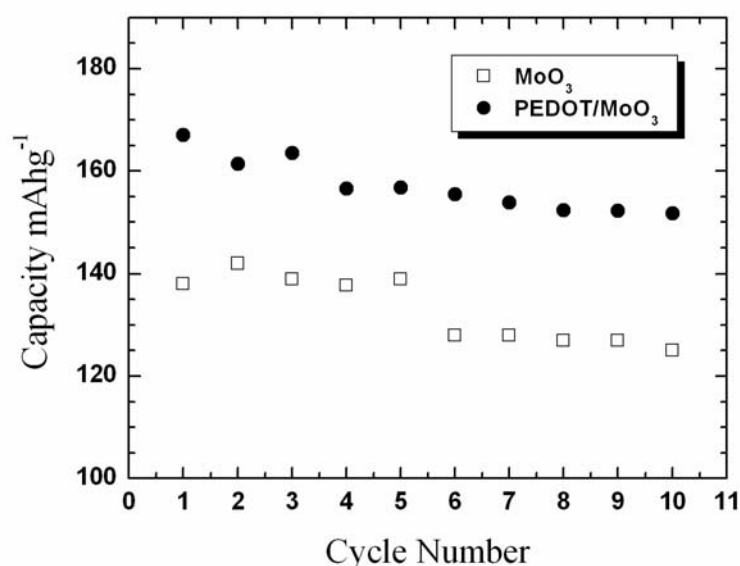


Figure 4.10. Evolution of discharge capacity with number of cycles for pristine VS<sub>2</sub> and PEDOT/VS<sub>2</sub>. The data were obtained at a current density of 0.5 mA/cm<sup>2</sup>. in the potential range of 2.0 ~ 4.4 V vs. Li reference electrode.

extended cycling, the variation of discharge capacities were measured on MoO<sub>3</sub> and PEDOT/ MoO<sub>3</sub> as shown in Figure 4.10. For PEDOT/ MoO<sub>3</sub> there is only a small loss in capacity over the first four cycles, indicating nearly 96% coulombic efficiency for the discharge process. In contrast, for the pristine MoO<sub>3</sub>, the cell capacity drops substantially after five cycles (Figure 4.10). The reason for poor cyclability in MoO<sub>3</sub> is thought to be the result of



irreversible reactions of  $\text{Li}^+$  with the lattice, and structural modifications.<sup>27</sup> These appear to be somewhat suppressed on incorporation of the PEDOT. However, PEDOT/  $\text{MoO}_3$  nano composite maintains capacities over 150 mAh/g for ten cycles and this nanohybrid provides larger capacity and better cyclability than the pristine  $\text{MoO}_3$ . The improved performance is presumably due to a higher electrical conductivity and to the altered separation between molybdenum oxide layers, due to an enhanced bidimensionality.

## 4.4 Conclusions

In conclusion, a novel approach to prepared poly (3,4-ethylenedioxythiophene)/  $\text{MoO}_3$  nanocomposite by using a soft chemistry route has been discussed in this chapter. This reaction takes place with the *in situ* oxidative polymerization in the presence of an external oxidizing agent. Our results suggest that the interlayer spacing, upon intercalation expands from 6.93Å to 13.46Å followed by exfoliation and restacking process. The resultant interlayer separation is consistent with the existence of two phases of organic and inorganic species in the nanocomposite corresponding to the intercalation of PEDOT in the  $\text{MoO}_3$  framework to produce a new composite. The experimental data presented here also suggest that the polymerization proceeds concomitantly with intercalation. Although, despite the relative conductivity is a linear function of PEDOT content and interestingly there is a three order of magnitude increase in conductivity compared to that of the pristine oxide afforded by incorporation of polymer, and we also observed that the effect of the polymer incorporation in between  $\text{MoO}_3$  layers is to improve the linearly current increase with scan rate is expected for a strongly adsorbed electrochemical species. It is interesting to note that the double layer capacitance of pristine  $\text{MoO}_3$  increases from ~40 mF/g to ~300 F/g. In addition during the discharge process, the second discharge capacity is found to be significantly enhanced from 130 mAh/g for pure  $\text{MoO}_3$  compared to 160 mAh/g for PEDOT/  $\text{MoO}_3$  nanocomposites under similar experimental conditions and the nanocomposite displays intriguing effects with respect to electrochemical  $\text{Li}^+$  insertion. Thus we conclude that the PEDOT/ $\text{MoO}_3$  nanocomposite is a promising electrode material for supercapacitor and better cathode for rechargeable lithium battery than the pristine alkali bronze oxide.

## 4.5 References

1. V.L. Colvin, M.C. Schlamp, and A.P. Alivisatos, *Nature*, **370** (1994) 354.
2. C. Arbizzani, M. Mastragostino, L. Meneghello and R. Paraventi, *Adv. Mater.* **8** (1996) 331.
3. M-I. Baraton, L. Merhara, J. Wang and K. E. Gonsalves, *Nanotechnology*, **9** (1998) 356.
4. B.Rajesh, K.R.Thambi, J.-M.Bonard, N.Xanthapolous, H.J.Mathieu and B.Viswanathan, *Electrochem Solid State Lett*, **5** (2002) E71.
5. B. R. Mattes, E. T. Knobbe, P. D. Fuqua, F. Nishid, E. W. Chang, B. M. Pierce, B. Dunn and R. B. Karner, *Synth. Metal* **43** (1991) 3183.
6. F. Bonino and B. Scrosati, *In Materials for Solid State Batteries*: B. V. R. Chowdari, S. Radhakrishna, Eds.; *World Scientific: Singapore*, (1986) P53.
7. -G.Wu,D.C.DeGroot, H.O. Marcy, J.L. Schindler, C.R. Kannewurf, Y.-J. Liu, W, Hirpo and M.G. Kanatzidis, *Chem.Mater.* **8** (1996) 1992.
8. T.A. Kerr, L.F. Nazar, *Chem. Mater.* **8** (1996) 2588.
9. E.Shouji, D. A. Buttry, *Langmuir*. **15** (1999) 669.
10. S. Kuwabata, S.Masui, H.Tomiyori, H.Yoneyama, *Electrochim. Acta*, **46** (2000) 91
11. P.Gomez-Romero,. *Adv Mater*, **13** (2001) 163.
12. A.Vadivel Murugan, B.B. Kale, C-W.Kwon, G.Campet, K.Vijayamohan, *J.Mater.Chem.* **11** (2001) 2470.
13. A.Vadivel Murugan, C-W.Kwon, G.Campet, B.B. Kale, T.Maddanimath and K.Vijayamohan *J.Power Sources*, **105** (2002) 1.
14. C-W.Kwon, A.Vadivel Murugan, G.Campet, J. Portier, B.B. Kale, K.Vijayamohan, J.H.Choy *Electrochem.Comm*, **4** (2002) 384.
15. G. Heywang and F. Jonas, *Adv. Mater.* **4** (1992) 116.
16. H. Yamato, M. Ohwa and W. Wernet, *J. Electroanal. Chem.* **397** (1995) 163.
17. I. Winter, C. Reese, J. Hormes, G. Heywang and F. Jonas, *Chem. Phys.* **194** (1995) 207.

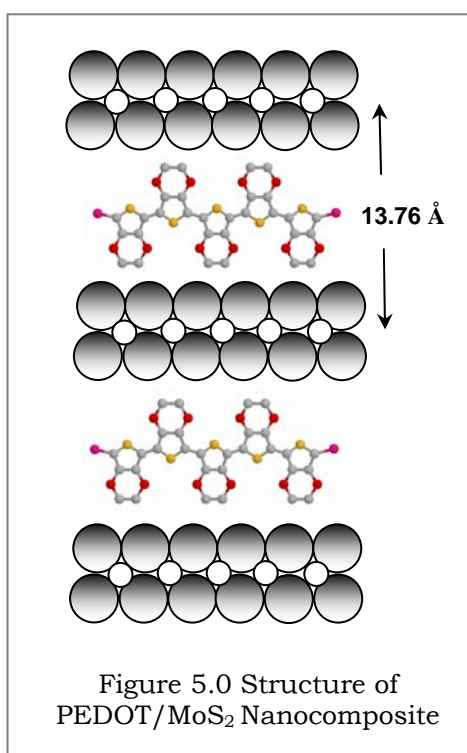
18. P. Novak, K. Muller, K. S. V. Santhanam, O. Haas, *Chem. Rev.* **97** (1997) 207.
19. N.Margalit, *J.Electrochem.Soc.*, 121 (1974) 1460; G.A.Nazri, C.Julien, *Solid State Ionics*, **68** (1994) 111.
20. N.Kumagai, N.Kumagai, K.Tanno, *J.Appl Electrochem*, 1988, **18**, 857.; S.K.Deb, *Proc. Roy. Soc., (London) Ser.A* **304** (1968) 211.
21. J.-P.Pereira-Ramos, N.Kumagai, N.Kumagai, *J.Power Sources* **56** (1995) 87.; M.Greenblatt, *Chem.Rev*, **88** (1988)31.
22. T.A. Kerr, H.Wu, L.F. Nazar, *Chem. Mater.* **8** (1996) 2005.
23. V.Hernandez, F.J.Ramirez, T.F.Otero, J.T.Lopez Navarrete, *J.Chem.Phys.* **100** (1994) 114.
24. G.Louarn, J.Kruszka, S.Lefrant, M.Zagorska, I.Kulshewicz-Bayer, A.Prón, *Synth.Met.* **61** (1993) 233.
25. N.B.Colthup, L.H.Daly, S.E.Wiberley, *Introduction to Infrared and Raman Spectroscopy*, Academic Press, New York, 1964, 276.
26. R.S.Tipson, H.S.Isbell, J.E.Stewart, *J.Res.Natl.Bur.Standards.* **62** (1959) 257.
27. J.O.Besenhard, R.Schollhorn, *J.Power Sources*, **1** (1976) 267.

# POLY (3,4-ETHYLENEDIOXYTHIOPHENE) NANOSHEET FORMATION IN BETWEEN MoS<sub>2</sub> LAYERS BY EXFOLIATION AND RESTACKING PROCESS

# 5

## Chapter

This chapter deals with a new type of layered poly (3, 4-ethylenedioxythiophene) PEDOT/ MoS<sub>2</sub> nanocomposite synthesized *via* flocculation of delaminated MoS<sub>2</sub> with subsequent *in situ* oxidative polymerization of 3,4-ethylenedioxythiophene. Intercalation produces an



expansion of the lattice in a direction perpendicular to the S-Mo-S dichalcogenide layers held together by van der Waals interactions. The resulting nanocomposite with PEDOT nanosheets in between MoS<sub>2</sub> layers is characterized by thermal analysis (TGA), powder X-ray diffraction, FTIR, SEM, TEM, XPS and four-probe electrical conductivity measurements. Chemical analysis and X-ray diffraction results indicate that the exfoliated MoS<sub>2</sub> and PEDOT are restacked to produce a novel nanoscale composite material containing alternate nanosheets of PEDOT in between MoS<sub>2</sub> with a basal distance of ~1.38 nm. The application potential of this nanocomposite as a cathode material for rechargeable lithium battery is also demonstrated by the

electrochemical intercalation of lithium into the PEDOT/ MoS<sub>2</sub> nanocomposite, where a significant enhancement in the discharge capacity is observed compared to that of respective pristine sulfide.

## 5.1 Introduction

Recently low dimensional materials have attracted much attention due to their novel physicochemical properties in comparison with bulk materials. For example, zero-dimensional nanoparticles and one-dimensional nanostructures, such as nanotubes, nanowires, and nanorods, have been intensively investigated both for their size and shape dependent fundamental properties and also potential applications.<sup>1-6</sup> Low dimensional systems comprising of a variety of two-dimensional lamellar nanocomposite has also been synthesized by chemically delaminating a layered host into molecular single layers.<sup>7-9</sup> One approach to modify the properties of a layered material such as layered inorganic oxides, sulfides and graphite is through the intercalation of guests into this host using suitable procedures.<sup>10-15</sup> For example, many transition metal dichalcogenides have lamellar structures which are amenable to intercalation, and such modified materials also have interesting applications.<sup>16</sup> In particular, MoS<sub>2</sub> has drawn great attention due to its several important applications as an inorganic host for polymers,<sup>17</sup> a high-energy density battery cathode,<sup>18</sup> an encapsulating support for magnetic materials,<sup>19</sup> a catalyst support for hydrodesulfurization (HDS) and a coal liquefaction catalyst.<sup>20</sup> In the continuing quest for preparing hybrid materials with novel or enhanced properties, insertion of conducting polymers in layered host materials and other structurally organized environments is a topic of considerable interest because the resulting organic-inorganic nanostructures can possess novel electrical, structural, and mechanical properties. Such systems can potentially show hybrid properties synergistically derived from both the host and the guest.<sup>13</sup>

In *Chapter-2*, we have demonstrated the synthesis of conducting poly (3,4-ethylene dioxythiophene) based nanocomposite and its important application as a cathode material for rechargeable lithium batteries.<sup>14</sup> Poly (3,4 ethylenedioxythiophene) (PEDOT), one of the recently found excellent conducting polymers, has been reported to exhibit greatly enhanced stability compared to polypyrrole and polyaniline.<sup>21,22</sup> Indeed, it appears to be one of the most stable conducting polymers currently available<sup>35</sup> and has been attracting growing interest for applications in supercapacitors and electrochromic devices.<sup>23,24</sup> In this chapter we focus on the synthesis and characterization of organo-inorganic PEDOT/ MoS<sub>2</sub> nanocomposite, where PEDOT forms nanosheets in the interlayer spacing. The primary objective is to understand the specific interactions between PEDOT and MoS<sub>2</sub> using various spectroscopic and electrochemical

techniques to demonstrate how these interactions contribute to enhance the properties of the PEDOT/MoS<sub>2</sub> nanocomposite. These observations are supported by several physicochemical data including the microstructure of PEDOT/ MoS<sub>2</sub> nanocomposite, after the polymer nanosheets formation in between the MoS<sub>2</sub> layers. To our knowledge, this the first study of the preparation of PEDOT/ MoS<sub>2</sub> nanocomposite which also demonstrates that, it is possible to increase the specific capacity for its possible applications in rechargeable lithium batteries in comparison with that of pristine MoS<sub>2</sub> cathodes.

## 5.2 Experimental Section

### 5.2.1 Materials

MoS<sub>2</sub> (99 %), Butyllithium (1.6 M solution in hexane), lithium metal foil (99.9%), LiClO<sub>4</sub> (99.99%), polytetrafluoroethylene (PTFE,99.99%), propylene carbonate (PC,99.9%) and dimethylcarbonate (DMC,99%) from Aldrich and n-hexanol (98%) from Fluka were used without any further purification. 3,4-ethylenedioxythiophene (EDOT, Bayer AG Germany) was distilled under vacuum prior to use. Ethylene carbonate (EC, Prolabo 99%) and ketjenblack were used as received. All experiments were conducted with deionized water.

### 5.2.2 Preparation of Li<sub>x</sub>MoS<sub>2</sub>

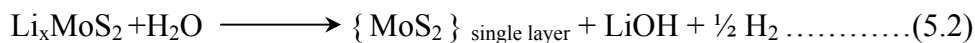
Li<sub>x</sub>MoS<sub>2</sub> was prepared by reacting three equivalents of standardized 1.6 M n-butyllithium to a dispersion of 2H- MoS<sub>2</sub> in hexane soaked for 48 h under N<sub>2</sub> atmosphere.



Following the intercalation of the MoS<sub>2</sub> by lithium, the product was washed repeatedly in hexane, dried and sealed. Li<sub>x</sub>MoS<sub>2</sub> formation was confirmed by powder X-ray diffraction as a single phase with a hexagonal unit cell having a=3.312(45) and c=6.394(18) Å. The lithium content, (x) was determined to be 1.02, while, Mo and S were analyzed by flame emission spectroscopy, X-ray fluorescence and CHNS-O analysis respectively.

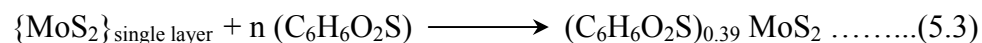
### 5.2.3 Preparation of Exfoliated and Reflocculated MoS<sub>2</sub>

All further stages of the reaction were carried out in air by adding sufficient de-ionized water to Li<sub>x</sub>MoS<sub>2</sub> in order to produce a suspension of 0.08 gml<sup>-1</sup> exfoliated MoS<sub>2</sub>-{represented by (MoS<sub>2</sub>)<sub>exfoliated</sub>}. The suspension was sonicated for 30 min, and the single layer dispersion was reflocculated after acidification to pH of 2 using concentrated HCl .



### 5.2.4 Polymer Intercalation and Restacking of MoS<sub>2</sub>

To this suspension, 3,4-ethylenedioxythiophene (EDOT) monomer (4.6 mM) was added drop wise and was refluxed with single layer dispersion of reflocculated MoS<sub>2</sub> for further 2h to ensure complete mixing. To this, 8.5 g of the oxidizing agent, iron (III) chloride in 10 ml of water was added drop wise under refluxed conditions for 10 h.



PEDOT/MoS<sub>2</sub> solid was filtered off and washed repeatedly with water and ethanol and the dark bluish black powder was dried in air. The Molybdenum content was determined by Inductive Coupled Plasma Optical Emission Spectroscopy (ICP-OES) to the sample solution that was prepared by dissolving the composite powder in concentrated sulfuric acid followed by dilution with water and filtration to remove the dispersed polymer. Elemental analysis of nanocomposite gave (C<sub>6</sub>H<sub>4</sub>O<sub>2</sub>S)<sub>0.39</sub> MoS<sub>2</sub> :C, 7.29%; H, 1.34%; S, 29.26 % and Mo, 40.97%.

### 5.2.5 Characterization techniques

The experimental detail of all physical characterization techniques carried out on the nanocomposite as well as the pristine MoS<sub>2</sub> has been discussed in *Chapter-3* (section.3.2.4).

### 5.2.6 Electrochemical measurements

Electrochemical measurements were carried out using the composite cathode, prepared by mixing the PEDOT/ MoS<sub>2</sub> nanocomposite powder and pristine VS<sub>2</sub> with carbon black and PTFE binder (70:25:5 by weight), followed by compaction and drying under a primary vacuum for 3 hrs at 80°C. This composite cathode was coupled with a lithium foil anode in 1M LiClO<sub>4</sub>

dissolved in a mixture of ethylene and dimethyl carbonate (EC/DMC 1:1) to form the electrochemical cell. All the charge discharge measurements were performed in a galvanostatic mode using a computer controlled potentiostat/ galvanostat. All manipulations of air sensitive materials as well as the cell assemblies were carried out in an argon filled glove box.

## 5.3 Results and Discussion

### 5.3.1 Synthesis of MoS<sub>2</sub> Intercalation compound

The synthetic techniques used here for the intercalation of MoS<sub>2</sub> and other hosts have been discussed previously.<sup>25</sup> Molybdenum disulfide is Hexagonal, space group-P63/mmc (2/m 2/m 2/m) with lattice parameters as,  $a=3.15$ ,  $b=3.15$ ,  $c=12.3$  (Å);  $\alpha=90^\circ$   $\beta=90^\circ$  and  $\gamma=120^\circ$ . When Li is intercalated between the sulfide layers of the 2H- MoS<sub>2</sub> (undistorted) this compound becomes metallic since it gets transformed to the CdI<sub>2</sub> structure of 1T- MoS<sub>2</sub> (distorted). 1T- MoS<sub>2</sub> adopts a structured type closely related CdI<sub>2</sub> except that the Mo ions are in trigonal prismatic coordination, rather than in octahedral coordination.<sup>16</sup> However, 1T- MoS<sub>2</sub> structure contain sheets of edge sharing polyhedra (octahedrons or trigonal prisms) held together by van der Waals interactions between sulfur atoms although the intercalated with Li (i.e, Li<sub>x</sub>MoS<sub>2</sub>) reacts with H<sub>2</sub>O (in sonication bath to increase the rate of reaction), as per equation 5.2. During this reaction Li<sup>+</sup> cations get hydrated leaving negatively charge on MoS<sub>2</sub> layers, thus facilitating the reduction of H<sub>2</sub>O to H<sub>2</sub> gas. The microbubbles of H<sub>2</sub> gas produced between the MoS<sub>2</sub> sheets forces them apart (exfoliation) to give an aqueous colloidal suspension of partially negatively charged, single layers of MoS<sub>2</sub>.<sup>16</sup> Upon addition of H<sup>+</sup>, the layers are discharged, presumably with the formation of H<sub>2</sub>, and the single layers are flocculated to give “restacked” MoS<sub>2</sub>, followed by subsequent in situ polymerization of 3,4-ethylenedioxythiophene to the suspension of single-layer MoS<sub>2</sub>.

### 5.3.2 Structure of 1T-MoS<sub>2</sub>

The intercalation of 2H-MoS<sub>2</sub> by Li is known to induce a structural change.<sup>26</sup> In 2H- MoS<sub>2</sub>, the sulfur atoms are in hexagonal close-packed sheets. Planes of Mo atoms are sandwiched between alternating sulfur layers such that each Mo is coordinated to six S atoms in trigonal prismatic geometry. In the unit cell, there are two such sandwiches, with an *aBa bAb\** stacking pattern along the *c* lattice direction. The region between the sandwiches (the *a* and *b* sulfur



planes) is held together by weak van der Waals forces. Upon intercalation, the Li atoms donate electrons to the  $d$ -band of the MoS<sub>2</sub> host and Li<sup>+</sup> cations migrate into the interlamellar spacing. The reduced MoS<sub>2</sub> layers transform into the 1T-MoS<sub>2</sub> structural type with octahedrally coordinated Mo atoms and an  $aBc$   $aBc$  stacking pattern along the  $c$  axis direction, such that there is one sandwich layer per unit cell (*Figure 5.2b*).

### 5.3.3 Structure of PEDOT/MoS<sub>2</sub> Intercalation Compound

The fact that intercalation occurs upon restacking the MoS<sub>2</sub> in the presence of polymer guest is observed by X-ray diffraction when the sample is prepared such that the basal planes of the nanocomposite are parallel to the X-ray beam (*Figure 5.2c*). This orientation affords diffraction spots due to  $00l$  as  $c$  is perpendicular to the X-ray beam. Indexing these spot yields a  $c$  lattice parameter ( $13.7 \pm 0.1 \text{ \AA}$ ) which suggests a lattice expansion of  $7.62 \text{ \AA}$ , compared to 2H-MoS<sub>2</sub>. X-ray diffraction of the intercalated sample is also consistent with a lattice expansion in the  $c$  direction, when compared to 2H-MoS<sub>2</sub> (*Figure 5.2 a*). The powder patterns showed only 001 and 002 diffraction peaks at a  $2\theta$  value of  $14.4^\circ$ . *Table 5.1* summarizes the  $d$  spacings corresponding to the diffraction patterns presented in *Figure 5.2*. and similarly *Scheme 5.1* demonstrates the relation between the  $c$  lattice parameters of 2H-MoS<sub>2</sub>, intercalated MoS<sub>2</sub> and PEDOT/MoS<sub>2</sub>. As the layer thickness of 1T-MoS<sub>2</sub> is almost identical to a single layer of 2H-MoS<sub>2</sub> ( $c \approx 6.14 \text{ \AA} = d_{002}$  for 2H-MoS<sub>2</sub>) the  $c$  lattice parameter of the polymer intercalation represents an interlayer expansion ( $\Delta c$ ) of approximately  $7.62 \text{ \AA}$ , commensurate with the intercalation of one layer of the guest species. The introduction of polar substituents in thiophene favors a perpendicular orientation of the guest in the interlayer space, permitting a higher degree of organic incorporation

### 5.3.4 FTIR Spectroscopy

*Figure.5.1* shows a comparison of the FT-IR spectra of (a) 2H-MoS<sub>2</sub> (b) exfoliated 1T-MoS<sub>2</sub> (c) restacked PEDOT/ MoS<sub>2</sub> nanocomposite and (d) pristine PEDOT. Crystalline 2H-MoS<sub>2</sub> has a very narrow peak, poorly crystalline MoS<sub>2</sub>, a very broad peak, and amorphous MoS<sub>2</sub>, almost no infrared features.<sup>28</sup> The crystalline 2H-MoS<sub>2</sub> peak generally occurs at  $365 \text{ cm}^{-1}$  although *Figure 5.1a* shows this as narrow peak at  $\sim 370 \text{ cm}^{-1}$  may be due to Mo- S -Mo peaks of

the highly crystalline MoS<sub>2</sub>.<sup>28</sup> In comparison, *Figure 5.1b* shows the corresponding spectrum after exfoliation of Li<sub>x</sub>MoS<sub>2</sub> with well resolved broad Mo=S and Mo-S-Mo peak positions at

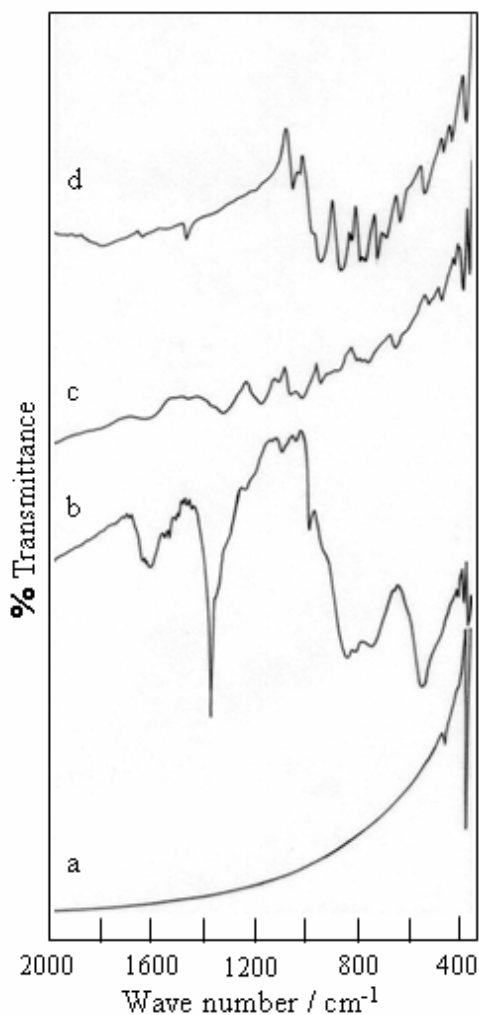


Figure 5.1. FTIR spectra of the (a) 2H-MoS<sub>2</sub> (b) exfoliated 1T-MoS<sub>2</sub> (c) PEDOT/ MoS<sub>2</sub> nanocomposite and (d) PEDOT

560, 754, 851 and 993 due to the  $\nu$  (Mo -S- Mo) doubly bounded S<sup>2-</sup>, doubly bridged S<sup>2-</sup> and  $\nu$  (Mo =S) terminal S stretches respectively. When we compare the spectrum of pristine polymer (*Figure 5.1d*) and MoS<sub>2</sub> (*Figure 5.1b*) separately, the intensity of the combined characteristic peaks of PEDOT/ MoS<sub>2</sub> are decreased as revealed in *Figure 5.1c*. This could be attributed to the restacking of MoS<sub>2</sub> layers along with polymer nanosheets. The vibrational spectrum of PEDOT/ MoS<sub>2</sub> is a combination of the vibrational features of PEDOT and that of MoS<sub>2</sub>. The 500-1500 cm<sup>-1</sup> region of the infrared spectrum is sensitive to C-H vibrations and consequently, any shift in this region can be used to identify the prominent changes in the polymer structure. The positions of the vibrational peaks arising from the encapsulated PEDOT are close to those of pure PEDOT polymer peak vibrations at 1512, 1470 and 1388 cm<sup>-1</sup> originated from the stretching of C=C and C-C in the thiophene ring<sup>29,30</sup> Further vibration from C-S bond in the thiophene ring can be seen at 930, 832 and 694 cm<sup>-1</sup> <sup>29,30</sup> Vibrations at 1142-1128,

1093-1076 and 1052-1047 cm<sup>-1</sup> are assigned to the stretching of the alkylendioxy group.<sup>31, 32</sup> Doping induced bands originating from changes in the conjugated backbone due to electron withdrawing (oxidation) from the polymer chain and counter balance also seen during polymerization appear at 1332, 1202, 1142, 1048 and at 918cm<sup>-1</sup> which are interpreted to be from stretching in the ethylendioxy ring and from the doping of C-S bond with Cl<sup>-</sup>.

### 5.3.5 Powder X- ray diffraction (XRD)

The encapsulation of polymers inside the interlayer galleries of MoS<sub>2</sub> is demonstrated by X-ray powder diffraction, which shows an expansion of the gallery space. For instance, *Figure 5.2 a, b and c* shows a comparison of typical XRD patterns of (a) crystalline 2H-MoS<sub>2</sub>, (b) 1T-MoS<sub>2</sub> and (c) poly (3,4-ethylenedioxy thiophene) PEDOT/ MoS<sub>2</sub> nanocomposite, where sharp and intense (001) reflections indicate the distinct stacking of MoS<sub>2</sub> layers. An increase in the interlayer distance of the pristine sulfide, MoS<sub>2</sub>, from 6.15 to 13.76 Å, indicates substantial incorporation of conducting polymeric material between the layers. The introduction of polar substituents to thiophene favors a perpendicular orientation of the guest in the interlayer space, permitting a higher degree of organic incorporation. In addition, the change in the interlayer distance is consistent with the interstitial PEDOT chains being oriented with the planes of the thiophene rings perpendicular to the layers as evident from the intense sharp peaks. For the PEDOT<sub>0.35</sub> MoS<sub>2</sub> nanocomposite, the polymer chains

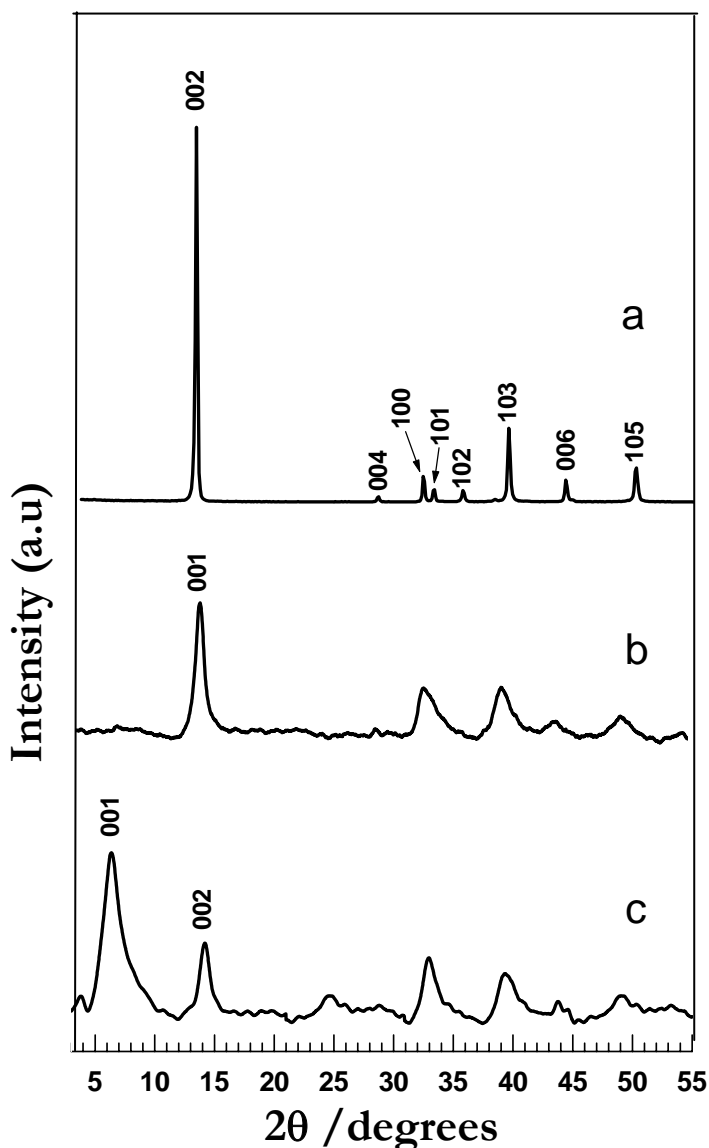
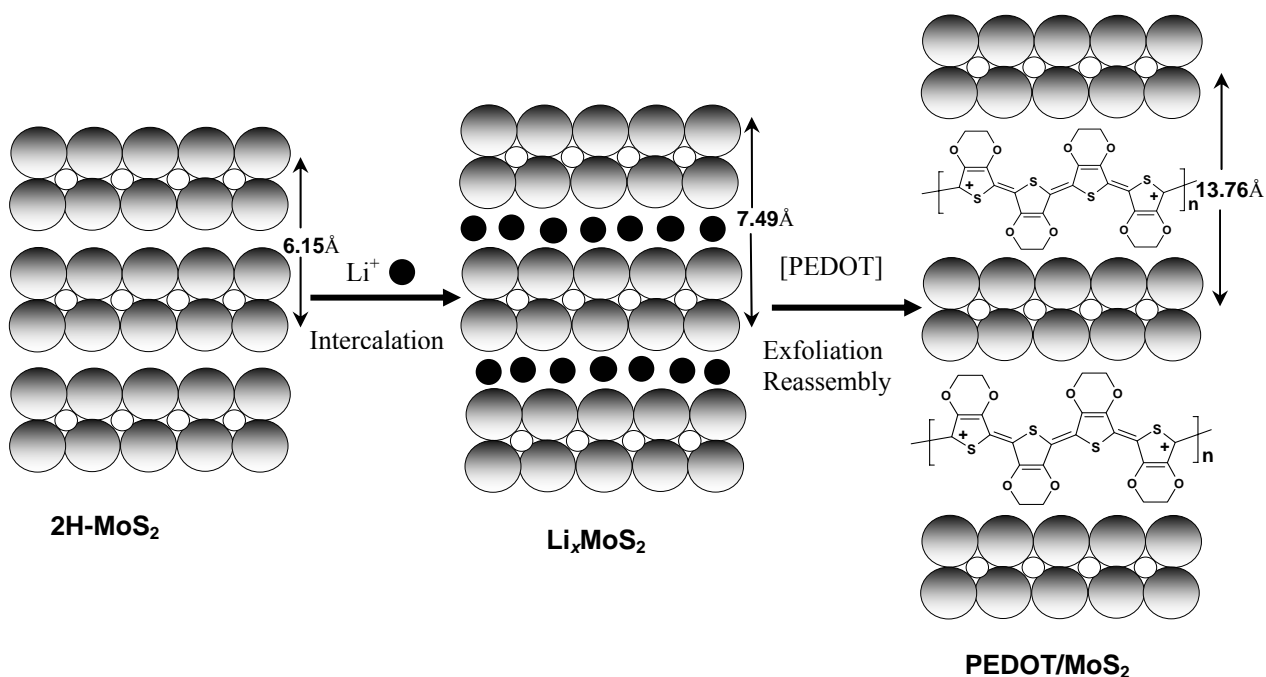


Figure 5.2. A comparative powder X - ray diffraction patterns of (a) 2H-MoS<sub>2</sub> powder and (b) 1T-MoS<sub>2</sub> (c) PEDOT/ MoS<sub>2</sub> nano composite

appear to be fixed in the interlamellar space, and the high degree of ordering is evident from the oriented powder XRD patterns suggesting that the PEDOT chains are aligned, at least to some extent, in the *ac* (basal) plane. Therefore, considerable bonding interaction between the organic

and inorganic components is expected probably due to the hydrogen bonding. These results also suggest that the polymer chains lie parallel to each other in the “valleys” of the sulfide sheets. Thus it is likely that these materials constitute a new PEDOT / MoS<sub>2</sub> composite phase consisting of a monolayer of PEDOT chains intercalated within the MoS<sub>2</sub> interlayer spacing and this is summarized in *Scheme 5.1*. This high degree of ordering is also supported by several groups working on similar organic-inorganic hybrid materials of conducting polymers with transition metal sulfide/oxide hosts.<sup>33</sup>



**Scheme 5.1. Schematic representation of Organo-Inorganic Poly(3,4-ethylenedioxythiophene)PEDOT/MoS<sub>2</sub> Nanocomposite by Intercalation**

### 5.3.6 X-ray Photoelectron Spectroscopy (XPS)

PEDOT and PEDOT/MoS<sub>2</sub> composite material were subjected to XPS analysis and the results from molybdenum 3d and sulfur 2p core levels of the above samples are shown in *Figures 5.3a and 5.3b*, respectively. Composite material was made into pellets and the surface was

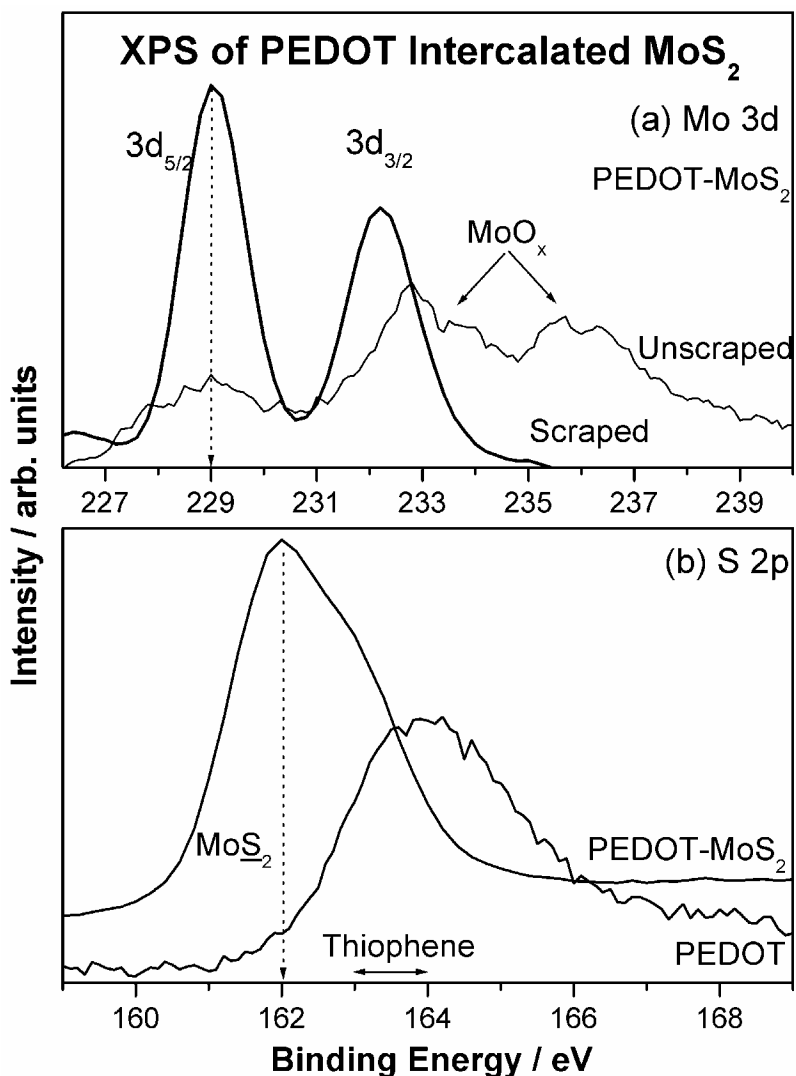


Figure 5.3 XPS of (a) Mo 3d core level and (b) S 2p core level from PEDOT and PEDOT intercalated MoS<sub>2</sub>; unscraped PEDOT-MoS<sub>2</sub> surface shows MoO<sub>x</sub> species due to atmospheric oxidation although physical scraping removes the contamination.

scraped *in situ* in the XPS chamber to remove any degradation/air oxidation product on the composite surface. Interestingly, the PEDOT/MoS<sub>2</sub> surface analyzed prior to scraping (*dotted line in Fig 5.3. a*) shows large amount of oxidation of Mo-species to MoO<sub>x</sub>. This could be attributed to the surface oxidation by air leading to above molybdenum oxides in addition to carbonates and hydroxides, which have been completely removed by scraping. Mo 3d core level spectrum shows spin-orbit doublet peaks at 229.1 and 232.3 eV respectively, for PEDOT/MoS<sub>2</sub> composite (bold line) after scraping, which is typical for MoS<sub>2</sub> sulphide<sup>34</sup>. This procedure ensures that the surface analyzed after scraping offers an uncontaminated surface

representative of PEDOT/MoS<sub>2</sub> and the atmospheric degradation is limited to only the top surface.

S 2p core level from PEDOT displays a peak at 164 eV, typical for thiophene sulfur<sup>34</sup>. The main S 2p peak at 162 eV on PEDOT/MoS<sub>2</sub> after scraping is due to S from MoS<sub>2</sub>. However, the S 2p core level from PEDOT/MoS<sub>2</sub> also shows a shoulder around 163 eV which suggests that on PEDOT intercalation, there is some charge transfer from Mo to thiophene units. On the whole, the XPS studies hint a reduction of PEDOT after intercalation into MoS<sub>2</sub> and there is also associated charge transfer from MoS<sub>2</sub> to thiophene sulfur. Thus XPS results are in good agreement with the results of the other studies.

### 5.3.7 Thermogravimetric Analysis (TGA)

The thermal analysis of PEDOT/ MoS<sub>2</sub> nanocomposite in air was examined by TGA experiments as shown in *Figure 5.4*. The TG curve shows a two step decomposition of the

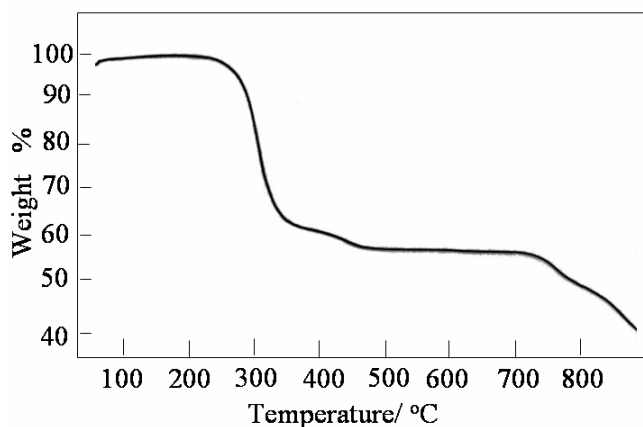


Figure 5.4. TGA curve of the PEDOT/ MoS<sub>2</sub> nanocomposite

intercalated PEDOT/MoS<sub>2</sub> nanocomposite (*Figure 5.4*). The mass loss which occurs at the first step, up to ~ 310°C could be attributed to the combustion of the organic polymer component. This is in agreement with the DTA curve where a large, relatively sharp exothermic peak at 280-310°C is distinct due to the degradation/oxidation of the poly (3,4-ethylenedioxythiophene) between the V<sub>2</sub>O<sub>5</sub> layers as has been recently reported.<sup>14</sup> Further more, the weight loss from TGA curve at 740°C is due to the phase transformation (melting) of MoS<sub>2</sub> to MoO<sub>3</sub> in the nanocomposite, which is in good agreement with the DTA curve of PEDOT/ MoO<sub>3</sub> where, a relatively sharp endotherm at 780°C, is apparent (*Chapter-4, section 4.3.3*). Thus the change in these thermal profiles could be attributed to the insertion and external oxidative polymerization of the 3,4-ethylenedioxythiophene (EDOT) between the MoS<sub>2</sub> layers.

### 5.3.8 Scanning Electron Microscopy (SEM)

A comparison of the SEM images of the MoS<sub>2</sub> and PEDOT / MoS<sub>2</sub> composite is presented in *Figure 5.5 a & b* respectively. It is apparent that PEDOT<sub>0.39</sub> MoS<sub>2</sub> composite forms a

continuous and relatively homogeneous matrix with a clearly lamellar morphology. It is evident that the incorporation of PEDOT into the MoS<sub>2</sub> accompanies morphological changes in agreement with the results of XRD patterns, although it can be seen only at a higher resolution. SEM micrographs also suggest that there is no bulk deposition of polymer on the surface of the micro-crystallites.

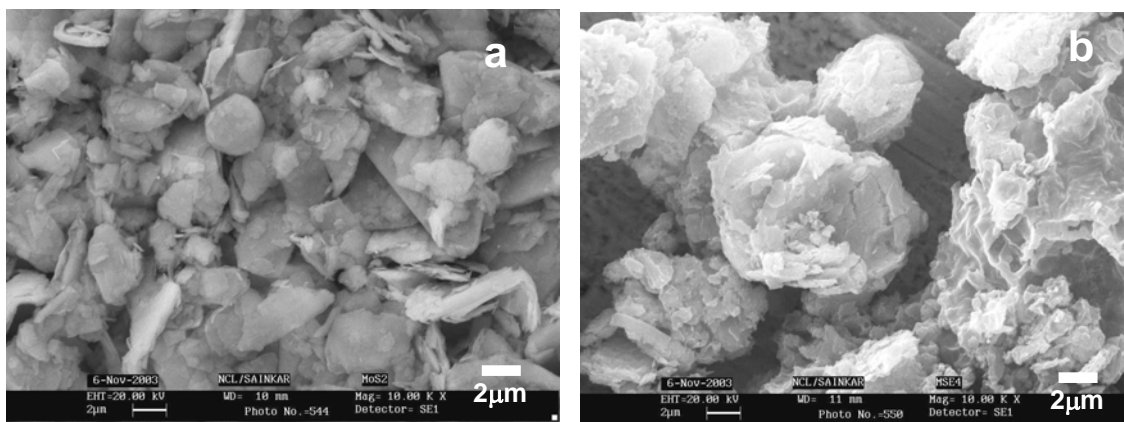


Figure 5.5. SEM micrographs of (a) MoS<sub>2</sub> and (b) PEDOT/ MoS<sub>2</sub> nanocomposite

### 5.3.9 Transmission Electron Microscopy (TEM)

The transmission electron microscopy (TEM) image shows thick particles of MoS<sub>2</sub> with few micrometer dimensions (*Figure 5.6 a*), where as the nanosheet morphology of the PEDOT/ MoS<sub>2</sub> nanocomposite, is illustrated in *Figure 5.6b*, suggesting that the *in situ* oxidative polymerization by “*Chimie douce*” is topotactic. As can be seen from TEM image, low scattering power causes bright contrast for white lines of conducting polymer nanosheets between dark

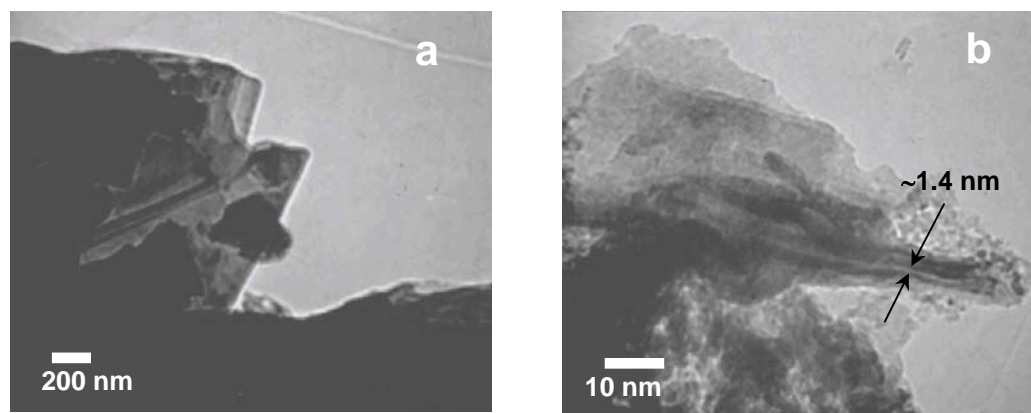


Figure 5.6. TEM images of (a) MoS<sub>2</sub> and (b) PEDOT nanosheets intercalated into MoS<sub>2</sub> layers to form a nanocomposite

fringes of MoS<sub>2</sub> host layers. It can be evaluated from the most pronounced intensity maximum found in the broad X-ray diffraction pattern  $d(001)$  (Figure. 5.2c). Thus, from the TEM image of the nanocomposite material, we conclude that highly crystalline MoS<sub>2</sub> is separated by alternating organic conducting polymer nanosheets in this hybrid which is also supported by the recently reported PEDOT nanosheet formation upon intercalation between V<sub>2</sub>O<sub>5</sub> layers.<sup>35</sup>

### 5.3.10 Electronic conductivity

The electron transport behavior of MoS<sub>2</sub> is expected to be significantly modified by the intercalation of PEDOT as the carrier density can undergo dramatic change. Four probe dc electronic conductivity of PEDOT/ MoS<sub>2</sub> nanocomposite measured at variable temperature shows

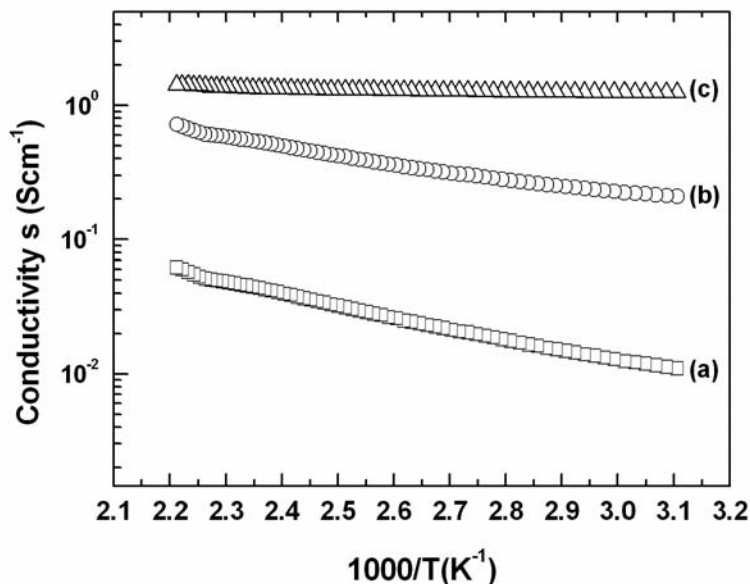


Figure 5.7. Four-probe variable-temperature electrical conductivity of (a) crystalline-MoS<sub>2</sub> (b) PEDOT/ MoS<sub>2</sub> nano composite and (c) PEDOT

a linear increase in conductivity indicative of thermally activated electron transport behavior as shown in Figure 5.7. Similar behavior of other nanocomposites was discussed in Chapter-4 (section 4.3.7). The room temperature conductivity for the PEDOT/ MoS<sub>2</sub> composite is  $2.09 \times 10^{-1} \text{ Scm}^{-1}$ , although pristine molybdenum disulfide is a semiconductor with a room temperature conductivity of  $1.09 \times 10^{-2} \text{ Scm}^{-1}$ .<sup>36</sup> The conductivity of PEDOT/ MoS<sub>2</sub> is therefore substantially increased over that of pristine MoS<sub>2</sub> which itself is higher than that of crystalline Li<sub>x</sub>MoS<sub>2</sub>. Surprisingly, it is not lower than that of bulk PEDOT ( $\sim 1.25 \text{ Scm}^{-1}$ ) and unlike what we observe for PEDOT/V<sub>2</sub>O<sub>5</sub> where the conductivity is a linear function of PEDOT content and interestingly there is a three order of magnitude increase in conductivity compared to that of the pristine oxide.<sup>14, 35</sup> The comparative electronic conductivity, open circuit voltage and discharge capacity of nanocomposite and their counterpart are listed in Table 5.1.



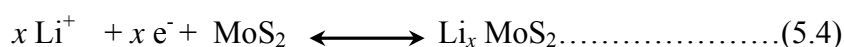
**Table 5.1. Comparison of the Interlayer Spacing, Electronic conductivity, Discharge capacity and Open circuit voltage of PEDOT/ MoS<sub>2</sub> nanocomposite with that of the individual components.**

Sample	Interlayer Spacing/ Å	Electronic conductivity, $\sigma/\text{Scm}^{-1}$ (R.T)	Discharge capacity/mAhg <sup>-1</sup>	Open circuit voltage* / V
MoS <sub>2</sub>	6.15	$1.09 \times 10^{-2}$	40	2.25
PEDOT/MoS <sub>2</sub>	13.76	$2.09 \times 10^{-1}$	96	2.62
PEDOT	-	$1.248 \times 10^0$	-	-

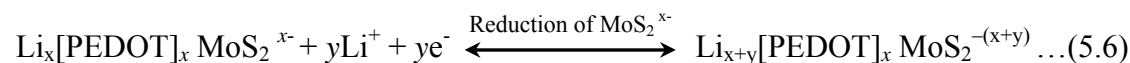
\*The open circuit voltage was obtained from the discharge measurements of MoS<sub>2</sub> and PEDOT/MoS<sub>2</sub> nanocomposite, as a cathode material by coupling with lithium metal anode using 1M LiClO<sub>4</sub> in propylene carbonate

### 5.3.11 Electrochemical lithium insertion

It is well known that the electronic property of MoS<sub>2</sub> can be altered significantly by the insertion of alkali metal ions into the van der Waals gap of this layered compound and accordingly electronic conductivity measurement shows a transition from semiconductor to a metal.<sup>37, 38</sup> For example, MoS<sub>2</sub> forms a stable lithium intercalation phase into Li<sub>x</sub>MoS<sub>2</sub> for  $0 < x < 1$  at room temperature, and the structure changes from the  $\alpha$ -phase (2H-MoS<sub>2</sub>) to a  $\beta$ -phase (1T-MoS<sub>2</sub>). During this first-order structural phase transition, the Mo coordination changes from trigonal prismatic to octahedral and the change in the structure is related to the difference in the electronic band structure of the two phases.<sup>39</sup> The electrochemical insertion of Li in MoS<sub>2</sub> material can be described by the following redox couple.



For the case of PEDOT/ MoS<sub>2</sub> nanocomposite, we can write analogous electrochemical reactions after incorporating lithium ions between the layers as;



### 5.3.12 Cyclic Voltammetry

A comparative cyclic voltammograms of (a) crystalline MoS<sub>2</sub> and (b) layered PEDOT/ MoS<sub>2</sub> nanocomposite, at several scan rates in 1M LiClO<sub>4</sub> in EC/DMC (1:1 v/v) is shown in *Figure 5.8*, illustrating a change in the electrochemical properties induced by the polymer insertion. For instance, during the first cathodic scan, from -2.5 to 0.25 V vs Ag/Ag<sup>+</sup>, the crystalline MoS<sub>2</sub>

undergoes a well-known structural phase transformation from the  $\alpha$ -phase (2H-MoS<sub>2</sub>) to a  $\beta$ -phase (1T-MoS<sub>2</sub>) after the lithium ion, (Li<sup>+</sup>) intercalation. During this first-order phase transition,

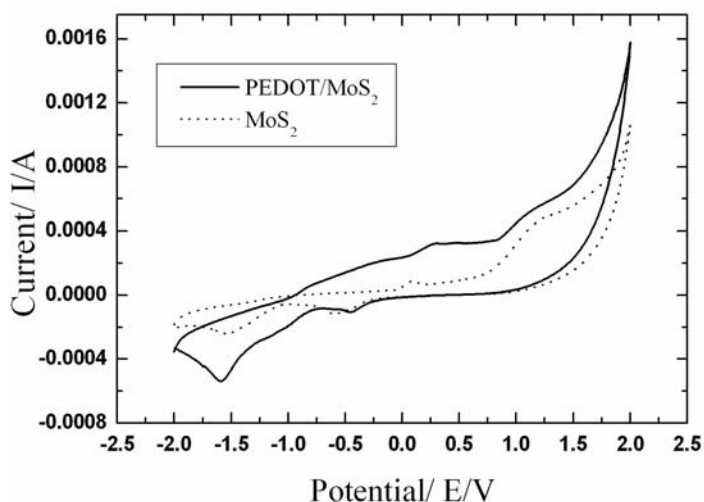


Figure 5.8. Cyclic Voltammograms of crystalline MoS<sub>2</sub> and layered PEDOT/ MoS<sub>2</sub> nanocomposite, using 1M LiClO<sub>4</sub> in EC/DMC (1:1 v/v)

the Mo coordination change from trigonal prismatic to octahedral<sup>39</sup> and *Figure 5.8* suggests that the structural change is permanent. Further, the weak interactions between the interlamellar layers allow fast insertion of Li<sup>+</sup> ions between the polymer ribbons rather than that in the crystalline molybdenum disulfide. In contrast, for the PEDOT/ MoS<sub>2</sub> hybrids, there is no sign of any irreversible structural change (*Figure 5.8*) although, the broad cathodic peak, resembles that of 2D inorganic layered compounds.<sup>14</sup> The broad and diffuse peak shape can, therefore, be correlated with the layer stacking derived by the polymer incorporation, as previously deduced from the X-ray diffraction data.

### 5.3.13 Charge-Discharge Properties

*Figure 5.9* demonstrates the potential vs. capacity curve for the third discharge carried out for MoS<sub>2</sub> and the PEDOT/ MoS<sub>2</sub> hybrid respectively, at a constant current density of 15 mA/cm<sup>2</sup> in the voltage range of 1.0 ~ 4 V (vs. Li<sup>+</sup>/Li), corresponding to an uptake of ~ 1.5 lithium per MoS<sub>2</sub> unit. Also the open-circuit voltage (OCV) of the composites when coupled with lithium metal anode is found to be a function of the PEDOT/ MoS<sub>2</sub> ratio and clearly all nanocomposite give higher OCV value (2.62V) than that observed (2.25V) for pure MoS<sub>2</sub> (*Table 5.1*). The discharge capacity is also found to be significantly enhanced from 40 mAh/g for pure MoS<sub>2</sub> to ca.100 mAh/g for the nanocomposite and the improvement in charging efficiency as well as cyclability for PEDOT/ MoS<sub>2</sub> nanocomposite is also evident under similar experimental conditions. The nanocomposite displays intriguing effects with respect to electrochemical Li<sup>+</sup> insertion. For example, despite relative increase in conductivity afforded by the incorporation of

the polymer, the effect of the polymer is perhaps to enhance the battery performance of the PEDOT eliminating water from the interlamellar region which can augment the discharge capacity due to the additional redox capabilities of the polymer. These results also suggest that the polymer nanocomposite is a better cathode material than the pristine  $\text{Li}_x\text{MoS}_2$  due to the

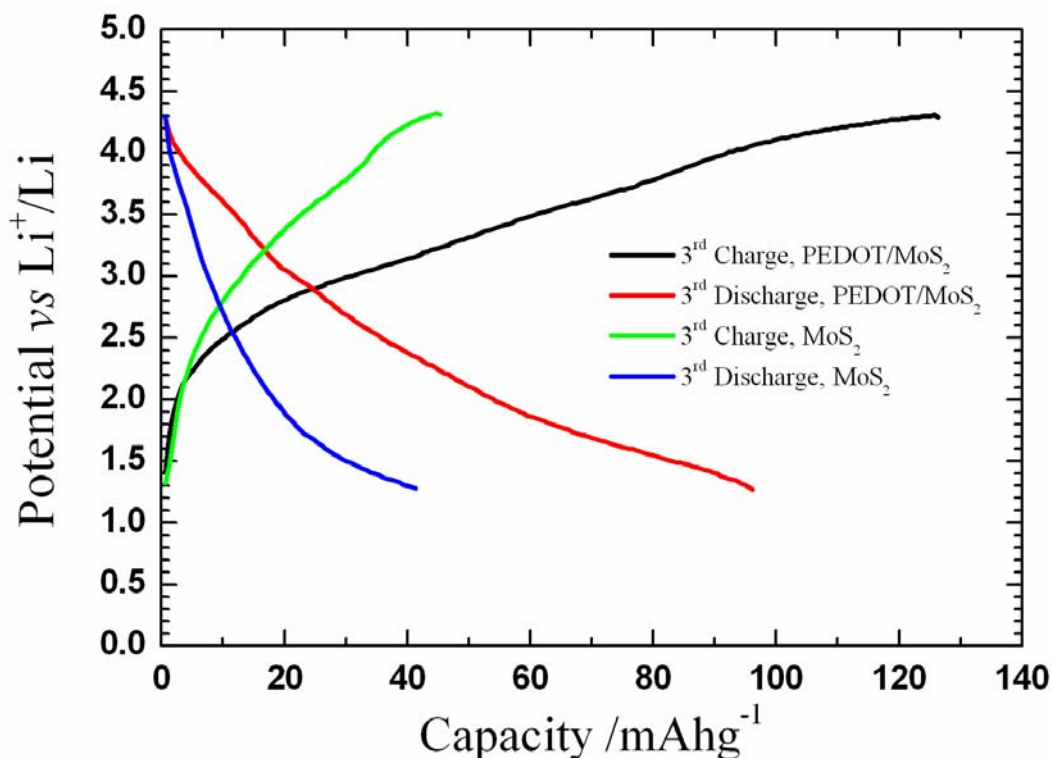


Figure 5.9. Potential vs. specific capacity for the third cycle of pristine  $\text{MoS}_2$ , and PEDOT/  $\text{MoS}_2$  nanocomposite. The potential range was selected to be 1.0 ~ 4.0 V vs. Li after coupling with lithium metal anode using 1M  $\text{LiClO}_4$  in a mixed electrolyte of ethylene and dimethyl carbonate using a constant current density of 15 mA/cm<sup>2</sup>.

effect of PEDOT intercalated into the  $\text{MoS}_2$  framework in enhancing the discharge capacity of  $\text{MoS}_2$  material and this could be attributed to the changes in the interlayer spacing due to more facile lithium ion diffusion.

### 5.3.14 Cycle life

In order to clarify the role of the polymer incorporation on the electrochemical performance for extended cycling, the variation of discharge capacities were measured for both  $\text{MoS}_2$  and PEDOT/  $\text{MoS}_2$  cathodes for several cycles as shown in *Figure 5.10*. For PEDOT/

MoS<sub>2</sub> composite there is only a small loss in capacity over the first two cycles, indicating better coulombic efficiency for the discharge process. In contrast, for the pristine MoS<sub>2</sub>, the cell

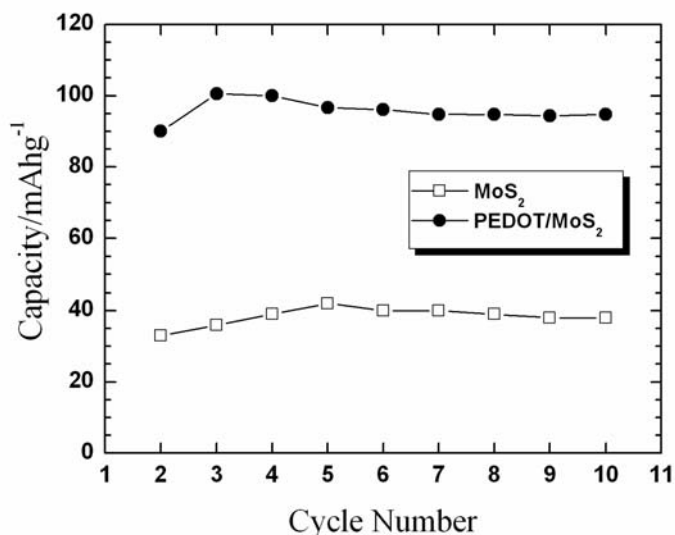


Figure 5.10. Evolution of discharge capacity with the number of cycles for pristine MoS<sub>2</sub> and PEDOT/ MoS<sub>2</sub>. The data were obtained at a current density of 15 mA/g. The potential range was set to 2.0 ~ 4.4 V vs. Li

capacity drops substantially up to five cycles (Figure 5.10). The reason for poor cyclability in MoS<sub>2</sub> is thought to be the result of irreversible reactions of Li<sup>+</sup> with the lattice, and structural phase transformation<sup>40</sup> from  $\alpha$ -phase (2H-MoS<sub>2</sub>) to  $\beta$ -phase (disordered 1T-MoS<sub>2</sub>) after the fifth cycle. This phase transition appears to be somewhat suppressed on the incorporation of the PEDOT and this can explain why the PEDOT/ MoS<sub>2</sub> nanocomposite maintains capacities over 90 mAh/g for several cycles than that of pristine MoS<sub>2</sub>. The improved

performances could also arise presumably due to a higher electrical conductivity and to the altered separation between MoS<sub>2</sub> layers, leading to enhanced bidimensionality.

## 5.4 Conclusions

We have found a novel method of interleaving poly (3,4-ethylenedioxythiophene) between the layers of MoS<sub>2</sub> using the soft chemistry route of intercalation. This reaction takes place with the *in situ* oxidative polymerization method in the presence of an external oxidizing agent. Analysis of the experimental data presented here suggests that the polymerization proceeds concomitantly along with intercalation. The fact that two distinct phases rather than a continuum of compositions is obtained in this system suggests the existence of a significant interaction between the host and guest beyond a simple insertion into the van der Waals gaps-perhaps closer to the formation of true compounds. Our results also suggest that the discharge capacity is also found to be significantly enhanced from 40 mAh/g for pure MoS<sub>2</sub> to ca.100 mAh/g for the nanocomposite and the improvement in charging efficiency as well as cyclability for PEDOT/ MoS<sub>2</sub> nanocomposite is also evident under similar experimental conditions.

## 5.5 References

1. J.A.Nelson, M.J.Wagner, *Chem.Mater*, **14** (2002) 915.
2. S.O'Brien, L.Brus, C.B.Murray, *J.Am. Chem.Soc*, **123** (2001)12085.
3. S.Iijima, *Nature*, **354** (1991) 56.
4. G.R.Patzke, F.Krumeich, R.Nesper, *Angew. Chem., Int.Ed.***41** (2002)2446.
5. X.F.Duan, Y.Huang, Y.Cui, J.-F.Wang, C.M.Leiber, *Nature*, **409** (2001) 66.
6. Z.-R.Tian, J.A.Liu,B.Mckenzie,M.J.Mcdermott. *J.Am.Chem.Soc.***124** (2002)12954.
7. D.M.Kaschak, S.A.Johnson, D.E.Hooks, H.-N.Kim,M.D.Ward, T.E.Mallouk, *J.Am.Chem.Soc.*, **120** (1998) 10887.
8. Y.-S.Han, I.Park, J.-H.Choy, *J.Mater.Chem*, **11** (2001) 1277.
9. T.Sasaki, M.Watanabe, *J.Am.Chem.Soc.*, **120** (1998) 4682.
10. -G.Wu,D.C.DeGroot, H.O. Marcy, J.L. Schindler, C.R. Kannewurf, Y.-J. Liu, W, Hirpo and M.G. Kanatzidis, *Chem.Mater.* **8** (1996) 1992.
11. T.A. Kerr, L.F. Nazar, *Chem. Mater* **8** (1996) 2588.
12. E.Shouji, D. A. Buttry, *Langmuir.* **15** (1999) 669.
13. P.Gomez-Romero,. *Adv Mater*,**13** (2001) 163.
14. A.Vadivel Murugan, B.B. Kale, C-W.Kwon, G.Campet, K.Vijayamohanan, *J.Mater. Chem.***11** (2001) 2470.
15. P.Bernier, J.E.Fischer, S.Roth, S.A.Solin, *Chemical Physics of Intercalation II*, Eds, Plenum, New York, 1993.
16. K.E.Dungey, M.D.Curtis, and J.E.Penner-Hahn, *Chem. Mater.* **10** (1998) 2152
17. L.Wang, J.L. Schindler, J.A.Tomas, C.R. Kannewurf, M.G. Kanatzidis, *Chem.Mater.* **7** (1995) 1753.
18. T.L.Templeton, Y.Yoshida, X.-Z.Li, A.S. Arrott, A.E.Curzon, F.Hamed, M.A.Gee, P.J.Schurer, J.L.LaCombe, *IEEE, Trans.Magn*, **29** (1993) 2625
19. B.K.Miremadi, S.R.Morrison, *J.Catal.* **112** (1988) 418.
20. B.C.Bockrath, D.S.Parfitt., *Catal. Lett* **33** (1995) 201.

21. G. Heywang and F. Jonas, *Adv. Mater.* **4**(1992) 116.
22. H. Yamato, M. Ohwa and W. Wernet, *J. Electroanal. Chem.* **397**(1995) 163.
23. I. Winter, C. Reese, J. Hormes, G. Heywang and F. Jonas, *Chem. Phys.* **194** (1995) 207.
24. S. Ghosh, and O. Inganas, *Adv. Mater.* **11**(1999)1214.
25. M.A.Gee, R.F.Frindt, P.Joensen, S.R.Morrison, *Mater.Res.Bull.* **21** (1986) 543.
26. K.Chrissafis, M.Zamani, K.Kambas, J.Stoelmenos, N.A.Economou, I.Samaras, C.Julien, *Mater.Sci.Eng.B*, **3** (1989)145.
27. W.Y.Liang, *Intercalation in Layered Materials*, Plenum Press, New York **148** (1986) 31.
28. R.R.Chianelli and M.B.Dines, *Inorganic Chemistry* **17** (1978) 2758.
29. V.Hernandez, F.J.Ramirez, T.F.Otero, J.T.Lopez Navarrete, *J.Chem.Phys.***100** (1994) 114.
30. G.Louarn, J.Kruszka, S.Lefrant, M.Zagorska, I.Kulszewicz-Bayer, A.Prón, *Synth.Met.* **61** (1993) 233.
31. N.B.Colthup, L.H.Daly, S.E.Wiberley, *Introduction to Infrared and Raman Spectroscopy*, Academic Press, New York, 1964, 276.
32. R.S.Tipson, H.S.Isbell, J.E.Stewart, *J.Res.Natl.Bur.Standards.* **62** (1959) 257.
33. A.V.Powell, L.Kosidowski, A.McDowall, *J.Mater.Chem*, **11**(2001) 1086.
34. Wagner, C.D. ; Riggs, W.M.; Davis, L.E. ; Moulder, J.F.; Muilenberg, G.E. *Handbook of X-rayphotoelectron spectroscopy*;Perkin-Elmer Corporation:Eden Prairie,Minnesota,1979
35. A.Vadivel Murugan,C. W. Kwon, G. Campet, B. B. Kale, A. B. Mandale, S.R.Sainker, Chinnakonda S.Gopinath, and K. Vijayamohanam, *J.Phys Chem B.* **108** (2004) 10736.
36. T.A. Kerr, L.F. Nazar, *Chem. Mater.***8** (1996) 2005.
37. A.M.Hermann, R.B.Somoano, V.Hadek and A.Rembaum, *Solid State Commun*, **13** (1973) 1065.
38. R.B.Somoano, V.Hadek and A.Rembaum, *J.Chem Phys*, **58** (1973) 697.
39. M.A.Py and R.R.Haring, *Cur.J.Phys*, **61** (1983) 76.
40. C.Julien, S.I.Saikh and G.A.Nazri, *Mater Sci & Engg B* **15** (1992) 73-77.

# SUMMARY AND FUTURE PROSPECTS

## Chapter

# 6

---

**T**his last chapter deals with significant conclusions of the present study of the synthesis and characterization of organo-inorganic poly (3,4-ethylenedioxythiophene) with transition metal oxides and sulfides such as  $V_2O_5$ ,  $MoO_3$ ,  $VS_2$  and  $MoS_2$  by various intercalative polymerization. We believe that the unprecedented results reported here on several organo-inorganic nanocomposites, facilitating larger capacities and better reversibility for rechargeable lithium batteries and supercapacitors provide an example of fundamental advancement in the chemistry of materials with a promising technological potential. This chapter also outlines the general stability limitations of such hybrid materials for sustained electrochemical performance upon prolonged cycling. Finally the future prospects for next 5-10 years is presented within a broad perspective, keeping in view of the interest in nanostructured hybrid materials justifying why different types of chemists and materials scientist are working harmoniously in the area of nanotechnology, electrochemical materials science and molecular electronics. Consequently, several detailed studies to overcome these limitations and to offer new robust hybrid materials alleviating the disadvantages are expected to be abundant in the coming years.

---

**A**fter an initial period of rediscovery of conjugated polymers as electronically conducting materials in the seventies and a period of detailed studies of their properties and possible applications, came the realization that conducting polymers could also be used as components of more complex systems. For example, when a conducting polymer is used as a part of hybrid materials, sometimes they could merge the best properties of both the organic and inorganic species giving rise to synergistic effects in electrical, optical or mechanical behavior. Consequently, the design of nanocomposite materials based on conducting polymer has thrived during the recent years. This broad goal has been tackled using many different approaches, leading to a wide variety of conducting polymer based composite materials. Examples range from organic polymer structures doped with inorganic host structures (O-I materials) to hybrids of the inverse nature where extended inorganic nanoparticles are incorporated into the matrix of a conducting polymer (I-O materials). In between are materials where no structure clearly dominates or where nanosized particles are dispersed in polymers forming nanocomposite materials useful for various applications and particularly electrode materials for electrochemical power sources as discussed in *Chapter-1*.

Recently, many p-doped conducting polymers such as polyaniline and polypyrrole have been inserted into layered transition metal oxides and sulfides to form Organo-inorganic nanocomposites. Unfortunately, owing to the possible presence of benzidine moieties in the polymer backbone, the application of these systems is limited as they might yield toxic (carcinogenic) products upon degradation. Consequently, numerous industrial and academic groups have considered alternatives to polyaniline including the (hetero) aromatic polypyrrole and polythiophene, two more “environment friendly” systems. Polythiophene and its derivatives have been investigated to a lesser extent only and it may be better to use poly (3,4-ethylene dioxythiophene) (PEDOT), one of the recently found excellent conducting polymers, as it has generated more attraction due to enhanced stability compared to polypyrrole and polyaniline. Indeed, it appears to be one of the most stable conducting polymers currently available and has been attracting growing interest for several applications. More significantly, the field of PEDOT chemistry is relatively young and hence several possibilities exist for modifying its structure as well as its functional behavior.

In this regard, we focused our attention on the synthesis and characterization of poly (3,4-ethylenedioxythiophene) based organo-inorganic nanocomposites using various inorganic



transition metal oxides as well as disulfides ( $V_2O_5$ ,  $MoO_3$ ,  $VS_2$ ,  $MoS_2$ ). These composites with PEDOT nanoribbons/ nanosheets and inorganic hosts were characterized by thermal analysis (TGA), powder X-ray diffraction, FTIR, SEM, TEM, XPS and four-probe electrical conductivity measurements. A systematic study of these nanocomposites and the experimental data presented here suggests that the polymerization proceeds concomitantly with intercalation. The fact that two distinct phases rather than a continuum of compositions is obtained in these systems suggests the existence of a significant interaction between the host and guest beyond a simple insertion into the van der Waals gap. However, common to all these nanocomposite materials is the underlying search for synergy and the hybrid approach endeavors in general to create a material that is superior to the sum of their parts for possible applications in electrochemical power sources particularly as electrodes for rechargeable lithium batteries and supercapacitors.

Subsequently, we are the first to demonstrate the interleaving of poly (3,4-ethylenedioxy thiophene) between the layers of  $V_2O_5$  as explicitly discussed in the **Chapter-2**. More specifically, a novel method of interleaving poly (3,4-ethylenedioxythiophene) between the layers of  $V_2O_5$  has been demonstrated using a soft process of intercalation. The reaction takes place with the *in situ* polymerization of EDOT within the framework of  $V_2O_5$  with different nominal EDOT/ $V_2O_5$  ratios to give two distinct phases. These two phases can be distinguished by different interlayer spacing as detected from powder X-ray diffraction patterns. The interlayer spacing of  $V_2O_5$  expands in two stages, i.e., first from 4.32 to 13.84 Å and further to 19.04 Å and is consistent with the existence of two phases in the PEDOT/  $V_2O_5$  system corresponding to the intercalation of one and two mono-layers of PEDOT respectively, in the  $V_2O_5$  framework. The fact that two distinct phases rather than a continuum of compositions is obtained in this system suggests the existence of a significant interaction between the host and guest beyond simple insertion into the van der Waals gaps. Analysis of the experimental data presented here suggests that the polymerization proceeds concomitantly with the intercalation. The polymer chains appear fixed in the interlamellar space, and the ring flips observed in the bulk form of PEDOT are frozen in these materials. Therefore, there is considerable bonding interaction between the organic and inorganic components, probably due to hydrogen bonding. In addition, X-ray photoelectron spectrum shows the presence of both  $V^{4+}/V^{5+}$  species in the nanocomposite suggesting the increased number of  $V^{4+}$  centers in the  $V_2O_5$  frame work. These results also do confirm the redox intercalation and charge transfer from the polymer to the  $V_2O_5$  framework, while the

HRTEM suggests that the interlayer distance of crystalline  $V_2O_5$  expands upon the incorporation of the polymer nanoribbons. The improvement of electrochemical performance compared with other nanocomposites is attributed to the redox intercalative polymerization producing well-ordered compounds with enhanced bidimensionality. The influence of intercalants on  $Li^+$  diffusion rates and charge capacity in the PEDOT/ $V_2O_5$  nanocomposite is increased relative to that for other nanocomposites. The results also suggest that, the polymer nanocomposite acts as a better cathode material than the pristine  $V_2O_5$  material by enhancing lithium diffusion due to well-ordered bidimensional compound.

Molybdenum oxide is considered to be an attractive cathode material for non-aqueous lithium batteries. However, the orthorhombic phase ( $\alpha$ - $MoO_3$ ) has two dimensional layered structure which is favorable for  $Li^+$  intercalation as it exhibits higher electrochemical activity, and exceptional stability, despite its disadvantages including relatively slow kinetics for Li-ion transport, electronically insulating state upon full oxidation and poor cycling behavior. Thus one approach to modify the properties of a host material is through the intercalation of electronically conducting large guest species into the interlayer van der Waals gap, albeit with some difficulty. Consequently, **Chapter-4** describes attempts to successfully prepared poly (3,4-ethylenedioxy thiophene)/  $MoO_3$  nanocomposite by using a soft chemistry route. This reaction takes place with the *in situ* oxidative polymerization in the presence of an external oxidizing agent. Our results suggest that the interlayer spacing, upon intercalation expands from 6.93Å to 13.46Å followed by exfoliation and restacking process. The resultant interlayer separation is consistent with the existence of two phases of organic and inorganic species in the nanocomposite corresponding to the intercalation of PEDOT in the  $MoO_3$  framework to produce a new composite. The experimental data presented here also suggests that the polymerization proceeds concomitantly with intercalation. Interestingly there is a three order of magnitude increase in conductivity compared to that of the pristine oxide afforded by incorporation of polymer. We also observe that the effect of the polymer incorporation in between  $MoO_3$  layers is to improve the conductivity and there is a linear current increase with scan rate as expected for a strongly adsorbed electrochemical species. It is interesting to note that the double layer capacitance of pristine  $MoO_3$  increases from ~40 mF/g to ~300 F/g. In addition, when these composite are used as cathode for rechargeable lithium batteries using nonaqueous electrolytes the discharge capacity is found to be significantly enhanced from 130 mAh/g for pure  $MoO_3$  to 160 mAh/g for PEDOT/

MoO<sub>3</sub> nanocomposites under similar experimental conditions demonstrating intriguing effects with respect to electrochemical Li<sup>+</sup> insertion. Thus we conclude that the PEDOT/MoO<sub>3</sub> nanocomposite is a promising electrode material for supercapacitors and rechargeable lithium batteries than the pristine oxide.

Although, transition-metal dichalcogenides have been extensively investigated for their interesting electrical properties and their applications as cathode materials for rechargeable lithium batteries, VS<sub>2</sub> and MoS<sub>2</sub> have received only scanty attention. This presumably due to its lack of ability to undergo intercalation with organic molecules and macromolecule like PEDOT. In this regard, the exfoliation and restacking properties of both VS<sub>2</sub> and MoS<sub>2</sub> have been exploited to produce a novel molecular nanocomposite materials containing PEDOT, although no serious attempt has been made to date, to verify this. Thus, **Chapters 3 and 5** describe the study of a new class of nanocomposites including their synthesis by direct *in situ* oxidative polymerization of EDOT with VS<sub>2</sub> & MoS<sub>2</sub> as a host material followed by flocculation/delamination facilitating the expansion of the lattice in a direction perpendicular to the dichalcogenide layers. Upon intercalation, the interlayer spacing of VS<sub>2</sub> expands from 5.79Å to 14.01Å, and X-ray diffraction results also indicate that the exfoliated MoS<sub>2</sub> and PEDOT are restacked to produce a novel nanoscale composite material containing alternate nanosheets of PEDOT in between MoS<sub>2</sub> with a basal distance of ~13.8 Å. These changes in interlayer separations are consistent with the existence of two phases of organic and inorganic species in the nanocomposite corresponding to the intercalation of PEDOT in VS<sub>2</sub> and MoS<sub>2</sub> frameworks. The application potential of these nanocomposites as cathode materials for rechargeable lithium batteries is also demonstrated by the electrochemical intercalation of lithium into the PEDOT/ VS<sub>2</sub> and PEDOT/ MoS<sub>2</sub> nanocomposites, where a significant enhancement in the discharge capacity is observed compared to that for respective pristine sulfides. The enhancement in discharge capacity could be explained by the disturbed layer stacking scheme, derived from the separation of layers due to structural disorders (enhanced “bidimensionality”). Since conductive additives like graphite and carbon black are often used for fabricating Li/MoS<sub>2</sub> and VS<sub>2</sub> rechargeable battery electrodes, the intrinsic conductivity of PEDOT/MoS<sub>2</sub> and PEDOT/Vs<sub>2</sub> molecular composites reported here, would eliminate the need for such additives during electrode fabrication.

The future prospects and applications of conducting polymer based nanocomposites are as varied as the materials themselves due to the amazing combination of both conjugated type polymers and layered hosts available with structural and functional compatibility. Several number of nanocomposites described here are based on electro-active inorganic oxides and sulfides with electronically conducting polymers, where the electrochemical activity is preeminent. Although, these nanocomposites show enhancement in discharge capacity and cycle life, a rigorous evaluation of the long term stability concerning high energy storage applications like both supercapacitors and rechargeable lithium batteries is desirable. In addition, these types of intercalative nanocomposites may also be useful for the study of applications like electro-catalyst for fuel cells and electrochromic properties for opto electronic devices.

Although, the applications of these hybrid materials are promising and varied primarily due to their superior device performance, these are also interesting from a fundamental point of view, as the anchoring of electronically conducting polymers between inorganic hosts offers an opportunity to modulate their electrochemistry. Also much remains to be learned about the nanostructural features of hybrid materials in general, since their behavior changes with respect to the dimensionally constrained environment. For instance, the behavior of conducting polymer in the interlayer region is unknown and studies are needed to understand the role of conformation of the polymers upon insertion into these inorganic layers. It is hoped that the new development of this field in the coming decade will allow us to expect exciting developments dealing with both fundamental aspects and applications. As this happens, even more exotic applications in molecular electronics may emerge, enabling intercalative nanocomposites and its analogues to maintain their position as one of the important useful materials.

\*\*\*\*\*

